IDENTIFICATION AND CHARACTERIZATION OF MYCN-EXPRESSING TRIPLE-NEGATIVE BREAST CANCER: IMPLICATIONS FOR THERAPETUIC STRATEGIES

By

Johanna Marlies Schafer

Dissertation

Submitted to the Faculty of the

Graduate School of Vanderbilt University

in partial fulfillment of the requirements

for the degree of

DOCTOR OF PHILOSOPHY

in

Biochemistry

December 14, 2019

Nashville, Tennessee

Approved:

Jennifer Pietenpol, Ph.D.

John York, Ph.D.

Stephen Fesik, Ph.D.

Scott Hiebert, Ph.D.

Christine Lovly, M.D., Ph.D.

To my parents
and Román

ACKNOWLEDGEMENTS

This work would not have been possible without the support from my family, friends, co-workers and mentors. I have immense appreciation for each and every person who has contributed mentorship, scientific discussions, challenging feedback, and words of encouragement over the years. I would first like to thank Dr. Jennifer Pietenpol. Her unwavering enthusiasm and scientific rigor have driven me to work hard and dream big. I find myself at a level I did not foresee when I started graduate school. During all of the time, effort, and experimental heartache I endured in pursuit of a meaningful scientific discovery, Jennifer has been nothing but helpful and encouraging. Jennifer has expressed care for my mental and physical health, the development of my scientific abilities, and my pursuit of a research career. Her positive attitude and intense love for science has made this journey an overall pleasant and exciting experience. She sent me to both smaller specialized symposiums and large conferences and selected me to be an integral part of several collaborations that included a pharmaceutical company and individuals at Vanderbilt. Under Jennifer's guidance, I found myself surrounded by multiple teams of talented scientists that shared a similar passion for translational medicine and progressing the breast cancer research field to the next level.

My graduate school experience was also enhanced by my wonderful colleagues. I joined the Pietenpol lab with three other graduate students, Tim Shaver, Scott Beeler, and Gaby Santos. We went through classes together, our qualifying exams together, and worked side by side at the bench together. Our time spent inside and outside of the Pietenpol lab will forever link us. I would like to thank them for their collaborative efforts

and insights during project discussions. I would also like to thank the other members of the Pietenpol lab – Dr. Brian Lehmann for his time and openness to discuss any question I had, no matter how big or small; Dr. Clayton Marshall and Kimberly Johnson for their assistance on high-end experiments and for creating an efficient lab environment; Dr. Hanbing An for her interest in my project and career development; Hailing Jin for assisting me with several experimental techniques and her friendly morning chats; and Lindsay Redman, the newest graduate student of the Pietenpol lab, for her willingness to review material, team spirit, and overall pleasant demeanor.

Over the years, I have had several key mentors that took the time to work with me and enlighten me on the path to becoming a scientist. My interest in research started during the summer of my junior year in college where I participated in an undergraduate summer research program at Virginial Commonwealth University and worked in the lab of Dr. Ben Churn. Overall, it was one of the most enjoyable and fulfilling summers I've ever had. Together, Dr. Churn and Dr. John Campbell created a lab environment that shifted my interest from medical to graduate school and jump-started my pursuit for additional research experience. I would like to thank Dr. Amy Grunden for her mentorship during my Capstone research project at North Carolina State University and Dr. Steven Simmons for allowing me to shadow him at the US Environmental Projection Agency. While preparing for graduate school, I worked in the lab of Dr. Mohanish Deshmukh at the University of North Carolina, Chapel Hill where Dr. Deshmukh and Dr. Vivian Gama perpetuated a driving force for scientific discovery. I would like to thank Mohanish for involving me in a very interesting, thought-provoking project and for creating such an enjoyable work atmosphere. I worked closely with Vivian during my time at UNC. I

consider her one of the most genuine and scientifically savvy people I have ever met. Her detail-oriented focus greatly assisted in the development of my technical skills leading up to graduate school.

I am also tremendously grateful for the mentorship I received in graduate school. I would like to thank Dr. John York, the chair of my committee, for his straight-forward and candid views on my project and personal development as a scientist. He recognized my strengths and encouraged me to further development other skillsets. I thank Dr. Scott Hiebert for his generosity in allowing me to spend time in his lab to learn a specialized experimental method and for taking the time to discuss next steps in my career. I thank Dr. Steve Fesik for pushing me to conduct high-throughput screens and for his advice on effective presentation techniques. I would be remiss not to also thank Dr. Christine Lovly. Her extensive knowledge and sharp wit contributed greatly to project discussions and future directions.

I attribute my mental strength over these years to my family - my mom for keeping me company during the late-night walks to my car and for being overly excited about every little positive result or accomplishment - and my dad for always checking in to see how I'm doing and for reminding me of how proud he is of me. I would like to thank my sisters and best friends, Jessica and Jennifer, for being my own personal cheerleaders. They attended both my white coat ceremony and defense and have always been a phone call away to brighten my day. I also appreciate both brothers - Jared for his support and excitement over my graduate school journey - and Justin for always pushing me to take the hard road and strive for a career that could potentially benefit the world around me.

I am also very grateful for my friends far and near. I would like to thank my best friends made before graduate school, Megan Cooke, Savanna Edmiston, and Stefanie Boenig, for their phone calls, surprise gifts, and visits - and the friends I made along the way - first Katie Sprinkel and Rachel Lippert, who were both great workout buddies and dance partners, my unstoppable American Outlaws soccer team, and friends made during the latter half of graduate school, Liz Conrad, Matt Bach, Mal Hacker, Henry Horne, and Roberto Vanacore. I will always look back fondly on the numerous cycling sessions, festive dinner parties, and exciting get togethers for sporting events that helped balance my life. Finally, I would like to thank mi amor, Román Covarrubias. While I met him on the soccer field, Román also received his doctorate at Vanderbilt through the Interdisciplinary Graduate Program and could relate to challenges faced and efforts needed to get through the program. I would like to thank Román for providing a silver lining on life when needed, for always encouraging me to go the extra mile to set myself apart from others, and for his never-ending joyful sense of humor. I appreciate every aspect of his personality and feel immensely fortunate to have him in my life.

TABLE OF CONTENTS

LIST OF TABLES

LIST OF FIGURES

LIST OF ABBREVIATIONS

AR	androgen receptor
AACR	American Association for Cancer Research
ACS	American Cancer Society
ADCC	antibody-dependent cellular cytotoxicity
AML	acute myeloid leukemia
AOD	approved oncology drug
ATCC	American Type Culture Collection
ATP	adenosine triphosphate
BET	bromodomain and extra-terminal motif
BETi	bromodomain and extra-terminal motif inhibitor
BID	twice a day
BL1	basal-like 1
BL2	basal-like 2
BRCA	breast invasive carcinoma
BRD	bromodomain
CCLE	cancer cell line encyclopedia
CBR	clinical benefit rate
CDC	Centers for Disease Control and Prevention
CDK	cyclin-dependent kinase
CDX	cell line-derived xenograft
CFA	colony formation assay

CRPC	castration-resistant prostate cancer
CI	confidence interval
CN	copy number
CTC	circulating tumor cell
CRPC	castration-resistant prostate cancer
DAB	3,3′-Diaminobenzidine
DFS	disease free survival
DHSR	Digital Histology Shared Resource
DMEM	Dulbecco's modified Eagle's medium
DNA	deoxyribonucleic acid
EDTA	ethylenediaminetetraacetic acid
EGFR	epidermal growth factor receptor
ERK1/2	mitogen-activated protein kinase 3/1 (gene: MAPK3/1)
EMT	epithelial-to-mesenchymal transition
ER	estrogen receptor (gene: ESR1)
ERE	estrogen response element
FDA	Food and Drug Administration
FISH	fluorescence *in situ* hybridization
FFPE	formalin-fixed paraffin-embedded
GBM	glioblastoma multiforme
GE	gene expression
GENIE	genomics evidence neoplasia information exchange
GLS	glutaminase

GSEA	gene set enrichment analysis
HER2	human epidermal growth factor receptor 2 (gene: ERBB2)
HTS	high-throughput screening
HR	hormone receptor
HR	homologous recombination
HRP	horseradish peroxidase
HSC	hematopoietic stem cell
IACUC	Institutional Care and Use Committee
IC_{50}	half-maximal inhibitory concentrations
iPS	induced pluripotent stem
IRB	institutional review board
ISB	isotonic swelling buffer
IHC	immunohistochemistry
IDT	Integrated DNA Technologies
IM	immunomodulatory
LAR	luminal androgen receptor
LCM	laser-capture microscopy
LB	ligation buffer
M	mesenchymal
MAPK	mitogen-activated protein kinase
MBC	metaplastic breast cancer
MEC	mammary epithelial cells
MEK1/2	mitogen-activated protein kinase kinase 1/2 (gene: MAP2K1/2)

MEKi	MEK inhibitor
METABRIC	Molecular Taxonomy of Breast Cancer International Consortium
mRNA	messenger RNA
MTA	material transfer agreement
mTOR	mammalian target of rapapmycin
MYC	V-Myc avian myelocytomatosis viral oncogene homolog
MYCL	V-Myc avian myelocytomatosis viral oncogene homolog 1, lung
MYCN	V-Myc avian myelocytomatosis viral oncogene neuroblastoma
NAC	neoadjuvant chemotherapy
NST	non-special type
NB	neuroblastoma
NCBI	National Center for Biotechnology Information
NCI	National Cancer Institute
NEB	New England Biolabs
NEPC	neuroendocrine prostate cancer
NIH	National Institutes of Health
NSG	NOD *scid* gamma
NT	non-targeting
NTP	nucleotide triphosphate
OR	odds ratio
PARP	poly (ADP-ribose) polymerase
PCA	principal component analysis
pCR	pathologic complete response

PI3K	phosphoinositide 3-kinase
PI3Ki	phosphoinositide 3-kinase inhibitor
PI3KiR	phosphoinositide 3-kinase inhibitor-resistant
PIM1	pim-1 proto-oncogene, serine/threonine kinase
PBS	phosphate-buffered saline
PDX	patient-derived xenograft
PFS	progression-free survival
PK	pharmacokinetic
PLK1	polo-like kinase 1
PMSF	phenylmethylsulfonyl fluoride
PTEN	phosphatase and tensin homolog
PR	progesterone receptor (gene: PGR)
PRO-seq	precision nuclear run-on sequencing
QC	quality control
QD	every day
RNA	ribonucleic acid
RNA-seq	RNA-sequencing
RNA pol II	RNA polymerase II
RPKM	reads per kilobase per million
RPPA	reverse phase protein array
RT	room temperature
RT	reverse transcriptase
OS	overall survival

scRNA-seq	single-cell RNA sequencing
SD	standard deviation
siRNA	small interfering RNA
SEER	Surveillance, Epidemiology, and End Results
SEM	standard error mean
SNP	single nucleotide polymorphism
SPORE	Specialized Program of Research Excellence
SPRM	selective progesterone receptor modulators
TBST	tris-buffered saline plus tween
TCGA	The Cancer Genome Atlas
TDLU	terminal ductal lobular unit
TGI	tumor growth inhibition
TKI	tyrosine kinase inhibitor
TIL	tumor-infiltrating lymphocytes
TNBC	triple-negative breast cancer
TPM	transcripts per million
TPSR	Translational Pathology Shared Resource
TMA	tissue microarray
TSA-IF	tyrosine signal-amplified immunofluorescence
TTP	Time to Progression
VANTAGE	Vanderbilt Technologies for Advanced Genomics
VICC	Vanderbilt-Ingram Cancer Center
VUMC	Vanderbilt University Medical Center

CHAPTER I

INTRODUCTION

This dissertation focuses on the discovery and preclinical characterization of drug combinations to inhibit the tumor cell growth of a subset of triple-negative breast cancer (TNBC) tumors that aberrantly expresses the transcription factor, MYCN. TNBC, a subtype of breast cancer known for both its heterogeneity and poor prognosis, is characterized by the absence of estrogen receptor (ER) and progesterone receptor (PR) expression and amplification/over-expression of the human epidermal growth factor receptor 2 (HER2) gene (ERBB2). These three receptors currently direct therapeutic strategies for the other breast cancer subtypes. Given the lack of ER, PR, and elevated HER2 levels in TNBC, the standard-of-care for patients with TNBC primarily involves cytotoxic chemotherapy in the primary setting.

Development of strategies to treat TNBC has been challenging due to genetic and epigenetic differences in tumor makeup between patients (intertumoral heterogeneity) as well as between individual cells within a given tumor (intratumoral heterogeneity). Investigators who focus on the study of TNBC have approached these issues by (1) further dividing TNBC into additional subtypes based on gene and protein expression or by specific oncogenic genomic alterations; and (2) evaluating genetic modifications and shifts in cellular composition within tumor cell populations before and after treatment with various chemotherapeutics and targeted therapies. The most prevalent genetic alteration in TNBC involves the mutation or loss of TP53, followed by aberrant *MYC* amplification/overexpression and alterations in genes involved in PI3K pathway signaling.

Results presented in Chapters III and IV focus on the identification and characterization of a subset of tumors that aberrantly express two members of the MYC family (MYC and MYCN) and how tumor expression of these onco-proteins changes in response to leading chemotherapeutics and agents under clinical development.

Strategies to target receptor-positive and triple-negative breast cancer

Breast cancer subtype identification and significance

Breast cancer is the most commonly diagnosed malignancy in females worldwide, accounting for greater than two million diagnoses annually *(1)*. The National Cancer Institute (NCI), American Cancer Society (ACS), and Centers for Disease Control and Prevention (CDC) collaborate yearly to analyze and report cancer incidence and mortality patterns across the United States. The most current report from Surveillance, Epidemiology, and End Results (SEER) states that, among women, breast cancer is the second leading cause of cancer-related deaths across all racial and ethnic groups *(2)*. Although incidence rates of breast cancer in the U.S. have increased approximately 0.4% per year since 2004, mortality rates have been on the decline *(2)*. The latter is due, in part, to the discovery of biomarkers in breast cancer that effectively guide selection of targeted therapies and the ongoing development of new therapeutics.

We have known since the 1930s that aberrant expression of hormones (namely estrogen and progesterone), which are involved in normal mammary gland development, is one of the primary drivers of breast cancer and characterizes a breast cancer subtype that represents about 70-75% of all breast cancer cases *(3)*. Screening new breast cancer diagnoses for the expression of nuclear hormone receptors (HRs), ER and PR, through

immunohistochemical (IHC) methods has become routine to guide selection of therapy. Where it was once believed that surgical removal of the ovaries [oophorectomy (source of estrogen and progesterone production)] or breast tissue [lumpectomy (breast-conserving, wide local excision of tumor tissue); mastectomy (full removal of a breast)] were the only avenues to disrupt hormone-driven breast cancer, we now know that pharmacological inhibition of ER and associated upstream hormone signaling to ER and PR are both effective methods to inhibit the growth of tumors that express these receptors *(3)*.

In 1987, Slamon and his colleagues described another subtype of breast cancer *(4)* shortly after the discovery of the ERBB2 gene and its transforming activity by the Weinberg laboratory, which they further characterized by 1984 *(5, 6)*. Overexpression of ERBB2 (encoding the protein HER2) in 10-15% of all breast cancer cases is typically due to amplification of ERBB2. In addition to the assessment of HER2 protein levels through IHC, breast tumors are also frequently screened for ERBB2 gene-amplification through fluorescence *in situ* hybridization (FISH) techniques. Discovery and development of therapeutics against HER2+ disease was a considerable breakthrough in breast cancer research. Once considered a poor prognosis, patients with HER2+ breast cancer now experience prolonged survival after first line therapy *(7)*.

TNBC, representing 15% of breast cancer cases, is a subset of breast cancer that lacks ER and PR expression and HER2 gene-amplification/over-expression; and, is therefore, unresponsive to the leading targeted therapeutics in the breast cancer field. Due to the scarcity of effective targeted therapies for TNBC, standard of care for early stage disease entails the use of cytotoxic chemotherapy. Patients with a TNBC diagnosis

are typically of younger age and experience a worse survival outcome compared to the other breast cancer subtypes. The following sections will explain genomic and morphological differences between the breast cancer subtypes, mechanisms to which effective therapeutics are known to inhibit growth of receptor-positive (ER, PR, and HER2) breast cancer, and current avenues under exploration for the treatment of TNBC.

Standard of care for patients with receptor-positive breast cancer

Hormone receptor-directed therapeutic intervention: While estrogen receptors, ERα and ERβ, are expressed at similar levels within normal mammary epithelium, ERα is expressed at higher levels in breast cancer and is the only isoform evaluated in breast cancer biopsies for diagnostic purposes *(8)*. ERα is expressed in the majority of breast cancer and plays a critical role in hormone-regulated breast cancer progression; therefore, therapeutic strategies have been deployed to target ER signaling. Given that estrogen is an essential component of the menstrual cycle and reproduction, tamoxifen, the current leading breast cancer therapeutic, was originally synthesized in the 1960s for contraceptive purposes *(9)*. One of the earliest observations supporting a relationship between breast cancer progression and the ovaries (where estrogen is produced) came from a study that found a reduction in mammary cancer development in high-incidence strains of mice after early oophorectomy (removal of ovaries) *(10)*. Tamoxifen is considered a selective estrogen-receptor modulator (SERM), or estrogen antagonist, and was designed to compete with estrogen for ER binding (Figure 1A) *(8, 9, 11)*. In 1973, tamoxifen was repurposed for the treatment of breast cancer in the United Kingdom and four years later in the United States *(9)*.

Although the clinical application of tamoxifen resulted in decreased ER+ tumor cell growth, mechanisms of inhibition were initially unclear; *in vitro* assays indicated the affinity between tamoxifen and ER was very low *(12)*. Discovering that tamoxifen was converted in the liver to 4-hydroxytamoxifen, a molecule with greater than 100 times the affinity to ER than tamoxifen, launched the study of structure-activity relationships of antiestrogens and ultimately led to the development of raloxifene (3-hydroxytamoxifen, another leading clinical estrogen antagonist) and the majority of all current SERMs (Figure 1A) *(9)*. Other treatments for ER+ breast cancer include the use of selective ER downregulators (SERDs), a class of steroidal anti-estrogens (e.g. fulvestrant) that causes an ER conformational change and subsequent proteasomal degradation *(13)*, and aromatase inhibitors (e.g. exemestane, anastrozole, and letrozole) that prevent the conversion of androgen to estrogen (Figure 1A) *(14)*.

ER+ breast cancers, representing the majority of all breast cancer cases (70-75%) (Figure 1A), are largely well-differentiated, less aggressive, and associate with better survival outcomes compared to HER2+ and TNBC subtypes *(15)*. Tamoxifen treatment after surgical resection provides a response rate of nearly 70% in premenopausal women as well as substantially reduces the rate of recurrence and mortality by at least 40% and 30%, respectively *(16, 17)*. Extending administration of tamoxifen from two to five years will generally prolong time to metastatic recurrence, indicating selective pressure on ER for an extended period of time is an effective measure to control outgrowth of disseminated dormant tumor cells and should be continuously administered beyond five years. Unfortunately, nearly a third of patients will relapse after tamoxifen treatment within

A

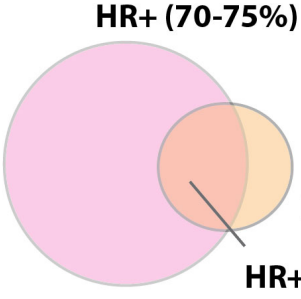

Leading therapies for receptor-positive BC	Drug target
Tamoxifen	ER antagonist[a]
Raloxifene	ER antagonist[a]
Fulvestrant	ER degradation[b]
Exemestane	Aromatase inhibitor
Anastrozole	Aromatase inhibitor
Letrozole	Aromatase inhibitor
Trastuzumab	Extracellular HER2
Pertuzumab	Extracellular HER2
Lapatinib	Intracellular HER2

B

Therapies for TNBC	Leading compounds	Target	Tumor criteria	FDA-approval
Chemotherapy	Anthracyclines Taxanes	DNA damage Microtubules	No specific criteria	All stages
PARP inhibitor	Olaparib Talazoparib	PARP PARP	germline *BRCA1/2*-mutant	Advanced or metastatic
Immunotherapy	Atezolizumab	PD-L1	PD-L1 expression	Advanced or metastatic[†]

C

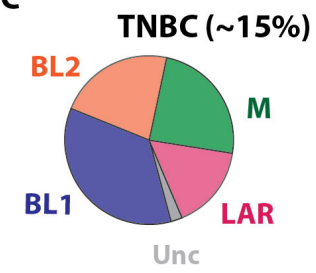

TNBC subtype	Gene Ontology	Mutational enrichment	Drug sensitivity
BL1	Cell cycle/DDR	BRCA1/2	Platinum agents/NAC/ PARP inhibition
BL2	MET/EGFR genes and myoepithelial features		mTOR, Growth factor receptors
M	NOTCH/TGFß and trans-differentiation features		mTOR, Growth factor receptors, Src inhibition
LAR	Luminal androgen receptor signaling	PIK3CA	AR antagonist/ PI3K inhibition
*IM**	Immune signaling		Chemotherapy/ Immunotherapy

Figure 1. Therapeutic strategies to target HR+ and triple-negative breast cancer. (**A**) Leading therapies and corresponding drug targets to treat receptor-positive (HR+ and HER2+) breast cancer (BC). a, selective estrogen receptor modulator. b, selective estrogen receptor down-regulator. (**B**) Leading therapies and corresponding drug targets, along with stage and molecular tumor criteria, to treat triple negative breast cancer (TNBC). †Unresectable. (**C**) Gene ontology, mutational enrichment, and drug sensitivity for the four TNBCtype-4 subtypes [basal-like 1 (BL1), basal-like 2 (BL2), mesenchymal (M), and luminal androgen receptor (LAR)]. Unc, unclassified. *, tumors with immunomodulatory (IM) gene expression from presence of tumor infiltrating lymphocytes (TILs).

15 years; however, second-line therapeutic options, such as SERDs and aromatase inhibitors, are generally effective to treat tamoxifen-resistant disease.

Since ER is involved in transcription of PR, breast cancer expressing both receptors typically respond well to endocrine therapies. However, individual hormone receptor expressing tumors, ER+/PR- versus ER-/PR+, represent approximately 15% and 3% of all breast cancer, respectively, and have been determined as separate distinct types of cancer in terms of biological features and prognosis *(17)*. ER+/PR- tumors more frequently affect elderly, postmenopausal women, are classified as ductal or unspecified carcinomas, and are associated with a better prognosis compared to ER-/PR+ expressing tumors *(17, 18)*. ER-/PR+ tumors, on the other hand, affect younger, premenopausal women and are often associated with biomarkers of poor prognosis, such as basal cytokeratins and reduced E-cadherin expression; counterintuitively, patients with dual positive (ER+/PR+) breast cancer demonstrate a better overall survival (OS) than patients that express either receptor alone *(17)*.

Despite the understanding that PR signaling is a major component of breast cancer progression, drug development has primarily focused on disrupting ER signaling. The disproportional effort is due, at least in part, to severe clinical side effects (liver toxicity) from first line PR antagonists [selective progesterone receptor modulators (SPRMs)] generated in the 1960s *(19)*. Although less toxic newer generation SPRMs are currently under investigation, additional avenues of PR-mediated signaling are being developed that target downstream effectors involved in paracrine signaling (WNT4 and RANKL) or proliferation (cyclin D1) that promote breast carcinogenesis *(19–21)*. These therapeutics

are suspected to benefit patients with ER-/PR+ tumors or with expression of both receptors that are unresponsive to endocrine therapies designed to target ER signaling.

HER2-directed targeted therapies: HR+ and HER2+ tumors are not mutually exclusive; approximately 10% of breast cancers are both HR+ and HER2+ and 5% are HER2+ only (Figure 1A). Unlike the nuclear HRs, HER2 is a transmembrane protein with no known direct activating ligand; instead, HER2-mediated growth factor signaling is initiated at the plasma membrane after homo- or heterodimerization with related family members, HER3, HER4, or epidermal growth factor receptor (EGFR/HER1), another frequently amplified receptor in cancer *(22)*. After dimerization, catalytic activity within the cytoplasmic domain of the receptors results in autophosphorylation of tyrosine residues and initiates various growth stimulating pathways including phosphatidylinositol-4,5-bisphosphate 3-kinase (PI3K), mitogen-activated protein kinase (MAPK), and protein kinase C (PKC) signaling *(22, 23)*. HER2 overexpression is generally a result of enhanced transcription and/or amplification of the ERBB2 gene.

The development of HER2-targeted therapies has been one of the most productive areas of drug development for breast cancer over the last three decades. Upon the discovery of HER2 overexpression in breast tumors, two main approaches were taken to target HER2+ breast cancer. The first involved the use of monoclonal antibodies designed to bind to the extracellular domain of HER2, and the second entailed the use of tyrosine kinase inhibitors that bind to the intracellular domain of HER2. Trastuzumab and pertuzumab are the two leading Food and Drug Administration (FDA)-approved monoclonal antibodies to treat patients with HER2+ breast cancer (Figure 1A). Both

therapies induce antibody-dependent cellular cytotoxicity (ADCC), recruitment of immune innate effector cells, and immune cell Fc receptor-dependent tumor cell lysis *(24)*. Further, HER2 antibody-drug conjugates, such as trastuzumab-emtansine (T-DM1), that utilize antibody-mediated delivery of potent toxins to HER2+ tumor cells, are also under clinical development *(24)* (Figure 1A). Currently, trastuzumab in combination with the microtubule inhibitor, paclitaxel, is the current standard of care for patients with treatment-naïve HER2+ breast cancer *(25)*. Lapatinib, neratinib, and afatinib are examples of a class of oral receptor tyrosine kinase inhibitors (TKIs) that compete with adenosine triphosphate (ATP) binding to prevent auto-phosphorylation and inhibit subsequent activation of growth-stimulating signal transduction pathways (Figure 1A) *(24)*. The use of TKIs result in decreased cell proliferation and induction of apoptosis; however, they are generally suggested as a treatment for later stage disease once tumors have stopped responding to the various anti-HER2 monoclonal antibodies in combination with chemotherapy.

Although IHC and FISH are the two clinically-developed methods for identification of HER2+ breast cancer, overexpression of HER2 can also be identified through RNA-based methods such as RNA-sequencing and quantitative reverse transcription polymerase-chain reaction (qRT-PCR); however, these techniques have been primarily used in preclinical studies or to evaluate changes in gene expression after treatment in clinical samples *(23)*. The magnitude of benefit between expression levels and HER2-targeted therapies in primary and metastatic breast cancer has been extensively studied. The greatest correlation between HER2 levels and response to HER2-targeted therapies have been in the neoadjuvant setting (treating patients prior to surgical resection) *(26, 27)*. No association with disease-free survival (DFS) nor OS could be made in the

adjuvant setting (treating patients after surgical resection and/or radiation therapy) *(28)*. Studies evaluating response to HER-targeted therapies in the metastatic setting were variable. While patients with tumors harboring elevated HER2 mRNA levels responded well to targeted treatment, patients with lower HER2-expressing tumors also exhibited clinical benefit *(29)*.

Around 10-15% of patients that present with early stage HER2+ breast cancer will experience disease recurrence after the first round of anti-HER2 treatment *(23)*. Known mechanisms of resistance to monoclonal antibody-mediated therapies include steric hindrance of the HER2 receptor itself (e.g. activating truncations and kinase domain mutations), expression of alternative receptors (e.g. HER1, HER3, IGF-1R, and VEGFR), and activation of downstream effectors (e.g. development of PIK3CA mutations, PTEN loss, or mTOR activation) *(30)*. The discovery of resistance mechanisms to HER2-targeted therapy have led to the initiation of various clinical trials to investigate the integration of agents that target the other HER2 family members, the PI3K pathway, or mTOR signaling in combination with anti-HER2 treatment. Currently, patients with metastatic HER2+ breast cancer have a median survival comparable to HR+ breast cancer with a life expectancy of more than 4.5 years (compared to 1.5 years achieved 18 years ago); unfortunately, metastatic breast cancer is not considered curable, so across every breast cancer subtype, treatment goals for metastatic disease involve prolonging survival and improving quality of life as much as possible *(25)*.

Standard of care for patients with TNBC

As previously mentioned, TNBC represents ~15% of all breast cancer; however, the subtype also accounts for ~26% of all locally-advanced disease *(31)* and ~25% of all breast cancer-related deaths *(32)*. TNBC affects women of younger age (<40 years) compared to the other breast cancer subtypes and is enriched for women of African-decent *(33)*. The clinical definition for what constitutes negativity for ER, PR, and HER2 expression has varied over the decades, namely the definition of ER/PR positivity. Currently, positivity greater than or equal to one percent for either ER or PR by IHC defines criteria for assigning an ER+/PR+ breast cancer classification by the American Society of Clinical Oncology *(34)*. HER2 positivity is defined by the presence of 3+ IHC levels and/or *ERBB2* gene amplifications greater than 2.0 by FISH *(35)*. Therefore, the now universal pathology screening assay-based definition for TNBC is zero for ER/PR expression and ≤1+ for HER2 expression by IHC, and the lack of *ERBB2* gene amplifications by FISH.

Subtype-specific clinical features: A description for what this subtype lacks, rather than what it contains, provides a misconception that tumors within the TNBC subtype are of similar biology. TNBC tumors are actually a composite of breast cancers with numerous histological variants that are both genetically and morphologically distinct, making the development of universal therapy for TNBC extremely difficult. The majority of TNBC tumors are invasive ductal carcinomas that frequently present with elevated EGFR and/or keratin 5/6 expression; however, the TNBC subtype also contains relatively rare histotypes, including medullary, metaplastic, adenoid cystic, and apocrine carcinomas

(36). MBC represents 0.5-5.0% of all invasive breast cancers and are characterized by a differentiation of neoplastic epithelium into squamous and/or mesenchymal elements (i.e. chondroid, spindle, rhabdoid, or osseous cells) entirely or in admixture with glandular components *(37)*. Although MBCs present with a wide range of histological appearances, they are perceived clinically as a single subtype that is typically recalcitrant to chemotherapy and associated with a poor prognosis *(38)*

Aside from differing in gene expression and presenting with unique histological elements, additional attributes distinguish TNBC from the other breast cancer subtypes, including aberrant multimodality imaging features at diagnosis in the primary setting. These include spiculated margins, irregular mass shape, and low levels of calcification *(31)*. Calcium deposition is the primary means to detect tumors using mammographic methods; therefore, despite the relatively large size at diagnosis, nearly 20% of TNBC are occult upon initial mammographic imaging, indicating mammography alone is a suboptimal tool for initial diagnostic evaluation *(31)*. Combining mammography with ultrasonographic assessment has been shown to enhance detection levels to 92-100% of TNBC tumors. Further, given the increased sensitivity of magnetic resonance imaging (MRI), institutions are implementing this technology as a screening tool, alongside biopsy evaluation, for patients that are at high risk for developing breast cancer (i.e. patients with a family history of breast cancer or that carry BRCA1/2 mutations, discussed below) *(31)*.

The current standard of care for patients with early stage TNBC remains systemic cytotoxic chemotherapy, primarily through use of anthracyclines (DNA-damaging agents) and taxanes (microtubule inhibitors, Figure 1B). Compared to the receptor-positive breast cancer subtypes, patients with TNBC display the highest rates of pathologic complete

response (pCR, no observable disease in breast and regional lymph nodes after treatment) after neoadjuvant chemotherapy *(39, 40)*. A pCR for patients with TNBC is associated with infrequent relapse and favorable long-term clinical outcomes; however, patients with residual disease experience progression and a poor prognosis *(39, 40)*. To further elucidate the natural history and clinical behavior between breast cancer subtypes, Dent *et al.* analyzed the clinical correlates of TNBC versus receptor-positive breast cancer for 1,601 patients diagnosed with early-stage disease over a ten-year time span *(32, 41)*. Similar to previous studies, patients with TNBC were of younger mean age (53.0 versus 57.7, $p<0.0001$) and presented with tumors that were of higher grade (grade III: 66% versus 28%, $p<0.0001$), larger in size (>2cm: 63.5% versus 37.3%, $p<0.0001$), and associated with a higher lymph node positivity (54.6% versus 45.6%, $p<0.02$). While size of receptor-positive tumors correlated with lymph node positivity ($p<0.0001$), no correlation was found for patients with TNBC; at least one positive lymph node was found in 55% of patients with tumors $\leq$1 cm *(32)*. These analyses illustrated patients with TNBC had an increased likelihood of distant recurrence [hazard ration (HR) 2.6, $p<0.0001$] and death (HR 3.2, $p<0.001$) compared to patients with receptor-positive breast cancer. The average time to recurrence peaked at three years for patients with TNBC; whereas, receptor-positive breast cancer patients exhibited a constant rate of recurrence over time *(32)*. Visceral relapses, including lung and brain metastases, are more prevalent in patients with TNBC, whereas patients with HR+ and HER2+ disease recur more often to the bone and liver, respectively *(42–44)*.

Genomic alterations and biomarker-directed therapies: The most highly mutated gene in TNBC, representing ~80% of cases, is the tumor suppressor *TP53* (encoding protein p53), a critical regulator of genome maintenance that functions to regulate the cell cycle and prevent adverse effects from DNA damage *(45, 46)*. To ensure proper genomic fidelity, activated p53 will initiate growth arrest to repair DNA lesions, or if DNA damage is too severe, induce an apoptotic cell death *(45, 47)*. Hotspot mutations that occur in the DNA binding domain of *TP53* result in a loss of p53 transcription factor activity and DNA damage-induced cell cycle checkpoint control, which allows for the accumulation of genetic alterations and predisposes cells to transformation *(45)*. Germline mutations in *TP53* can lead to Li-Fraumeni syndrome, a rare autosomal-dominant hereditary disorder, that ultimately results in a 80-100% risk of females developing cancer in their lifetime *(48, 49)*. While the association between inactivated p53 and cancer was discovered in the 1970s, it still remains an active area in cancer research.

BRCA1 and *BRCA2* are well-characterized tumor suppressors that are directly involved in the homologous recombination (HR)-mediated repair of double-stranded breaks *(50)*. Individuals carrying germline mutations in *BRCA1/2* face a 60-85% risk of developing breast cancer in their lifetime *(51)*. The majority (~75%) of all tumors that harbor a *BRCA1/2* mutation are TNBC, representing ~15% of the TNBC tumor population *(52)*. Regardless of whether a *BRCA1/2* mutation is hereditary or sporadic, a mutation in one copy of either gene can lead to defects in HR-mediated DNA repair and thereby sensitize tumor cells to damage by DNA crosslinking agents, such as platinum salts (e.g. cisplatin and carboplatin) *(53, 54)*. Further, phenotypic and molecular characteristics of *BRCA1*-mutant cancers have been found in TNBC tumors without *BRCA* gene mutations.

These tumors are hypothesized to have "*BRCA*ness" through epigenetic silencing of *BRCA* expression or defects in HR through unknown variants and be responsive to therapies that demonstrate efficacy in *BRCA1/2*-mutant cancers *(55)*.

Despite only consisting of ten patients with *BRCA1* germline mutations, results from a proof-of-concept study brought tremendous excitement to the breast cancer research field; nine of the ten patients (90%) achieved a pCR after four cycles of single-agent neoadjuvant cisplatin *(56)*. As a result, clinical trials in both the primary *(57–59)* and metastatic *(60–62)* settings were initiated, with the majority of trials reporting promising results in favor of adding platinum agents to standard-of-care chemotherapy. For example, in the GeparSixto randomized phase II neoadjuvant trial, 315 patients with primary TNBC were treated with paclitaxel, liposomal doxorubicin, and bevacizumab, with or without weekly carboplatin *(58)*. Patients treated with the addition of carboplatin achieved a higher pCR (53.2% versus 36.9%, p=0.005) *(58)*. In a randomized phase II study, 53 patients with metastatic TNBC were treated with docetaxel combined with either cisplatin or capecitabine in the first-line setting *(60)*. Patients that received cisplatin achieved a better overall response rate (63.0% versus 15.4%, p=0.001) and progression-free survival (PFS, 10.9 versus 4.8 months, $p \leq 0.001$) *(60)*. In contrast, the Triple Negative Breast Cancer Trial (TNT), a large randomized phase III trial based in the U.K., treated 376 TNBC patients with either carboplatin or docetaxel monotherapy as first-line treatment with crossover on progression *(62)*. No difference was found with initial treatments or after crossover regimens; however, when evaluating benefit in select populations, patients with a germline *BRCA1* mutation had double the objective response rate when treated with carboplatin (68% versus 33%, p=0.01) *(62)*. Of note, a benefit was

not observed for patients with tumors expressing low *BRCA1* mRNA or exhibiting "BRCAness" using the Myriad HRD assay *(62)*.

Another approach to target *BRCA1/2*-mutant tumors was discovered in 2005 when two independent groups determined *BRCA1/2*-mutant tumors were hypersensitive to PARP inhibition *(63, 64)*. PARP is another protein involved in DNA double-strand break repair and is able to compensate for the loss-of-function phenotype observed in *BRCA1/2*-mutant cancers. The combined lethal effect of two genetic variations that are otherwise nonlethal in isolation is referred to as "synthetic lethality" and has been attributed to the efficacy of dual BRCA and PARP inactivation *(65)*. With promising preliminary results from phase II trials for patients with TNBC in the primary and metastatic setting *(66, 67)*, a large randomized phase III trial (OlympiaD) was initiated to evaluate olaparib, a PARP inhibitor (PARPi), as a monotherapy compared to standard-of-care treatment in germline *BRCA*-mutant HER2-negative metastatic breast cancers. Patients treated with PARPi had a greater response rate (59.9% versus 28.8%), lower grade III adverse events (36.6% versus 50.5%), and lower rates of discontinuation due to toxicity (4.9% versus 7.7%) *(68)*. In response to results from the OlympiaD trial, olaparib became the first FDA-approved targeted therapy for TNBC. Olaparib is approved for women with germline *BRCA*-mutant metastatic HER2-negative breast cancer (Figure 1B) *(69)*. Current efforts are focused on improving patient response by combining a PARPi with platinum agents and other chemotherapeutics for early-stage and metastatic *BRCA*-mutant cancers *(70, 71)*. Dosing strategies for PARPi and platinum agents still need to be optimized to ensure compounds added to chemotherapeutic regimens do not lead to increased rates of discontinuation or toxicity-induced adverse events *(72)*. Preclinical

efforts in *BRCA*-proficient tumors indicate PI3K, CDK1, HDAC, EGFR, ATM, and AR inhibitors are synthetic lethal with PARPi by inducing "BRCAness;" and thus, these combinations are also being evaluated clinically *(69)*.

Immunotherapy and immunoconjugates: The advent of immunotherapy has revolutionized the landscape of translational cancer research over the past decade. In normal physiology, the immune system performs a process called tumor immune surveillance where immune cells, such as CD8+ T-cells, recognize tumor-associated antigens and attack tumor cells *(73)*. When present in an inflammatory environment, activated T-cells, B-cells, natural killer cells, and other lymphocytes express an inhibitory receptor called PD-1 (programmed cell death protein 1) *(73, 74)*. Immune cells will become inactivated when PD-1 binds to its ligands, PD-L1 and PD-L2, which are normally expressed on the cells surface of T-cells and antigen-presenting cells *(75, 76)*. To escape immune surveillance, many tumor cells develop the ability to express PD-L1 and thus evade immune cell detection and activity *(73)*. A similar tumor cell-mediated deactivation of the immune system is carried out through tumor cell expression of the ligand, CTLA-4 (cytotoxic T-lymphocyte-associated antigen 4) *(77)*. Discovery of these interactions has led to the development of monoclonal antibodies designed against either the receptor or ligand to block the interaction and allow for immune cells to recognize the tumor cells as pathogenic.

High levels of tumor-infiltrating lymphocytes (TILs) are associated with ER-negativity, higher-grade tumors, poor-prognostic clinicopathological features, higher proliferation rates, and lymph node positivity *(78–81)*. These features generally associate

with advanced stage disease and a worse prognosis *(82)*. Counterintuitively, high TIL levels are associated with a superior response to NAC treatment and are predictive of pCR rates, DFS, and a greater OS *(83–85)*. For example, specimens analyzed from two large neoadjuvant clinical trials (GeparDuo and GeparTrio) demonstrated that patients with lymphocyte-predominant breast cancer (>60% stroma or tumor infiltration) had a higher pCR rate compared to patients with no TILs (GeparDuo: 41.7% versus 2.8%, p=0.012; GeparTrio: 40.0% versus 7.2%, p=0.001) *(85)*. Efficacy of NAC in TIL-rich tumors suggest that the immune component plays a substantial role in the response to NAC.

Immunotherapy, in the form of checkpoint inhibitors, first demonstrated substantial improvements in patient care when used to treat patients with metastatic melanoma. Until a phase III clinical trial evaluating antibodies designed against CTLA-4, no therapy had shown an improvement in overall survival for patients with metastatic melanoma in any phase III, randomized, controlled trial *(86)*. This study demonstrated the addition of anti-CTLA-4 (ipilimumab) alone, or in combination with a gp100 peptide vaccine, improved median OS (ipilimumab alone versus gp100 alone: 10.1 versus 6.4 months, HR 0.66, p=0.003; ipilimumab plus gp100 versus gp100 alone: 10.0 versus 6.4 months, HR 0.68, p<0.001) *(87)*. A randomized, controlled, phase III study for advanced melanoma designed to compare anti-PD-1 (pembrolizumab) to anti-CTLA-4 (ipilimumab) determined that treatment with pembrolizumab resulted in superior response rates (32.9% versus 11.9%, p=<0.001), 6-month PFS rates (46.4% versus 26.5%, HR 0.58, p<0.001), and 12-month OS rates (68.4% versus 58.2%, HR 0.69, p=0.0036) after 3-week treatments of either compound *(88)*. Further, patients treated with pembrolizumab had less high-grade

toxicity than those treated with ipilimumab (10.1% versus 19.9%) *(88)*. Treatment with pembrolizumab every 2 weeks further improved efficacy in all categories but also resulted in elevated rates of high-grade toxicity (13.3%) *(88)*. Tumor immunotherapy is now being evaluated in nearly all tissue types, alone or in combination with other forms of treatment, with the goal of increasing tumor-associated antigens and associated immunogenicity.

A randomized phase III trial (IMpassion130) evaluating patients with unresectable, locally-advanced or metastatic TNBC treated with anti-PD-L1 (atezolizumab) plus nab-paclitaxel versus placebo plus nab-paclitaxel demonstrated that the addition of atezolizumab resulted in superior PFS (7.2 versus 5.5 months, HR 0.80, p=0.002) and OS (21.3 versus 17.6 months, HR 0.84, p=0.08), with greater differential efficacy when patients were selected based on high PD-L1 expression (PFS: 7.5 versus 5.0 months, HR 0.62, p<0.001; OS: 25.0 versus 15.5 months, HR 0.62) *(89)*. Results from Impassion130 led to the first FDA approval for immunotherapy in breast cancer; atezolizumab is approved for patients with unresectable, locally advanced or metastatic TNBC that are positive for PD-L1 by IHC (Figure 1B). Understanding the relevance of immune targets in disease etiology has brought to light a new era of therapeutic strategies and the continued exploration of checkpoint inhibitors, immune antagonists, and cancer-related vaccines.

TNBC subtypes and corresponding gene expression

Technological advances in the epigenetic analysis of tumors have enabled further insight to transcriptional programs and signal transduction pathways that govern the biological differences between tumors. Through use of complementary DNA microarrays

on mRNA from 84 experimental tumor samples, Perou and colleagues published a landmark study in 2000 demonstrating that expression patterns could be grouped through use of unsupervised hierarchical clustering to identify discrete intrinsic subtypes of breast cancer *(90)*. A subset of 496 genes (termed the 'intrinsic' gene subset) had considerable variation between tumors and could be used to reproducibly classify tumors into individual subtypes: normal-like, luminal A, luminal B, HER2+/ER-, and basal-like *(90, 91)*. Further, tumors classified as luminal stained positive for luminal markers (keratin 8/18), and basal-like tumors stained positive for basal/myoepithelial markers (keratin 5/6) by IHC *(90)*. Of importance, HR and HER2 expression status was one of the driving factors that dictated clustering [ER and/or PR expression in luminal A, luminal B, and 'normal-like' subtypes; elevated HER2 expression in Luminal B and HER2+ subtypes; and the lack of ER, PR, and elevated HER2 expression (aka triple-negative) in the basal-like subtype] and could therefore be joined with histopathological assessments to direct clinical prognoses and treatment decisions *(90)*. Similar to previously identified histological subtype correlations with TNBC, patients with basal-like breast cancer represented a higher proportion of premenopausal women from African descent, and along with the HER2+ subtype, had the shortest survival outcomes *(91)*.

Subsequent studies identified a subset of unique tumors, termed "claudin-low", that were characterized by low expression of *Claudin 3, 4,* and *7*, as well as *Occludin* and *E-cadherin (92, 93)*. They also exhibit low expression of luminal genes, have inconsistent basal gene expression, and highly express lymphocyte and endothelial cell markers *(92, 93)*. Prat *et al.* report that claudin-low tumors were enriched for EMT markers, cancer stem cell-like features, and immune response genes *(93)*. Importantly, these tumors were

identified clinically as TNBC with metaplastic and medullary differentiation, further highlighting the heterogeneous nature of TNBC biology through gene expression studies *(93)*. Collectively, nearly all “basal-like” breast cancers, as identified through the 496 intrinsic gene subset, are classified as TNBC; however, only 50-80% of TNBC tumors, as identified through clinical IHC assessment, are considered to have the intrinsic basal subtype *(94–96)*. These data highlighted the basic nature of TNBC subtype classification and signified the necessity to refine and classify TNBC tumors based on transcriptional profiling.

To further characterize the spectrum of gene expression across TNBC, Pietenpol and colleagues analyzed gene expression in 587 TNBC tumors from 21 Affymetrix datasets that were identified through a bimodal expression filter to exclude ER+, PR+, and HER2+ cases *(97)*. Cumulative expression was renormalized and subjected to k-means clustering to determine the most differentially expressed genes and identify stable clusters; the six resulting groups [basal-like 1 (BL1), basal-like 2 (BL2), immunomodulatory (IM), mesenchymal (M), mesenchymal stem-like (MSL), and luminal androgen receptor (LAR)] demonstrated vastly different gene expression profiles, gene ontologies, and mutational enrichments *(97)*. Briefly, the BL1 and BL2 subtypes were enriched in genes known to regulate the cell cycle and DNA replication. The BL2 subtype expressed genes involved in EGF/MET/WNT β-catenin pathways. The IM subtype exhibited high expression of genes involved in immune-cell signaling, the M and MSL subtypes were enriched for extracellular matrix (ECM) and EMT-related genes, and the LAR subtype demonstrated gene expression associated with androgen receptor signaling (Figure 1C) *(97, 98)*.

Given the growing focus on TILs and the advent of immune therapy, focus was given to determining if immune and stromal cells within the tumor microenvironment contributed to the TNBC subtype classifications. By performing laser-capture microscopy (LCM) on stromal-rich TNBC tumors and sequencing RNA isolated from cells within the stroma and tumor compartments separately, the Pietenpol Lab determined that IM and MSL subtypes were impacted by tumor-infiltrating immune and associated stromal cells, respectively; therefore, TNBC subtype classifications were refined to four subtypes (BL1, BL2, M, and LAR) and termed TNBCtype-4 (Figure 1C) *(98)*. To determine the significance of TNBC subtyping, retrospective analyses on TNBC gene expression from clinical trials were performed. Genomic alterations, clinical behavior, and sensitivity to therapeutic agents associated with TNBCtype-4 subtype correlations, and how these results could contribute to future clinical trial design, are described in the sections below.

TNBC subtype-specific therapies

TNBC subtypes and neoadjuvant chemotherapy: As previously mentioned, *BRCA1/2* mutations have long been associated with basal-like breast cancer and increased sensitivity to DNA-damaging agents such as cisplatin and other platinum-based agents. Similarly, a higher frequency of *BRCA1/2* mutations were found in BL1-subtype TNBC cell line models compared to the other TNBC subtypes and demonstrated increased sensitivity to cisplatin both *in vitro* and *in vivo* (Figure 1C) *(97)*. By performing retrospective analyses on TNBC tumors from The Cancer Genome Atlas (TCGA) and several clinical trials, TNBCtype-4 correlates were able to further delineate the clinical, histological, and genomic differences between subtypes and determine the predictive

value of each subtype with response to neoadjuvant chemotherapy. Consistent with previous studies that associate high grade TNBC with increased immune infiltrate and an improved overall patient survival *(83–85)*, BL1-subtype tumors were of the highest grade, contained the most immune infiltrate, and when treated with neoadjuvant A-T (adriamycin and taxanes) *(99)*, achieved a significantly higher pCR compared to the other subtypes (49% versus 31%, p=0.0441) *(98)*. Similar results were found after patients with TNBC were treated with neoadjuvant AC-T (A-T plus cyclophosphamide) *(99)*; BL1-subtype tumors displayed the highest pCR (49%) and best long-term RFS (72%) seven years post-treatment *(98)*. In contrast, tumors stratified to the BL2 and LAR subtypes demonstrated the least favorable clinical outcomes. To determine the likeliness that a patient with a specific TNBC subtype would respond to NAC, an odds ratio (OR) was calculated for each subtype (BL1-OR: 1.44, BL2-OR: 0.44, M-OR: 1.21, LAR-OR: 0.81), with the highest values indicating increased odds of an achieved pCR *(98)*. These data further characterize the clinical characteristics of TNBC tumors grouped according to gene expression similarities and demonstrate an association between the BL1 subtype and an increased response to NAC (Figure 1C), a result that could aid in future clinical trial design by stratifying patients more likely to respond to NAC.

Androgen receptor signaling: The androgen receptor (AR) is a hormone receptor reliant on testosterone for signaling and has been studied as a therapeutic target for AR-dependent prostate cancer for decades. With prospects of reappropriating antiandrogenic therapies, the discovery that a subset of TNBC (~16%) express genes involved in AR signaling created tremendous excitement in the breast cancer research field, especially

since LAR-subtype TNBC tumors have a poor response to NAC *(98–100)*. Counterintuitively, patients with AR-expressing TNBC generally experience more favorable survival outcomes compared to those harboring AR-negative tumors *(101)*. This is due to the lower overall mitotic score, histological grade, and clinical stage typically detected at diagnosis, and could explain why chemotherapy is less effective for this subtype *(101)*.

Initial efforts to target AR-expressing TNBC using first generation antiandrogens, such as bicalutamide, have been promising. By assessing differential sensitivity to bicalutamide across a panel of TNBC cell lines, LAR-subtype cells demonstrated a statistically significant increased sensitivity to bicalutamide compared to lines without AR expression (Figure 1C) *(97)*; however, only a six month clinical benefit rate (CBR) of 19% and a median progression-free survival of 12 weeks (95% confidence interval (CI), 11-22 weeks) was achieved with bicalutamide in patients with metastatic AR-expressing TNBC (TBCRC011) *(102)*. Two large, randomized, phase II trials evaluating patients with prostate cancer confirmed superior efficacy with a second generation AR-antagonist, enzalutamide, compared to bicalutamide *(103, 104)*. Similarly, a greater CBR (28%, 95% CI, 19% to 39%) to enzalutamide was achieved at six months in patients with AR-expressing TNBC in a phase II clinical trial (NCT01889238) *(102)*.

With the goal of developing effective drug combinations and improving the CBR of AR-antagonists for patients with LAR-subtype TNBC, I started my graduate studies in the Pietenpol Lab working alongside Brian D. Lehmann, Ph.D. Mutational analysis of clinical samples demonstrated an enrichment of *PIK3CA* activating mutations within AR-expressing TNBC (40%) compared to AR-negative TNBC (4%) *(105)* (Figure 1C).

Similarly, all four LAR-subtype TNBC cell lines contained activating *PIK3CA* mutations compared to 6% found in the other TNBC subtypes *(97, 105)*. *PIK3CA* and *PTEN* are among the most highly mutated genes in TNBC *(106)*. Mutations within the regulatory (E542) and kinase (H1047) domains of PI3Kα, the protein product of *PIK3CA*, and loss-of-function mutations or chromosomal deletions of *PTEN*, are known to result in constitutive oncogenic phosphatidylinositol-3 kinase (PI3K) signaling and therefore, increased protein translation and tumor cell growth *(107)*. Reverse phase protein arrays (RPPA), IHC, and Western analyses confirmed co-occurrence of AR expression with markers of activated PI3K pathway signaling (phospho-AKT and phospho-S6) *(105)*.

Importantly, combined pharmacological inhibition of AR and PI3K resulted in an additive or synergistic decrease in cell growth across every LAR-subtype cell line tested, *in vitro* and *in vivo*, using adherent and nonadherent cell viability assays and cell line-derived xenograft (CDX) animal studies, respectively *(105)*. Preclinical studies evaluating PTEN-deficient prostate cancer, and now LAR-subtype TNBC, demonstrate a greater reduction in viability after combined AR and PI3K inhibition compared to treatment with either inhibitor alone *(105, 108)*. Currently, enzalutamide in combination with the PI3K inhibitor, BYL719, is being evaluated clinically for AR-expressing metastatic breast cancer (NCT03207529).

Immunotherapy for IM-subtype TNBC: As previously discussed, initial gene expression analyses from whole TNBC tumor sections identified a subset of specimens with immune gene ontology *(97)*. While the IM gene signature is no longer classified as a TNBC subtype, it remains a descriptor that highlights tumor populations enriched for TILs and

high immune-related gene expression, including *PD-L1*, *PD-1*, and *CTLA-4 (97, 98)*. Consistent with other studies, tumors displaying an IM gene signature associated with increased RFS and distant metastasis-free survival compared to tumors without IM association *(97)*. Of significance, the anti-PD-1 monoclonal antibody, pembrolizumab, was reported to have clinical activity in a patient with advanced-stage BL1-subtype TNBC with IM gene ontology (BL1/IM) and no expression of the PD-1 ligand (PD-L1) (Figure 1C) *(109, 110)*. This case study indicates that the IM gene signature could be a surrogate biomarker to identify a patient population responsive to checkpoint inhibitors who would not be identified through conventions IHC analyses of their tumors.

Additional high-frequency alterations in TNBC

Genomic instability in TNBC has also been characterized by elevated mutational burdens, complex structural rearrangements, and high-frequency CN alterations *(46, 111)*. Additional genetic alterations found in DNA-repair and cell-cycle genes include *RB1*, *ATM*, *CHEK2*, *CCNE1*, *RAD51C*, *BRIP1*, and *NBN (106, 112, 113)*. Significant CN alterations include amplifications in *MYC, PIK3CA*, *KRAS*, *BRAF*, *EGFR*, and *CCNE1* and deletions in *TP53*, *RB1*, *PTEN*, *INPP4B*, and *MAP2K4*, many of which lead to activation of oncogenic pathways and could be targeted therapeutically *(113)*. Of significance, *MYC* alterations occur in ~30% of ER-negative breast cancer with resulting *MYC* levels disproportionately elevated in TNBC compared to the other breast cancer subtypes *(46, 114)*. MYC drives tumorigenesis by increasing the transcription of genes involved in numerous oncogenic signal transduction pathways *(115)*. Given the focus of my research and results presented in Chapter III and IV on MYC and MYCN expression

in TNBC, the next section will review MYC proteins in tumorigenesis and the development of therapeutic strategies to target the MYC family.

MYC-family isoform function in normal physiology and tumorigenesis

Tissue specific MYC-family isoform expression

The MYC family of proto-oncogenes includes three isoform paralogs, *MYC*, *MYCN*, and *MYCL*, encoded by proteins MYC, MYCN, and MYCL, respectively. These isoforms comprise one of the most extensively studied gene families due to their critical role in vertebrate development and oncogenesis. Their function primarily involves the transcriptional regulation of genes representing at least 15% of the human genome; genes that encode proteins involved in ribosome biogenesis, metabolism, protein translation, and cell cycle progression, and orchestrate a broad range of biological processes such as differentiation, cell proliferation, survival, and immune surveillance *(116, 117)*. Since the >50% of all human cancers that exhibit deregulated MYC-family isoform expression associate with unfavorable clinical prognoses and patient outcomes, targeting the MYC family in tumor development has been a highly sought-after therapeutic strategy *(118)*.

MYC family members are thought to function similarly but differ with respect to tissue-specificity, with each isoform having unique spatial and temporal tissue-specific expression patterns necessary for proper organogenesis in a developing mammal *(119–122)*. While *MYC* expression is generally ubiquitously expressed during murine embryogenesis, *MYCN* expression is primarily restricted to the brain, kidney, intestine, and pre-B-cells, and *MYCL* expression is primarily restricted to the brain, kidney, and lung

(123). Overexpression of each isoform is thought to result in tumors that are of similar tissue origin. Elevated *MYC* levels lead to a broad spectrum of blood-borne malignancies and solid tumors across numerous tissue types, *MYCN* overexpression results in tumors of neural or neuroendocrine origin, and high *MYCL* expression generates small-cell lung carcinomas *(124–126)*. A discussion of the ever-evolving literature on MYC-family isoform expression and regulation, and how the general perception of tissue-specific isoform expression is not entirely accurate, will be presented in the next several sections.

Discovering MYC

MYC was the first family member to be discovered, stemming from experiments that began in the 1960s. In Sofia, the capital city of Bulgaria, a strain of virus, MC29, was propagated from a Rhode Island Red Chicken that had succumbed to spontaneous development of anemia and promyelocytic solid tumors *(127)*. Isolation and animal-mediated viral passaging revealed that MC29 predominantly resulted in hematopoietic neoplasia in recipient fowl *(127)*. While other avian leukosis viruses typically result in leukemia, MC29 transformed myeloid cells into solid tumor *my*elo*c*ytomas, which is how the *MYC* oncogene received its name. Further characterization of MC29 revealed the virus could induce transformation in a variety of cell types that resemble tumor morphology *in vivo (128–131)*. Through a series of experiments that predominantly entailed the use of radiolabeling and genomic assessment, *v-myc* was found to be the single gene functionally transmitted by MC29 *(132–134)* and was a gene that resembled a cellular homolog in uninfected vertebrate cells, termed *c-myc (135, 136).* In 1982, *c-myc* was officially cloned and characterized, events that solidified *c-myc* (also known as

MYC) as a *bona fide* oncogene *(137)* and led to an era of research evaluating MYC protein structure, regulation, and function and the search for related genes.

The first mechanism identified that showed enhanced *MYC* transcription came from a seminal discovery where a retroviral promoter inserted before the *MYC* gene led to tumor development *(138–140)*. Soon after, the MYC locus was found to be translocated in Burkitt's lymphoma, placing *MYC* under the control of the immunoglobulin μ heavy chain enhancer and resulting in high levels of *MYC* transcription *(141, 142)*. While similar gene rearrangements are not frequently observed in other cancers, *MYC* expression is commonly upregulated through transcriptional overexpression or gene amplification, which can take the form of large amplifications, small focal amplification, or double-minute chromosomes *(113, 143, 144)*. Additional genomic alterations include high-frequency mutations around the Thr58 phosphorylation site within the degron of MYC. Thr58 mutations stabilize MYC and lead to increased growth and transformation *(145, 146)*. Another noteworthy nucleotide variant, rs6983267, discovered by Haiman and colleagues, located more than one megabase away from the *MYC* gene, conferred an increased risk to colorectal and prostate cancer *(147)*. Subsequent studies demonstrated that this polymorphism stimulates binding of the activator TCF-4 to an enhancer and results in increased *MYC* transcription *(148, 149)*. The identification of a distant variant with no apparent genomic connection to the *MYC* gene location suggests other remote mutations could be leading to deregulated *MYC* expression.

MYC is typically under control of numerous signal transduction pathways activated in tumors. The loss of tumor suppressor adenomatous polyposis coli (APC) in colorectal cancer leads to ß-catenin accumulation, activation of TCF-4, and constitutive high *MYC*

transcription *(150)*. Similarly, potent induction of *MYC* expression can result from aberrant Sonic hedgehog, Notch, PI3K, and MAPK pathway signaling *(151–154)*. The majority of studies to date that focus on elevated *MYC* copy number (CN) and RNA levels do not consider other perturbations that lead to increased MYC protein, such as increased translation or a slower rate of protein degradation; meaning, the number of tumors with aberrant MYC signaling could be much higher than realized. For example, overexpression of eIF4E, a translation factor, has been found in a variety of malignancies and results in the increased export of *MYC* mRNA from the nucleus *(155)*. Stability of *MYC* message itself can lead to increased *MYC* levels *(156)*. Loss of the SCF^{Fbw7} ubiquitin ligase, which occurs in approximately 6% of all human cancers, leads to stabilization of MYC protein *(157)*. Taken together, the various ways in which *MYC* levels can be deregulated signifies its prominent and widespread role in tumorigenesis.

Originally identified in neuroblastoma, *MYCN* was the second family member to be discovered *(158)*. Soon after, *MYCL* was identified and characterized in human small-cell lung cancer *(159)*. Each MYC-family isoform resides on a separate chromosome (*MYC*: 8q24.21, *MYCN*: 2p24.3, *MYCL*: 1p34.2) and are related due to high sequence and structure homology conserved across all metazoan life *(160)*. The general MYC family protein architecture includes five highly-conserved domains called MYC-boxes (I, II, IIIa, IIIb, and IV) located at the N-terminus of the protein and a nuclear localization sequence (NLS) and basic-region/helix-loop-helix/leucine-zipper (bHLHZip) motif at the C-terminus of the protein *(161)*. MYC-boxes participate in protein-protein interactions and the regulation of MYC-family isoform stability and function; whereas, the bHLHZip motif heterodimerize with the bHLHZip motif of other transcription factors (e.g. MAX) and binds

to DNA with highest affinity through recognition of the Enhancer box (E-box) consensus sequence, CACGTG *(162, 163)*. Unlike *MYCL*, the loss of *MYC* and *MYCN* are embryonic lethal in murine development (*MYC*-/- at E10.5 and *MYCN*-/- at E11.5) *(122)*. Given the lack of experimental evidence for MYCL function in breast cancer, the remainder of this Introduction and chapters that follow are focused on MYC and MYCN.

Defining MYC target genes

Defining target genes that are directly regulated by MYC family members across cell types that are essential for its oncogenic properties has been a challenge. While previous studies have indicated that MYC is a regulator of specific target genes, further experimentation across a greater variety of cell types demonstrates MYC can act as both a transcriptional activator and repressor and can regulate thousands of genes, possibly even every active gene within a given cell type *(164, 165)*. Similarly, MYCN has been shown to bind to thousands of promoters in open chromatin within embryonic stem cells and in several MYCN-driven types of cancer *(166, 167)*. Some of the difficulties determining MYC/MYCN-specific target genes have likely been due to differing epigenetic patterns between cell types and pathological states that govern active chromatin regions. Further, the amount of MYC protein within a given cell can dictate the number and extent to which genes are expressed. Collectively, a consensus on MYC target genes has not been reached in this evolving field due to the breadth of model systems tested, the varying experimental methods taken, the vast range of expression levels, and the numerous mechanisms in which the MYC family regulates gene transcription.

As MYC levels increase, it is speculated that MYC becomes increasingly nonspecific and can “invade” promoters and enhancers with lower-affinity binding sites to drive the transcription of proteins that regulate nutrient transport, responses to hypoxia, and cell adhesion, processes more associated with the growth and survival of tumors *(165, 168–170)*. Despite numerous failed attempts to determine a core set of target genes present across different cell types *(171, 172)*, a study by Ji *et al.* identified ~50 MYC target genes that were shared between mouse and human embryonic stem cells and several cancer cell lines that also highly correlated with *MYC* levels across over 300 additional cell models *(173)*. This core set of target genes represent high-affinity MYC binding sites and highlight a role for MYC in RNA processing, ribosome biogenesis, and macromolecular synthesis *(173)*.

Lessons learned from the myriad of experimental results across various tissue types with differing levels of MYC have led to new theories about the role of MYC in normal and oncogenic cells. Two studies published in 2012 introduced the “amplifier” model, in which MYC does not act as a typical sequence-specific transcription factor but rather, is able to drive the expression of all preexisting genes already “on” within a given cell type *(164, 165)*. These results align with findings that demonstrate MYC is typically present at both active and transcriptionally-poised chromatin alongside RNA polymerase II *(174–176)*. The transcriptional amplification of active genes was largely uniform and dose-dependent, with a similar broad activation specific to individual cell types *(164, 165)*. Consequently, when MYC is highly expressed in a tumorigenic state, the upregulation of all biochemical pathways creates a massive flux towards the acceleration of cellular processes involved in survival and cell growth while retaining the same cell lineage. The

MYC family has greatest affinity for E-boxes located in close proximity to CpG islands, regions that define active euchromatin *(177, 178)*, and therefore, the chromatin structure that governs the differentiation state of a cell dictates which E-box or DNA sequences will be available for transcriptional activity *(179)*. The strongest data to support the notion that the primary function of each MYC-family isoform is to maintain the survival and growth properties of a given cell type in which it is expressed comes from a study where the *MYCN* coding sequence is able to functionally replace *MYC* alleles in murine development *(180)*. Expression of *MYCN* from the *MYC* locus resulted in normal cell growth and differentiation, with the transgenic mouse surviving until adulthood and capable of reproducing *(180)*. Collectively, these data indicate MYC and MYCN have similar biochemical properties, but their physiological roles and target genes differ with respect to the transcriptional regulation and differentiation state in which each isoform is expressed.

In the amplifier model, suspending MYC expression would enable more rapid and efficient reprogramming. Once a cell has differentiated, elevated MYC levels would return to reinforce the new cell state. Such biphasic MYC expression has been reported in several models during the development of erythroleukemia *(181–183)*. Of relevance to this dissertation research, I would like to highlight the concept of biphasic expression of MYCN to MYC in cells transitioning between distinct states. An example of this occurs during early stages of hematopoiesis. Data from an elegant study using endogenous *MYC* and *MYCN* allelic fluorescent fusions demonstrate that expression of MYC and MYCN isoforms are mutually exclusive, with MYCN being highly expressed in the most primitive hematopoietic stem cell (HSC) state that switches to MYC expression during

differentiation into transit-amplifying progenitors *(167)*. In concert with these results, ectopic expression of MYC in HSCs results in exit from the stem cell niche and the expansion of proliferative differentiated cell types *(184)*. Conversely, conditional elimination of MYC in HSCs results in accumulation of defective HSCs and a failure to initiate normal stem cell differentiation *(184, 185)*.

Similar to hematopoietic stem cells, the development of skeletal and connective tissue requires coordinated MYCN and MYC activity. MYCN is essential for the proliferative expansion of undifferentiated mesenchymal progenitors from the emergent limb bud *(186, 187)*. As the undifferentiated mesenchyme expands, the most distal cells downregulate MYCN, condense, and exit the cell cycle *(188)*. Chondrogenic progenitors expressing little to no expression of either isoform emerge from the condensing mesenchyme, induce MYC expression, and proliferate as chondrocytes within cartilaginous growth plates *(187, 189)*. The condensing mesenchyme also gives rise to MYC-expressing osteoblasts and other connective tissue lineages and are thought to be a result of epigenetic reprogramming of the MYCN-expressing undifferentiated mesenchymal progenitors that gives rise to lineages necessary for the development of skeletal and connective tissue *(189)*. While the amplification model challenges previous reports that the MYC family regulates a specific set of discrete genes, it offers an intuitive explanation for the prevalence of cell type-specific binding sites and aligns well with studies focused on investigating MYC-family isoform expression patterns during vertebrate development and tumorigenesis.

MYC and MYCN expression in vertebrate development

MYC and *MYCN* expression appear to be mutually exclusive with elevated levels that vary across tissue types at differing stages of development. Deletion of either *MYC* or *MYCN* is embryonic lethal in murine development at midgestation. Homozygous null *MYCN* embryos perish around embryonic day 12 (E12) due to severe hypoplasia and structural defects of the lungs, heart, intestines, kidneys, skeleton, genitourinary system, and central nervous system *(186, 190, 191)*. Mouse models with epiblast-restricted loss of *MYC*, or that contain conditional tissue-specific deletions, demonstrate MYC is dispensable for the development of tissues and organs up until E11 but is critical for the growth, proliferation, and cellularity necessary for further development and maintenance of most organs *(192, 193)*. Lethality resulting from loss of *MYC* is primarily due to a failure of proper hematopoiesis in extraembryonic tissues *(194–196)*.

A clear dose-dependent effect on organ system development can be seen through *MYCN* heterozygotes and mice engineered to express hypomorphic alleles. For example, mice carrying homozygous hypomorphic *MYCN* alleles that express ~15-25% of normal *MYCN* levels were not embryonic lethal but did exhibit severe lung and cardiac hypoplasia *(197–199)*. Site-specific conditional *MYCN* deletions confirm the essential role of MYCN in the development of the lung and heart *(200, 201)*, as well as the developmental of limbs *(187)*, kidneys *(202)*, inner ears *(203)*, and the central nervous system *(204)*. The constellation of developmental defects observed in these mouse models largely recapitulates organs and tissues affected by Feingold syndrome (type 1), a human disease that develops as a result of *MYCN* haploinsufficiency *(205)*. While the spectrum of phenotypes can be variable between patients, individuals with Feingold syndrome

experience digital abnormalities, renal disorders, inner ear malformations, esophageal and gastrointestinal atresia, microcephaly, and defects in intellectual development *(206)*.

The extensive use of mouse models evaluating *MYCN* and *MYC* expression during early vertebrate development illustrates that *MYCN* is widely expressed during late gastrulation, immediately before the onset of organogenesis, and during the early stages of organogenesis and is critical for the initial establishment and expansion of stem and progenitor cell populations (Figure 2). Once organogenesis commences, *MYCN* levels subside and low *MYC* expression supports stem and progenitor cell maintenance that give rise to various cell lineages (Figure 2). Often under the control of WNT/ß-catenin signaling *(202, 207–209)*, *MYC* levels elevate and lead to stem cell mobilization and proliferative expansion of specific cell lineages *(207, 210–212)*. The general effect of MYC and MYCN stimulation on poised and active transcription provides a new paradigm where expression below some threshold level may increase cellular plasticity and when highly expressed, amplifies transcriptional targets that reinforce the differentiation state initiated by cell-specific pioneer factors (Figure 2).

MYCN and *MYC* levels are reduced across the majority of cells in an organ system as they reach terminal differentiation and are no longer proliferating *(213–215)* (Figure 2). However, low levels of *MYC* appear to maintain stem and progenitor cell populations in various tissue types, including kidney *(216)*, pancreas *(202, 217)*, lung *(218)*, mammary gland *(219, 220)*, and intestinal epithelium *(221, 222)*. *MYC* is also expressed in proliferative transit-amplifying compartments of intestinal crypts alongside a single *MYCN*-expressing cell, lacking *MYC* expression, located at the base of the crypt that is thought to be an intestinal stem cell *(222)*. The coordinated efforts between MYC and

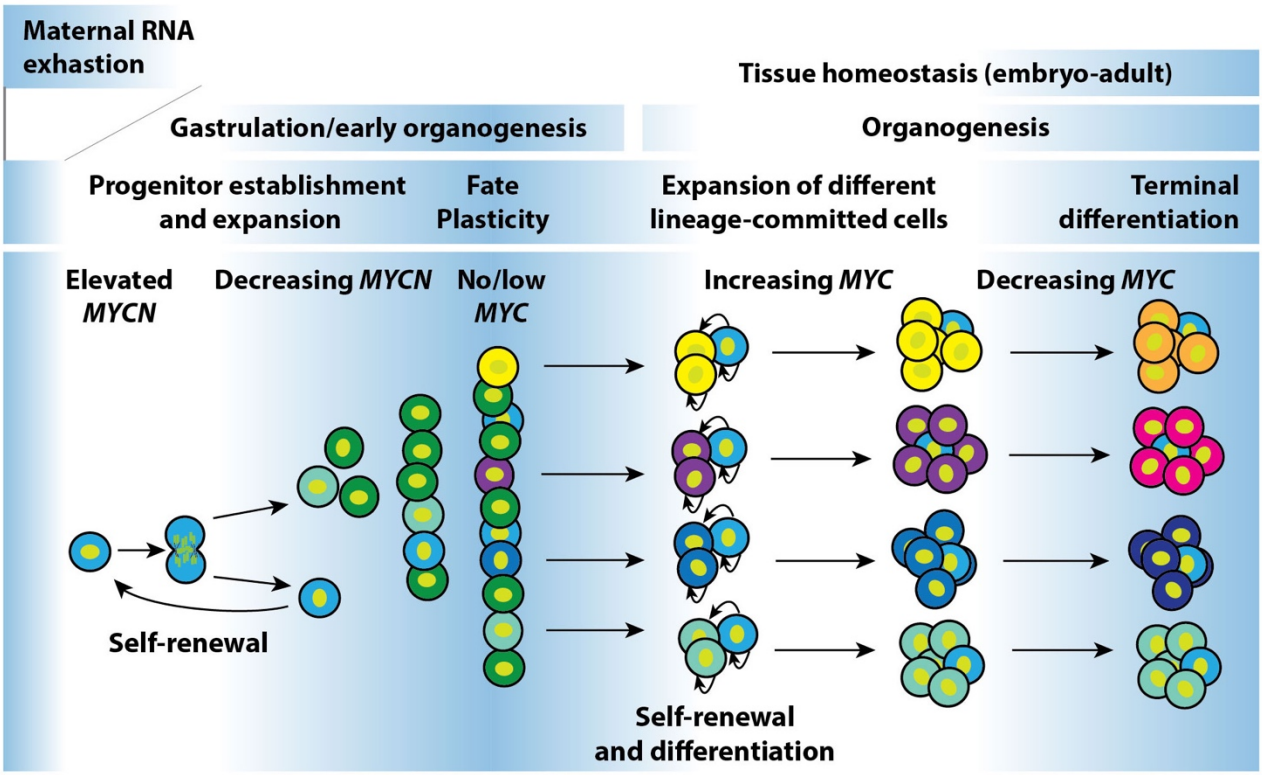

Figure 2. *MYCN* and *MYC* expression in vertebrate development. Modified figure from Hurlin *el al.* demonstrating expression of *MYCN* and *MYC* during vertebrate development. Background colors represent stages where MYC-family isoform expression is highest (white) and lowest (blue).

MYCN in organogenesis and in adult tissue maintenance, such as in the hematopoietic system, skeletal tissue, and intestinal track, indicate a relationship between these two isoforms that likely contributes to the development of additional organ systems and when deregulated, could also contribute to tumorigenesis.

MYC and MYCN in tumor development

Historically, ectopic or overexpression of MYC or MYCN has been the primary way to study the cellular effects of elevated MYC-family isoform expression. Either isoform can regulate genes involved in cell cycle progression, such as cyclins and cyclin-dependent kinases (CDKs) *(223, 224)*. Overexpression of MYC or MYCN generally leads to the prevention of cell cycle exit and increased proliferative potential, even in post-mitotic cells *(225)*. For example, forced expression of MYC *in vivo* results in cell-cycle reentry of postmitotic myocytes, keratinocytes, and forebrain neurons *(226–228)*. MYCN overexpression supports cell-cycle reentry of cultured postmitotic sympathetic neurons *(229)*. However, this is not always the case; elevated MYCN levels do not result in postmitotic cortical neuron proliferation *(229)*. Similarly, forced MYC expression leads to cell-cycle reentry of structurally unorganized epithelial cells of mammary acini but does not cause the proliferation of cells within mature acini *(230)*. Postmitotic cells that retain transcriptionally poised or active low-level proliferation-associated genes may be the reason some postmitotic cells are more receptive to MYC- or MYCN-mediated transformation than others.

In many cases, MYC- and MYCN-driven tumors arise from cell lineages that express either isoform during normal development. *MYC*, ubiquitously expressed in the

developing mammal, is elevated within a subset of nearly every tumor type. *MYCN*, best known for having elevated expression in neurons during vertebrate development, is overexpressed in several cancer types of the sympathetic and central nervous system (i.e. neuroblastoma, medulloblastoma, retinoblastoma, astrocytoma, and glioblastoma multiforme) *(231)* as well as non-neuronal tissues as described later. Approximately 20% of neuroblastoma cases harbor *MYCN*-amplification, which correlate with unfavorable biologic features, advanced stage, and poor patient outcome *(232, 233)*. Similarly, *MYCN* is amplified in ~5% of medulloblastoma (both Sonic Hedgehog-driven and non-Sonic Hedgehog-driven) *(234)* and associates with a worse prognosis *(235)*. MYCN amplifications are found to be a key factor in tumor progression in preclinical medulloblastoma models *(234)*. Deregulated *MYCN* expression that occurs in a subset of glioblastoma multiforme is independent of low-grade gliomas and astrocytomas and leads to forebrain rather than hindbrain tumors *(236)*. Recurrent functional mutations in the epigenetic modulator histone 3 gene (*H3F3A*) have been found in both adult and pediatric glioblastoma multiforme, which results in enhanced *MYCN* transcription and proliferation *(237, 238)*. While *MYCN* is amplified in only a subset of retinoblastoma, *MYCN* is overexpressed in the majority of cases and is thought to reflect the embryonal cell of origin *(239–241)*. Cases with *MYCN* amplifications are mutually exclusive to germline or somatic mutations of the retinoblastoma gene (*RB1*), present unilaterally at an early age (median 4.5 months), and are clinically aggressive *(242)*.

Similar to the variety of cell types expressing *MYCN* in normal development described in the previous section, aberrant amplification and/or overexpression of *MYCN* is also found in a variety of non-neuronal cancers, including hematopoietic malignancies

(243, 244), Wilms tumor *(245)*, rhabdomyosarcoma *(246)*, small-cell lung cancer *(247)*, pancreatic tumors *(248)*, and prostate cancer *(249)*. While a subset of rhabdomyosarcoma presents with *MYCN* amplification, the vast majority of all rhabdomyosarcoma cases express *MYCN* RNA and protein *(246, 250)*. *MYCN* amplifications are frequently observed in hematopoietic malignancies such as lymphomas and acute myeloid leukemia (AML) *(243)*. The *MYCN* locus is also a common site for retroviral integration in mouse T-cell lymphoma *(244)*. Elevated MYCN expression in hematopoietic malignancies is considered one of the main "drivers" in tumor formation, depending on the cell of origin *(231)*. Mouse bone marrow cells transduced with *MYCN,* but not *MYC,* stimulated the self-renewal and proliferation of myeloid cells *in vitro* and rapidly generated AML in *vivo (251).* Additionally, elevated *MYCN* expression in adult AML is predictive of unfavorable outcomes and a poor OS *(252)*.

Solid cancers, including lung and prostate, contain both MYC- and MYCN-expressing tumors. While there is insufficient evidence to demonstrate MYCN plays a role in the development of lung cancer, 15-20% of small-cell lung cancer cases are *MYCN*-amplified and associate with rapid tumor growth, a poor response to chemotherapy, and a shorter survival outcome *(247, 253, 254)*. On the other hand, the development and progression of prostate cancer has been well characterized. Prostate cancer is generally driven by AR signaling; therefore, therapies targeting AR are primarily used to treat the disease. Following exposure to therapy, a subset of prostate cancer develops resistance to treatment in form of AR-independent signaling [i.e. castration-resistant prostate cancer (CRPC)] and typically spreads to distal sites *(255–257)*. MYC is overexpressed in early-stage, high-grade intraepithelial neoplasia and localized adenocarcinomas, and MYCN is

amplified and/or overexpressed in late stage disease in the form of CRPC with adenocarcinoma or neuroendocrine histology *(258)*. Recent studies demonstrate neuroendocrine prostate cancers (NEPC) often arise from preexisting adenocarcinoma during the development of resistance to AR therapies and are a result of lineage switching, a shift from *MYC*-expressing epithelial cells to *MYCN*-expressing neuroendocrine cells *(249, 258, 259)*. Therefore, compared to MYC-expressing prostate cancer, MYCN-expressing cases are typically late stage, differ in histology and response to AR inhibitors, and associate with disease progression and a poor patient outcome. In concert with the previously described associations between MYCN expression and unfavorable outcomes across nearly every tumor cell type, MYCN overexpression has also been associated with poor prognostic features and worse clinical outcomes for a subset of breast cancers *(260, 261)*.

Preclinical and clinical strategies to target MYC- and MYCN-driven tumors

While conditional mouse models demonstrate MYC-family isoform expression is sufficient to induce tumorigenesis *(262–264)*, transient inactivation of these isoforms are able to elicit tumor regression *(265)*, implying the downregulation of oncogenic MYC expression is a potential strategy to treat patients with tumors driven by one of the MYC-family isoforms. However, directly targeting MYC has proved to be a challenge. Given that MYC proteins are composed of bHLHZip motifs devoid of any active catalytic sites, therapeutic strategies using small molecule design have been difficult *(161)*. Further, the MYC family is predominantly located in the nucleus, creating an obstacle for targeting the

family through monoclonal antibodies *(266)*. Therefore, numerous methods have been proposed to indirectly abrogate MYC function.

Targeting transcription: The bromodomain and extraterminal (BET) motif family of transcriptional regulators, comprised of *BRD2*, *BRD3*, *BRD4*, and *BRDT* (testes-specific), binds to hyperacetylated lysines on active histone complexes and positively regulates transcription through recruitment of positive-transcription elongation factor b (p-TEFb) *(267)*. pTEFb-mediated phosphorylation at the carboxyl-terminal domain of paused RNA polymerase II (RNA pol II), located at promoter-proximal gene regions, results in RNA pol II pause-release and transcriptional elongation *(267, 268)*. Given that BRD4 is a regulator of *MYC* and *MYCN* transcription, inhibitors designed to outcompete lysine-binding to the BRD-family N-terminal bromodomains result in displacement of BRD4 from the *MYC* promoter and associated enhancers, thus decreasing transcription of *MYC* or *MYCN* *(269–271)*. BET inhibitors (BETis) have demonstrated potent preclinical anti-growth effects using hematopoietic and solid tumor models with deregulated *MYC* (i.e. multiple myeloma) and *MYCN* (i.e. neuroblastoma) expression, respectively *(271–273)*, and are therefore currently in early stage clinical development.

In contrast to classic cyclin-dependent kinases (CDKs) that regulate cell cycle progression, CDK9 and CDK7 have critical roles in transcriptional regulation *(268, 274)*. The phosphorylation of RNA pol II by p-TEFb mentioned above is mediated by the CDK9 kinase subunit of p-TEFb *(275)*. CDK7 is the catalytic subunit of the transcription factor IIH complex *(276)*. Together, both kinases facilitate RNA pol II pause-release and elongation, and therefore, similar to BETis, inhibition of CDK9 or CDK7 results in reduced

MYC transcript as well as MYC-mediated transcriptional regulation *(277)* and have become another strategy to target MYC- and MYCN-driven tumors. Potent preclinical anti-tumor effects have been described in several tissue types overexpressing either isoform, such as T-cell acute lymphoblastic leukemia, mixed-lineage leukemia, small-cell lung cancers, and neuroblastomas *(278–280)*. Similar to BETis, CDK7/9 inhibitors are being evaluated clinically across a large variety of malignancies and tissue types.

Targeting translation: As previously mentioned, PI3K/AKT/mTOR signaling is a prominent growth-stimulating pathway frequently altered in TNBC as well as a variety of other cancer tissue types *(281)*. mTOR complexes 1 and 2 (mTORC1 and mTORC2) are serine/threonine kinases, with mTORC1 having a central role in protein synthesis *(282, 283)*. Upon phosphorylation by mTORC1, the eukaryotic translation initiation factor 4E (eIF4E) binding protein 1 (4EBP1) is released from eIF4E, thus allowing for translation of mRNAs with long 5'-untranslated regions, such as *MYC* and *MYCN (282, 283)*. Pharmacological inhibition of PI3K, AKT, or mTOR decreases translation globally, including the protein synthesis of both MYC-family isoforms, and demonstrates antitumor effects in many MYC- and MYCN-driven tumors *(281, 284–286)*.

Targeting stability: Several promising therapeutic strategies have been employed to target proteins responsible for the stability of MYC and MYCN. The primary focus in this approach involves the MYC-family isoform degron, located within MYC-box I at the C-terminus of the protein *(161)*. Two phosphorylation sites, four amino acids apart (Ser62/Thr58 for MYC; Ser54/Thr50 for MYCN), are phosphorylated in a similar

sequential fashion for each MYC-family isoform *(224, 287)*. Ser62/54 is phosphorylated first, by MAPK/ERK for MYC and CDK1 for MYCN, which stabilizes either isoform and promotes proliferative potential *(224, 287, 288)*. GSK3ß is downstream in the PI3K pathway. GSK3bß is inactivated when the PI3K pathway is actively signaling. However, upon PI3K pathway inhibition, GSK3ß translocates to the nucleus and phosphorylates Thr58/50; wherein, the ubiquitin ligase, SCF^{FBXW7}, and associated complexes are recruited for MYC-family proteasomal degradation *(289, 290)*. Therefore, inhibition of the MAPK or PI3K pathway generally results in decreased MYC levels and inhibition of CDK1 or PI3K pathway signaling generally results in decreased MYCN levels *(224, 287)*. Further, polo-like kinase 1 (PLK1) binds to and phosphorylates SCF^{FBXW7}, leading to self-polyubiquitination and degradation *(291)*. Therefore, PLK1 inhibition stabilized FBXW7 and results in increased degradation of MYC and MYCN *(291)*.

AURKA, encoding the protein Aurora-A, is a regulator of chromosome segregation and cytokinesis and has been the most studied aurora kinase in conjunction with MYC-family isoform function in cancer *(292)*. While MYC exhibits several tumorigenic functions with Aurora-A, such as MYC-mediated transcription of *AURKA* in B-cell lymphomas *(293)* and joint enhancement of hTERT promoter activity in ovarian and breast epithelial cells *(294)*, the latest enthusiasm in targeting Aurora-A has been to deregulate the MYCN stability. Aurora-A binds to the MYCN degron and blocks SCF^{FBXW7}-mediated ubiquitination *(295)*. Since Aurora-A binding is independent of its catalytic activity, allosteric inhibitors have been developed to alter the conformation of Aurora-A and disrupt its ability to bind to MYCN *(296–298)*. By disrupting protein-proteins interactions with allosteric inhibitors, instead of compounds that compete with ATP for the Aurora-A ATP-

binding site, not only do MYCN levels decrease but the cell-cycle function of Aurora-A in healthy cells remains intact *(299)*. While Aurora-A allosteric inhibitors are thought to result in decreased toxicity *(299)*, these inhibitors are yet to enter clinical trials.

Targeting protein-protein interactions: Another approach to target the MYC family has involved disruption of protein-protein interactions that mediate MYC-family isoform transcriptional regulation. Currently, the two leading strategies involve interrupting the binding interface between the MYC-family proteins and the bHLHZip transcription factor, MAX, or the epigenetic regulator, WDR5 *(231, 266)*. Through interacting bHLHZip motifs, MYC and MAX have been described as obligate dimers necessary for DNA-binding and the transcriptional activation across thousands of target genes *(300)*. In part, the interaction between MYC and MAX is controlled by post-translational modifications, including the phosphorylation of three residues in the bHLHZip motif of MYC; when phosphorylated, the binding interface between MYC and MAX is disrupted *(301)*. Mutagenesis of glutamate and asparagine residues in the bHLHZip motif of MYC has revealed an additional binding site critical for proper MYC/MAX binding and function *(302–304)*.

Approximately 80% of MYC DNA-binding sites are also bound by WDR5 through interactions with the evolutionarily conserved MYC-box IIIb motif *(305)*. WDR5 acts as a scaffold for the assembly of multiple epigenetic regulatory complexes, including various histone acetyltransferases and methyltransferases *(306)*. In conjunction with WDR5 histone binding and euchromatin formation, MYC is recruited to open chromatin to mediate corresponding target gene regulation *(306)*. Given that WDR5 is aberrantly

expressed in a variety of cancers *(307)*, has been shown to a prominent role in EMT *(308)*, and operates as a co-factor for MYC binding *(305, 309)*, significant effort has been given towards inhibition of WDR5 function, both together and independent of MYC. Through use of high-throughput screens and fragment-based methods and structure-based design, highly-specific small molecule inhibitors have been synthesized to target the WDR5 interaction (WIN) site within WDR5 *(310, 311)*. Not only do these compounds displace WDR5 from chromatin, but they disrupt MYC-WDR5 protein-protein interactions *(307, 311)*. WDR5 has also been shown to support MYCN transcriptional complexes in neuroblastoma *(312)*. Together, strategies to disrupt the interface between MYC and MAX or WDR5 are highly anticipated approaches for the treatment of numerous tumor types.

Additional strategies: Several studies have demonstrated MYC-driven tumors contain high surface expression of glutamine transporters and rely on exogenous glutamine for survival *(313)*. Given that glutamine is converted to glutamate by glutaminase (GLS), selective GLS inhibitors have been developed to target MYC-driven glutamine metabolism and are currently in early phase clinical development *(314, 315)*. *MYCN*-amplified neuroblastoma cell lines exhibited hypersensitivity to inhibitors that target the antiapoptotic proteins BCL2/BCLxL (venetoclax) *(316)*. Treating these cells with an Aurora-A inhibitor (alisertib) led to mitotic arrest, decreased p4EBP1-mediated translation, and decreased MCL1 levels (another antiapoptotic protein) *(316)*. Combined treatment with venetoclax and alisertib demonstrated greater efficacy in *MYCN*-amplified tumor cells than with either agent alone *(316)*. Lastly, as previously noted, late stage prostate

cancer progresses from a CRPC to NEPC phenotype. EZH2, the enzymatic component of the polycomb repressive complex, has been shown to cooperate with MYCN to facilitate progression to a neuroendocrine cell lineage *(256)*. Treatment with EZH2 inhibitors reverses MYCN target gene expression that supports a NEPC phenotype and abrogates associated tumor cell growth *(256)*. EZH2 inhibitors have advanced clinically to investigate efficacy in patients with MYCN-expressing CRPC and NEPC.

Characterization of MYCN in TNBC and strategies to inhibit MYCN-expressing TNBC tumor cell growth: Goals of this dissertation

TNBC tumors are characterized by the lack of therapeutic targets expressed in the other breast cancer subtypes. Therefore, patients with TNBC have few treatment options and experience a shorter time to relapse and a worse survival outcome compared to the other breast cancer subtypes. Given that the TNBC subtype is a heterogeneous collection of tumors with no unifying biological features to exploit therapeutically, cytotoxic chemotherapy remains the primary means to treat patients with primary TNBC. For the >70% of patients that progress or recur during or subsequent to treatment, PARP inhibitors and monoclonal antibodies are used to target *BRCA*-mutant and unresectable PD-L1-expressing disease, respectively. Identification of new therapeutic targets are needed to improve outcomes for patients with TNBC. Given the prevalence of MYCN-expressing tumors, of both neuronal and non-neuronal cell origin, and the notion that a subset of breast cancer expresses MYCN, we sought to determine the prevalence of MYCN expression in TNBC and whether MYCN-expressing tumors represented a patient population to direct clinical efforts.

The primary goal of Chapter III was to assess levels of MYCN expression during the progression of TNBC. This was accomplished by developing an IHC stain capable of detecting non-amplified levels of MYCN and the use of clinical specimens from patients with primary treatment-naïve, primary NAC-treated, or locally-recurrent/metastatic TNBC. Conclusions from this study were validated by analyzing MYCN expression in single-nuclei sequencing data from patients before and after NAC treatment. By isolating individual cells from a TNBC tumor-derived cell line, we created unique preclinical models that allowed us to investigate tumor cell growth properties and drug sensitivities associated with MYCN expression.

Chapter IV encompasses results from primary and validation high-throughput drug screens using the NCI FDA-approved oncology drug (AOD) library and compounds of interest on our newly-generated MYCN- and MYC-expressing TNBC clonal cell line models. “Hits” from the validation screen were evaluated further through precision nuclear run-on sequencing (PRO-seq) and RNA-sequencing (RNA-seq) methods. To investigate the cellular effects of drug treatment on MYCN and MYC levels, we created a dual immunofluorescence stain capable of simultaneously detecting cellular MYCN and MYC expression within TNBC cell lines and patient-derived xenografts (PDX) that heterogeneously expressed both isoforms. Combination treatments using our leading compounds under investigation were performed on mice harboring TNBC PDX models with varying levels of MYCN and MYC expression. Together, our preclinical data provide a rationale to advance our proposed drug combination to clinical investigation for patients with advanced or recurrent MYCN-expressing TNBC with the goal of eventually providing patients with TNBC an additional treatment option.

CHAPTER II

MATERIALS AND METHODS

Breast cancer subtype determination

Gene expression for the MET500 dataset was kindly provided by Dr. Arul M. Chinnaiyan from the University of Michigan. RNA expression from TCGA (BRCA, RNA-Seq), METABRIC (microarray), Siegal *et al* (RNA-Seq), and MET500 (RNA-Seq) were log_2-transformed and density plotted for ER (ESR1), PR (PGR), and HER2 (ERBB2). Breast cancer subtypes were identified with discrete cutoffs in the bimodal distribution of positive and negative expression for each gene. A tumor was categorized as TNBC if the ER, PR and HER2 RNA levels were in the peak for negative expression of each gene. TNBC subtypes were determined from log_2-normalized expression using the publicly available TNBCtype tool *(98, 317)*.

Clinical sample RNA-Seq analyses

MYCN transcript comparisons between TNBC and other *MYCN*-expressing cancers were achieved through upper-quantile normalization across RNA-seq (FPKM) data from TCGA [TNBC (BRCA, n=197), AML (LAML, n=173), GBM (GBM, n=156)], the NCI-funded TARGET initiative *(318)* (NB, n=161), and two CRPC studies *(259, 319)* [adenocarcinoma, n=123; NE, n=15]. For those patients whom had multiple samples sequenced, the most current sequencing submission was analyzed. Pairwise Wilcox tests were performed between TNBC and each dataset, and p-values were adjusted by false

discovery rate. Patient-matched primary and metastatic lesion RNA-Seq analyses evaluating *MYCN* transcript levels were performed on RNA-Seq (RSEM) data *(320)* after identifying corresponding breast cancer subtypes as described in the "Breast cancer subtype determination" section.

TNBC587 differential gene expression analyses

Differential gene expression analyzes were conducted using median-centered $\log_2$ normalized gene expression from the TNBC587 dataset. We created a rank order list that segregated the top MYCN-expressing tumors with the least amount of MYC expression ($MYCN^{RatioHigh}$) from high MYC-expressing tumors with little MYCN expression ($MYC^{RatioHigh}$). The number of statistically significant differentially expressed genes (FDR <= 0.05, absolute fold change >= 1.5) using the R-package, limma, between the top percentage (individual evaluations for each percentage, 1-10%) of $MYCN^{RatioHigh}$ versus $MYC^{RatioHigh}$ TNBC tumor samples was compared to an analysis comparing the same number of tumor samples selected at random. Volcano and principal component analysis (PCA) plots were generated using R-package, ggplot2.

Patient tissue and tissue microarrays (TMAs)

Immunohistochemistry (IHC) was performed on 344 previously collected and formalin-fixed paraffin-embedded (FFPE) primary or recurrent (local and distal) TNBC tumors, of which 314 were present within TMAs. Tumors were identified as TNBC by pathologist evaluation of IHC staining for ER, PR, and HER2. TMA101, TMA102, TMA11-4-09, TMA2 Mixed, TMA2 TNBC and TMA9936 were constructed from surgically resected

primary tumor samples from patients with breast cancer diagnosed at Vanderbilt University Medical Center. One-millimeter tumor cores (2 per surgical specimen) were punched from representative areas containing invasive carcinoma selected by a pathologist. Clinical and pathologic data were retrieved from medical records under institutionally approved protocols, IRB# 030747 and 130916, for patients in TMA101 and TMA11-4-09, respectively. TMAs P1, P2, and P3 were constructed from surgically resected primary tumors from patients with breast cancer diagnosed at the Instituto Nacional de Enfermedades Neoplásicas (Lima, Perú) *(321)*. Three 1 mm tumor cores were punched per surgical specimen. Clinical and pathologic data were retrieved from medical records under an institutionally approved protocol (INEN 10-018). TMAs BR1901 and BR1201a were purchased from US Biomax and contained two cores per tumor (1 and 1.5 mm punches, respectively).

Twenty-three surgically resected brain metastases, three needle core biopsies from lung metastases, and five paired surgically resected primary tumors from patients with TNBC diagnosed at VUMC were collected under an institutionally approved protocol (IRB# 171983). Two 1 mm tumor cores from representative areas containing invasive carcinoma selected by a pathologist were punched from 19 of the brain metastases to construct TMA111. An additional 19 TNBC samples from VUMC patients were identified from the American Association for Cancer Research (AACR) project genomics evidence neoplasia information exchange (GENIE) database, including six primary, eleven locally recurrent, and two metastatic tumors to the lung. These tissues were curated for IHC analysis under an institutionally approved protocol (IRB# 180146). See Table 2 and 4 for additional patient and sample characteristics.

Immunohistochemical (IHC) staining

For IHC experiments, 4 μm formalin-fixed, FFPE sections were deparaffinized with xylene and rehydrated with graded alcohol incubations. For tissue undergoing MYC staining (Abcam, ab32072), pressurized antigen retrieval was performed at 125°C for 10 seconds (Dako, S2367) and then cooled to 90°C prior to incubation with 3% hydrogen peroxide (H_2O_2) for 10 minutes. Sections were subjected to a protein block (Dako, X0909) and incubated with antibody overnight at 4°C in antibody diluent (Dako, S0809). HRP-conjugated secondary antibody (Dako, K4003) was applied to tissue for 30 minutes, followed by DAB reagent (Dako, K3468) for 5 minutes. Hematoxylin was used as a counterstain and all washes were conducted with tris-buffered saline (TBS) with 0.1% Tween-20 (TBST). For MYCN staining (Cell Signaling, 51705S), pressurized antigen retrieval was performed at 125°C for 4 minutes (BioGenex, HK080-9K), followed by a 30-minute depressurization period and an additional 30-minute room temperature (RT) cooling period. Sections were treated with 3% H_2O_2 for 10 minutes, permeabilized with 0.1% Tween-20 for 20 minutes, and blocked with Image-iT FX Signal Enhancer (Invitrogen, I36933) for 30 minutes. An additional block was performed with 5% goat serum/0.3% Triton X-100 in phosphate-buffered saline (PBS) for 1 hour prior to incubation with primary antibody overnight at 4°C in PBS with 5% goat serum. Subsequent incubations were performed as described with MYC staining; however, all washes were done with either PBS or PBS with 0.1% Tween-20. Whole slide bright field imaging was performed with the Zeiss Axio Scan.Z1 microscope (20x objective lens). H-scores were determined by a certified pathologist (Gonzalez-Ericsson) and were generated by

calculating the sum of the percent positive nuclei multiplied by IHC staining intensity (0-3). See Table 1 for additional specifications on antibodies used.

Tyrosine-signal amplification (TSA) immunofluorescence (IF) staining

Tumor sections: Antigen retrieval and all blocking steps (H_2O_2, Image-iT FX Signal Enhancer, and 5% goat serum/0.3% Triton X-100 in PBS) were performed similar to the methodology for MYCN IHC staining. Slides were incubated overnight with the first primary antibody (MYC, Abcam, ab32072) in PBS with 5% goat serum. HRP-conjugated secondary antibody (ThermoFisher Scientific, 31462) was applied for 1 hour at RT and slides incubated with TSA reagent (PerkinElmer, NEL741B001KT (fluorescein) plus 0.0015% H_2O_2) according to manufacturer's recommendations. Additional rounds of antigen retrieval and re-blocking steps were performed prior to incubation with a second primary antibody (MYCN, Cell Signaling, 51705S), HRP-conjugated secondary antibody, and TSA reagent (PerkinElmer, NEL744B001KT (cyanine 3) plus 0.0015% H_2O_2). Lastly, sections were incubated in DAPI (1:50,000, Sigma-Aldrich, D9542) for 15 minutes and mounted with SlowFade Gold Antifade Mountant (ThermoFisher Scientific, S36937). All washes were done with either PBS or PBS/0.25% goat serum/0.1% Triton X-100. Whole slide fluorescence imaging was performed with the Zeiss Axio Scan.Z1 microscope (20x objective lens). See Table 1 for additional specifications on antibodies used.

Chamber slide cell line cultures: Cells were washed briefly with PBS and fixed with 100% methanol for 10 minutes. TSA-IF for MYCN and MYC was performed on cells similar to methods described for tumor sections. Briefly, blocking steps were applied, followed by

sequential overnight incubations of MYC-family isoform antibodies. Antigen retrieval and blocking steps were performed between MYC and MYCN antibody incubations and after the last TSA reaction. For the nuclear stain, an antibody for histone H3 (Abcam, ab1791) was incubated overnight and a Cy5-conjugated secondary antibody (Invitrogen, A10523) applied for one hour at RT. Whole slide fluorescence imaging was performed with the Zeiss Axio Scan.Z1 microscope (20x objective lens).

Single-nucleus RNA-Seq analyses

Single-nucleus RNA-sequencing (SNRS) expression from TNBC tumors, pre- and post-NAC, were kindly provided by Dr. Nicholas E. Navin from a previously published study *(322)*. Expression in TPM was log-transformed and scaled using the Seurat v3.0 R package *(323)*. Tumor samples (KTN615, KTN132, KTN102, and KTN152) with persistent disease after NAC were evaluated for *MYCN* expression. tSNE dimensionality reduction, violin, and balloon plots were created using Seurat v3.0.

Survival analyses

Disease/progression-free and overall survival of patients represented in the TNBC587 dataset have been previously published *(98)*. Analyses compared survival characteristics of patients with positive versus negative median-centered $\log_2$ normalized *MYCN* expression. In accordance with protocols described in the section "*Patient tissue and tissue microarrays (TMAs)*," survival data for patients with tissue in the three TNBC cohorts (primary, treatment-naïve; primary, NAC-treated; and recurrent) was curated and

analyzed with respect to MYCN H-scores. Survival curves for these datasets were generated using Graphpad Prism 7.0a.

Cell culture and in vitro assays

Cell culture: TNBC cell lines, CAL-51 (DSMZ, ACC 302) and MDA-MB-468 (ATCC, HTB-132), and neuroblastoma cell line, SK-N-BE(2)C (kindly provided by Dr. Dai H. Chung, Vanderbilt University), were cultured and maintained in DMEM (Gibco, 11965-092), 5% (v/v) FBS (Gemini, 100-106), 100U/ml penicillin, and 100 µg/ml streptomycin (Gemini, 400-109). Clonal cell lines were generated by seeding serial dilutions into 96-well plates (Costar, 3997). Wells containing single cells were identified the following day and expanded into clonal cell lines. Short tandem repeat DNA fingerprinting analyses (performed by Cell Line Genetics) were conducted on CAL-51 and MDA-MB-468 (March, 2011) and five CAL-51 clonally-derived cell lines (Cln3, Cln5, Cln15, Cln37, and Cln39) (April, 2016). All cell lines were routinely tested with results negative for the presence of *mycoplasma* (Lonza Bioscience).

Cell line-derived xenograft (CDX) tumor growth: CAL-51, MDA-MB-468, and SK-N-BE(2)C cell lines were resuspended in PBS at $5.0X10^6$ cells per 200 µl and injected subcutaneously into the flanks of NSG mice. CDX tumor dimensions were measured with calipers and tumor volumes estimated using the formula, ($width^2$ X length/2). Once tumors reached ~1000 mm^3, CDXs were collected, placed in 10% buffered formalin overnight at RT, transferred to 70% ethanol, and paraffin-embedded at the Translational Pathology Shared Resource (TPSR) of Vanderbilt University Medical Center. All experiments were

conducted in accordance with approved protocols by the Institutional Care and Use Committee for animal research at Vanderbilt University Medical Center.

Development of PI3K inhibitor-resistance: CAL-51 cells were initially treated with PI3K inhibitor, taselisib (GDC-0032), at the IC_{50} for CAL-51 (100 nM). Media was replaced at least once a week and cultures treated with the same dose, or 25% higher, the day following each passage. CAL51 cells were considered PI3Ki-resistant after demonstrating a >10-fold increase in IC_{50} to taselisib, compared to the starting parental CAL-51 cell line, after a two-week "drug holiday." Taselisib was not applied at time of single-cell isolation or thereafter.

Drug sensitivity assays: Compounds were either purchased from commercial vendors or supplied under a material transfer agreement (MTA) through Genentech or Incyte Corporation (tables S6 and S7). VU661013 was kindly provided by Dr. Stephen W. Fesik, Vanderbilt University. CAL-51 cell lines were seeded in quadruplicate (1,500 cells/well) in 96-well plates (Costar, 3997) and treated with a six-point, three-fold dose-escalation alongside untreated controls for 72 hours. AlamarBlue (ThermoFisher Scientific, DAL1100) was applied to all assays according to manufacture recommendations and fluorescence analyzed with microplate data collection and analysis software Gen5 (Biotek). Viability and IC_{50} analyses were determined in Prism (Graphpad, 7.0a) by performing a non-linear fit to $\log_{10}$ normalized fluorescence values.

Bliss independence analyses were performed to determine synergy between combination treatments *(324, 325)*. The theoretical Bliss expectation (C) between the fractional growth of drug A and B, at a given dose, was calculated by C = (A+B) – (A*B). The delta Bliss is the difference between the Bliss expectation and the observed growth inhibition between drug A and B at the same dose. A Bliss score = 0 indicates the combination treatment is additive and effects are likely through independent pathways. Therefore, a Bliss score > 0 is considered synergistic and < 0 antagonistic.

Proliferation assays: CAL-51^{Parental} clonal cell lines were seeded at 10,000 cells per well in triplicate into adherent (Sarstedt, 83.3920) or ultra-low adherent (Corning, 3471) six-well plates. Cells were collected daily and counted using the TC20 automated cell counter (Bio-Rad). Doubling rate was calculated between day one and five for adherent cells and due to a latency in initial proliferation, between day three and five for forced-suspension cells, using the formula:

$$DoublingTime = \frac{Duration * \log(2)}{\log(FinalConcentration) - \log(InitialConcentration)}$$

Chamber slides: CAL-51 and MDA-MB-468 cell populations were seeded into eight-well chamber microscope slides (Corning, 354108) at 10,000 and 16,000 cells per well, respectively. After three days, chamber slides were treated with a dose-escalation of 0.25, 0.5, or 1.0 μM INCB054329 or JQ1 for 24 hours. For combination treatment assays, cells were treated with 0.25 μM trametinib, 0.5 μM INCB054329, or 0.5 μM JQ1 alone, or with the combination of trametinib and either BETi, for 48 hours.

Colony formation assays: For single-agent colony formation assays (CFAs), CAL-51 clonal cell lines were seeded into six-well plates (Sarstedt, 83.3920) or twelve-well plates (Corning, 353043) at 1,000 cells per well and treated with either 0.5 μM or 1.0 μM INCB054329 for six days. For combination treatment CFAs, CAL-51 and MDA-MB-468 cell populations were seeded at 1,500 and 3,000 cells per well in 48-well plates (Costar,3548) and treated with a dose escalation of INCB054329 [CAL-51 (0.13, 0.25, 0.5 μM), MDA-MB-468 (0.03, 0.06, 0.13 μM)], JQ1 [CAL-51 (0.13, 0.25, 0.5 μM), MDA-MB-468 (0.06, 0.13, 0.25 μM)], or trametinib [CAL-51 (2.5, 5, 10, 20, 40 nM), MDA-MB-468 (0.63, 1.25, 2.5, 5, 10 nM)] as single-agents or with trametinib in combination with either BETi for six days. Colonies were washed with PBS, fixed with 100% methanol for 10 minutes, and stained with a 1:1 mixture of methanol and crystal violet aqueous solution (Electron Microscopy Sciences, 26106-01) at RT for 1 hour. Cells were washed three times with dH_2O before placing inverted to dry. Quantification was performed using the Odyssey infrared imaging system and Odyssey software (Li-COR Biosciences).

siRNA-mediated knockdown: CAL-51 clonal cell lines were seeded into six-well plates at 100,000 cells per well and knockdown of *MYCN* (10 or 25 nM, Dharmacon, D-003918-08), alongside a non-targeting control (Dharmacon, D-001810-10), was performed according to the DharmaFECT Transfection Reagents siRNA transfection protocol using Dharmacon transfection reagent (Dharmacon, T-2004-03): https://dharmacon.horizondiscovery.com/uploadedFiles/Resources/basic-dharmafect-protocol.pdf.

Transfection medium was replaced with complete medium after six hours and plates incubated at 37°C for four days. Viability was assessed by incubating cells with alamarBlue prior to cell collection for immunoblot analyses.

Table 1. Specifications for antibodies used

Protein Target	Company	Catalog #	Species	Immunoblot	IHC	IF	TSA-IF
MYCN	Santa Cruz	sc-53993	Mouse	1:500			
MYCN	Cell Signaling	9405	Rabbit	1:500			
MYCN	Cell Signaling	51705	Rabbit	1:500	1:150†		1:500
MYC	VAPR	9E10	Rabbit	1:500			
MYC	Cell Signaling	5605	Rabbit	1:1000			
MYC	Abcam	ab32072	Rabbit	1:1000	1:150		1:500
pERK1/2	Cell Signaling	4370	Rabbit	1:2000			
ERK1/2	Cell Signaling	9107	Mouse	1:2000			
Cleaved PARP	Cell Signaling	5625	Rabbit	1:1000			
Cleaved Caspase-3	Cell Signaling	9661	Rabbit	1:500			
Beta-Actin	Santa Cruz	sc-47778	Mouse	1:500			
GAPDH	Millipore	MAB374	Mouse	1:25000			
Histone H3	Abcam	ab1791	Rabbit			1:100	

† General concentration, titrations and optimal concentration should be determined per antibody lot

Immunoblotting and antibodies

All cells were lysed using RIPA (pH 7.4) buffer [150mM NaCl, 50mM Tris-HCl (pH 7.5), 0.1% SDS, 1.0% NP-40, 0.5% Deoxycholic Acid, 5mM EDTA] supplemented with protease and phosphatase inhibitors (Chymostatin: Calbiochem, 230790; Leupeptin: Calbiochem, 108975; Antipain: Calbiochem, 178220; Pepstatin A: Millipore, 195368; AEBSF: Calbiochem, 101500; PMSF: Sigma, P-7626; NaVan: Sigma, S6508). Equal amounts of protein were separated on SDS polyacrylamide gels and transferred onto PVDF membrane (Millipore, IPVH00010). Antibodies used for cell line immunoblot analyses were against MYCN (Santa Cruz, sc-53993), MYC (VAPR, 9E10), and Actin (Santa Cruz, sc-47778). For PDX lysate, antibodies were against MYCN (Cell Signaling, 9405), MYC (Cell Signaling, 5605), cleaved-Caspase 3 (Cell Signaling, 9661), cleaved-

PARP (Cell Signaling, 5625), and GAPDH (Millipore, MAB374). Additional antibodies included pERK1/2$^{T202/Y204}$ (Cell Signaling, 4370) and ERK1/2 (Cell Signaling, 9107).

Oncology drug screens

Primary and secondary drug screens were conducted at the High-Throughput Screening (HTS) facility at Vanderbilt University. The primary drug screen contained 158 drugs and was comprised of compounds from the NCI FDA-approved AOD library set (http://dtp.cancer.gov), Selleck Chemicals, and other venues (see table S6 for vendor and catalog numbers). The screen was conducted in 384-well plates using a ten-point, three-fold dose escalation of each compound for 72 hours. AlamarBlue was applied (see 'Drug sensitivity assays' section) and IC_{50} results determined in Prism (GraphPad, 7.0a) by performing a non-linear fit to log_{10} normalized (to DMSO-treated control) fluorescence values. Compounds with a greater or less than two-fold change in IC_{50} between MYCN^{Low} and MYCN^{High} clonal cell lines were used in a secondary screen, alongside additional related compounds (see table S7 for source and catalog numbers), for a total of 40 drugs. The secondary screen was conducted with the same conditions as the primary screen.

RNA isolation, sequencing, and analyses

CAL-51 clonal cell lines were treated with 0.5 μM INCB054329 or DMSO control for 4 hours and total RNA collected using the Aurum Total RNA Mini Kit (Bio-Rad, 732-6820) according to manufacturer recommendations. All RNA samples were assessed for quality and quantified using a NanoDrop One Spectrophotometer (Thermo Fisher Scientific, ND-ONE-W). Samples were further analyzed using the Qubit RNA assay and

Agilent BioAnalyzer 2100. Library preparation and sequencing was performed at the Vanderbilt Technologies for Advanced Genomics (VANTAGE). Libraries were prepared using the Illumina TruSeq RNA Library Preparation Kit (poly-A capture, stranded) and sequenced on the Illumina HiSeq 3000 (20-30 million 75 base-pair (bp), paired-end reads per sample). Reads were trimmed to remove TruSeq adapter sequences using Flexbar v2.5 and aligned to hg19 with STAR v2.5.2a using default parameters and GENCODE v25lift37 annotations *(326–328)*. Transcript assembly and abundance estimation was performed using Cufflinks v2.2.1 *(329)*. Gene-level FPKM estimates were converted to TPM. DESeq2 v1.24.0 *(330)* was used to determine differential gene expression (FDR-adjusted, $p < 0.1$) and heatmap was generated using the pheatmap package *(331)*. The Gene Set Enrichment Analysis (GSEA, v3) *(332)* was used to identify enriched signatures in the MSigDB database (v6.1) *(333)*.

Precision nuclear run-on sequencing (PRO-seq)

Four CAL-51 clonal cell lines were treated with 0.5 μM INCB054329 or DMSO control for 15 minutes and nuclei isolated by incubating cells with isotonic swelling buffer (ISB: 10 mM Tris-Cl pH7.4, 300 mM Sucrose, 3 mM $CaCl_2$, 2 mM $MgCl_2$, 1 mM PMSF) plus RNAse (Applied Biosystems, N8080119) and EDTA-free protease and phosphatase inhibitors (see 'immunoblotting and antibodies' section) for 5 minutes. Cells were scraped, spun down, and lysed in isotonic lysis buffer (ISB plus 0.4% Triton X-100 and 10% glycerol) for 5 minutes. Cells were further lysed via dounce-homogenization and stored at -80°C in glycerol storage buffer (50 mM Tris-Cl pH8.3, 5 mM $MgCl_2$, 0.1 mM EDTA, 40% glycerol) plus inhibitors at a concentration of $1.5x10^7$ million cells/100 μl.

All buffers were made with DEPC-treated, nuclease-free water. Biotin run-on was conducted by incubating nuclei with Sarkosyl nucleotide buffer (10 mM Tris-Cl pH8.0, 5 mM $MgCl_2$, 0.1 mM DTT, 300 mM KCl, 380 µM NTPs (ATP, GTP, and UTP; ThermoFisher Scientific), 500 µM biotin-11-CTP (PerkinElmer, NEL542001), 1% Sarkosyl, SUPERase In RNase Inhibitor (ThermoFisher Scientific, AM2694)) for 3 minutes at 30°C. RNA was isolated through TRIzol LS/chloroform extraction and ethanol (EtOH) precipitation. Base hydrolysis was performed by dissolving air-dried RNA pellet in DEPC-treated dH_2O, heating RNA to 65°C for 40 sec, and incubating samples with 0.2 N NaOH for 10 minutes on ice. After neutralization with an equal volume of 1M Tris-HCl pH6.8, nascent RNA-capture was performed by incubating samples with Dynabeads® MyOne™ Streptavidin T1 magnetic beads (ThermoFisher Scientific, 65601) according to manufacturer recommendations for 20 minutes at RT. RNA-bound beads were subjected to a series of wash steps using high salt wash buffer (HS: 50 mM Tris pH7.4, 2 M NaCl, 0.1% Triton X-100), medium salt (MS: 10 mM Tris pH 7.4, 300mM NaCl, 0.1% Triton X-100), and low salt wash buffer (LS: 5 mM Tris pH7.4, 0.1% Triton X-100). RNA was extracted twice from beads with TRIzol/chloroform, mixed with 2 µl of 20 mg/ml glycogen, and EtOH precipitated.

To ligate adapters to the 3' end of RNA, pellets were resuspended in 5 µl of 2 µM Reverse 3' RNA adapter (5'-GAUCGUCGGACUGUAGAACUCUGAAC-3', Integrated DNA Technologies (IDT)) and mixed with ligation buffer (LB: T4 RNA ligase (NEB), 1X T4 RNA ligase buffer, 1mM ATP, SUPERase In) for 6 hours at 20℃. Adapter-bound RNA was subjected to another round of streptavidin bead capture, gradient salt washes, and EtOH precipitation. To cap the 5' end, RNA was resuspended in 5 µl DEPC-treated dH_2O

and incubated with CAP mix (CAP CLIP (CellScript, C-CC15011H), 1X CAP CLIP buffer, SUPERase In) at 37°C for 2 hours. Again, RNA was extracted via TRIzol/cholorform incubations, mixed with glycogen, and EtOH precipitated. To repair the 5' hydroxyl after capping, RNA pellets were resuspended in 5 µl DEPC dH_2O and mixed with PNK buffer (T4 PNK (NEB), 1X PNK buffer, 1 mM ATP, SUPERase In) at 37°C for 1 hour. For 5' adapter ligation, RNA pellets were resuspended in 2 µM Reverse 5' RNA adapter (5'-CCUUGGCACCCGAGAAUUCCA-3', IDT) and incubated with LB at 20°C for 6 hours.

After streptavidin-mediated RNA-capture and TRIzol/chloroform extraction, dried pellets were resuspended in 5 µM RNA PCR Primer RP1 (5'-AATGATACGGCGACCAC CGAGATCTACACGTTCAGAGTTCTACAGTCCGA-3', IDT) and incubated with reverse transcriptase (RT) mix (1.6 mM dNTP mix (NEB, N0446S), 1x first strand synthesis buffer, 25 mM DTT, SUPERase In) for 3 minutes at 48°C. Superscript III RTase (ThermoFisher Scientific, 18080093) was added to each sample, and RNA incubated in thermocycler (44°C for 20 minutes, 52°C for 45 minutes, 4°C hold). After performing test amplifications, optimal RNA dilutions were determined and subjected to full-scale amplifications by mixing RT product with PCR mix (Phusion polymerase (NEB), 1x HF buffer, 1M betaine, 250 µM dNTP mix, and 1.25 µM RP1) and one of eight RPI-indices (TruSeq barcodes, Illumina). RNA was amplified using thermocycling previously described *(334)*, ran through 8% native polyacrylamide gels, and extracted using soaking buffer (1X TE buffer, 150 mM NaCl, 0.02% Tween-20) via two overnight incubations at 37°C. Samples were passed through Costar Spin-X centrifuge filters to remove gel debris, RNA phenol-chloroform extracted, EtOH precipitated, and resuspended in 10 µM DEPC-treated dH_2O for sequencing.

PRO-Seq quality control (QC) and sequencing were performed at VANTAGE. Nascent RNA quality and quantification was assessed using the Qubit RNA assay and Agilent BioAnalyzer 2100. Sequencing was performed using the Illumina NextSeq 5000 (30-45 million 75 bp, single-end reads per sample). Reads were trimmed to remove TruSeq adapter sequences using Flexbar v2.5, converted to their reverse complement using FASTX-Toolkit v0.0.13 "fastx_reverse_complement" command, and aligned to hg19 with BWA-MEM v0.7.13 using default parameters *(326, 335, 336)*. Aligned reads with a quality score less than 30 were removed with SAMtools v1.3.1 *(337)*. Nascent RNA sequencing analysis (NRSA) was used to quantify nascent RNAs, identify paused genes as well as active enhancers, and detect transcriptional changes between INCB054329- and DMSO-treated cells *(338)*.

In vivo patient-derived xenograft (PDX) experiments performed at VUMC

Mice were housed and treated in accordance with protocols approved by IACUC for animal research at Vanderbilt University. Female 6-8 week-old NOD *scid* gamma (NSG) or athymic nude mice (Jackson Laboratory) were anesthetized with isoflurane and subjected to subcutaneous engraftment of a 2 mm^3 TNBC PDX [Jackson Laboratory (TM00096, TM00090, TM01273), Baylor University (BCM-2147), Xentech (HBCx1)] fragment into the lateral dorsal side of each mouse. Ten to fourteen days post-surgical implantation and daily monitoring, the mice were anaesthetized and wound clips removed. Once PDX tumors reached approximately 150-250 mm^3, mice were randomized into single-agent and combination treatment groups and administered MEK inhibitor, trametinib (0.1mg/kg, once daily), and/or a BET inhibitor, INCB054329 or JQ1

(50mg/kg, twice daily), in 0.5% methylcellulose with 0.2% Tween-80 or 5% N,N-Dimethylacetamide, respectively, through orogastric gavage for 14 or 22 days. Tumor volume was calculated twice a week by caliper measurements ($width^2$ X length/2) and body weight measured once a week. Tumors were not allowed to reach the maximum size of 2,000 mm^3. Tumors used for subsequent molecular analyses were snap-frozen and deposited in a liquid nitrogen storage tank.

In vivo PDX experiments performed at Champions Oncology

The PDX study analyzing BETi and MEKi treatment on CTG-1475 PDX tumor growth was performed at Champions Oncology and conducted according to the guidelines of Institutional Animal Care and Use Committee (IACUC) of Champions Oncology. Subcutaneous engraftments were performed on 5-8 week-old female immune compromised mice. Once tumors reach 150-300 mm^3, mice were matched by tumor size, placed into treatment arms, and administered trametinib (0.1mg/kg, once daily) or INCB057643 (10mg/kg, once daily) in sterile water with 0.5% methylcellulose and 5% N,N-Dimethylacetamide through orogastric gavage, as single-agents or in combination for 30 days. Mouse weight and tumor size were measured twice a week and volume calculated with the formula, $width^2$ X length X 0.52.

PDX TMA construction and analyses

For molecular analyses on PDX tissue, samples were collected after initial (two days) and final (22 days) doses for the TM00096, HBCx1, and BCM-2147 models. Tissues were fixed in 10% neutral-buffered formalin (Thermo Fisher Scientific, 5701) at

RT overnight, transferred to 70% ethanol, and paraffin-embedded at TPSR at VUMC. Three 1 mm cores were punched from each FFPE block in regions selected by a pathologist to construct three TMAs. Four-micron sections from each TMA were used to perform IHC staining for Ki67 (Leica Biosystems) through services provided at TPSR. Whole slide imaging and quantification of immunostaining were performed at the Digital Histology Shared Resource (DHSR) at VUMC using the Leica SCN400 bright field microscope (40x objective lens; 0.25 μm/pixel) and Digital Image Hub slide-hosting software (Leica Microsystems). In parallel, TSA-IF for MYCN and MYC was applied to additional TMA sections, alongside positive controls, MYCN-amplified neuroblastoma patient tumor and cell line-derived xenograft SK-N-BE(2)C. Slides were scanned using the Aperio Versa 200 or Zeiss Axio Scan.Z1 fluorescence microscopes (20x objective lens). TMAs were de-arrayed into individual fluorescence channels (Leica, Review) and mean pixel intensities for each fluorophore quantified per nuclei for each treatment timepoint using the Cellprofiler software package *(339)*. Results were displayed as violin plots using R package ggplot2.

CHAPTER III

CHARACTERIZATION OF MYCN EXPRESSION IN TRIPLE-NEGATIVE BREAST CANCER DISEASE ETIOLOGY AND PROGRESSION

Introduction

The development of targeted therapies for TNBC is challenging due to its molecular heterogeneity and lack of therapeutically targetable, high-frequency "driver" alterations *(106)*. Aside from *TP53*, the majority of mutations found in TNBC are within the PI3K/mTOR or RAS/RAF/MEK signaling pathways. The most frequent oncogenic mutations in TNBC occur in 'hotspot' regions of the *PIK3CA* gene (E545 helical domain and H1047 kinase domain) *(340)*, and the most frequently amplified oncogene is *MYC (321, 341)*. MYC family members, *MYC*, *MYCN*, and *MYCL* (encoding proteins MYC, MYCN, and MYCL, respectively), are transcription factors that regulate the expression of genes involved in normal development, cell growth, proliferation, metabolism, and survival *(161)*. Aberrant expression of MYC family members has been considered tumorigenic in a tissue-specific manner [e.g. *MYCN* in neuronal *(271, 273)* or neuroendocrine tumors *(256, 342)* and *MYCL* in the lung *(161)*]. However, recent reports have shown elevated *MYCN* expression in non-neuronal tissues, such as ovarian *(343)* and prostate cancer *(344)*, as well as hematopoietic cells that give rise to acute lymphoblastic *(345)* and myeloid *(251)* leukemias. Further, there is increasing evidence that *MYCN* expression is deregulated in a subset of breast cancers with both unfavorable prognostic features and clinical outcomes *(260, 261, 346)*. *MYCN* transcript has been

found in circulating breast tumor cell clusters within the bloodstream of breast cancer patients *(347)* and is associated with a stem-cell program found in tumor-initiating metastatic cells *(261)*, implicating a role for *MYCN* in recurrence and the metastatic spread of breast cancer.

Through experiments described in this chapter, we determined the frequency and levels of MYCN expression in primary TNBC, the relative expression of MYCN versus MYC in tumor cell populations, and if MYCN expression levels change in response to neoadjuvant chemotherapy (NAC). Further, we provide evidence that MYCN-expressing cells have survival advantages after cellular stress and acquire resistance to anti-cancer agents. While this chapter focuses on the discovery and initial characterization of MYCN expression in TNBC, subsequent chapters will focus on therapeutic strategies to target MYCN-expressing TNBC and other breast cancer subtypes.

Results

A significant fraction of primary TNBC express MYCN

To evaluate *MYCN* expression in TNBC, we first identified TNBC tumors from primary, treatment-naïve cases in The Cancer Genome Atlas (TCGA) Breast Invasive Carcinoma (BRCA) dataset (Figure 3A) *(340)*. *MYCN* transcript was expressed in all tumors [transcript per million (TPM) >0] and elevated [>12 TPM, >1 standard deviation (SD) above the mean] in 10.2% (20/197) of cases (Figure 4A). Likewise, we detected elevated *MYCN* expression in a similar proportion of primary TNBC cases in two other datasets, TNBC587 (>0.65 median-centered $\log_2$ normalized, n=65/587) *(97)* and Molecular Taxonomy of Breast Cancer International Consortium (METABRIC) (>7 $\log_2$

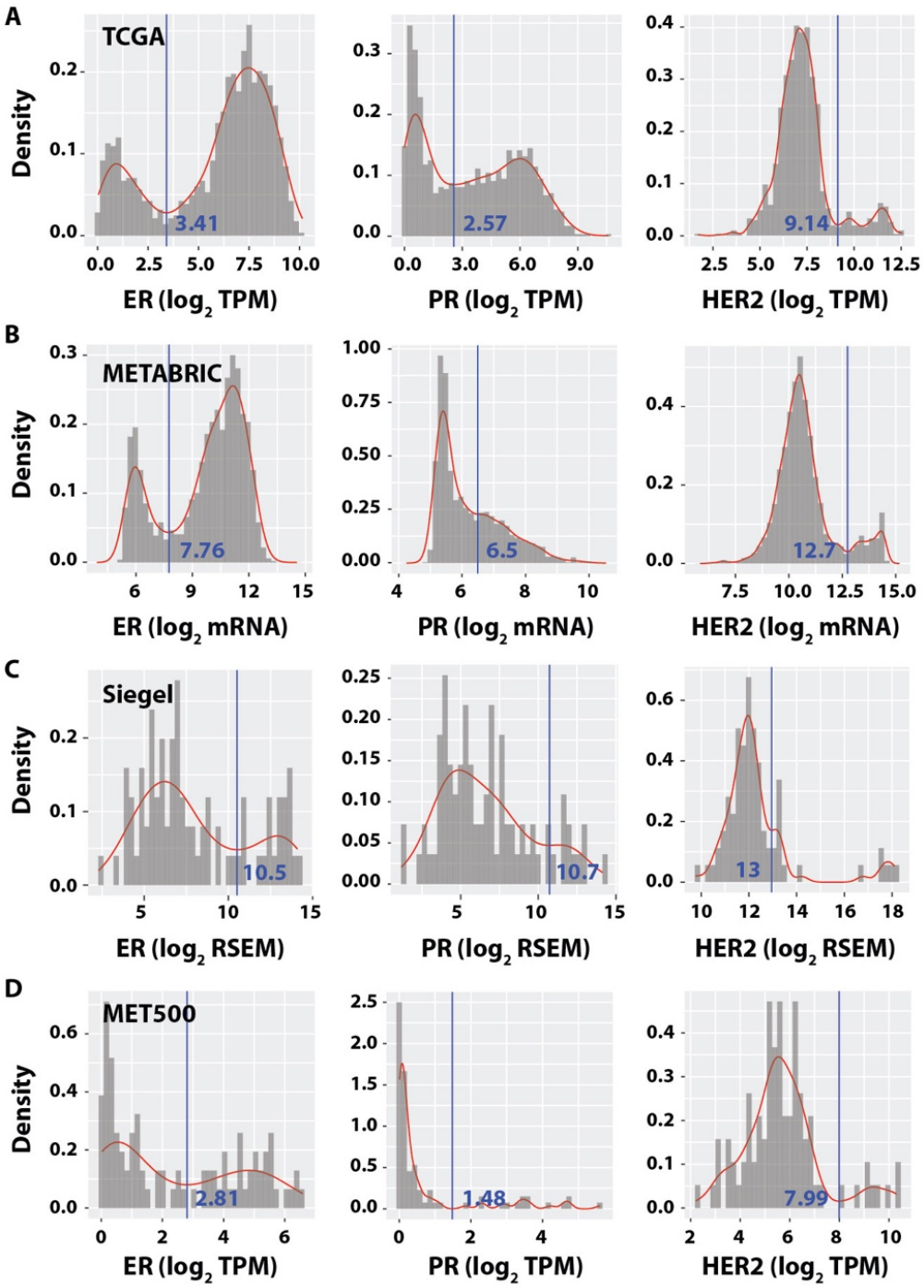

Figure 3. Identification of TNBC breast cancers in TCGA, METABRIC, Siegel, and MET500 breast cancer datasets. (**A-D**) Histograms showing discrete RNA-Seq mRNA expression cutoffs for the estrogen receptor (ER), progesterone receptor (PR), and human epidermal growth factor receptor 2 (HER2) to identify TNBC tumors in TCGA (BRCA) (**A**), METABRIC (**B**), Siegel *(320)* (**C**), and MET500 (**D**) datasets. A tumor was categorized as TNBC if the ER, PR, and HER2 RNA levels were in the first peak of the bimodal distribution.

normalized, n=48/323) *(348)* (Figure 3B and Figure 5, A and B). To gain insight to the biological relevance of *MYCN* expression in TNBC, we compared *MYCN* transcript levels in primary, treatment-naïve TNBC (source: TCGA, BRCA) to expression levels in known MYCN-driven cancers *(349)* (Figure 4B). Cancers with *MYCN* gene amplification such as neuroblastoma (NB), glioblastoma multiforme (GBM), and acute myeloid leukemia (AML) originate from migrating neural crest cells, neural stem cells, or hematopoietic stem cells, respectively *(349)*. *MYCN* is also amplified or overexpressed in at least 20% and 60% of adenocarcinoma (Adeno) and neuroendocrine (NE) castration-resistant prostate cancer (CRPC) cases, respectively *(256, 344)*. While transcript levels in TNBC were not as high as NB *(318)*, AML (source: TCGA, LAML), or GBM (source: TCGA, GBM), *MYCN* expression was similar to NE-CRPC and signifcantly higher ($p<0.0001$) than Adeno-CRPC *(259, 319)* (Figure 4B). Further, elevated *MYCN*-expressing TNBC cases identified in TCGA (Figure 4A) had higher *MYCN* expression levels than the top *MYCN*-expressing NE-CRPC tumors (Figure 4B).

The TNBC587 dataset, curated from 21 Affymetrix breast cancer datasets, was used to identify distinct TNBC transcriptional subtypes [basal-like (BL1 and BL2), mesenchymal (M), and luminal androgen receptor (LAR)] with unique gene expression and molecular ontologies *(97, 98)*. We evaluated *MYCN* expression within the TNBC587 dataset to determine if the expression was associated with a particular TNBC subtype. *MYCN* transcript levels were significantly enriched in M-subtype tumors (one-way ANOVA, $p=0.0225$), which exhibit higher expression of genes involved in cell motility and epithelial-to-mesenchymal transition (EMT) (Figure 5C) *(97)*. By applying the same methodology to identify TNBC subtypes in TCGA and METABRIC datasets, we found *MYCN* had the

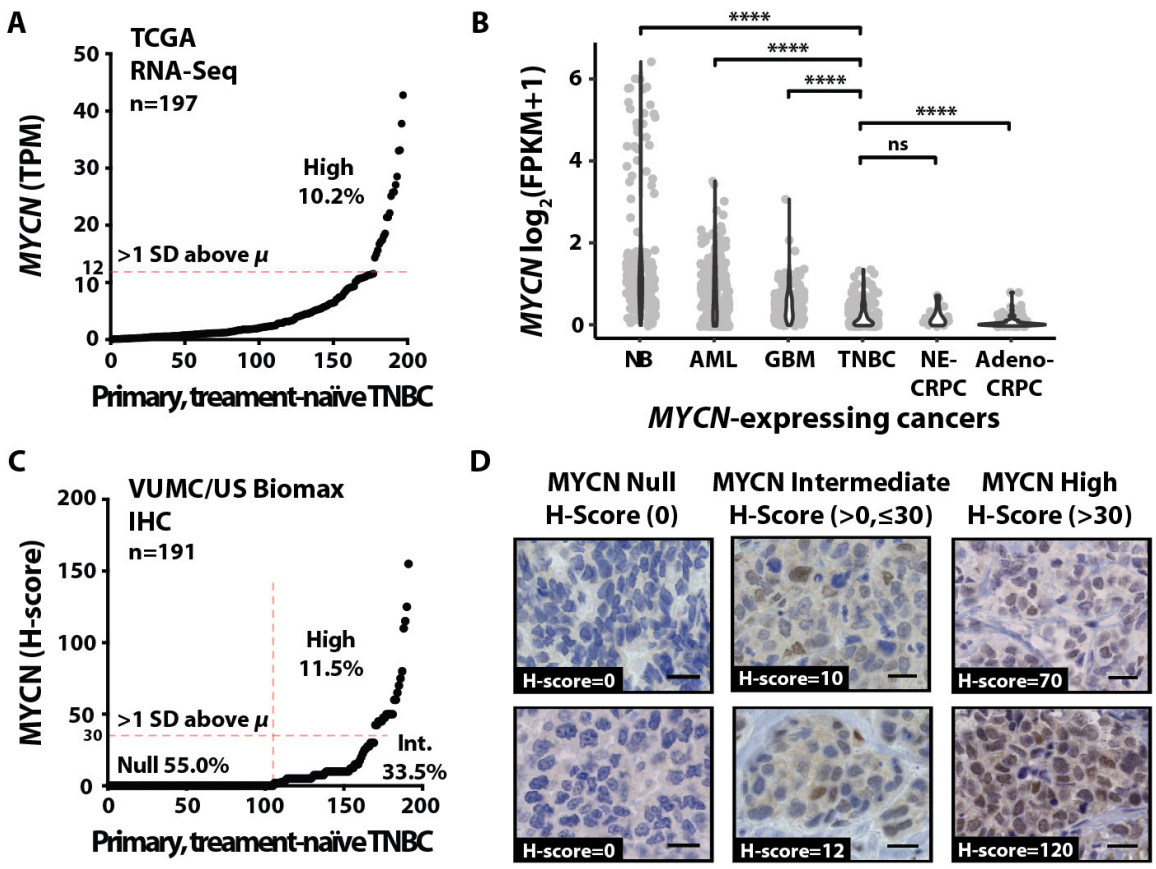

Figure 4. *MYCN* RNA and MYCN protein expression in primary, treatment-naïve TNBC. (**A**) *MYCN* transcript levels (TPM) from 197 primary, treatment-naïve TNBC [source: TCGA (BRCA)]. SD, standard deviation. μ, mean. (**B**) Violin plot showing *MYCN* expression in TNBC [source: TCGA (BRCA), n=197] compared to neuroblastoma (NB, n=161) *(318)*, acute myeloid leukemia (AML) [source: TCGA (LAML), n=173], glioblastoma multiforme (GBM) [source: TCGA (GBM), n=156], and castration-resistant prostate cancer (CRPC), including neuroendocrine (NE, n=15) and adenocarcinoma (Adeno, n=123) *(259, 319)*. Pairwise Wilcox t-test between TNBC and the other cancer types, ****p<0.0001. ns, not significant. (**C**) MYCN protein levels (H-scores) from 191 primary, treatment-naïve TNBC [source: Vanderbilt University Medical Center (VUMC) and US Biomax]. Int., intermediate. (**D**) Representative MYCN IHC images in TNBC devoid of MYCN protein expression (H-score=0), that contain intermediate levels of MYCN (H-score between >0 and ≤30), or that have high MYCN (H-score >30). Scale bar, 20 μM.

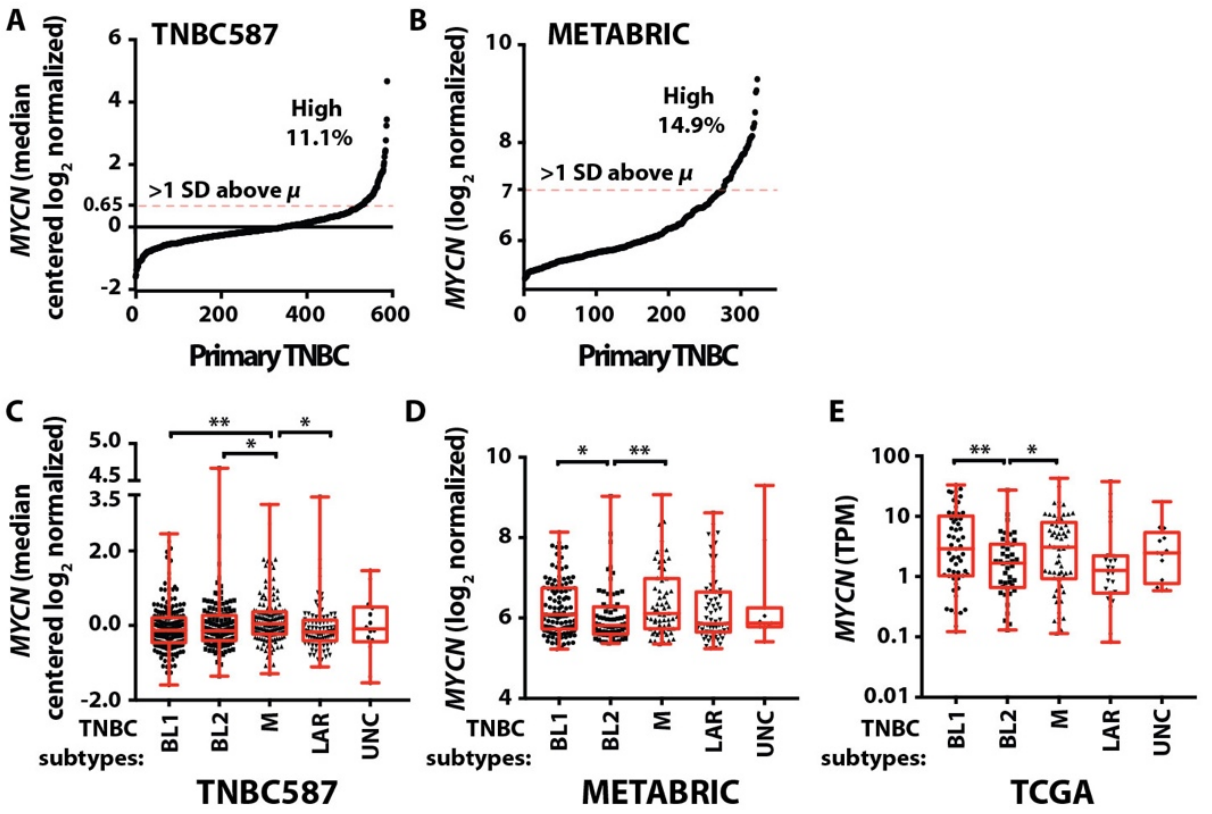

Figure 5. Distribution of *MYCN* expression across TNBC and within TNBC subtypes. (**A**) Median-centered log_2 normalized *MYCN* expression from 587 TNBC cases in the TNBC587 dataset *(97, 98)*. SD, standard deviation. μ, mean. (**B**) *MYCN* expression from 323 primary TNBC cases identified in the METABRIC dataset (fig. S1B). (**C-E**) Distribution of normalized *MYCN* expression according to TNBC subtype in the TNBC587 (n=587) (**C**), METABRIC (n=323) (**D**), and TCGA (n=197) (**E**) datasets. See the TNBC587 publication *(98)*, table S1, and table S2 for TNBC subtype correlations. Unpaired t-test between all TNBC subtype comparisons, *p<0.05, **p<0.01.

highest median expression in M-subtype tumors (Figure 5, D and E). *MYCN* expression was also elevated in BL1-subtype TNBC, the subtype characterized by elevated DNA damage response gene expression *(97, 98)*. Similarly, MYCN-expressing NE-CRPC has an enrichment in DNA damage response pathway gene expression *(350, 351)*.

Since the *MYCN* transcript in clinical specimens could have originated from the tumor or tumor-infiltrating immune or stromal cells, we performed MYCN immunohistochemistry (IHC) to identify the cellular distribution of MYCN protein in an independent cohort of 191 primary, treatment-naïve TNBC tumors, curated at VUMC and US Biomax. IHC demonstrated 45% of specimens contained nuclear MYCN within tumor cells, and similar to our RNA analyses, 11.5% of cases had elevated expression (H-score >30, >1 SD above the mean) (Figure 4, C and D, and Table 2). Of note, IHC specificity was confirmed with positive and negative controls from PDXs and CDXs, including SK-N-BE(2)C, a validated *MYCN*-amplified neuroblastoma CDX (Figure 6, A and B, and Table 3) *(352)*. *MYCN* transcript levels highly correlated with IHC protein levels (H-score) across two PDX cohorts (cohort1: R^2=0.968, cohort2: R^2=0.822), further validating antibody specificity (Figure 6, C and D, and Table 3). Collectively, these data demonstrated the prevalence of MYCN protein in TNBC tumor cell nuclei and provided the rationale to further characterize MYCN-expressing cells in the context of disease etiology.

MYCN expression in metaplastic TNBC

Clinical correlates were evaluated to better understand TNBC tumor cell populations associated with MYCN expression. First, we evaluated the histological

Table 2. IHC of MYCN and MYC in primary, treatment-naïve; primary, NAC-treated; and recurrent TNBC cases

						MYCN		MYC	
Specimen ID	Tissue Block	Tissue Source	Primary/Recurrence	Sample Site	Naïve/Treated	% Positive Tumor	H-Score	% Positive Tumor	H-Score
A9	TMA101	VUMC	Primary	Breast	Naïve	80	155	5	5
G7/G8	TMA BR1901	US Biomax	Primary	Breast	Naive	100	125	NA	NA
E5/E6	TMA BR1201a	US Biomax	Primary	Breast	Naive	100	115	NA	NA
A8	TMA101	VUMC	Primary	Breast	Naïve	60	110	30	35
B10/J8	TMA 11-4-09	VUMC	Primary	Breast	Naïve	80	80	40	45
H5/H6	TMA BR1201a	US Biomax	Primary	Breast	Naive	75	75	NA	NA
A7	TMA102	VUMC	Primary	Breast	Naïve	60	70	0	0
E3/E4	TMA BR1901	US Biomax	Primary	Breast	Naive	62.5	65	NA	NA
C5/C6	TMA BR1201a	US Biomax	Primary	Breast	Naive	60	60	NA	NA
B1	TMA102	VUMC	Primary	Breast	Naïve	50	60	10	10
D9/D10	TMA BR1901	US Biomax	Primary	Breast	Naive	50	50	NA	NA
H1/H2	TMA BR1201a	US Biomax	Primary	Breast	Naive	50	50	NA	NA
D6/L4	TMA 11-4-09	VUMC	Primary	Breast	Naïve	50	50	0	0
A8	TMA102	VUMC	Primary	Breast	Naïve	40	50	20	26
A8/9	TMA2 Mixed	VUMC	Primary	Breast	Naïve	40	50	0	0
L13/L14	TMA BR1901	US Biomax	Primary	Breast	Naive	47.5	47.5	NA	NA
H9/H10	TMA BR1901	US Biomax	Primary	Breast	Naive	40	47.5	NA	NA
L9/L10	TMA BR1901	US Biomax	Primary	Breast	Naive	42.5	45	NA	NA
C1/C2	TMA BR1901	US Biomax	Primary	Breast	Naive	45	45	NA	NA
D10/J4	TMA2 TNBC	VUMC	Primary	Breast	Naïve	40	45	7	9
A7/A8	TMA BR1901	US Biomax	Primary	Breast	Naive	42.5	42.5	NA	NA
E3/E4	TMA BR1201a	US Biomax	Primary	Breast	Naive	42.5	42.5	NA	NA
D5/L3	TMA 11-4-09	VUMC	Primary	Breast	Naïve	30	30	15	17
B6	TMA102	VUMC	Primary	Breast	Naïve	20	30	10	14
B9	TMA102	VUMC	Primary	Breast	Naïve	25	30	20	37
H5/H6	TMA BR1901	US Biomax	Primary	Breast	Naive	27.5	27.5	NA	NA
F3/F4	TMA BR1901	US Biomax	Primary	Breast	Naive	27.5	27.5	NA	NA
L3/4	TMA2 Mixed	VUMC	Primary	Breast	Naïve	17	26	18	31
K7/K8	TMA BR1901	US Biomax	Primary	Breast	Naive	25	25	NA	NA
I5/I6	TMA BR1901	US Biomax	Primary	Breast	Naive	22.5	22.5	NA	NA
G5/G6	TMA BR1201a	US Biomax	Primary	Breast	Naive	20	20	NA	NA
C3/C4	TMA BR1201a	US Biomax	Primary	Breast	Naive	17.5	17.5	NA	NA
H9/H10	TMA BR1201a	US Biomax	Primary	Breast	Naive	15	15	NA	NA
E9/E10	TMA BR1901	US Biomax	Primary	Breast	Naive	15	15	NA	NA
D1/2	TMA2 Mixed	VUMC	Primary	Breast	Naïve	5	15	12	20
L1/L2	TMA BR1901	US Biomax	Primary	Breast	Naive	12.5	12.5	NA	NA
D7/D8	TMA BR1201a	US Biomax	Primary	Breast	Naive	12.5	12.5	NA	NA
A2/3	TMA101	VUMC	Primary	Breast	Naïve	10	12	10	15
B3/B4	TMA BR1201a	US Biomax	Primary	Breast	Naive	7.5	10	NA	NA
J9/J10	TMA BR1201a	US Biomax	Primary	Breast	Naive	10	10	NA	NA
L3/L4	TMA BR1901	US Biomax	Primary	Breast	Naive	10	10	NA	NA
K11/K12	TMA BR1901	US Biomax	Primary	Breast	Naive	10	10	NA	NA
K9/K10	TMA BR1901	US Biomax	Primary	Breast	Naive	10	10	NA	NA
J7/J8	TMA BR1201a	US Biomax	Primary	Breast	Naive	10	10	NA	NA
C1/C2	TMA BR1201a	US Biomax	Primary	Breast	Naive	10	10	NA	NA
C7	TMA101	VUMC	Primary	Breast	Naïve	10	10	40	66
C3	TMA101	VUMC	Primary	Breast	Naïve	10	10	15	29
E3/M1	TMA 11-4-09	VUMC	Primary	Breast	Naïve	10	10	5	5
D10/L8	TMA 11-4-09	VUMC	Primary	Breast	Naïve	10	10	1	1
C6	TMA101	VUMC	Primary	Breast	Naïve	10	10	10	21
A18	Surgical Resection	VUMC	Primary	Breast	Naïve	10	10	20	40
C5/6	TMA2 Mixed	VUMC	Primary	Breast	Naïve	10	10	0	0
E9/K3	TMA2 TNBC	VUMC	Primary	Breast	Naïve	10	10	0	0
H3/4	TMA2 Mixed	VUMC	Primary	Breast	Naïve	3	9	85	125
J5/J6	TMA BR1201a	US Biomax	Primary	Breast	Naive	7.5	7.5	NA	NA
H3/H4	TMA BR1901	US Biomax	Primary	Breast	Naive	7.5	7.5	NA	NA
J1/J2	TMA BR1901	US Biomax	Primary	Breast	Naive	7.5	7.5	NA	NA
F3/F4	TMA BR1201a	US Biomax	Primary	Breast	Naive	7.5	7.5	NA	NA
D1/D2	TMA BR1901	US Biomax	Primary	Breast	Naive	7.5	7.5	NA	NA
D13/D14	TMA BR1901	US Biomax	Primary	Breast	Naive	7.5	7.5	NA	NA
D9/D10	TMA BR1201a	US Biomax	Primary	Breast	Naive	7.5	7.5	NA	NA
A6	TMA101	VUMC	Primary	Breast	Naïve	6	6	5	5
H3/H4	TMA BR1201a	US Biomax	Primary	Breast	Naive	5	5	NA	NA
H11/H12	TMA BR1201a	US Biomax	Primary	Breast	Naive	5	5	NA	NA
L11/L12	TMA BR1901	US Biomax	Primary	Breast	Naive	5	5	NA	NA
K1/K2	TMA BR1901	US Biomax	Primary	Breast	Naive	5	5	NA	NA
D15/D16	TMA BR1901	US Biomax	Primary	Breast	Naive	5	5	NA	NA
E11/E12	TMA BR1201a	US Biomax	Primary	Breast	Naive	5	5	NA	NA
E7/E8	TMA BR1901	US Biomax	Primary	Breast	Naive	5	5	NA	NA
A7/A8	TMA BR1201a	US Biomax	Primary	Breast	Naive	5	5	NA	NA
B6	TMA101	VUMC	Primary	Breast	Naïve	5	5	8	11
B7	TMA102	VUMC	Primary	Breast	Naïve	5	5	0	0

A5	TMA102	VUMC	Primary	Breast	Naïve	5	5	35	65
B8	TMA102	VUMC	Primary	Breast	Naïve	5	5	55	130
G5/6	TMA2 Mixed	VUMC	Primary	Breast	Naïve	5	5	30	50
F1/2	TMA2 Mixed	VUMC	Primary	Breast	Naïve	5	5	60	95
F6/K10	TMA2 TNBC	VUMC	Primary	Breast	Naïve	5	5	8	15
C9/I3	TMA2 TNBC	VUMC	Primary	Breast	Naïve	5	5	80	150
J1/J2	TMA BR1201a	US Biomax	Primary	Breast	Naive	4	4	NA	NA
A9/G6	TMA2 TNBC	VUMC	Primary	Breast	Naïve	3	3	15	15
J5/J6	TMA BR1901	US Biomax	Primary	Breast	Naive	2.5	2.5	NA	NA
E7/E8	TMA BR1201a	US Biomax	Primary	Breast	Naive	2.5	2.5	NA	NA
A7	TMA101	VUMC	Primary	Breast	Naïve	2	2	25	35
B5	TMA101	VUMC	Primary	Breast	Naïve	2	2	30	50
C1	TMA101	VUMC	Primary	Breast	Naïve	2	2	0	0
C4	TMA101	VUMC	Primary	Breast	Naïve	2	2	0	0
F1/M9	TMA 11-4-09	VUMC	Primary	Breast	Naïve	0	0	0	0
A5	TMA101	VUMC	Primary	Breast	Naïve	0	0	5	12
C2	TMA101	VUMC	Primary	Breast	Naïve	0	0	15	20
B8	TMA101	VUMC	Primary	Breast	Naïve	0	0	30	46
F9/F10	TMA BR1201a	US Biomax	Primary	Breast	Naïve	0	0	NA	NA
I9/I10	TMA BR1901	US Biomax	Primary	Breast	Naïve	0	0	NA	NA
B7	TMA101	VUMC	Primary	Breast	Naïve	0	0	0	0
E10/M8	TMA 11-4-09	VUMC	Primary	Breast	Naïve	0	0	5	5
A8/I6	TMA 11-4-09	VUMC	Primary	Breast	Naïve	0	0	0	0
E2/N10	TMA 11-4-09	VUMC	Primary	Breast	Naïve	0	0	40	53
E8/M6	TMA 11-4-09	VUMC	Primary	Breast	Naïve	0	0	5	5
B5/J3	TMA 11-4-09	VUMC	Primary	Breast	Naïve	0	0	80	220
A1/H9	TMA 11-4-09	VUMC	Primary	Breast	Naïve	0	0	5	5
I9/I10	TMA BR1201a	US Biomax	Primary	Breast	Naïve	0	0	NA	NA
J11/J12	TMA BR1201a	US Biomax	Primary	Breast	Naïve	0	0	NA	NA
C7/C8	TMA BR1201a	US Biomax	Primary	Breast	Naïve	0	0	NA	NA
D5/D6	TMA BR1201a	US Biomax	Primary	Breast	Naïve	0	0	NA	NA
C9/C10	TMA BR1201a	US Biomax	Primary	Breast	Naïve	0	0	NA	NA
J3/J4	TMA BR1201a	US Biomax	Primary	Breast	Naïve	0	0	NA	NA
I3/I4	TMA BR1201a	US Biomax	Primary	Breast	Naïve	0	0	NA	NA
A9/A10	TMA BR1201a	US Biomax	Primary	Breast	Naïve	0	0	NA	NA
I7/I8	TMA BR1201a	US Biomax	Primary	Breast	Naïve	0	0	NA	NA
E1/E2	TMA BR1201a	US Biomax	Primary	Breast	Naïve	0	0	NA	NA
I5/I6	TMA BR1201a	US Biomax	Primary	Breast	Naïve	0	0	NA	NA
D1/D2	TMA BR1201a	US Biomax	Primary	Breast	Naïve	0	0	NA	NA
G3/G4	TMA BR1201a	US Biomax	Primary	Breast	Naïve	0	0	NA	NA
B1/B2	TMA BR1201a	US Biomax	Primary	Breast	Naïve	0	0	NA	NA
D3/D4	TMA BR1201a	US Biomax	Primary	Breast	Naïve	0	0	NA	NA
K15/K16	TMA BR1901	US Biomax	Primary	Breast	Naïve	0	0	NA	NA
J9/J10	TMA BR1901	US Biomax	Primary	Breast	Naïve	0	0	NA	NA
A9/A10	TMA BR1901	US Biomax	Primary	Breast	Naïve	0	0	NA	NA
I3/I4	TMA BR1901	US Biomax	Primary	Breast	Naïve	0	0	NA	NA
A13/A14	TMA BR1901	US Biomax	Primary	Breast	Naïve	0	0	NA	NA
C13/C14	TMA BR1901	US Biomax	Primary	Breast	Naïve	0	0	NA	NA
I11/I12	TMA BR1901	US Biomax	Primary	Breast	Naïve	0	0	NA	NA
L5/L6	TMA BR1901	US Biomax	Primary	Breast	Naïve	0	0	NA	NA
K3/K4	TMA BR1901	US Biomax	Primary	Breast	Naïve	0	0	NA	NA
J13/J14	TMA BR1901	US Biomax	Primary	Breast	Naïve	0	0	NA	NA
I1/I2	TMA BR1901	US Biomax	Primary	Breast	Naïve	0	0	NA	NA
K5/K6	TMA BR1901	US Biomax	Primary	Breast	Naïve	0	0	NA	NA
B3/B4	TMA BR1901	US Biomax	Primary	Breast	Naïve	0	0	NA	NA
L7/L8	TMA BR1901	US Biomax	Primary	Breast	Naïve	0	0	NA	NA
B4	TMA101	VUMC	Primary	Breast	Naïve	0	0	20	25
B9	TMA101	VUMC	Primary	Breast	Naïve	0	0	30	35
B10	TMA101	VUMC	Primary	Breast	Naïve	0	0	40	65
B1	TMA101	VUMC	Primary	Breast	Naïve	0	0	2	2
G5	Surgical Resection	VUMC	Primary	Breast	Naïve	0	0	35	45
E7/O5	TMA 11-4-09	VUMC	Primary	Breast	Naïve	0	0	6	8
F1/F2	TMA BR1201a	US Biomax	Primary	Breast	Naïve	0	0	NA	NA
I1/I2	TMA BR1201a	US Biomax	Primary	Breast	Naïve	0	0	NA	NA
H13/H14	TMA BR1901	US Biomax	Primary	Breast	Naïve	0	0	NA	NA
E15/E16	TMA BR1901	US Biomax	Primary	Breast	Naïve	0	0	NA	NA
C15/C16	TMA BR1901	US Biomax	Primary	Breast	Naïve	0	0	NA	NA
C11/C12	TMA BR1901	US Biomax	Primary	Breast	Naïve	0	0	NA	NA
J7/J8	TMA BR1901	US Biomax	Primary	Breast	Naïve	0	0	NA	NA
A5/A6	TMA BR1901	US Biomax	Primary	Breast	Naïve	0	0	NA	NA
K13/K14	TMA BR1901	US Biomax	Primary	Breast	Naïve	0	0	NA	NA
I15/I16	TMA BR1901	US Biomax	Primary	Breast	Naïve	0	0	NA	NA
E13/E14	TMA BR1901	US Biomax	Primary	Breast	Naïve	0	0	NA	NA
A10	TMA101	VUMC	Primary	Breast	Naïve	0	0	5	9
A1	TMA101	VUMC	Primary	Breast	Naïve	0	0	5	9
B9/J7	TMA 11-4-09	VUMC	Primary	Breast	Naïve	0	0	5	5

B1/I10	TMA 11-4-09	VUMC	Primary	Breast	Naïve	0	0	45	70
G11/G12	TMA BR1201a	US Biomax	Primary	Breast	Naïve	0	0	NA	NA
G15/G16	TMA BR1901	US Biomax	Primary	Breast	Naïve	0	0	NA	NA
A1/A2	TMA BR1901	US Biomax	Primary	Breast	Naïve	0	0	NA	NA
A11/A12	TMA BR1901	US Biomax	Primary	Breast	Naïve	0	0	NA	NA
I11/I12	TMA BR1201a	US Biomax	Primary	Breast	Naïve	0	0	NA	NA
H7/H8	TMA BR1201a	US Biomax	Primary	Breast	Naïve	0	0	NA	NA
G9/G10	TMA BR1201a	US Biomax	Primary	Breast	Naïve	0	0	NA	NA
H11/H12	TMA BR1901	US Biomax	Primary	Breast	Naïve	0	0	NA	NA
F5/F6	TMA BR1901	US Biomax	Primary	Breast	Naïve	0	0	NA	NA
B15/B16	TMA BR1901	US Biomax	Primary	Breast	Naïve	0	0	NA	NA
C5/C6	TMA BR1901	US Biomax	Primary	Breast	Naïve	0	0	NA	NA
J3/J4	TMA BR1901	US Biomax	Primary	Breast	Naïve	0	0	NA	NA
A15/A16	TMA BR1901	US Biomax	Primary	Breast	Naïve	0	0	NA	NA
F1/M9	TMA 11-4-09	VUMC	Primary	Breast	Naïve	0	0	10	11
E1/L9	TMA 11-4-09	VUMC	Primary	Breast	Naïve	0	0	15	17
A10	TMA102	VUMC	Primary	Breast	Naïve	0	0	0	0
A2	TMA102	VUMC	Primary	Breast	Naïve	0	0	10	13
B2	TMA102	VUMC	Primary	Breast	Naïve	0	0	0	0
B3	TMA102	VUMC	Primary	Breast	Naïve	0	0	0	0
B5	TMA102	VUMC	Primary	Breast	Naïve	0	0	0	0
A9	TMA102	VUMC	Primary	Breast	Naïve	0	0	5	5
A1	TMA102	VUMC	Primary	Breast	Naïve	0	0	8	8
B4	TMA102	VUMC	Primary	Breast	Naïve	0	0	10	19
A3/A4	TMA102	VUMC	Primary	Breast	Naïve	0	0	20	33
F3/4	TMA2 Mixed	VUMC	Primary	Breast	Naïve	0	0	0	0
G3/4	TMA2 Mixed	VUMC	Primary	Breast	Naïve	0	0	0	0
H7/8	TMA2 Mixed	VUMC	Primary	Breast	Naïve	0	0	5	5
I5/6	TMA2 Mixed	VUMC	Primary	Breast	Naïve	0	0	5	5
G7/8	TMA2 Mixed	VUMC	Primary	Breast	Naïve	0	0	6	8
B1/2	TMA2 Mixed	VUMC	Primary	Breast	Naïve	0	0	11	12
C7/8	TMA2 Mixed	VUMC	Primary	Breast	Naïve	0	0	12	14
J7/8	TMA2 Mixed	VUMC	Primary	Breast	Naïve	0	0	10	19
D7/8	TMA2 Mixed	VUMC	Primary	Breast	Naïve	0	0	25	30
H5/6	TMA2 Mixed	VUMC	Primary	Breast	Naïve	0	0	15	30
K1/2	TMA2 Mixed	VUMC	Primary	Breast	Naïve	0	0	35	35
D9/10	TMA2 Mixed	VUMC	Primary	Breast	Naïve	0	0	30	62
F5/6	TMA2 Mixed	VUMC	Primary	Breast	Naïve	0	0	60	115
C1/H5	TMA2 TNBC	VUMC	Primary	Breast	Naïve	0	0	0	0
F4/K8	TMA2 TNBC	VUMC	Primary	Breast	Naïve	0	0	2	2
A4/G1	TMA2 TNBC	VUMC	Primary	Breast	Naïve	0	0	10	10
D5/I9	TMA2 TNBC	VUMC	Primary	Breast	Naïve	0	0	10	12
D6/I10	TMA2 TNBC	VUMC	Primary	Breast	Naïve	0	0	40	45
B7/8/9	TMA P3	VUMC	Primary	Breast	NAC	90	180	0	0
C9	TMA101	VUMC	Primary	Breast	NAC	75	120	15	21
D7/8/9	TMA P2	VUMC	Primary	Breast	NAC	80	110	5	5
J1/2/3	TMA P2	VUMC	Primary	Breast	NAC	80	100	0	0
E7/8/9	TMA P2	VUMC	Primary	Breast	NAC	90	100	50	95
E1/2/3	TMA P2	VUMC	Primary	Breast	NAC	60	90	0	0
I4/5/6	TMA P1	VUMC	Primary	Breast	NAC	70	80	30	35
F4/5/6	TMA P3	VUMC	Primary	Breast	NAC	45	65	60	120
D7/8/9	TMA P1	VUMC	Primary	Breast	NAC	60	60	20	25
G7/8/9	TMA P3	VUMC	Primary	Breast	NAC	54	60	25	30
A1	Surgical Resection	VUMC	Primary	Breast	NAC	40	60	21	42
A5	Surgical Resection	VUMC	Primary	Breast	NAC	40	55	80	155
J4/5/6	TMA P2	VUMC	Primary	Breast	NAC	52	54	5	5
C7/8/9	TMA P2	VUMC	Primary	Breast	NAC	40	40	20	25
G4/5/6	TMA P2	VUMC	Primary	Breast	NAC	40	40	25	28
A7	Surgical Resection	VUMC	Primary	Breast	NAC	30	40	10	15
A17	Surgical Resection	VUMC	Primary	Breast	NAC	30	40	40	80
C5	TMA101	VUMC	Primary	Breast	NAC	15	40	25	45
G6	Surgical Resection	VUMC	Primary	Breast	NAC	30	40	70	140
E4/5/6	TMA P1	VUMC	Primary	Breast	NAC	30	30	25	30
J4/5/6	TMA P1	VUMC	Primary	Breast	NAC	30	30	0	0
H4/5/6	TMA P1	VUMC	Primary	Breast	NAC	30	30	25	25
F4/5/6	TMA P1	VUMC	Primary	Breast	NAC	30	30	35	65
G1/2/3	TMA P1	VUMC	Primary	Breast	NAC	30	30	40	40
F4/5/6	TMA P2	VUMC	Primary	Breast	NAC	30	30	20	20
I4/5/6	TMA P2	VUMC	Primary	Breast	NAC	30	30	0	0
F7/8/9	TMA P2	VUMC	Primary	Breast	NAC	25	25	10	15
A1/2/3	TMA P3	VUMC	Primary	Breast	NAC	25	25	5	5
H4/5/6	TMA P3	VUMC	Primary	Breast	NAC	20	20	13	16
A4/5/6	TMA P2	VUMC	Primary	Breast	NAC	20	20	0	0
G7/8/9	TMA P1	VUMC	Primary	Breast	NAC	20	20	0	0
H1/2/3	TMA P1	VUMC	Primary	Breast	NAC	20	20	0	0
I7/8/9	TMA P1	VUMC	Primary	Breast	NAC	20	20	5	5

K4/5/6	TMA P1	VUMC	Primary	Breast	NAC	20	20	0	0
D4/5/6	TMA P1	VUMC	Primary	Breast	NAC	20	20	0	0
L4/5/6	TMA P1	VUMC	Primary	Breast	NAC	20	20	0	0
J4/5/6	TMA P3	VUMC	Primary	Breast	NAC	20	20	3	3
G1	Surgical Resection	VUMC	Primary	Breast	NAC	10	20	30	58
J7/8/9	TMA P2	VUMC	Primary	Breast	NAC	15	15	4	5
F7/8/9	TMA P3	VUMC	Primary	Breast	NAC	15	15	5	5
H1/2/3	TMA P3	VUMC	Primary	Breast	NAC	15	15	0	0
A4/5/6	TMA P3	VUMC	Primary	Breast	NAC	15	15	10	10
H1/2/3	TMA P2	VUMC	Primary	Breast	NAC	15	15	20	20
D1/2/3	TMA P3	VUMC	Primary	Breast	NAC	15	15	0	0
F1/2/3	TMA P3	VUMC	Primary	Breast	NAC	15	15	10	10
J1/2/3	TMA P3	VUMC	Primary	Breast	NAC	10	12	8	8
D7/8/9	TMA P3	VUMC	Primary	Breast	NAC	10	10	50	90
C1/2/3	TMA P1	VUMC	Primary	Breast	NAC	10	10	5	5
C4/5/6	TMA P1	VUMC	Primary	Breast	NAC	10	10	5	5
A7/8/9	TMA P1	VUMC	Primary	Breast	NAC	10	10	0	0
J1/2/3	TMA P1	VUMC	Primary	Breast	NAC	10	10	25	36
J7/8/9	TMA P1	VUMC	Primary	Breast	NAC	10	10	0	0
I7/8/9	TMA P2	VUMC	Primary	Breast	NAC	10	10	3	6
A7/8/9	TMA P2	VUMC	Primary	Breast	NAC	10	10	0	0
G7/8/9	TMA P2	VUMC	Primary	Breast	NAC	10	10	5	8
H7/8/9	TMA P2	VUMC	Primary	Breast	NAC	10	10	5	5
B4/5/6	TMA P3	VUMC	Primary	Breast	NAC	10	10	20	20
C4/5/6	TMA P3	VUMC	Primary	Breast	NAC	10	10	20	25
I4/5/6	TMA P3	VUMC	Primary	Breast	NAC	5	10	5	6
D4/5/6	TMA P3	VUMC	Primary	Breast	NAC	10	10	50	85
B7/8/9	TMA P2	VUMC	Primary	Breast	NAC	10	10	10	13
25	TMA9936	VUMC	Primary	Breast	NAC	10	10	0	0
D6	TMA101	VUMC	Primary	Breast	NAC	8	8	15	17
C10	TMA101	VUMC	Primary	Breast	NAC	5	5	8	8
F1/2/3	TMA P1	VUMC	Primary	Breast	NAC	5	5	5	5
E4/5/6	TMA P2	VUMC	Primary	Breast	NAC	5	5	0	0
I1/2/3	TMA P2	VUMC	Primary	Breast	NAC	5	5	7	9
C8	TMA101	VUMC	Primary	Breast	NAC	5	5	18	30
D7	TMA101	VUMC	Primary	Breast	NAC	2	4	5	5
E2	TMA101	VUMC	Primary	Breast	NAC	4	4	35	63
D3	TMA101	VUMC	Primary	Breast	NAC	2	4	12	14
C2	TMA102	VUMC	Primary	Breast	NAC	3	3	40	70
E1	TMA101	VUMC	Primary	Breast	NAC	3	3	18	32
B10	TMA102	VUMC	Primary	Breast	NAC	2	2	13	16
A4	TMA101	VUMC	Primary	Breast	NAC	0	0	0	0
A4/5/6	TMA P1	VUMC	Primary	Breast	NAC	0	0	0	0
K1/2/3	TMA P1	VUMC	Primary	Breast	NAC	0	0	20	25
32	TMA9936	VUMC	Primary	Breast	NAC	0	0	5	9
A3/I1	TMA 11-4-09	VUMC	Primary	Breast	NAC	0	0	0	0
D4/L2	TMA 11-4-09	VUMC	Primary	Breast	NAC	0	0	3	3
A1/2/3	TMA P2	VUMC	Primary	Breast	NAC	0	0	0	0
E4/5/6	TMA P2	VUMC	Primary	Breast	NAC	0	0	5	5
E7/8/9	TMA P2	VUMC	Primary	Breast	NAC	0	0	0	0
H4/5/6	TMA P2	VUMC	Primary	Breast	NAC	0	0	10	12
B1/2/3	TMA P3	VUMC	Primary	Breast	NAC	0	0	5	5
B2	TMA101	VUMC	Primary	Breast	NAC	0	0	85	115
34	TMA9936	VUMC	Primary	Breast	NAC	0	0	0	0
L1/2/3	TMA P1	VUMC	Primary	Breast	NAC	0	0	0	0
K7/8/9	TMA P1	VUMC	Primary	Breast	NAC	0	0	0	0
B4/5/6	TMA P1	VUMC	Primary	Breast	NAC	0	0	0	0
B1/2/3	TMA P1	VUMC	Primary	Breast	NAC	0	0	0	no tissue
E1/2/3	TMA P1	VUMC	Primary	Breast	NAC	0	0	0	0
F7/8/9	TMA P1	VUMC	Primary	Breast	NAC	0	0	15	15
G4/5/6	TMA P1	VUMC	Primary	Breast	NAC	0	0	0	0
I1/2/3	TMA P1	VUMC	Primary	Breast	NAC	0	0	0	0
D1/2/3	TMA P2	VUMC	Primary	Breast	NAC	0	0	10	10
G1/2/3	TMA P2	VUMC	Primary	Breast	NAC	0	0	30	35
A7/8/9	TMA P3	VUMC	Primary	Breast	NAC	0	0	8	8
K7/8/9	TMA P3	VUMC	Primary	Breast	NAC	0	0	0	0
G4/5/6	TMA P3	VUMC	Primary	Breast	NAC	0	0	5	5
E4/5/6	TMA P3	VUMC	Primary	Breast	NAC	0	0	60	90
H7/8/9	TMA P3	VUMC	Primary	Breast	NAC	0	0	0	0
I1/2/3	TMA P3	VUMC	Primary	Breast	NAC	0	0	13	18
G1/2/3	TMA P3	VUMC	Primary	Breast	NAC	0	0	5	5
J7/8/9	TMA P3	VUMC	Primary	Breast	NAC	0	0	5	7
C7/8/9	TMA P1	VUMC	Primary	Breast	NAC	0	0	0	0
E1/2/3	TMA P2	VUMC	Primary	Breast	NAC	0	0	5	5
A13	Surgical Resection	VUMC	Primary	Breast	NAC	0	0	21	42
C1	TMA102	VUMC	Primary	Breast	NAC	0	0	5	8

40	TMA9936	VUMC	Primary	Breast	NAC	0	0	10	13
G4	Surgical Resection	VUMC	Primary	Breast	NAC	0	0	60	110
D2	TMA101	VUMC	Primary	Breast	NAC	0	0	35	55
G7	Surgical Resection	VUMC	Primary	Breast	NAC	0	0	80	165
D4	TMA101	VUMC	Primary	Breast	NAC	0	0	0	0
D5	TMA101	VUMC	Primary	Breast	NAC	0	0	10	10
G2	Surgical Resection	VUMC	Recurrence, Distant Metastasis	Lung	Naïve	80	180	50	135
A4	Surgical Resection	VUMC	Recurrence, Distant Metastasis	Lung	NA	80	130	0	0
A2	Surgical Resection	VUMC	Recurrence, Local	Chest Wall	NA	65	120	10	12
A9	Surgical Resection	VUMC	Recurrence, Local	Skin	NA	50	95	0	0
A8/9	TMA111	VUMC	Recurrence, Distant Metastasis	Brain	NAC	50	70	75	150
A12	Surgical Resection	VUMC	Recurrence, Local	Skin	NA	40	60	25	50
G8	Surgical Resection	VUMC	Recurrence, Distant Metastasis	Lung	NAC	35	45	70	140
G3	Surgical Resection	VUMC	Recurrence, Distant Metastasis	Lung	Naïve	30	40	60	120
F1	Surgical Resection	VUMC	Recurrence, Distant Metastasis	Brain	NAC	30	40	70	150
D11/12	TMA111	VUMC	Recurrence, Distant Metastasis	Brain	Naïve	20	35	30	60
A10/11	TMA111	VUMC	Recurrence, Distant Metastasis	Brain	Naïve	20	35	85	150
A10	Surgical Resection	VUMC	Recurrence, Local	Chest Wall	NA	20	30	20	35
A19	Surgical Resection	VUMC	Recurrence, Local	Chest Wall	NA	20	20	70	125
C1/2	TMA111	VUMC	Recurrence, Distant Metastasis	Brain	Naïve	10	10	15	30
C8/9	TMA111	VUMC	Recurrence, Distant Metastasis	Brain	Naïve	10	10	10	17
A11	Surgical Resection	VUMC	Recurrence, Local	Skin	NA	10	10	40	80
A6	Surgical Resection	VUMC	Recurrence, Local	Skin	NA	10	10	90	200
C3/4	TMA111	VUMC	Recurrence, Distant Metastasis	Brain	Naïve	7	9	15	30
C12/D1	TMA111	VUMC	Recurrence, Distant Metastasis	Brain	Naïve	5	8	30	59
C5/6	TMA111	VUMC	Recurrence, Distant Metastasis	Brain	Naïve	2	6	10	12
B2/3	TMA111	VUMC	Recurrence, Distant Metastasis	Brain	Naïve	5	5	60	105
F3	Surgical Resection	VUMC	Recurrence, Distant Metastasis	Brain	Naïve	0	0	35	75
A3/4	TMA111	VUMC	Recurrence, Distant Metastasis	Brain	Naïve	0	0	25	47
B6/8	TMA111	VUMC	Recurrence, Distant Metastasis	Brain	Naïve	0	0	70	130
C10/11	TMA111	VUMC	Recurrence, Distant Metastasis	Brain	Naïve	0	0	75	140
A5/6	TMA111	VUMC	Recurrence, Distant Metastasis	Brain	Naïve	0	0	80	150
F2	Surgical Resection	VUMC	Recurrence, Distant Metastasis	Brain	NAC	0	0	30	50
D2/3	TMA111	VUMC	Recurrence, Distant Metastasis	Brain	NAC	0	0	55	100
E1/2	TMA111	VUMC	Recurrence, Distant Metastasis	Brain	NAC	0	0	15	22
B11/12	TMA111	VUMC	Recurrence, Distant Metastasis	Brain	NAC	0	0	40	60
F5	Surgical Resection	VUMC	Recurrence, Distant Metastasis	Brain	NA	0	0	30	60
A16	Surgical Resection	VUMC	Recurrence, Distant Metastasis	Lung	NA	0	0	50	110
A1/2	TMA111	VUMC	Recurrence, Distant Metastasis	Brain	NA	0	0	12	19
B4/5	TMA111	VUMC	Recurrence, Distant Metastasis	Brain	NA	0	0	15	20
B9/10	TMA111	VUMC	Recurrence, Distant Metastasis	Brain	NA	0	0	60	125
A8	Surgical Resection	VUMC	Recurrence, Local	Skin	NA	0	0	5	10
A15	Surgical Resection	VUMC	Recurrence, Local	Chest Wall	NA	0	0	60	120
A14	Surgical Resection	VUMC	Recurrence, Local	Chest Wall	NA	0	0	90	180

TMA, tissue microarray
VUMC, Vanderbilt University Medical Center
NAC, neoadjuvant chemotherapy

Table 3. *MYCN* and *MYC* expression and TNBC subtype correlations in breast cancer PDX models

A

	MYC-family isoforms		TNBC subtype		TNBC subtype correlations			
PDX models	***MYCN***	***MYC***	**Primary**	**Secondary**	**BL1**	**BL2**	**M**	**LAR**
TM00089	0.42	94.48	BL2	UNS	-0.21973	0.33605	-0.31315	-0.08316
TM00090	1.22	43.10	LAR	UNS	-0.31497	0.03350	-0.01061	0.05965
TM00096	23.94	47.12	M	UNS	-0.03825	-0.28093	0.33473	0.03649
TM01117	0.20	83.44	UNS	UNS	-0.18411	0.00289	-0.48297	-0.12211
TM01273	2.17	60.64	M	BL1	0.09660	-0.02203	0.43481	-0.17311
TM01278	4.18	53.10	BL2	LAR	-0.26615	0.49817	-0.08718	0.19395

B

	MYC-family isoforms	
PDX models	***MYCN***	***MYC***
CTG-1475	5.35	0.86
CTG-0018	3.32	2.69
CTG-1325	2.89	6.48
CTG-1408	2.83	6.63
CTG-0869	2.52	7.55
CTG-1340	2.53	6.48
CTG-1684	2.85	4.38
CTG-1151	2.09	4.99
CTG-0017	1.85	6.17
CTG-1019	2.82	6.52

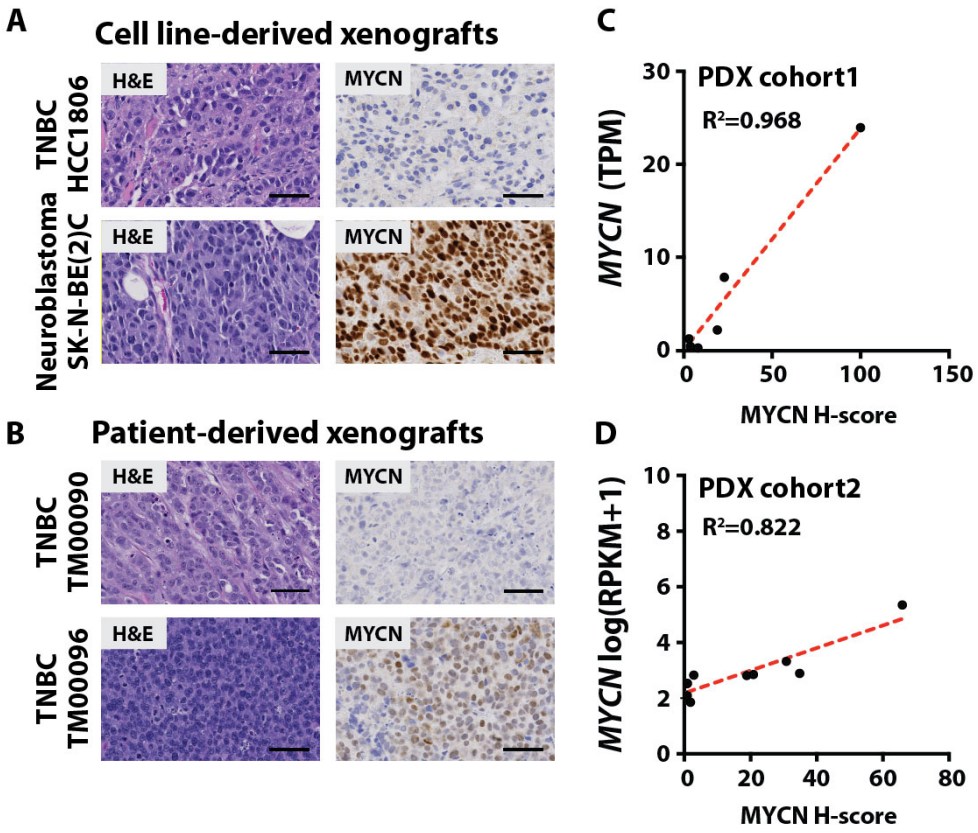

Figure 6. IHC detection of MYCN in cell line- and patient-derived xenograft tissue. (**A-B**) IHC of MYCN using cell line-derived xenografts (CDXs) positive for MYCN (SK-N-BE(2)C) (**A**) and patient-derived xenografts (PDXs) positive for MYCN (TM00096) (**B**). Scale bar, 50 μM. (**C-D**) Analysis comparing gene expression to protein expression (H-score) for MYCN across PDXs from Jackson Laboratory (n=6) (**C**) and Champions Oncology (n=10) (**D**).

characteristics of tumors in the primary, treatment-naïve TNBC cohort. Although the majority of MYCN-expressing tumors were invasive carcinomas, non-special type (NST), a relatively rare form of breast cancer called metaplastic breast cancer (MBC) was enriched for tumors that were considered 'MYCN High' (11%, 2/18), including the top MYCN-expressing case (H-score = 155, Figure 7A). MBCs represent 0.5-5.0% of all invasive breast cancers, typically (>90%) display a triple-negative phenotype, and do not respond well to chemotherapy *(37)*. To explore MYCN expression in MBC further, we analyzed *MYCN* expression in a recently published study investigating gene expression and genetic alterations across a relatively large cohort of metaplastic TNBC tumors (n=17) *(353)*. Whereas 11.5% of all TNBC cases from TCGA (BRCA) demonstrated elevated *MYCN* expression (>12 TPM; Figure 4C), 35.3% (6/17) of metaplastic TNBC expressed *MYCN* at similar levels (Figure 7B), indicating an enrichment for elevated *MYCN* expression in metaplastic TNBC.

To expand on these analyses and evaluate MYCN protein expression within the metaplastic disease, we performed MYCN IHC on 15 metaplastic TNBC cases with different histological features (spindle cell, mesenchymal, squamous, and adenosquamous) curated at VUMC (Figure 7C). Similar to differences in *MYCN* gene expression between all TNBC and metaplastic TNBC, a greater percentage of metaplastic TNBC contained elevated MYCN expression [H-score >30, 73% (11/15)] (Figure 7, C and D). MYCN expression was observed across all metaplastic tissue types, with tumors of spindle cell morphology being among the top expressers (Figure 7, C and D). Of note, the majority of neoadjuvant chemotherapy (NAC)-treated metaplastic TNBC contained MYCN expression, suggesting either MYCN expression was induced or pre-existing

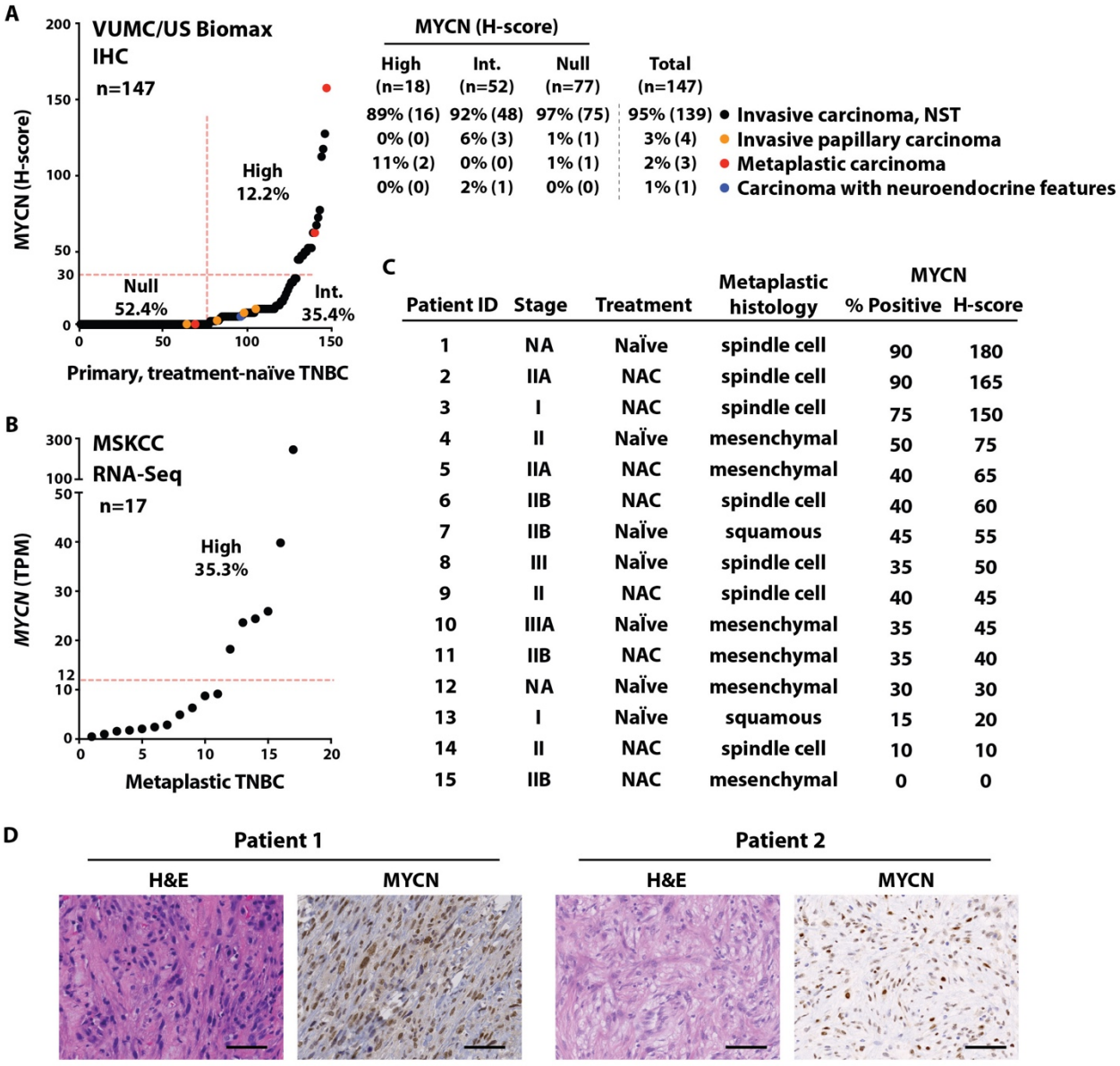

Figure 7. *MYCN* RNA and MYCN protein expression in metaplastic triple-negative and HER2+ breast cancer. (**A**) MYCN H-scores for primary, treatment-naïve TNBC colored according to histological subtype [invasive carcinoma, NST (black), invasive papillary carcinoma (orange), metaplastic carcinoma (red), and carcinoma with neuroendocrine features (blue)]. Quadrants in graph contain the percentage of cases that are MYCN high (H-score >30), intermediate (Int; H-score <30, >0), or null (H-score=0), with percentages also calculated per histological subtype on right. NST, non-special type. (**B**) *MYCN* expression (TPM) in metaplastic TNBC (n=17) *(353)* (**C**) Histological subtypes with metadata and associated MYCN H-scores for 15 metaplastic breast cancer cases curated at VUMC. NA, not available. NAC, neoadjuvant chemotherapy. (**D**) Representative H&E and MYCN IHC images for the top two metaplastic TNBC cases. Scale bar, 50 μM.

MYCN-expressing tumor cells persisted in TNBC cell populations (Figure 7, C and D). These data further characterize a subtype of breast cancer currently associated with a poor prognosis and highlights the presence of MYCN-expressing cells after chemotherapy.

Increased fraction of MYCN-expressing cells in residual TNBC after neoadjuvant chemotherapy

Due to the lack of therapeutic targets in TNBC, patients are primarily treated with combination chemotherapy and less than 30% of patients achieve a pathological complete response (pCR) after NAC *(354, 355)*. Patients with residual disease after NAC exhibit poor overall survival due to an enrichment of chemotherapy-resistant tumor cells and a lack of subsequent therapeutic options *(322, 356)*. To evaluate MYCN expression in residual tumor cells after NAC, we performed IHC for MYCN on a primary TNBC cohort (n=115) comprised of residual disease surgically resected after NAC *(321)* (Figure 8A and Table 4A). MYCN expression was significantly (p=0.001) higher in the post-NAC-treated TNBC cohort (Figure 8B and Table 4B) compared to cases in the treatment-naïve TNBC cohort (Figure 4C), with 65% vs. 45% of cases having an H-score greater than zero (Figure 8, A and B, and Table 4B). The majority (90%) of patients in the NAC-treated TNBC cohort had stage III disease at the time of diagnosis, while the treatment-naïve cohort consisted primarily of patients with stage I (11%) and stage II (70%) disease (Table 4A). To remove a potential bias due to differences in clinical stage between cohorts, we restricted the comparison of MYCN expression to tumors from patients with stage III disease from each cohort; MYCN expression (H-score >0) remained significantly

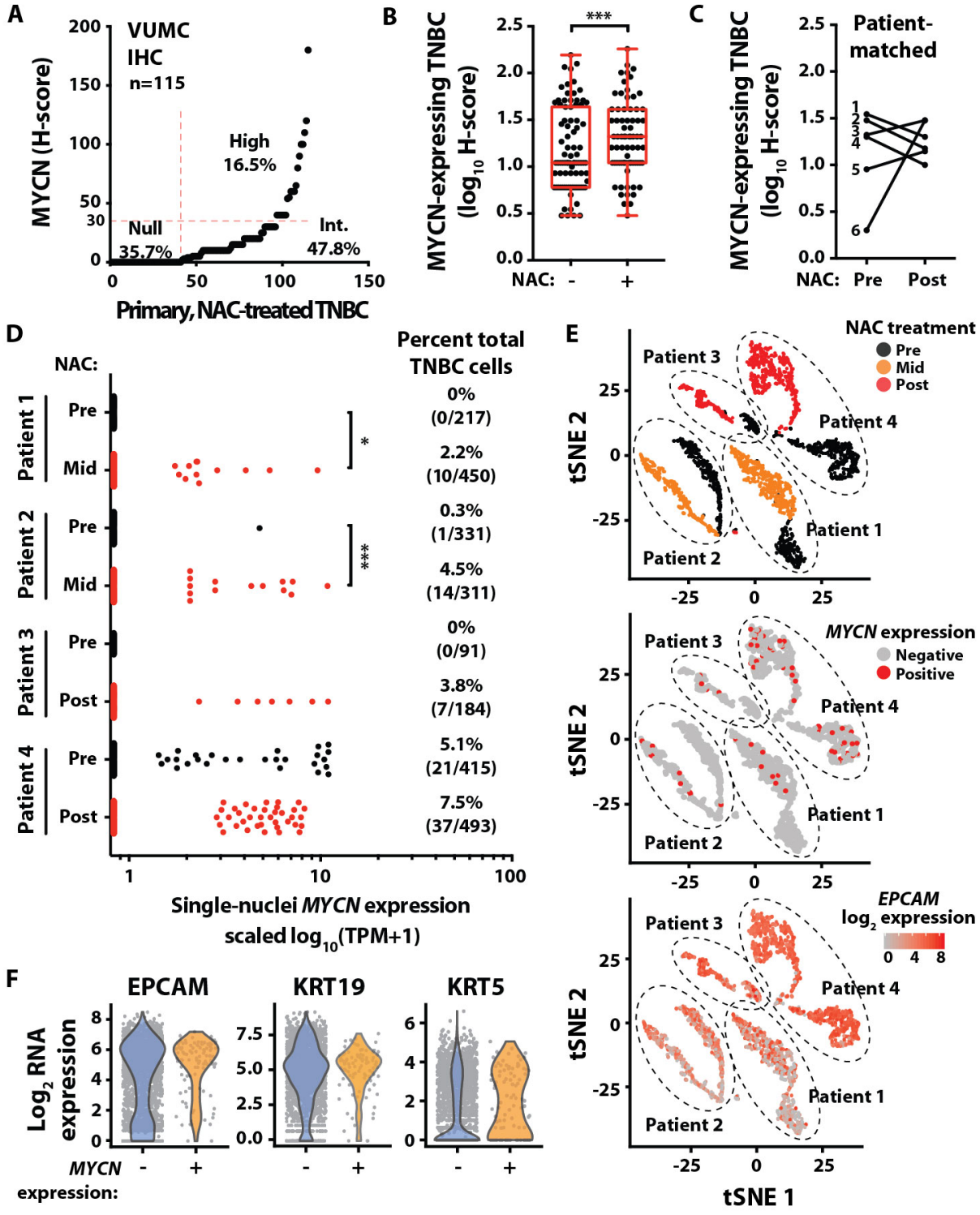

Figure 8. Increased percentage of MYCN-expressing cells in residual disease after neoadjuvant chemotherapy. (**A**) MYCN H-scores in residual disease from 115 primary, NAC-treated TNBC (source: VUMC). Int., intermediate, H-score >0 to ≤30. High, H-score >30.

(**B**) Box plot showing MYCN H-scores in primary, treatment-naïve TNBC cases (n=191, see Fig. 1B) compared to residual disease from primary, NAC-treated TNBC cases (n=115, see Fig. 2A). Mann Whitney t-test, ***p= 0.0001. (**C**) MYCN protein levels (H-scores) in patient-matched TNBC cases pre- and post-NAC (see table S5C for treatments and patient characteristics). (**D**) *MYCN* expression from single-nuclei RNA sequencing (SNRS) of dissociated primary, treatment-naïve TNBC before (Pre, pre-treatment), after two cycles (Mid, mid-treatment) of docetaxel and epirubicin, or after the mid-treatment regimen plus four additional cycles (Post, post-treatment) of docetaxel and epirubicin in combination with bevacizumab *(322)*. Percentages above represent quantification of *MYCN*-expressing cells per sample. Fisher exact test, *p<0.05, ***p<0.001. (**E**) t-SNE plots of SNRS from patient-matched TNBC tumor samples described in part D. Top: Patient treatment groups [pre-treatment cells (black), mid NAC-treated cells (orange), post NAC-treated cells (red)]. Middle: Distribution of *MYCN*-expressing cells [*MYCN*-negative (TPM=0, grey), *MYCN*-positive (TPM>0, red)]. Bottom: Heatmap of *EPCAM* expression. (**F**) Violin plots of *EPCAM*, *KRT19*, and *KRT5* expression in *MYCN*-expressing and non-expressing cells.

(p=0.014) higher in the residual disease of patients after NAC treatment (65%, 54/83) compared to cases from patients who were treatment-naïve (40%, 10/25) (Table 4B). Since the primary treatment-naïve and NAC-treated TNBC cohorts were independently assembled, we examined MYCN expression levels in patient-matched TNBC before and after NAC treatment (n=6) (Figure 8C). Compared to MYCN levels before treatment, MYCN protein expression was elevated or within a similar range post-NAC, demonstrating MYCN-expressing cells remained after treatment (Figure 8C and Table 4C).

To further investigate the distribution of MYCN expression across individual cells during NAC treatment, we analyzed previously published high-throughput single-nucleus RNA- sequencing (SNRS) data from patient-matched TNBC before and after NAC treatment *(322)*. Tumor core biopsies were taken prior to treatment (pre-treatment) and again after two cycles (mid-treatment) of NAC treatment [epirubicin (anthracycline) and docetaxel (taxane)], or after the mid-treatment regimen plus an additional four cycles (post- treatment) of NAC treatment [epirubicin and docetaxel in combination with

Table 4. Primary, treatment-naïve and NAC-treated TNBC patient characteristics

A

	Treatment-naïve	NAC-treated
Total number of cases	**191**	**115**
Age (n)	**140**	**106**
Mean age (range)	53 (30-87)	48 (24-78)
Stage (n)	**140**	**92**
IA,B	16 (11.4%)	1 (1.1%)
IIA,B	98 (70.0%)	8 (8.7%)
IIIA,B,C	26 (18.6%)	83 (90.2%)
Neoadjuvant anthracycline (n)		**112**
Yes		95 (84.8%)
No		17 (15.2%)
Neoadjuvant taxane (n)		**112**
Yes		65 (58.0%)
No		47 (42.0%)

B

Primary TNBC		MYCN-expressing cases (H-score>0)	Total cases	Percent total	p-value
All Stages	**Treatment-naïve**	86	191	45	**0.001**
	NAC-treated	74	115	64	
Stage III	**Treatment-naïve**	10	25	40	**0.014**
	NAC-treated	54	83	65	

C

Matched-pair	Age	Stage	Treatment (cycles)
Pt 1	46	IIIB	Anthracycline/cyclophosphamide (4), paclitaxel (2)
Pt 2	37	IIIA	Fluorouracil/anthracycline/cytoxan (5), paclitaxel (2)
Pt 3	38	IIIB	Anthracycline/cyclophosphamide (4), paclitaxel (2)
Pt 4	30	IIIB	Anthracycline (unknown)
Pt 5	46	IIIB	Anthracycline/cyclophosphamide (unknown)
Pt 6	33	IIIC	Anthracycline/cyclophosphamide (4)

bevacizumab (angiogenesis inhibitor)] *(322)*. Approximately 400 single nuclei from each patient-matched sample were isolated for RNA-sequencing *(322, 357)*. The percentage of *MYCN*-positive cells identified from single-nuclei *MYCN* transcripts increased from pre-treatment samples to residual disease collected mid- or post-NAC treatment for each patient [Patient 1: 0% to 2.2% (p=0.0353); Patient 2: 0.3% to 4.5% (p=0.0003); Patient 3: 0% to 3.8%; Patient 4: 5.1% to 7.5%] (Figure 8D). Dimensionality reduction using t-SNE was performed on single-nuclei expression from pretreatment and NAC-persistent samples to identify expressing *MYCN* cell types (Figure 8E). Cells from each patient clustered independently from each other and there was a separation between pretreatment and NAC-persistent cells (Figure 8E). *MYCN*-expressing and non-expressing cells resided within the same cluster, which contained elevated levels of the epithelial cell marker, EPCAM, indicating the majority of cells sequenced were of tumor cell origin (Figure 8E). By analyzing markers of epithelial (*KRT8*, *KRT18*, *KRT19*, *KRT5*, *KRT14*, and *EPCAM*), immune (*CD4*, *CD8A*, *CD8B*, *CD19*, and *MS4A1*), fibroblast (*PTPRC*, *ACTA1*, *CAV1*, and *FAP*), endothelial (*PECAM1* and *CD34*), and neuroendocrine (*CHGA*, *SYP*, *ENO2*, and *NCAM1*) cells *(322)*, we found *MYCN*-expressing cells were predominantly epithelial and had a similar distribution of epithelial cell marker expression to non-*MYCN*-expressing cells (Figure 8F and Figure 9). Together, MYCN-expression was increased in bulk tumor (IHC) and individual tumor cells (SNRS) post-NAC, further suggesting either pre-existing MYCN-expressing tumor cells persisted in TNBC cell populations or MYCN expression was induced after chemotherapy.

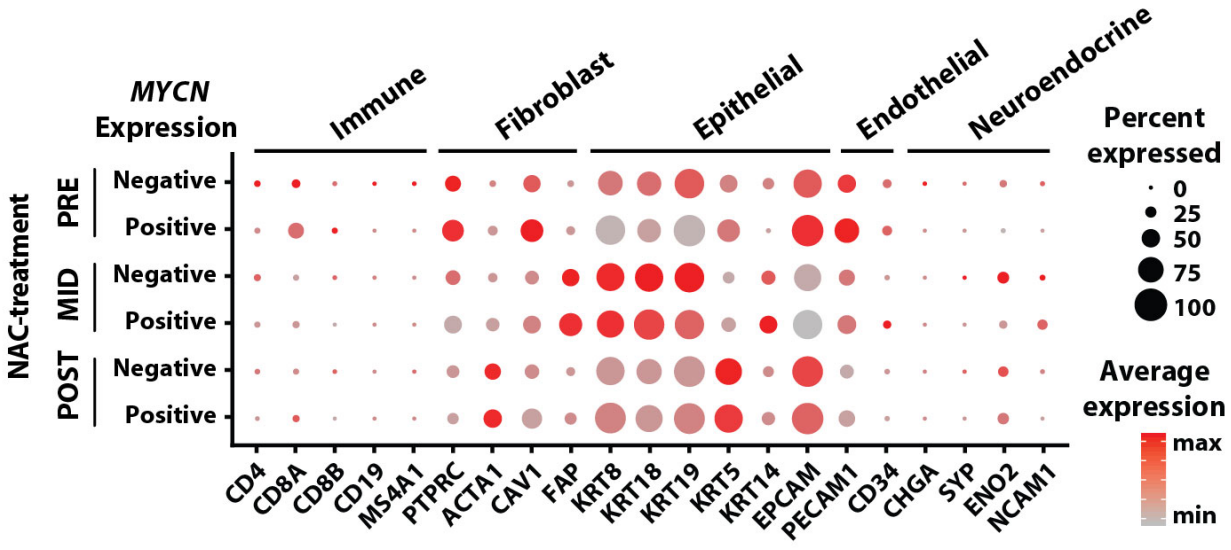

Figure 9. Features of *MYCN*-expressing and non-expressing cells from TNBC tumors before and after NAC treatment. Average expression and distribution of immune (CD4, CD8A, CD8B, CD19, and MS4A1), fibroblast (PTPRC, ACTA1, CAV1, and FAP), epithelial (KRT8, KRT18, KRT19, KRT5, KRT14, and EPCAM), endothelial (PECAM1 and CD34), and neuroendocrine (CHGA, SYP, ENO2, and NCAM1) cell markers across pretreated and NAC-treated TNBC samples *(322)* grouped according to if the cells do (TPM>0, Positive) or do not (TPM=0, Negative) express *MYCN*. The relative sphere size and color represent percentage of cells that express a given cell marker and their relative expression levels, respectively.

Primary and metastatic TNBC display heterogeneous MYCN and MYC protein expression

Despite better initial responses to NAC in TNBC compared to the other breast cancer subtypes, patients with TNBC experience higher rates of relapse and worse overall survival in the metastatic setting *(354)*. Given that nearly all women with metastatic TNBC ultimately die of their disease (36), we evaluated *MYCN* expression in the context of disease recurrence. We analyzed the TNBC cases from a recent study (37) evaluating transcriptional changes between primary and metastatic breast cancer (Figure 10). *MYCN* levels were elevated or similarly expressed in nearly all metastatic specimens compared to matched primary TNBC, and *MYCN* was expressed at all metastatic sites evaluated [adrenal gland, lymph node, liver, lung, chest (chest wall, rib, pleura, mediastinum), neural (brain, spine), kidney, skin] (Figure 10). Similarly, we performed MYCN IHC on 10 locally recurrent (five chest wall and five skin) and 28 metastatic (five lung and 23 brain) surgically resected TNBC tumors and detected MYCN protein expression (H-score >0) in 55% (21/38) of the recurrent TNBC tumors analyzed [lung: 80% (4/5); skin: 80% (4/5); chest wall: 60% (3/5); brain: 43% (10/23)] (Figure 11A and Table 2).

Since *MYCN*-expressing TNBC cell populations are thought to seed metastatic lesions, then expand and differentiate into high *MYC*-expressing proliferative tumors *(261)*, we investigated the relationship between MYC-family isoforms (MYCN and MYC) in both primary and recurrent TNBC. We performed MYC IHC on tissue representing each of our TNBC patient cohorts [primary, treatment-naïve TNBC (Figure 4C); primary, NAC-treated TNBC (Figure 8A); and recurrent TNBC (Figure 11A)] previously analyzed for MYCN. Thirty-four percent (29/86) of primary, treatment-naïve TNBC; 49% (56/114) of

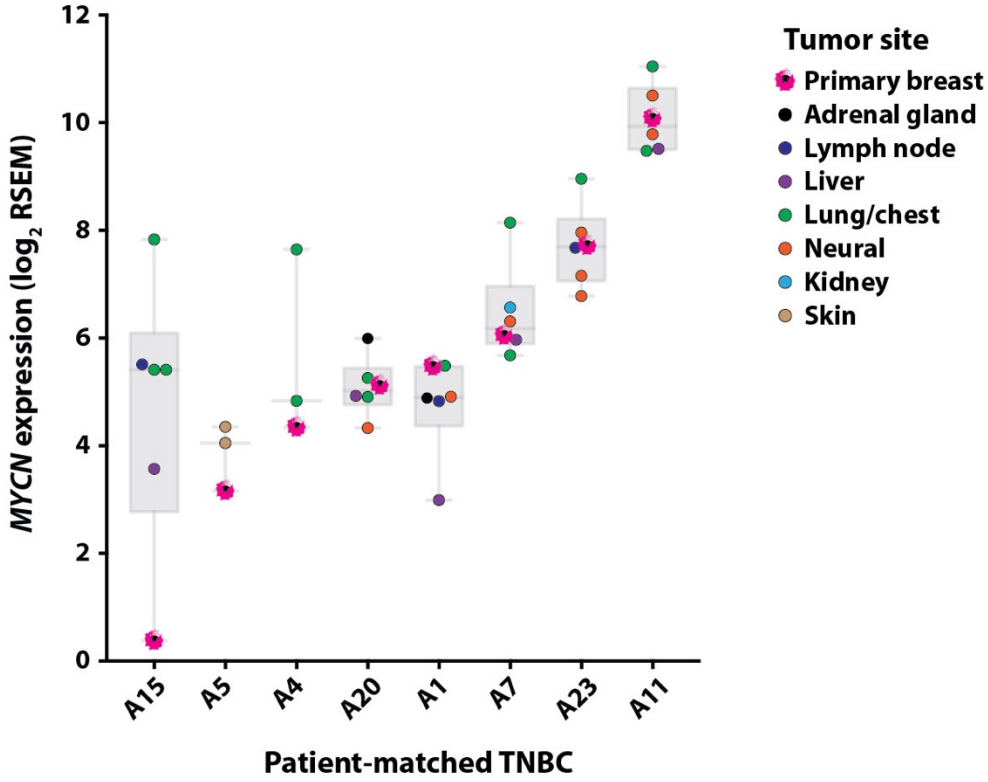

Figure 10. *MYCN* expression in primary TNBC and patient-matched metastases. *MYCN* expression (RSEM) in primary TNBC (pink) and patient-mached metastatases [adrenal gland (black), lymph node (dark blue), liver (purple), lung/chest (green), neural (orange), kidney (light blue), and skin (beige)] *(320)*. Chest = chest wall, rib, pleura, mediastinum. Neural = brain, spine.

primary, NAC-treated TNBC; and 50% (19/38) of recurrent TNBC expressed both MYC-family isoforms (Figure 11B). *MYCN* and *MYC* can be expressed both spatially and temporally in a mutually exclusive manner during normal tissue development *(358)*; thus, we assessed the distribution of these proteins in individual cells within a given tumor section using dual MYC-family isoform tyrosine signal-amplified immunofluorescence (TSA-IF). We found that both MYCN and MYC were heterogeneously expressed in tumor cells throughout the sections, and the majority of cell nuclei robustly expressed only one MYC family member (Figure 11C). These data demonstrate the cell-to-cell heterogeneity of MYC-family isoform expression in TNBC and the dynamic distribution of expression of these oncogenes at both primary and metastatic sites.

Preclinical models of MYCN-expressing TNBC

To identify MYCN-expressing TNBC cell line models for preclinical evaluation, we assessed *MYCN* expression across TNBC cell lines in the Cancer Cell Line Encyclopedia (CCLE) *(359)*. CAL-51 and MDA-MB-468, M- and BL1-subtype TNBC cell lines respectively *(97)*, both established from pleural effusions *(360, 361)*, displayed the highest levels of *MYCN* transcript (Figure 12A). These results are consistent with our findings that M- and BL1-subtype TNBC tumors had higher *MYCN* expression (Figure 5, C-E), and MYCN was elevated in TNBC lung and chest metastases (Figure 10 and Figure 11A). Given that TNBC clinical specimens displayed heterogenous MYCN and MYC expression (Figure 11C), we evaluated if this heterogeneity existed within TNBC cell line models. We adapted our TSA-IF staining procedure used on FFPE tumor sections to cells fixed *in situ* after growth as adherent cultures and analyzed cellular MYCN and MYC

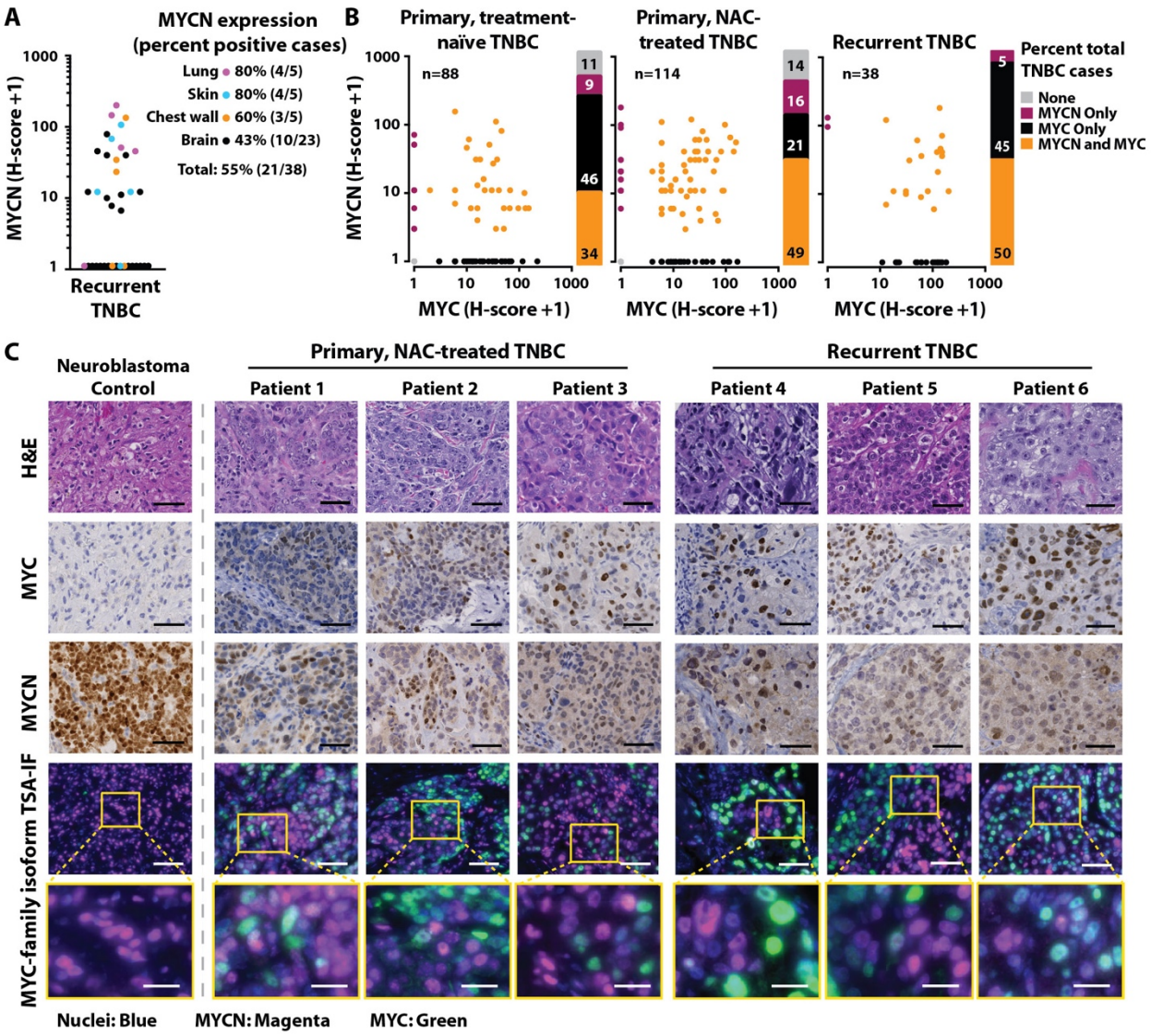

Figure 11. Intratumoral heterogeneity of MYCN and MYC expression in TNBC. (**A**) MYCN H-scores from 38 recurrent TNBC cases with quantification of percent positive cases (H-score >0) for each site of recurrence, labeled by color [lung (magenta), skin (blue), chest wall (orange), brain (black)]. (**B**) MYCN and MYC H-scores for each of the 88 primary, treatment-naïve; 114 primary, NAC-treated; and 38 recurrent TNBC cases. Stacked bar graph represents quantification of TNBC cases positive (H-score >0) for each MYC-family isoform [alone (MYCN Only, MYC Only); both isoforms (MYCN and MYC); or neither isoform (None)]. (**C**) Representative hematoxylin and eosin (H&E), IHC, and TSA-IF stains of MYCN and MYC in primary and recurrent TNBC. The dotted line separating a *MYCN*-amplified neuroblastoma positive control from TNBC cases represents the same exposure times for all samples but a diminished brightness adjustment for MYCN in the NB control due to over-expression of MYCN. Tumor images do not represent serial sections. Scale bar, 50 μM (top four rows), 20 μM (bottom row).

expression within the CAL-51 and MDA-MB-468 cell populations. Individual cells in either cell line culture robustly expressed either nuclear MYCN or MYC (Figure 13A), consistent with observed MYC-family isoform heterogeneity in clinical specimens (Figure 11C). To further evaluate the biological characteristics of MYCN-expressing tumor-derived cells, we isolated single cells from the CAL-51 parental cell line and generated clonally-derived cell lines. Individual clones displayed varying levels of MYCN and MYC protein expression, with 6% (2/33) of cells exhibiting elevated MYCN expression (Figure 13B). MYCN and MYC protein levels were consistent with *MYCN* and *MYC* transcript levels in six of the clonal cell lines evaluated (Cln3, Cln5, Cln8, Cln15, Cln37, Cln39; Figure 12, B and C), and individual MYC-family isoform RNA and protein levels were expressed at higher levels in the clonal lines as compared to the CAL-51 cell population (Figure 12, B and C). Thus, the CAL-51 cell line is composed of a heterogeneous population of cells with varying levels of MYC-family isoform expression.

CAL-51 cells harbor an activating *PIK3CA* mutation (E542K) and their growth is dependent on PI3K pathway signaling *(362)*. Given the frequent evolution of tumor cell drug-resistance in response to PI3K-targeted cancer therapies *(363)*, we hypothesized that MYCN-expressing cells in the CAL-51 population (Figure 13, A and B) would have a growth advantage under selective pressure with PI3K inhibitor (PI3Ki) treatment. To test this hypothesis, we treated CAL-51 with increasing concentrations of the PI3Ki, taselisib (GDC-0032), over time to generate PI3Ki-resistant cells (CAL-51^{PI3KiR}). After six months, single cells from CAL-51^{PI3KiR} were isolated to generate clonally-derived PI3Ki-resistant cell lines. To determine if the individual CAL-51^{PI3KiR} clonal cell lines displayed durable resistance to PI3Ki, we treated CAL-51^{PI3KiR} cells with taselisib or another PI3Ki, pictilisib

A

TNBC cell lines	MYC-family isoforms (RNA-seq Z-scores)	
	MYCN	*MYC*
CAL-51	1.63	3.20
MDA-MB-468	1.42	5.25
DU4475	1.06	3.87
HCC-1187	0.78	5.58
MDA-MB-453	0.38	4.74
HCC-1143	0.18	6.49
MDA-MB-436	-1.35	5.73
HDQP1	-3.45	4.36
MDA-MB-157	-3.72	4.09
MDA-MB-231	-3.89	5.03
HCC-1937	-4.39	4.71
CAL-851	-4.97	4.81
HCC-38	-5.03	4.22
BT-20	-5.26	4.54
CAL-148	-5.48	6.05
HCC-1806	-5.61	4.81
HCC-1599	-5.86	7.83
HCC-70	-6.54	4.66
HCC-1395	-6.94	5.36
BT-549	-7.64	5.27
HS-578-T	-8.25	4.91
CAL-120	-13.00	6.38

B

CAL-51 cell lines	MYC-family isoforms (TPM)	
	MYCN	*MYC*
Parental population	18.82	17.60
Clone 3	0.00	75.23
Clone 5	0.03	87.66
Clone 15	92.88	13.38
Clone 8	93.11	2.34
Clone 37	109.06	1.11
Clone 39	127.49	0.95

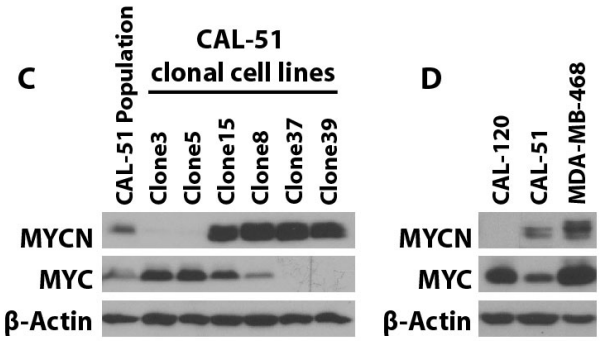

Figure 12. *MYCN* and *MYC* expression in TNBC cell populations and CAL-51 clonally-derived cell lines. (**A**) *MYCN* and *MYC* expression (RNA-Seq) in 22 TNBC cell lines from the Cancer Cell Line Encyclopedia (CCLE). (**B**) RNA (TPM) and (**C**) immunoblot analyses for MYCN and MYC in the CAL-51 parental cell population and the indicated six CAL-51 clonally-derived cell lines. (**D**) Immunoblot analysis for MYCN, MYC, and β-Actin in the indicated TNBC cell lines.

(GDC-0941), after the lines were cultured for two weeks in the absence of drug (a “drug holiday”). Five of the seven CAL-51^{PI3KiR} clonal cell lines maintained resistance to PI3K inhibition, whereas two of the lines had reverted to a PI3Ki-sensitive state (Figure 13C). CAL-51^{PI3KiR} clonal cell lines were evaluated for MYC-family isoform expression and those lines that had acquired durable resistance to PI3Ki also displayed higher MYCN protein expression (compare Figure 13C to 13D). In contrast to 6% (2/33) of the parental clonal cell lines, the majority (86%, 12/14) of CAL-51^{PI3KiR} clonal cell lines expressed MYCN (Figure 13D), suggesting that MYCN expression conferred a selective growth advantage to CAL-51 cells under the continuous selective pressure of PI3Ki treatment.

To evaluate MYC-family isoform expression within CAL-51 and MDA-MB-468 *in vivo*, both parental lines were grown in mice as CDXs. While MYC expression was not detected in the CAL-51 CDX, MYCN-expressing cells were present in both CAL-51 and MDA-MB-468 CDXs (Figure 14A). Similarly, after growth for 14 days in non-adherent forced suspension cultures, MYC expression was lost in CAL-51 and MYCN levels increased in both CAL-51 and MDA-MB-468 (Figure 14B). Given that MYCN-expressing circulating tumor cell clusters have been found in the bloodstream of patients with breast cancer *(347)*, we explored the relationship between differential MYC-family isoform expression and tumor cell growth in non-adherent cultures at the clonal level. To do this, we compared the proliferation of two CAL-51 MYCN^{Low} (MYC-expressing) and MYCN^{High} cell lines in adherent and non-adherent (forced suspension) culture settings. While all four lines grew robustly as adherent cultures (doubling rate: 14-21 hours), only the MYCN^{High} cell lines retained the ability to proliferate when grown in forced suspension (Figure 14C). Further, all MYCN^{High} cell lines (n=10) tested grew and remained metabolically active over

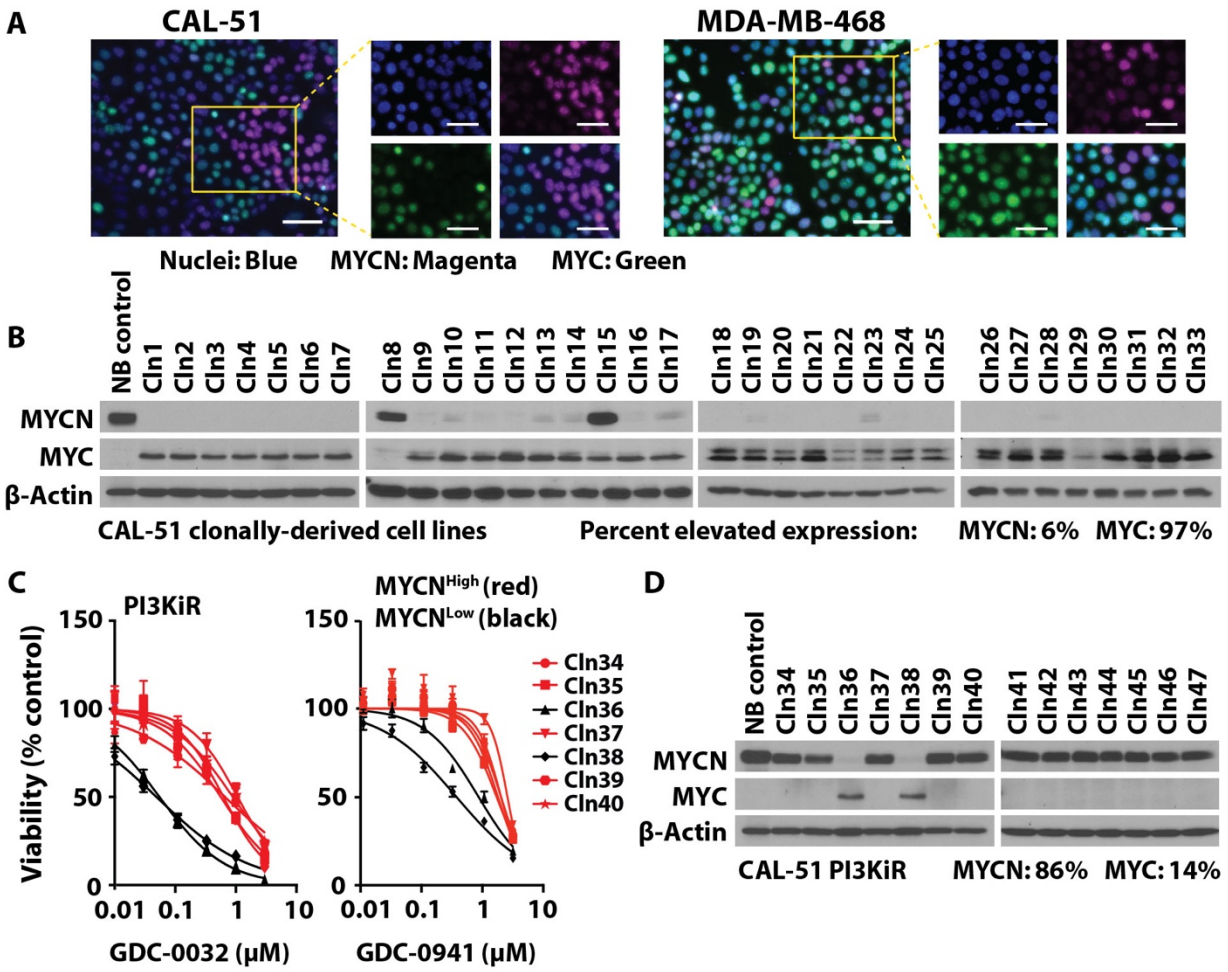

Figure 13. Evaluation of MYCN and MYC expression in TNBC cell lines models. (**A**) Representative TSA-IF stains of MYCN and MYC in the CAL-51 and MDA-MB-468 TNBC cell lines. Colors represent cell nuclei (blue), MYCN (magenta), and MYC (green). Scale bar, 50 μM for overlay fluorescence images at 20X magnification (left panel per cell line), 20 μM for individual fluorescence images at 40X magnification (right panels per cell line). (**B**) Immunoblot analysis of MYCN, MYC, and β-Actin in the indicated 33 clonally-derived cell lines established from CAL-51. NB control, MYCN-amplified SK-N-BE(2)C cell lysate. (**C**) Viability of PI3Ki-resistant (PI3KiR) CAL-51 clonally-derived cell lines after treatment with a dose-escalation of GDC-0032 or GDC-0941 for 72 hours. Black- and red-colored dose-response curves represent the indicated $MYCN^{Low}$ and $MYCN^{High}$ clonally-derived cell lines, respectively. Data shown represent the means ± standard error mean (SEM). (**D**) Immunoblot analysis of MYCN, MYC, and β-Actin in the 14 indicated CAL-51^{PI3KiR} clonally-derived cell lines.

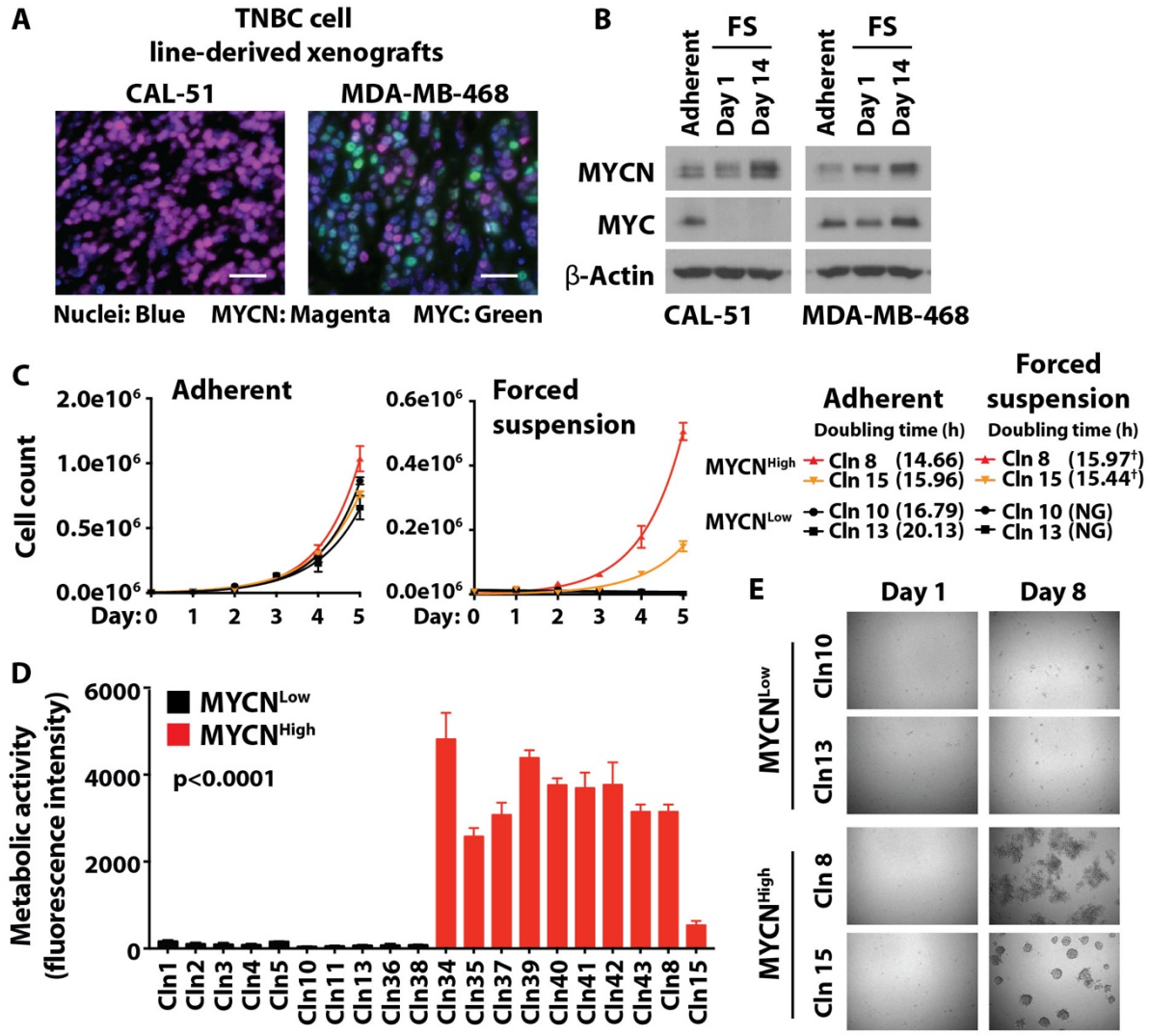

Figure 14. Evaluation of MYCN-expressing TNBC cell line growth properties. (**A**) Representative TSA-IF stains of MYCN and MYC in the CAL-51 and MDA-MB-468 TNBC cell line-derived xenografts. Colors represent cell nuclei (blue), MYCN (magenta), and MYC (green). Scale bar, 20 μM. (**B**) Immunoblot analysis of MYCN, MYC, and β-Actin in the indicated TNBC cell lines after one and eight in forced suspension (FS) compared to adherent cultures. (**C**) Proliferation assays of the two indicated $MYCN^{Low}$ and $MYCN^{High}$ cell lines in adherent and forced-suspension cultures over a five-day time course. Data shown represent the means ± SEM. NG, no growth. †Doubling rate was calculated between day one and five for adherent cells and between day three and five for forced-suspension cells due to a latency in initial proliferation in suspension. (**D**) Brightfield images of the two indicated $MYCN^{Low}$ and $MYCN^{High}$ cell lines after one and eight days in forced-suspension culture. (**E**) Metabolic activity as measured by alamarBlue for the indicated 10 $MYCN^{Low}$ and $MYCN^{High}$ cell lines after eight days in forced-suspension culture. Data shown represent the means ± SD of three biological replicates. Generalized linear mixed model for continuous outcome was used to determine statistical differences between $MYCN^{Low}$ and $MYCN^{High}$ cell line groups, $p<0.0001$.

eight days in forced suspension compared to little, if any, growth of the $MYCN^{Low}$ (MYC-expressing) cell lines (n=10, p<0.0001) (Figure 14, D and E). These data demonstrate that unlike MYC-expressing cells, MYCN-expressing cells from either CAL-51 or MDA-MB-468 possessed the ability to grow and proliferate in adherent as well as non-adherent culture systems and provide the rationale to evaluate MYCN in the context of patient survival.

Disease/progression-free and overall survival for $MYCN^{High}$ and $MYCN^{Low}$ TNBC

Given that MYCN-expressing cells from our TNBC cell line models grew in non-adherent culture conditions (Figure 14) and *MYCN* expression was detected in both primary and metastatic TNBC (Figure 10), we evaluated *MYCN* expression in relation to patient survival. We used the TNBC587 dataset to analyze disease/progression-free and overall survival of patients with TNBC that had either positive (*MYCN* High) or negative (*MYCN* low) median-centered log_2 normalized *MYCN* expression. Consistent with previous studies that correlate MYCN expression in breast cancer with unfavorable prognostic features and clinical outcomes *(260, 261, 346)*, a greater percentage of patients (60% versus 50%) relapsed if their tumor contained elevated *MYCN* expression. They also experienced a shorter time to progression (TTP) compared to patients with *MYCN* low TNBC (p=0.0355, Figure 15A); and, although the 15-year overall survival between cohorts was similar, patients with *MYCN* high tumors succumbed to their disease quicker than patients with *MYCN* low tumors (Figure 15A). Similar results were observed by evaluating patient disease/progression-free and overall survival from our primary and metastatic TNBC cohorts, on which we performed IHC (Figure 15, B and C).

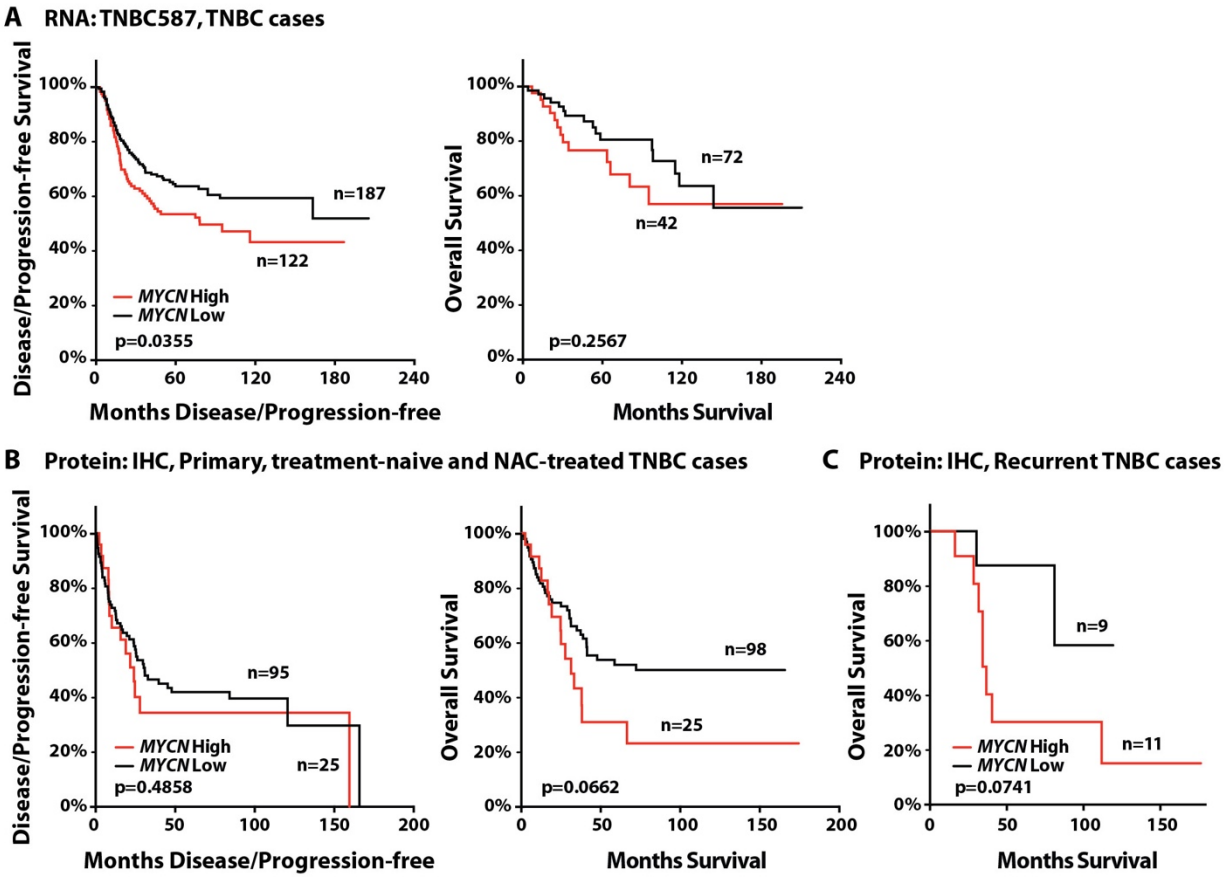

Figure 15. Disease/progression-free and overall survival for *MYCN*^{High} and *MYCN*^{Low} TNBC. (**A**) Left panel: Disease/progression-free survival and Right panel: Overall survival for patients with *MYCN*^{High} versus *MYCN*^{Low} TNBC in the TNBC587 dataset. *MYCN* High, median centered log_2 normalized expression >0; *MYCN* Low, median centered log_2 normalized expression <0. (**B**) Left panel: Disease/progression-free survival and Right panel: Overall survival for patients in the primary, treatment-naïve and NAC-treated TNBC IHC cohorts. *MYCN* High, H-score>30 (>1 SD above the mean); *MYCN* Low, H-score<30. (**C**) Overall survival for metastatic cases in the recurrent TNBC IHC cohort: *MYCN* High, H-score>30; *MYCN* Low, H-score<30.

Although additional cases were needed to reach significance, patients with elevated MYCN-expressing tumors (H-score >30) tended to experience a worse overall survival compared to patients with low (H-score <30) MYCN-expressing tumors (p=0.0662-0.0741; Figure 15, B and C).

Discussion

The lack of therapeutically targetable, high-frequency "driver" alterations across TNBC creates a challenge for developing strategies to treat patients with TNBC. Herein, we evaluate the occurrence of MYCN expression, a transcription factor recently associated with increased stemness, EMT, survival, and dormancy phenotypes in TNBC cells *(261)*. Through the use of IHC, we assessed MYCN protein expression in several TNBC patient cohorts, comprised of both primary tumors and metastatic disease, and report that a significant fraction (45-64%) of tumors heterogeneously express MYCN, including enrichment in a rare histological TNBC subtype (MBC) that is associated with chemotherapy recalcitrance *(38)*. Further, MYCN-expressing cells are present in residual disease after NAC treatment, as shown through both single-nuclei RNA-Seq and protein detection. MYCN expression was also expressed at a higher percentage in a TNBC cell line after acquired resistance to PI3Ki. These data suggest that induction or maintenance of MYCN expression confers a survival advantage for cells treated with compounds that target microtubule structure (taxanes), induce DNA damage (anthracyclines), or cause metabolic stress (PI3Ki). NE prostate cancer, a tumor type considered to be driven by MYCN expression *(364)*, is associated with castration- and androgen inhibitor-resistance and a poor prognosis *(364, 365)*. Unlike *MYCN*-amplified NB, AML, and GBM, which are

tumors that have retained a same-cell lineage, NE prostate cancers are thought to have differentiated from castration-resistant adenocarcinoma prostate cancer through MYCN-mediated mechanisms and lineage switching *(344, 366)*. Herein, we found *MYCN* transcript levels in primary, treatment-naïve TNBC to be comparable to *MYCN* expression in NE-CRPC, suggesting MYCN-expressing TNBC could represent a similar altered differentiation state, which could be investigated further.

In addition to TNBC tumors lacking therapeutic targets, the development of effective drug-treatment strategies for TNBC patients has also been hindered by the presence of highly heterogeneous intratumoral cell populations with different biological properties within an individual patient's tumor. Through the use of dual MYC-isoform TSA-IF, we report, for the first time, that MYCN and its family member MYC are heterogeneously expressed in separate cell nuclei within a given tumor in at least 40% of primary and metastatic TNBC tumors. By isolating and expanding single cells from heterogeneous TNBC tumor-derived cell line populations, we were able to generate novel MYCN- and MYC-expressing cell cultures with a similar genetic background, thus allowing us to assign the biological relevance of MYCN versus MYC expression. Unlike MYC-expressing clonal cells from the CAL-51 cell line, MYCN-expressing cells were able to grow and proliferate in nonadherent forced-suspension cultures. MYCN expression was also elevated in MDA-MB-468 after 14 days in forced suspension, and like CAL-51, MYCN-expressing cells were retained within the cell population when grown in mice as CDXs. These data are consistent with RNA-Seq data from primary TNBC and patient-matched metastatic lesions that demonstrate MYCN expression was present in primary tumors and retained after metastasis. Not only are MYCN-expressing cells within TNBC

tumors found in the metastatic setting, but like NE-CRPC, elevated MYCN expression correlated with a shorter TTP and overall worse prognosis.

Conclusions

In summary, we have identified MYCN-expressing TNBC cell populations within a significant fraction of tumors that can survive various forms of drug-induced cellular stress and have survival advantages *in vitro* under selective antiproliferative treatments. In part, this discovery was accomplished through the development of a novel immunofluorescence staining method that can simultaneously assess MYCN and MYC protein expression within individual TNBC tumor specimens. We found both isoforms were co-expressed in nearly half of primary and metastatic TNBC tumors and were retained in TNBC-derived cell lines. Single-cell isolation and clonal expansion allowed us to create highly relevant MYCN- and MYC-expressing TNBC cell line models to assess related phenotypes and determine associated drug sensitivity, which is the focus of the next chapter.

CHAPTER IV

TARGETING MYCN-EXPRESSING TRIPLE-NEGATIVE BREAST CANCER WITH BET AND MEK INHIBITORS

Introduction

The heterogeneity of MYC-family isoform expression in the CAL-51 and MDA-MB-468 cell lines is consistent with the heterogeneity observed in TNBC clinical specimens and supports the use of these two cell lines as preclinical tools to investigate differential drug sensitivity of MYCN-expressing cells. This chapter investigates the biological relevance of MYCN versus MYC expression in TNBC cells and if MYCN expression represented a biomarker of response to compounds currently or previously under clinical development [including the NCI FDA-Approved Oncology Drug (AOD) library]. Since the MYC-family are basic helix-loop-helix (bHLH) transcription factors lacking catalytic domains, strategies to inhibit their activity have been limited to indirect targeting of proteins that regulate MYC-family isoform stability or expression; these include the bromodomain (BRD)-containing family of transcriptional regulators, PIM1, MEK1/2, and Aurora kinase A *(271, 367–370)*.

Herein, we performed primary and validation high-throughput drug screens using the AOD library, alongside compounds selected to target the MYC family members. Top "hits" from the drug screen were examined further as single-agents and in combination, *in vitro* and in mice harboring TNBC patient-derived xenografts (PDXs) with differing levels of MYCN. We discovered that combined bromodomain and extra-terminal motif

(BET) and MEK inhibition synergistically inhibited the growth of MYCN-expressing PDX TNBC tumors. Our results provide a preclinical rationale for further development of BET and MEK inhibitors in combination for advanced or recurrent TNBC, with the evaluation of MYCN as a relevant biomarker for patient selection.

Results

MYCN-expressing TNBC cells have increased sensitivity to BETi

To gain insight to potential strategies for targeting MYCN-expressing TNBC, we performed a high-throughput drug sensitivity screen on two CAL-51 $MYCN^{Low}$ and two $MYCN^{High}$ clonally-derived cell lines (described in the previous chapter) for sensitivity to a library of 158 compounds, comprised of the 114 compounds in the NCI FDA-Approved AOD library and 44 additional compounds of interest. Analysis of half-maximal inhibitory concentrations (IC_{50}) demonstrated similar drug sensitivities between each clonal cell line set [$MYCN^{Low}$ (R^2=0.9476) and $MYCN^{High}$ (R^2=0.9439)], with $MYCN^{High}$ cell lines having greater sensitivity to compounds that target the BRD family, Aurora kinase A, and MAPK pathway proteins (Figure 16A, Table 5). We performed a secondary screen on $MYCN^{Low}$ (n=5) and $MYCN^{High}$ (n=5) cell lines with inhibitors that demonstrated a >2-fold increase or decrease in IC_{50}, plus additional related compounds of interest. Again, $MYCN^{High}$ cell lines displayed greater sensitivity to compounds previously shown to regulate MYC-isoform expression or activity (Figure 17A, Table 6), including compounds targeting the BRD family of transcriptional regulators (JQ1, INCB054329, and OTX-015) *(270, 371, 372)*.

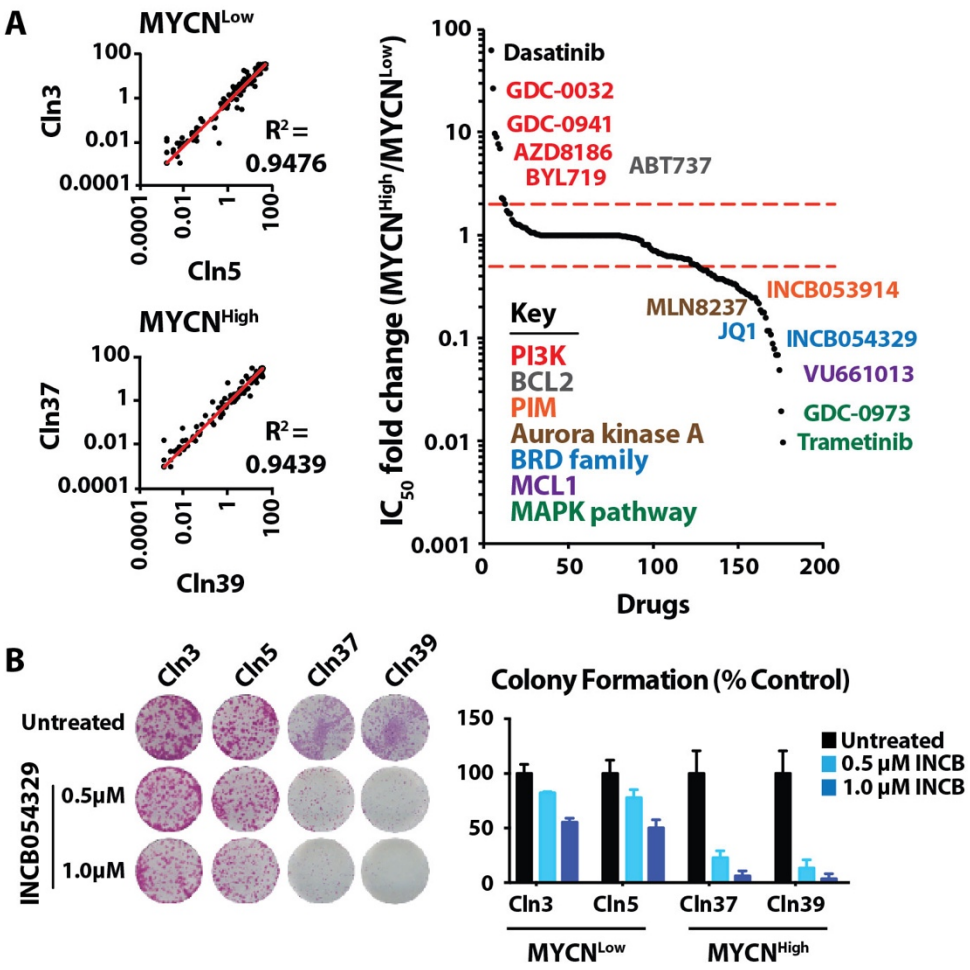

Figure 16. Drug sensitivity of CAL-51 MYCN^{High} and MYCN^{Low} cells. (**A**) Left: IC_{50} correlations for MYCN^{Low} and MYCN^{High} cell lines based on treatment with 158 compounds (NCI-AOD library supplemented with an additional 44 compounds of interest) for 72 hours. Right: Fold change in IC_{50} between MYCN^{Low} and MYCN^{High} cell lines after treatments described in the left panel. Font colors indicate the class to which compounds are associated [PI3K (red), BCL2 (gray), PIM (orange), Aurora kinase A (brown), BRD family (blue), MCL1 (purple), MAPK pathway (green)]. Horizonal red dotted lines represent a separation of compounds that had a greater or less than two-fold IC_{50} between MYCN^{Low} and MYCN^{High} cell lines. (**B**) Left: Representative crystal violet-stained colony formation assay (CFA) after treatment with INCB054329 (0.5 and 1.0 μM) for six days. Right: Quantification of CFAs for the indicated two MYCN^{Low} and MYCN^{High} cell lines analyzed in Part A. Data shown represent the means ± SD.

Table 5. Results from a primary drug screen on CAL-51 $MYCN^{High}$ and $MYCN^{Low}$ cell lines

				Average IC_{50} (µM)		Standard deviation (µM)		Fold change		Difference	
Compounds	Targets	Source	Catalog number	$MYCN^{Low}$	$MYCN^{High}$	$MYCN^{Low}$	$MYCN^{High}$	$MYCN^{High}$/ $MYCN^{Low}$	$MYCN^{Low}$/ $MYCN^{High}$	$MYCN^{High}$- $MYCN^{Low}$	$MYCN^{Low}$- $MYCN^{High}$
5-FU	Pyrimidine analog	Accord Healthcare, Inc	276-68	17.26	10.20	0.65	0.68	0.59	1.69	-7.06	7.06
Abiraterone	Cytochrome P450 17A1	AOD library	NA	23.83	24.37	2.31	0.28	1.02	0.98	0.54	-0.54
ABT737	BCL2	Selleckchem	S1002	2.31	17.63	0.94	1.32	7.64	0.13	15.32	-15.32
Afatinib	EGFR	AOD library	NA	0.96	1.13	0.42	0.17	1.18	0.85	0.18	-0.18
Allopurinol	Xanthine oxidase	AOD library	NA	0.00	0.00	0.00	0.00	0.73	1.37	0.00	0.00
Altretamine	Alkylating agent	AOD library	NA	>30.00	>30.00	0.00	0.00	1.00	1.00	0.00	0.00
Amifostine	Platinum/free radical scavenger	AOD library	NA	>30.00	>30.00	0.00	0.00	1.00	1.00	0.00	0.00
Aminolevulinic acid HCl	Photosensitizer	AOD library	NA	>30.00	>30.00	0.00	0.00	1.00	1.00	0.00	0.00
Anastrozole	Aromatase	AOD library	NA	24.42	25.24	2.37	1.32	1.03	0.97	0.83	-0.83
Arsenic trioxide	ROS	AOD library	NA	>30.00	>30.00	0.00	0.00	1.00	1.00	0.00	0.00
Axitinib	Tyrosine kinases - VEGFR, PDGFR, cRAF	AOD library	NA	2.08	0.58	0.85	0.11	0.28	3.58	-1.50	1.50
Azacitidine	Nucleoside analogue - DNA, RNA	AOD library	NA	>30.00	8.02	0.00	1.87	0.27	3.74	-21.98	21.98
AZD8186	PKCbeta	Selleckchem	S7694	3.07	27.39	0.29	3.04	8.91	0.11	24.31	-24.31
Belinostat	HDAC	Selleckchem	S1085	0.97	0.40	0.06	0.02	0.41	2.41	-0.57	0.57
Bendamustine HCl	Alkylating agent	AOD library	NA	>30.00	>30.00	0.00	0.00	1.00	1.00	0.00	0.00
BKM120	PI3K	Selleckchem	S2247	0.80	1.01	0.04	0.06	1.27	0.79	0.22	-0.22
Bleomycin sulfate	DNA damge	AOD library	NA	0.58	0.14	0.07	0.10	0.25	4.04	-0.43	0.43
Bortezomib	Proteasome	Selleckchem	S1013	0.02	0.01	0.00	0.00	0.62	1.62	-0.01	0.01
Bosutinib	Tyrosine kinases - ABL, SRC	AOD library	NA	1.28	1.21	0.14	0.61	0.95	1.05	-0.06	0.06
Busulfan	Alkylating agent	AOD library	NA	>30.00	29.39	0.20	0.43	0.98	1.02	-0.62	0.62
BYL719	PI3K (Alpha Specific)	Selleckchem	S2814	1.53	10.59	0.00	0.87	6.91	0.14	9.06	-9.06
Cabazitaxel	Antimicrotubule agent	AOD library	NA	0.00	0.00	0.00	0.00	1.00	1.00	0.00	0.00
Cabozantinib	Multi-receptor tyrosine kinase	AOD library	NA	4.94	4.57	2.32	1.32	0.93	1.08	-0.37	0.37
Capecitabine	Antimetabolite	AOD library	NA	>30.00	>30.00	0.00	0.00	1.00	1.00	0.00	0.00
Carboplatin	Alkylating agent	AOD library	NA	27.84	8.13	3.05	1.12	0.29	3.42	-19.71	19.71
Carfilzomib	Proteasome	AOD library	NA	0.01	0.00	0.00	0.00	0.52	1.91	0.00	0.00
Carmustine	Alkylating agent	AOD library	NA	>30.00	>30.00	0.00	0.00	1.00	1.00	0.00	0.00
CB-839	Glutaminase	Selleckchem	S7655	>30.00	>30.00	0.00	0.00	1.00	1.00	0.00	0.00
CD532	Aurora Kinase A	Millipore Sigma	532605	0.40	0.38	0.08	0.06	0.96	1.04	-0.02	0.02
Celecoxib	COX2	AOD library	NA	>30.00	>30.00	0.00	0.00	1.00	1.00	0.00	0.00
Ceritinib	ALK/multi-receptor tyrosine kinase	Selleckchem	S7083	1.12	1.50	0.50	0.47	1.34	0.75	0.38	-0.38
Chlorambucil	DNA Intercalation	AOD library	NA	28.97	7.74	1.46	1.82	0.27	3.74	-21.22	21.22
Cladribine	Antimetabolite	AOD library	NA	1.98	1.40	1.37	0.48	0.71	1.42	-0.58	0.58
Clofarabine	Nucleoside Analog	AOD library	NA	0.52	0.47	0.05	0.06	0.89	1.12	-0.06	0.06
Crizotinib	ALK	AOD library	NA	0.88	0.36	0.03	0.15	0.41	2.43	-0.52	0.52
Cyclophosphamide	Alkylating agent	AOD library	NA	23.32	27.97	3.69	2.88	1.20	0.83	4.65	-4.65
Cytarabine HCl	Nucleoside Analog	AOD library	NA	0.13	0.13	0.04	0.07	0.98	1.02	0.00	0.00
Dabrafenib mesylate	Mutant BRAF	AOD library	NA	2.14	0.67	0.78	0.03	0.31	3.20	-1.47	1.47
Dacarbazine	Alkylating agent	AOD library	NA	>30.00	>30.00	0.00	0.00	1.00	1.00	0.00	0.00
Dactinomycin	DNA Intercalation	AOD library	NA	0.00	0.00	0.00	0.00	1.00	1.00	0.00	0.00
Dasatinib	Bcr-Abl/Src	AOD library	NA	0.03	1.94	0.01	0.00	61.49	0.02	1.91	-1.91
Daunorubicin HCl	DNA Intercalation	AOD library	NA	0.01	0.00	0.01	0.00	0.53	1.88	0.00	0.00
Decitabine	DNA methylation	AOD library	NA	1.80	3.62	0.99	1.03	2.01	0.50	1.82	-1.82
Dexrazoxane	Fe Chelator/Topoisomerase II	AOD library	NA	9.70	9.12	0.03	5.34	0.94	1.06	-0.58	0.58
Docetaxel	Antimicrotubule agent	AOD library	NA	0.00	0.00	0.00	0.00	0.47	2.13	0.00	0.00
Doxorubicin HCl	DNA Intercalation	Pfizer, Inc	3032-20	0.93	0.07	0.86	0.02	0.07	13.73	-0.87	0.87
Doxorubicin HCl	DNA Intercalation	AOD library	NA	0.03	0.01	0.00	0.00	0.25	3.99	-0.02	0.02
Enzalutamide	AR	AOD library	NA	>30.00	>30.00	0.00	0.00	1.00	1.00	0.00	0.00
Epirubicin HCl	DNA	AOD library	NA	0.02	0.00	0.01	0.00	0.22	4.61	-0.01	0.01
Epothilone B	Antimicrotubule agent	Selleckchem	S1364	0.00	0.00	0.00	0.00	0.81	1.23	0.00	0.00
EPZ-6438	EZH2	Selleckchem	S7128	23.59	>30.00	9.07	0.00	1.27	0.79	6.42	-6.42
EPZ015666	PRMT5	Selleckchem	S7748	>30.00	>30.00	0.00	0.00	1.00	1.00	0.00	0.00
EPZ5676	DOT1L	Selleckchem	S7062	30.00	>30.00	0.01	0.00	1.00	1.00	0.01	-0.01
Erastin	Ferroptosis	Selleckchem	S7242	2.29	1.74	0.03	0.29	0.76	1.31	-0.55	0.55
Erlotinib HCl	EGFR	AOD library	NA	>30.00	>30.00	0.00	0.00	1.00	1.00	0.00	0.00
Estramustine Na_2SO_4	Alkylating agent	AOD library	NA	>30.00	>30.00	0.00	0.00	1.00	1.00	0.00	0.00
Etoposide	Topoisomerase	AOD library	NA	0.31	0.12	0.01	0.00	0.39	2.54	-0.19	0.19
Everolimus	mTOR	AOD library	NA	0.01	0.01	0.01	0.01	1.29	0.78	0.00	0.00
EX 527	Sirtuin	Selleckchem	S1541	>30.00	>30.00	0.00	0.00	1.00	1.00	0.00	0.00
Exemestane	Aromatase	AOD library	NA	15.16	21.55	6.77	8.66	1.42	0.70	6.39	-6.39
Floxuridine	Antimetabolite	AOD library	NA	0.60	0.05	0.31	0.03	0.08	12.47	-0.55	0.55
Fludarabine phosphate	Antimetabolite	AOD library	NA	29.66	>30.00	0.49	0.00	1.01	0.99	0.34	-0.34
Fluorouracil	Pyrimidine analog	AOD library	NA	7.42	4.35	2.36	0.52	0.59	1.70	-3.06	3.06
Fulvestrant	Estrogen receptor	AOD library	NA	>30.00	>30.00	0.00	0.00	1.00	1.00	0.00	0.00
Ganetespib	HSP90	Selleckchem	S1159	0.01	0.01	0.00	0.00	0.62	1.60	-0.01	0.01
GDC-0032	Pan-PI3K	Genentech	NA	0.09	2.49	0.08	0.57	26.28	0.04	2.40	-2.40
GDC-0068	Pan-AKT	Selleckchem	RG7440	0.41	0.27	0.09	0.14	0.67	1.49	-0.13	0.13
GDC-0449	Hedgehog - PTCH, SMO	Selleckchem	S1082	>30.00	>30.00	0.00	0.00	1.00	1.00	0.00	0.00
GDC-0941	Pan-PI3K	Genentech	NA	0.52	5.04	0.10	2.08	9.65	0.10	4.52	-4.52
GDC-0973	MEK1/2	Selleckchem	RG7420	5.11	0.13	0.98	0.03	0.02	40.30	-4.98	4.98
Gefitinib	EGFR	AOD library	NA	14.54	9.23	4.24	1.52	0.63	1.58	-5.31	5.31
Gemcitabine HCl	Deoxycytidine analogue	AOD library	NA	0.01	0.01	0.00	0.00	0.94	1.06	0.00	0.00
Hydroxyurea	Antimetabolite	AOD library	NA	>30.00	>30.00	0.00	0.00	1.00	1.00	0.00	0.00
Ibrutinib	Bruton's tyr kinase (BTK)	AOD library	NA	7.23	16.11	2.97	2.12	2.23	0.45	8.88	-8.88
Idarubicin HCl	DNA Intercalation	AOD library	NA	0.00	0.00	0.00	0.00	0.36	2.81	0.00	0.00
Idelalisib	PI3Kδ	Selleckchem	S2226	26.51	>30.00	4.94	0.00	1.13	0.88	3.49	-3.49
Ifosfamide	Alkylating agent	AOD library	NA	25.42	24.99	0.22	0.54	0.98	1.02	-0.43	0.43
Imatinib	multikinase v-Abl, c-Kit and PDGFR	AOD library	NA	23.44	14.94	0.39	0.16	0.64	1.57	-8.50	8.50
Imiquimod	Unknown	AOD library	NA	>30.00	>30.00	0.00	0.00	1.00	1.00	0.00	0.00
INCB024360	IDO	Incyte Corporation	NA	15.00	15.00	0.00	0.00	1.00	1.00	0.00	0.00
INCB039110	JAK1	Incyte Corporation	NA	15.00	15.00	0.00	0.00	1.00	1.00	0.00	0.00
INCB040093	PI3Kδ	Incyte Corporation	NA	15.00	15.00	0.00	0.00	1.00	1.00	0.00	0.00
INCB053914	Pan-PIM	Incyte Corporation	NA	7.22	2.77	0.50	0.65	0.38	2.60	-4.45	4.45
INCB054329	BRD family	Incyte Corporation	NA	15.00	1.34	0.00	0.19	0.09	11.22	-13.66	13.66
INCB054828	FGFR	Incyte Corporation	NA	1.88	0.33	0.81	0.12	0.18	5.71	-1.55	1.55
Irinotecan HCl	DNA/Topoisomerase I	AOD library	NA	6.44	2.42	0.83	0.04	0.38	2.66	-4.02	4.02
Ixabepilone	Antimicrotubule agent	AOD library	NA	0.01	0.00	0.00	0.00	0.61	1.63	0.00	0.00
JQ1	BRD4	Selleckchem	S7110	24.89	3.09	7.23	0.47	0.12	8.04	-21.79	21.79
Lapatinib	Tyrosine kinases - HER2, EGFR	AOD library	NA	>30.00	>30.00	0.00	0.00	1.00	1.00	0.00	0.00
Lenalidomide	Cereblon	AOD library	NA	>30.00	>30.00	0.00	0.00	1.00	1.00	0.00	0.00
Letrozole	Aromatase	AOD library	NA	23.84	22.98	2.69	4.26	0.96	1.04	-0.86	0.86
Lomustine	Alkylating agent	AOD library	NA	>30.00	>30.00	0.00	0.00	1.00	1.00	0.00	0.00
Mechlorethamine HCl	DNA Intercalation	AOD library	NA	4.06	4.85	1.65	4.56	1.19	0.84	0.79	-0.79
Megestrol acetate	Progesterone receptor	AOD library	NA	>30.00	>30.00	0.00	0.00	1.00	1.00	0.00	0.00

Melphalan HCl	**Alkylating agent**	**AOD library**	**NA**	8.97	3.20	6.74	1.45	0.36	2.80	-5.77	5.77
Mercaptopurine	**Nucleoside Analog**	**AOD library**	**NA**	>30.00	19.89	0.00	14.30	0.66	1.51	-10.11	10.11
Methotrexate	**Antimetabolite/Folic Acid**	**AOD library**	**NA**	1.39	0.52	1.59	0.50	0.37	2.70	-0.88	0.88
Methoxsalen	**DNA damge**	**AOD library**	**NA**	>30.00	>30.00	0.00	0.00	1.00	1.00	0.00	0.00
Mitomycin	**DNA Intercalation**	**AOD library**	**NA**	0.06	0.02	0.03	0.01	0.34	2.92	-0.04	0.04
Mitotane	**Unknown**	**AOD library**	**NA**	>30.00	>30.00	0.00	0.00	1.00	1.00	0.00	0.00
Mitoxantrone	**DNA Intercalation**	**AOD library**	**NA**	0.01	0.00	0.00	0.00	0.11	8.91	0.00	0.00
MK2206	**AKT**	**Selleckchem**	**S1078**	0.55	1.26	0.13	0.34	2.30	0.43	0.71	-0.71
MLN8237	**Aurora Kinase**	**Selleckchem**	**S1133**	0.14	0.03	0.03	0.01	0.25	4.05	-0.11	0.11
Nelarabine	**Antimetabolite**	**AOD library**	**NA**	>30.00	>30.00	0.00	0.00	1.00	1.00	0.00	0.00
Nilotinib	**Tyrosine kinases - BCR-ABL, PDGFR**	**AOD library**	**NA**	>30.00	21.06	0.00	12.64	0.70	1.42	-8.94	8.94
NU7441	**DNA-PK**	**Selleckchem**	**S2638**	2.25	3.70	0.82	0.04	1.64	0.61	1.44	-1.44
Nutlin	**MDM2**	**Cayman**	**10004372**	0.90	0.99	0.07	0.20	1.10	0.91	0.09	-0.09
Olaparib HCl	**PARP**	**AOD library**	**NA**	9.60	10.20	9.14	2.75	1.06	0.94	0.60	-0.60
Omacetaxine mepesuccinate	**Ribosomes**	**AOD library**	**NA**	0.02	0.01	0.00	0.00	0.35	2.85	-0.01	0.01
Oxaliplatin	**DNA**	**AOD library**	**NA**	5.40	1.54	1.87	0.40	0.29	3.50	-3.86	3.86
Paclitaxel	**Antimicrotubule agent**	**AOD library**	**NA**	0.00	0.00	0.00	0.00	0.90	1.11	0.00	0.00
Palbociclib	**CDK4/6**	**Selleckchem**	**S1116**	2.00	1.34	0.12	0.29	0.67	1.49	-0.66	0.66
Pazopanib	**Multi-receptor tyrosine kinase**	**Selleckchem**	**S1035**	28.68	12.25	1.87	3.15	0.43	2.34	-16.44	16.44
Pazopanib HCl	**Tyrosine kinases - VEGFR, PDGFR**	**AOD library**	**NA**	>30.00	>30.00	0.00	0.00	1.00	1.00	0.00	0.00
Pemetrexed	**Antimetabolite/Folic Acid**	**AOD library**	**NA**	>30.00	3.60	0.00	3.99	0.12	8.34	-26.40	26.40
Pentostatin	**Nucleotide analogue/adenine deaminase**	**AOD library**	**NA**	>30.00	>30.00	0.00	0.00	1.00	1.00	0.00	0.00
PF-4708671	**p70 ribosomal S6 kinase S6K1**	**Selleckchem**	**S2163**	12.46	7.63	1.77	0.55	0.61	1.63	-4.83	4.83
Pipobroman	**Alkylating agent**	**AOD library**	**NA**	22.26	4.14	10.95	1.38	0.19	5.38	-18.12	18.12
Plerixafor	**CXCR4**	**AOD library**	**NA**	26.35	27.90	5.16	2.98	1.06	0.94	1.55	-1.55
Plicamycin	**DNA Intercalation**	**AOD library**	**NA**	0.03	0.02	0.00	0.00	0.65	1.53	-0.01	0.01
Pomalidomide	**Cereblon**	**AOD library**	**NA**	>30.00	>30.00	0.00	0.00	1.00	1.00	0.00	0.00
Ponatinib	**Bcr-Abl**	**AOD library**	**NA**	0.39	0.13	0.16	0.02	0.33	3.02	-0.26	0.26
Pralatrexate	**Antimetabolite/Folic Acid**	**AOD library**	**NA**	0.12	0.03	0.16	0.04	0.26	3.88	-0.09	0.09
Procarbazine HCl	**Alkylating agent**	**AOD library**	**NA**	>30.00	>30.00	0.00	0.00	1.00	1.00	0.00	0.00
Quisinostat	**HDAC1**	**Selleckchem**	**S1096**	0.02	0.00	0.01	0.00	0.23	4.29	-0.01	0.01
Raloxifene	**Estrogen receptor**	**AOD library**	**NA**	26.89	13.48	1.80	1.07	0.50	2.00	-13.42	13.42
Regorafenib	**VEGFR2-TIE2**	**AOD library**	**NA**	4.18	1.40	0.51	0.18	0.34	2.97	-2.77	2.77
Romidepsin	**HDAC**	**AOD library**	**NA**	0.00	0.00	0.00	0.00	0.60	1.66	0.00	0.00
SAHA	**HDAC**	**Selleckchem**	**S1047**	3.25	1.90	0.32	0.13	0.58	1.71	-1.35	1.35
SCH772984	**ERK**	**Selleckchem**	**S7101**	>30.00	18.82	0.00	7.83	0.63	1.59	-11.18	11.18
SGC-CBP30	**CREBBP/EP300**	**Selleckchem**	**S7256**	29.37	18.55	0.89	4.21	0.63	1.58	-10.82	10.82
Sirolimus	**mTOR**	**AOD library**	**NA**	0.00	0.00	0.00	0.00	0.71	1.41	0.00	0.00
Sorafenib	**Kinases - RAF, VEGFR**	**AOD library**	**NA**	4.56	3.68	1.11	0.26	0.81	1.24	-0.88	0.88
Streptozocin	**DNA Intercalation**	**AOD library**	**NA**	>30.00	>30.00	0.00	0.00	1.00	1.00	0.00	0.00
Sunitinib	**c-KIT, FGFR, PDGFR, VEGFR**	**AOD library**	**NA**	2.93	1.25	1.32	0.00	0.43	2.34	-1.67	1.67
Tamoxifen citrate	**Estrogen receptor**	**AOD library**	**NA**	16.14	13.09	2.25	2.38	0.81	1.23	-3.05	3.05
Temozolomide	**Alkylating agent**	**AOD library**	**NA**	>30.00	>30.00	0.00	0.00	1.00	1.00	0.00	0.00
Temsirolimus	**mTOR**	**AOD library**	**NA**	0.01	0.01	0.01	0.00	1.24	0.81	0.00	0.00
Teniposide	**DNA Topoisomerase II**	**AOD library**	**NA**	0.07	0.01	0.05	0.00	0.18	5.47	-0.06	0.06
TGX-221	**PKCbeta**	**Selleckchem**	**S1169**	17.99	29.08	4.52	1.30	1.62	0.62	11.10	-11.10
Thalidomide	**Cereblon**	**AOD library**	**NA**	>30.00	>30.00	0.00	0.00	1.00	1.00	0.00	0.00
Thioguanine	**Antimetabolite**	**AOD library**	**NA**	13.93	5.29	2.93	2.55	0.38	2.64	-8.64	8.64
Thiotepa	**Alkylating agent**	**AOD library**	**NA**	4.00	1.82	0.57	0.57	0.46	2.20	-2.18	2.18
Topotecan HCl	**DNA Topoisomerase I**	**AOD library**	**NA**	0.03	0.02	0.01	0.00	0.61	1.63	-0.01	0.01
Trametinib	**MEK1/2**	**AOD library**	**NA**	6.51	0.04	4.93	0.00	0.01	162.14	-6.47	6.47
Tretinoin	**Retinoic acid receptors**	**AOD library**	**NA**	18.82	18.56	0.05	1.80	0.99	1.01	-0.26	0.26
Triethylenemelamine	**DNA**	**AOD library**	**NA**	0.43	0.20	0.16	0.01	0.46	2.17	-0.23	0.23
Uracil mustard	**Alkylating agent**	**AOD library**	**NA**	25.06	13.11	0.59	0.04	0.52	1.91	-11.96	11.96
Valrubicin	**DNA**	**AOD library**	**NA**	0.10	0.04	0.01	0.00	0.35	2.87	-0.07	0.07
Vandetanib	**Tyrosine kinases - VEGFR, EGFR**	**AOD library**	**NA**	2.27	2.40	0.16	0.36	1.06	0.94	0.13	-0.13
Vemurafenib	**Mutant BRAF**	**AOD library**	**NA**	21.25	10.15	9.61	0.40	0.48	2.09	-11.10	11.10
Vinblastine sulfate	**Antimicrotubule agent**	**AOD library**	**NA**	0.00	0.00	0.00	0.00	0.46	2.17	0.00	0.00
Vincristine sulfate	**Antimicrotubule agent**	**AOD library**	**NA**	0.00	0.00	0.00	0.00	0.30	3.38	0.00	0.00
Vinorelbine tartrate	**Antimicrotubule agent**	**AOD library**	**NA**	0.06	0.02	0.03	0.00	0.38	2.66	-0.04	0.04
Vismodegib	**Hedgehog - PTCH, SMO**	**AOD library**	**NA**	>30.00	>30.00	0.00	0.00	1.00	1.00	0.00	0.00
Vorinostat	**HDAC**	**AOD library**	**NA**	1.73	0.91	0.70	0.47	0.53	1.90	-0.82	0.82
VU661013	**MCL1**	**Stephen W. Fesik, Ph.D.**	**NA**	11.55	0.62	1.47	0.29	0.05	18.52	-10.93	10.93
Zoledronic acid	**Pyrophosphate synthase**	**AOD library**	**NA**	>30.00	>30.00	0.00	0.00	1.00	1.00	0.00	0.00

AOD, FDA-Approved Oncology Drug

Bromodomain and extra-terminal motif inhibitors (BETis) are a class of compounds currently under clinical development that broadly target the BRD family (predominantly BRD2, BRD3, and BRD4) *(373)*. Preclinical studies have demonstrated that BETis are a promising strategy to target *MYCN*-amplified neuroblastoma because BRD4 regulates transcription of *MYCN* and occupies MYCN target-gene enhancers and super-enhancers *(271, 273)*. Since BETi sensitivity has been reported to have a stronger positive correlation with *MYCN* expression than with *MYC* expression in both hormonally *(343)* and non-hormonally regulated malignancies *(271, 273)*, we investigated BETis further using our MYCN-expressing TNBC preclinical models. By treating additional CAL-51 clonally-derived cell lines (n=26) with varying MYCN levels with BETi, we validated results from our prior drug screens that MYCN-expressing cells were more sensitive ($p<0.0001$) to BETi (Figure 17B). Further, we performed longer-term drug treatments and evaluated the colony-forming ability of a subset of clonal cell lines (n=14) differing in MYCN and MYC expression. Again, MYCN-expressing cells were more sensitive to BETi, and longer-term treatments resulted in more profound differential sensitivity ($p<0.001$) (Figure 16B and Figure 17C). $MYCN^{High}$ cell lines had a ≥5-fold decrease in cell growth compared to $MYCN^{Low}$ cell lines in both short-term metabolic and long-term colony formation assays, demonstrating an association between MYCN expression and BETi sensitivity in TNBC. To assess the effects of BETi treatment on $MYCN^{High}$ cell lines in a forced suspension culture, we treated ten lines with BETi for seven days. Similar to adherent assays, MYCN-expressing cells had significantly ($p<0.0001$) reduced viability after BETi treatment in anchorage-independent culture systems (Figure 17D). Taken together, MYCN-expressing TNBC cells demonstrated increased sensitivity to BETi in both adherent and

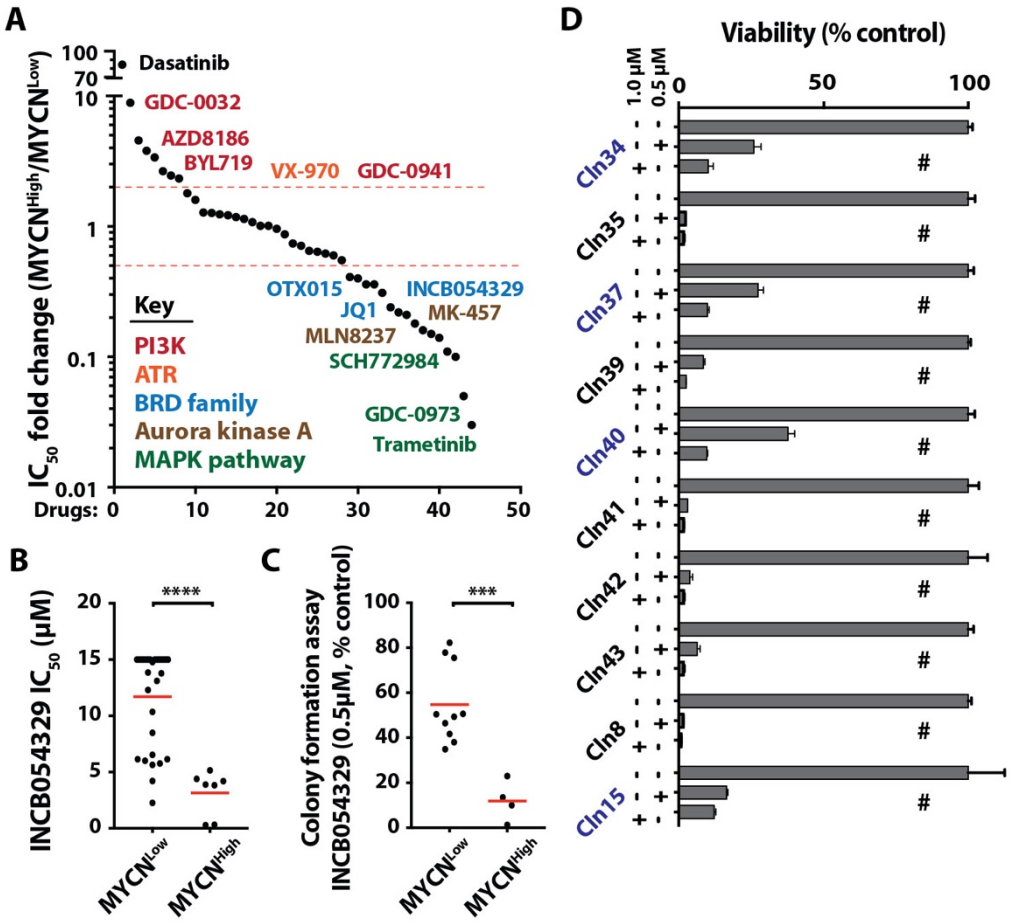

Figure 17. Evaluation of MYCN-expressing TNBC clonal cell line drug-sensitivity. (**A**) IC_{50} of 40 compounds used in a secondary screen to treat five $MYCN^{Low}$ and $MYCN^{High}$ cell lines for 72 hours. Colors associate with drug class [PI3K (red), ATR (orange), BRD family (blue), Aurora kinase A (brown), MAPK pathway (green)]. Horizonal red dotted lines represent a separation of compounds that had a greater or less than two-fold IC_{50} between $MYCN^{Low}$ and $MYCN^{High}$ cell lines. (**B**) IC_{50} of 31 CAL-51 clonally-derived cell lines after treatment with a dose-escalation of INCB054329 for 72 hours. Unpaired t-test, ****p<0.0001. (**C**) Quantification of crystal violet stained colonies compared to control for ten $MYCN^{Low}$ and four $MYCN^{High}$ cell lines treated with 0.5 μM INCB054329 for six days. Unpaired t-test, ***p<0.001. (**D**) Viability of the ten indicated $MYCN^{High}$ cell lines treated with 0.5 or 1 μM INCB054329 in forced suspension cultures for seven days. Data shown represent the means ± SD of three biological replicates. # indicates p<0.0001 for all untreated to treated unpaired t-tests. Cell lines with blue font represent lines with residual viability (>10% after 0.5 μM INCB054329) that were used in subsequent combination experiments.

Table 6. Results from a secondary drug screen on CAL-51 $MYCN^{High}$ and $MYCN^{Low}$ cell lines

				Average IC_{50} (μM)		Standard deviation (μM)		Fold change		Difference	
Compounds	Targets	Source	Catalog number	$MYCN^{Low}$	$MYCN^{High}$	$MYCN^{Low}$	$MYCN^{High}$	$MYCN^{High}$/ $MYCN^{Low}$	$MYCN^{Low}$/ $MYCN^{High}$	$MYCN^{High}$- $MYCN^{Low}$	$MYCN^{Low}$- $MYCN^{High}$
ABT-199	**BCL2**	**Selleckchem**	**S8048**	9.16	11.35	1.37	1.75	1.24	0.81	2.19	-2.19
ABT737	**BCL2**	**Selleckchem**	**S1002**	5.14	20.12	2.25	3.54	3.91	0.26	14.98	-14.98
AT101	**BCL2**	**Selleckchem**	**S2812**	1.85	1.37	0.33	0.30	0.74	1.35	-0.48	0.48
Azacitidine	**Nucleoside analogue**	**AOD library**	**NA**	7.78	9.20	4.04	7.48	1.18	0.85	1.42	-1.42
AZD8186	**PKCbeta**	**Selleckchem**	**S7694**	6.94	26.43	2.81	5.32	3.81	0.26	19.49	-19.49
BKM120	**PI3K**	**Selleckchem**	**S2247**	0.97	1.20	0.12	0.15	1.24	0.81	0.23	-0.23
Bleomycin Sulfate	**DNA Damage**	**AOD library**	**NA**	1.72	0.42	0.90	0.36	0.24	4.11	-1.30	1.30
BYL719	**PI3K (Alpha Specific)**	**Selleckchem**	**S2814**	2.91	9.76	1.04	1.95	3.35	0.30	6.85	-6.85
CBL0137	**FACT**	**Active Biochem**	**A-1961**	0.27	0.17	0.04	0.05	0.64	1.57	-0.10	0.10
CD532	**Aurora Kinase A**	**Millipore Sigma**	**532605**	0.82	0.84	0.11	0.16	1.03	0.97	0.02	-0.02
Dabrafenib mesylate	**Mutant BRAF**	**AOD library**	**NA**	>30.00	2.48	0.00	2.34	0.08	12.08	-27.52	27.52
Dasatinib	**Bcr-Abl/Src**	**AOD library**	**NA**	0.08	6.69	0.06	3.36	83.72	0.01	6.61	-6.61
Decitabine	**DNA methylation**	**AOD library**	**NA**	>30.00	5.55	0.00	3.58	0.19	5.40	-24.45	24.45
Floxuridine	**Antimetabolite**	**AOD library**	**NA**	0.02	0.02	0.01	0.01	0.87	1.15	0.00	0.00
GDC-0032	**Pan-PI3K**	**Genentech**	**NA**	0.35	3.14	0.12	0.70	8.88	0.11	2.78	-2.78
GDC-0068	**Pan-AKT**	**Selleckchem**	**RG7440**	0.41	0.47	0.05	0.18	1.14	0.88	0.06	-0.06
GDC-0941	**Pan-PI3K**	**Genentech**	**NA**	1.27	2.96	0.32	0.65	2.33	0.43	1.69	-1.69
GDC-0973	**MEK1/2**	**Selleckchem**	**RG7420**	6.63	0.33	2.94	0.20	0.05	19.96	-6.30	6.30
Gemcitabine HCl	**Deoxycytidine analogue**	**AOD library**	**NA**	0.01	0.01	0.00	0.00	1.00	1.00	0.00	0.00
Ibrutinib	**Bruton's tyrosine kinase**	**AOD library**	**NA**	11.18	20.20	1.89	5.85	1.81	0.55	9.02	-9.02
INCB053914	**Pan-PIM**	**Incyte Corporation**	**NA**	7.58	5.53	1.79	1.82	0.73	1.37	-2.05	2.05
INCB054329	**BRD family**	**Incyte Corporation**	**NA**	12.00	4.29	3.60	0.53	0.36	2.79	-7.71	7.71
JQ1	**BRD4**	**Selleckchem**	**S7110**	9.00	2.79	6.49	0.25	0.31	3.23	-6.21	6.21
KU55933	**ATM**	**Selleckchem**	**S1092**	14.04	15.11	2.11	2.65	1.08	0.93	1.07	-1.07
Methotrexate	**Antimetabolite/Folic Acid**	**AOD library**	**NA**	0.20	0.11	0.14	0.09	0.55	1.81	-0.09	0.09
MK-457	**Aurora Kinase**	**Selleckchem**	**S1048**	0.13	0.02	0.07	0.01	0.16	6.19	-0.11	0.11
MK2206	**AKT**	**Selleckchem**	**S1078**	1.58	3.90	0.25	0.82	2.46	0.41	2.31	-2.31
MLN8237	**Aurora Kinase**	**Selleckchem**	**S1133**	0.27	0.05	0.09	0.02	0.18	5.50	-0.22	0.22
NU7441	**DNA-PK**	**Selleckchem**	**S2638**	2.33	3.73	0.43	0.69	1.60	0.62	1.40	-1.40
OTX015	**BRD family**	**Selleckchem**	**S7360**	10.18	4.04	6.74	1.23	0.40	2.52	-6.15	6.15
Pemetrexed	**Antimetabolite/Folic Acid**	**AOD library**	**NA**	1.16	0.47	0.85	0.37	0.41	2.44	-0.68	0.68
PF-4708671	**p70 ribosomal S6 kinase S6K1**	**Selleckchem**	**S2163**	10.20	12.47	1.94	2.65	1.22	0.82	2.27	-2.27
Pralatrexate	**Antimetabolite/Folic Acid**	**AOD library**	**NA**	0.01	0.01	0.01	0.00	0.62	1.61	-0.01	0.01
SCH772984	**ERK**	**Selleckchem**	**S7101**	8.19	1.25	4.34	1.73	0.15	6.54	-6.94	6.94
TGX-221	**PKCbeta**	**Selleckchem**	**S1169**	23.51	29.89	5.02	0.24	1.27	0.79	6.38	-6.38
Thioguanine	**Antimetabolite**	**AOD library**	**NA**	7.16	4.66	2.86	2.83	0.65	1.54	-2.50	2.50
Trametinib	**MEK1/2**	**AOD library**	**NA**	4.09	0.12	0.81	0.11	0.03	33.19	-3.96	3.96
Vemurafenib	**Mutant BRAF**	**AOD library**	**NA**	28.21	16.84	2.46	7.62	0.60	1.67	-11.37	11.37
VU661013	**MCL1**	**Stephen W. Fesik, Ph.D.**	**NA**	11.86	1.18	1.91	0.33	0.10	10.02	-10.68	10.68
VX-970	**ATR**	**Selleckchem**	**S7102**	0.80	2.13	0.14	0.75	2.66	0.38	1.33	-1.33

AOD, FDA-Approved Oncology Drug

non-adherent growth conditions, providing the rationale for further drug development strategies for BETi in advanced TNBC.

Changes in MYC-family isoform expression in response to BETi treatment

To determine if the increased sensitivity of MYCN-expressing cells to BETi was MYCN-dependent, $MYCN^{Low}$ and $MYCN^{High}$ lines were subjected to *MYCN* siRNA-mediated knockdown. siRNAs targeting *MYCN* RNA decreased MYCN protein and decreased viability in a dose-dependent manner only in the $MYCN^{High}$ cell lines, without altering MYC levels in $MYCN^{Low}$ cells (Figure 18A). Of note, MYC expression increased with MYCN knockdown in $MYCN^{High}$ cells (Figure 18A), suggesting a feedback signaling mechanism between the MYC-family members to ensure cell survival under normal growth conditions. To determine if *MYCN* is a downstream target of BRD-mediated transcriptional regulation, we performed precision nuclear run-on sequencing (PRO-seq) on two $MYCN^{High}$ and two $MYCN^{Low}$ cell lines treated with BETi (0.5 μM INCB054329) for 15 minutes. Nascent RNA at the *MYCN* locus was observed only in $MYCN^{High}$ cells and *MYCN* transcripts were reduced after BETi treatment (Figure 18B). Nascent RNA at the *MYC* locus decreased in the $MYCN^{Low}$ cell lines after BETi treatment, consistent with reported responses to BETi in previous studies *(272, 374)* (Figure 18B). However, *MYC* RNA levels increased to basal levels by four hours (RNA-Seq; Figure 18C) in the $MYCN^{Low}$ cells, and protein levels were elevated at 24 hours (immunoblot; Figure 18D) in the $MYCN^{High}$ cells, in parallel experiments. Gene set enrichment analyses (GSEA) performed on RNA samples harvested after four hours of BETi treatment demonstrated

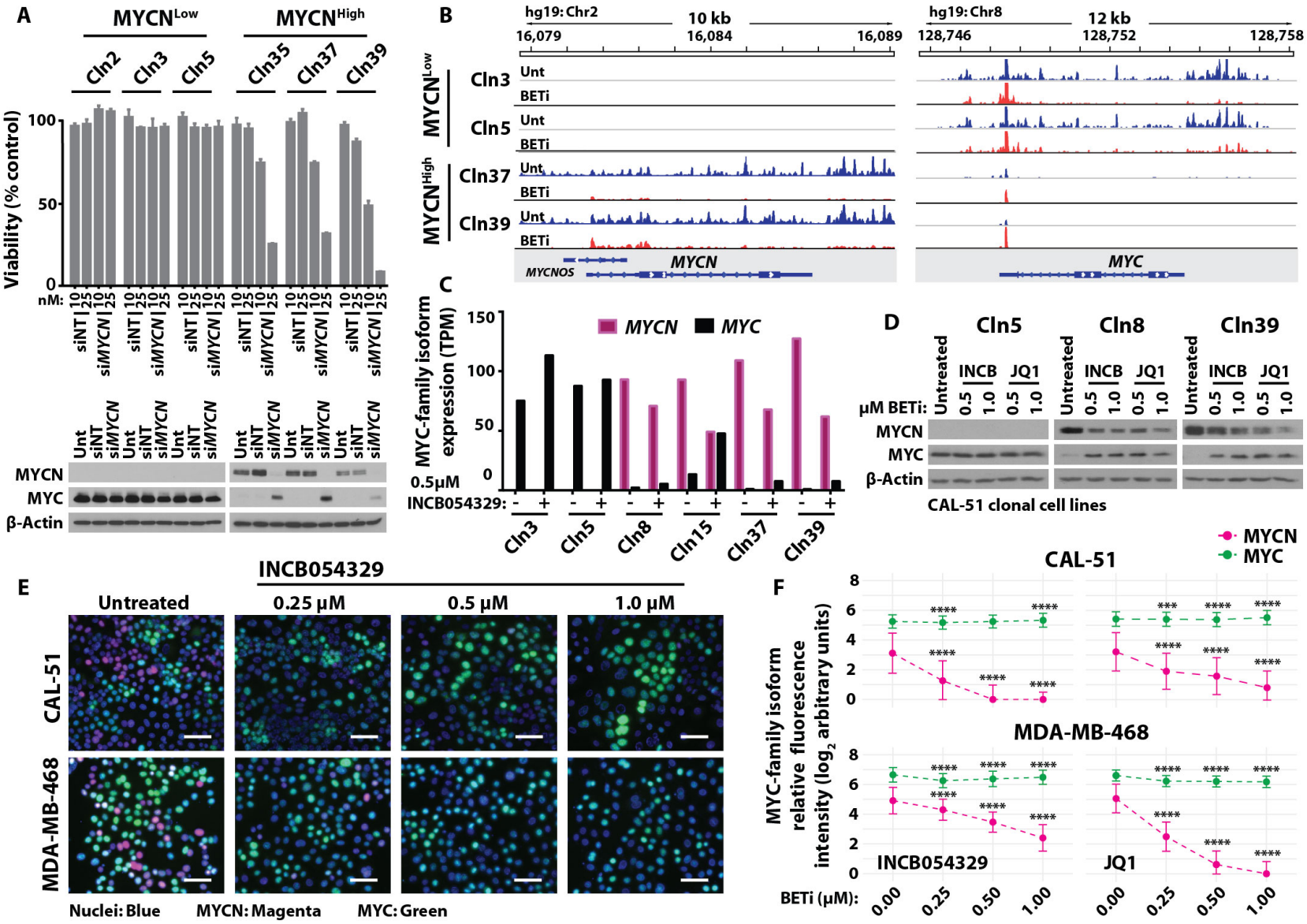
A
MYCN^Low
MYCN^High
Cln2
Cln3
Cln5
Cln35
Cln37
Cln39
Viability (% control)
100
50
0
nM:
siNT
siMYCN
MYCN
MYC
β-Actin
B
hg19: Chr2
10 kb
16,079
16,084
16,089
hg19: Chr8
12 kb
128,746
128,752
128,758
Unt
BETi
MYCNOS
MYCN
MYC
C
MYC-family isoform expression (TPM)
MYCN
MYC
0.5μM
INCB054329:
D
Cln5
Cln8
Cln39
Untreated
INCB
JQ1
μM BETi:
CAL-51 clonal cell lines
E
INCB054329
Untreated
0.25 μM
0.5 μM
1.0 μM
CAL-51
MDA-MB-468
Nuclei: Blue
MYCN: Magenta
MYC: Green
F
CAL-51
MDA-MB-468
MYC-family isoform relative fluorescence intensity (log2 arbitrary units)
INCB054329
JQ1
BETi (μM):
0.00
0.25
0.50
1.00

Figure 18. Evaluation of MYC-family isoform expression after BETi treatment. (**A**) Top: Viability of $MYCN^{Low}$ and $MYCN^{High}$ cell lines after siRNA-mediated knockdown using non-targeting (siNT) or anti-*MYCN* (si*MYCN*) siRNAs for 96 hours. Data shown represent the means ± SEM. Bottom: Immunoblot analysis of MYCN, MYC, and β-Actin in $MYCN^{Low}$ and $MYCN^{High}$ cell lines after the described knockdown with 25 nM siRNAs. (**B**) Genome viewer showing sequencing alignment tracks of nascent transcript PRO-seq mapping at the *MYCN* and *MYC* gene loci for the two indicated $MYCN^{Low}$ and $MYCN^{High}$ cell lines after treatment with DMSO control (Unt, blue) or 0.5 μM INCB054329 (BETi, red) for 15 minutes. (**C**) Fold change in *MYCN* and *MYC* expression in the two indicated $MYCN^{Low}$ (Cln3 and Cln5) and four $MYCN^{High}$ (Cln8, Cln15, Cln37, and Cln39) cell lines after treatment with 0.5 μM INCB054329 for four hours. (**D**) Immunoblot analysis of MYCN, MYC, and β-Actin in cell lines described in Part C after treatment with 0.5 and 1.0 μM INCB054329 or JQ1 for 24 hours. (**E**) MYC-family isoform TSA-IF on two MYCN-expressing TNBC cell lines (MDA-MB-468 and CAL-51) after 0, 0.25, 0.5, or 1.0 μM INCB054329 or JQ1 for 24 hours. Colors represent cell nuclei (blue), MYCN (magenta), and MYC (green). Scale bar, 50 μM. (**F**) Quanfication of fluorescence intensity for MYCN and MYC after BETi treatments described in Part E. Data shown represent the means ± SEM. TSA-IF images and quantification are representative of three biological replicates.

MYC target genes were significantly downregulated in response to BETi treatment in the $MYCN^{High}$ cells (Hallmark MYC targets V1, FDR q<0.0001; Hallmark MYC targets V2, FDR q<0.0001); Figure 19, A and B), consistent with BETi-mediated downregulation of MYCN-mediated transcriptional activity.

To evaluate MYC-family isoform dynamics in individual cells treated with BETi treatment, CAL-51 and MDA-MB-468 were treated with increasing doses of BETi (INCB054329 or JQ1) for 24 hours and TSA-IF performed for MYCN and MYC detection. Similar to MYC-family isoform expression changes observed in the CAL-51 clonal cell lines (Figure 18, C and D), BETi treatment decreased MYCN and increased MYC expression in a dose-dependent manner in the heterogeneous CAL-51 parental population (Figure 18, E and F). However, both MYCN and MYC expression decreased after BETi treatment in MDA- MB-468, suggesting isoform switching observed in the CAL-51 clonal cell line was not a universal cellular response to BETi treatment in TNBC cell lines.

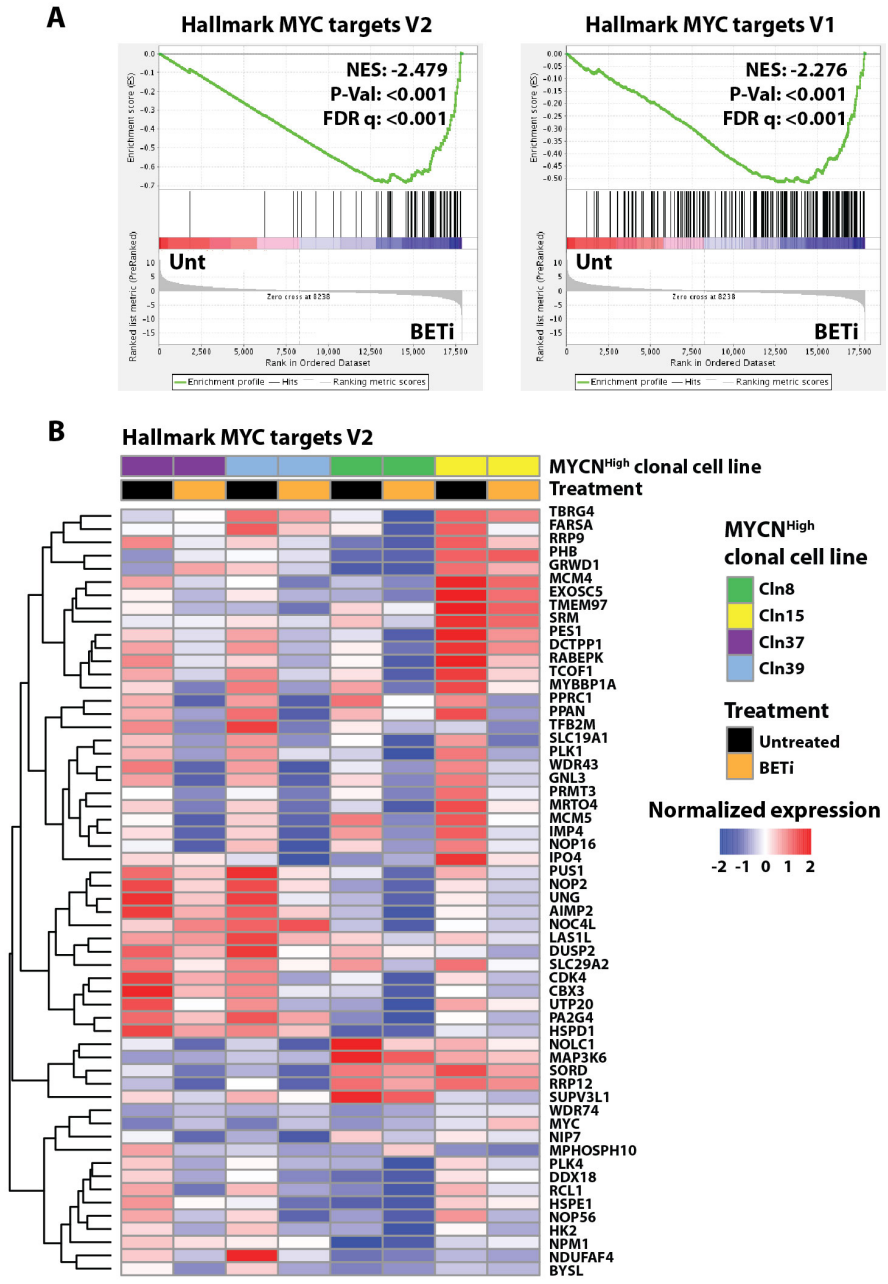

Figure 19. Changes in MYC target gene expression in CAL-51 MYCN^{High} cell lines after BETi treatment. (**A**) GSEA enrichment plots of the Hallmark MYC targets V1 and V2 genesets for MYCN-expressing CAL-51 clonal cell lines treated with DMSO control (Unt) or 0.5 μM INCB054329 (BETi) for four hours with corresponding statistical metrics shown. (**B**) Heatmap of normalized expression for genes in the Hallmark MYC targets V2 geneset after MYCN-expressing CAL-51 clonal cell lines were treated as described in Part A.

Combination BETi and MEKi treatment in MYCN-expressing TNBC cell lines

Given that the majority of MYCN-expressing TNBC also contains MYC-expressing tumor cells (Figure 11B), we sought to identify drug combinations that would result in decreased expression of both isoforms and thereby inhibit cell proliferation and tumor development. MYC protein stability can be regulated by both the MAPK and PI3K pathways *(375)*, and inhibition of either signaling pathway can lead to MYC instability and proteasomal degradation *(287)*. Given that MAPK pathway inhibitors are under preclinical investigation to treat aggressive relapsed MYCN-driven neuroblastoma *(376, 377)* and were among the top "hits" in our previously described drug screens (Figure 16A and Figure 17A), we evaluated if MAPK pathway inhibition would alter MYCN protein levels and/or be effective at decreasing MYC expression when combined with BRD inhibition. $MYCN^{High}$ and MYC-expressing $MYCN^{Low}$ CAL-51 clonal cell lines were treated with inhibitors targeting proteins in the MAPK pathway, including EGFR (erlotinib), RAF (TAK-632), MEK1/2 (trametinib and GDC-0973), and ERK1/2 (SCH772984). MEK inhibitors (MEKi) were most effective at inhibiting MAPK signaling, as evidenced by decreased ERK1/2 phosphorylation, and decreased MYC-family isoform levels within respective cell lines (Figure 20A). Since the FDA-approved MEKi, trametinib, demonstrated the greatest decrease in MYC and MYCN levels, we evaluated the effects of trametinib treatment alone or in combination with BETi. MYCN levels decreased while MYC levels increased in CAL-51 $MYCN^{High}$ clonal cell lines treated with either BETi agent alone (INCB054329 or JQ1, Figure 20B). However, trametinib in combination with either BETi attenuated MYC upregulation, thereby decreasing levels of both MYC-family isoforms (Figure 20B).

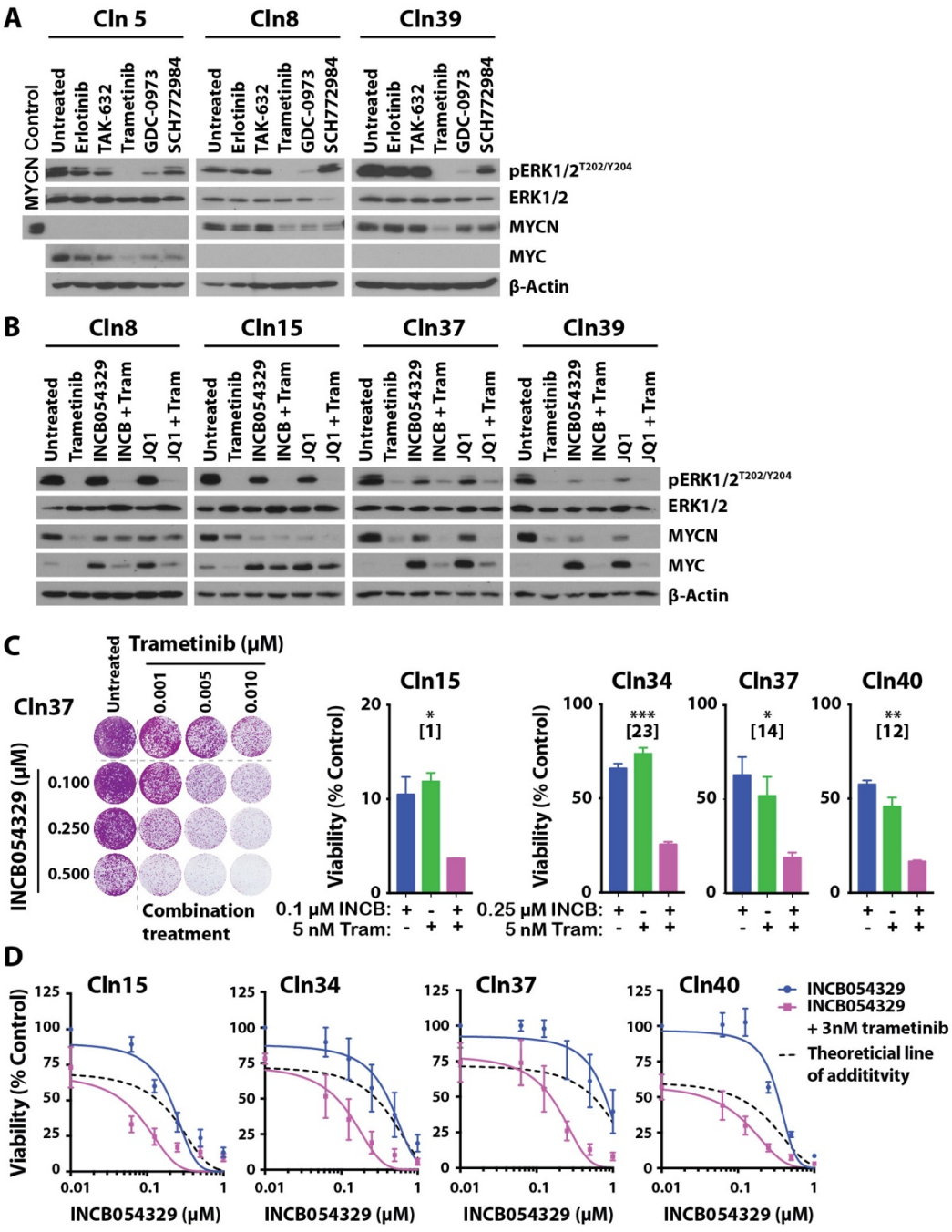

Figure 20. Effect of BETi and MEKi combination treatment on MYC-family isoform expression and cell viability of MYCN-expressing CAL-51 clonal cell lines. (**A-B**) Immunoblot analysis for pERK1/2, total ERK1/2, MYCN, MYC and β-Actin in the indicated CAL-51 clonal cell lines after treatment with MAPK pathway inhibitors at 0.25 μM for 24 hours (**A**) or treatment with 0.25 μM trametinib, 0.5 μM INCB054329, 0.5 μM JQ1, or the combination of trametinib with either BETi for 48 hours (**B**). All immunoblot experiments shown are representative of at least two biological replicates. (**C**) Left: Representative crystal violet-

stained colony formation assay (CFA) treated with INCB054329 (0.1, 0.25 and 0.5 μM) and trametinib (0.001, 0.005 and 0.01 μM), as single-agents or in combination, for six days. Right: Quantification of CFAs for the indicated four $MYCN^{High}$ cell lines representing one of the nine treatment combinations represented in the left panel. Data shown represent the means ± SD of two biological replicates. One-way ANOVA, *p<0.05, **p<0.01, ***p<0.001. Values in brackets represent synergy of combination treatment. (**D**) Forced suspension viability assays for the indicated four $MYCN^{High}$ cell lines treated with a dose escalation of INCB054329, 3 nM trametinib, or the combination of the two for seven days. Data shown represent the means ± SEM of four biological replicates. Dotted black lines represent the theoretical line of additivity, indicating data plotted below the theoretical line represents synergy between compounds evaluated in the combination treatment.

To determine the effects of BETi and MEKi on cell growth, we evaluated viability after single-agent and combination treatment in $MYCN^{High}$ cell lines in both adherent and non-adherent culture systems using colony formation assays and forced-suspension assays, respectively. Due to the high degree of single-agent efficacy in $MYCN^{High}$ cells to both 0.5 and 1.0 μM INCB054329 (Figure 17D), we evaluated the combination of BETi and MEKi on $MYCN^{High}$ clonally-derived lines that had demonstrated >10% residual viability after single-agent BETi (0.5 μM INCB054329) treatment (Figure 17D; Cln 15, 34, 37, and 40). Adherent and non-adherent cultures were treated with a dose escalation of low-dose INCB054329, as a single-agent or in combination with low-dose trametinib, for six and eight days, respectively (Figure 20, C and D). Cells grown as adherent cultures had a statistically significant synergistic decrease in cell growth in all lines tested [Cln15: ANOVA (p=0.0120), synergy (1); Cln34: ANOVA (p=0.0020), synergy (23); Cln37: ANOVA (p=0.0263), synergy (14); Cln40: ANOVA (p=0.0019), synergy (12)] (Figure 18C). By calculating the theoretical line of additivity between single-agents (see 'Drug sensitivity assays' in the materials and methods section for details), we also found cells cultured in forced suspension had a synergistic decrease in cell growth after BETi and MEKi combination treatment (Figure 20D).

To expand our analysis of effects of BETi and MEKi combination treatment on heterogeneous populations of MYCN-expressing TNBC, we treated CAL-51 and MDA-MB-468 cells with trametinib, INCB054329, or JQ1 as single-agents, or with either BETi in combination with trametinib, for 48 hours and examined MYC and MYCN expression. Treatment with either BETi alone decreased MYCN expression across both TNBC cell lines (Figure 21, A and B), consistent with previous single-agent results (Figure 18, E and F). While BETi treatment resulted in little to no change in MYC levels (Figure 21, A and B), single-agent trametinib decreased MYC expression to a greater extent than MYCN in both cell lines; and, when trametinib was combined with either BETi, MYC and MYCN decreased to a larger extent than with either agent alone (Figure 21, A and B). MDA-MB-468 and CAL-51 cell populations were treated with low-dose BETi and MEKi combinations to evaluate growth and viability in response to BETi and MEKi treatment. Both TNBC cell lines were treated with increasing doses of INCB054329 or JQ1, as single-agents, or in combination with increasing doses of trametinib, and colony-forming ability was assessed after six days (Figure 21C). MDA-MB-468, the higher MYCN-expressing cell line (Figure 12D, Figure 18F, and Figure 21B), displayed greater sensitivity to both single-agent BETi and MEKi treatments compared to CAL-51, and the combination of BETi and MEKi treatment resulted in a synergistic decrease in cell growth in both MYCN-expressing lines (Figure 21C). These data demonstrate low-dose BETi and MEKi combinations are effective in MYCN-expressing TNBC cell populations and provide the rationale to further evaluate the combination using *in vivo* model systems of MYCN-expressing TNBC.

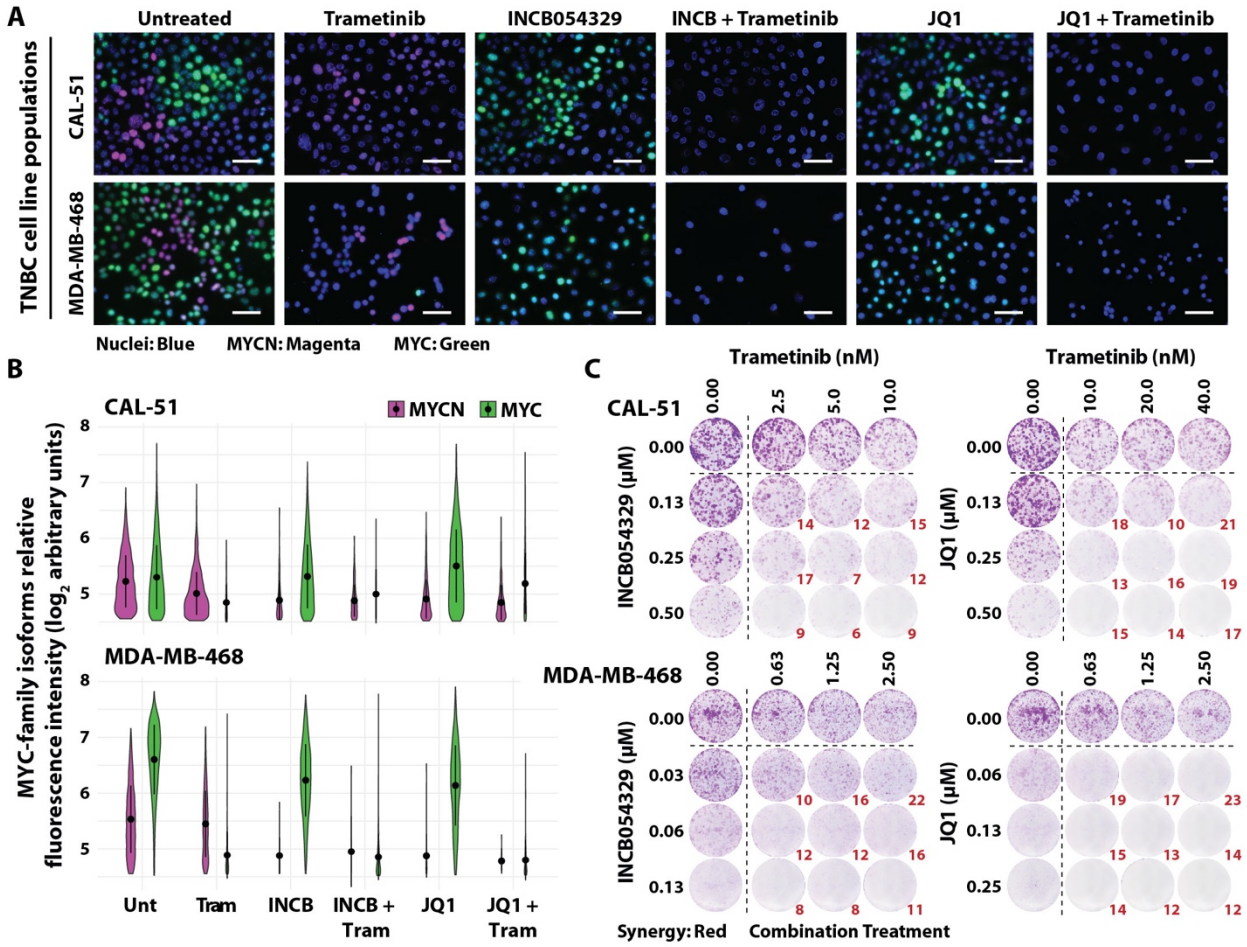

Figure 21. Effect of BETi and MEKi combination treatment on MYC-family isoform expression and cell viability of MYCN-expressing TNBC cell populations. (**A**) MYC-family isoform TSA-IF on two MYCN-expressing TNBC cell lines (MDA-MB-468 and CAL-51) after 0.25 μM trametinib, 0.5 μM INCB054329, 0.5 μM JQ1, or the combination of trametinib with either BETi for 48 hours. Colors represent cell nuclei (blue), MYCN (magenta), and MYC (green). Scale bar, 50 μM. (**B**) Violin plots showing quanfication of fluorescence intensity for MYCN and MYC after BETi treatments described in Part C. TSA-IF images and quantification are representative of three biological replicates. (**C**) Crystal violet colony formation assays for MDA-MB-468 and CAL-51 after treatment with the indicated concentrations of trametinib, INCB054329, or JQ1 alone, or either BETi in combination with trametinib, for six days. Values in red represent averaged synergy for combination treatments across three biological replicates.

Effects of BETi and MEKi treatment on in vivo growth of MYCN-expressing TNBC PDXs

To evaluate the preclinical efficacy of BET and MEK inhibition *in vivo*, we first confirmed MYCN and MYC protein expression in three TNBC PDX models with differing *MYCN* and *MYC* RNA expression (Figure 22A and Table 3A). The TM00096 PDX model is an M-subtype TNBC derived from a metastatic lung lesion (Table 3A) *(378)* and expresses MYCN and MYC in ~37% and ~51% of the tumor cells, respectively (Figure 22B). PDX models TM01273 and TM00090 both have a low percentage of MYCN-expressing cells (~2% and <1%, respectively) relative to MYC-expressing cells (~63% and ~32%, respectively) (Figure 22B). For all three models, a 2 mm^3 tumor was subcutaneously implanted into NOD *scid* gamma (NSG*)* mice and when xenograft tumor volumes reached ~150 mm^3, mice were treated with vehicle control, trametinib (0.1 mg/kg, QD), INCB054329 (50 mg/kg, BID), or the combination of the two agents at the indicated doses for 14 days. Compared to vehicle-treated controls, combined BET and MEK inhibitor treatment resulted in a synergistic and significant reduction in tumor growth only in the high MYCN-expressing PDX model (tumor growth inhibition (TGI): TM00096, 97%; TM01273, 58%; TM00090, 35%) (Figure 22C). These *in vivo* results were consistent with our *in vitro* observations and further confirmed an association between MYCN expression and efficacy of BETi and MEKi combination treatment.

To expand and reproduce our *in vivo* findings, we performed another PDX "trial" with TM00096 ($MYCN^{High}$) alongside two additional TNBC PDX models, HBCx1 and BCM2147, that have an intermediate ($MYCN^{Intermediate}$) or low ($MYCN^{Low}$) percentage of MYCN-expressing cells (~20% and ~2%, respectively) relative to MYC-expressing cells (~80% and ~95%, respectively) (Figure 22D). All three models were treated for 22 days

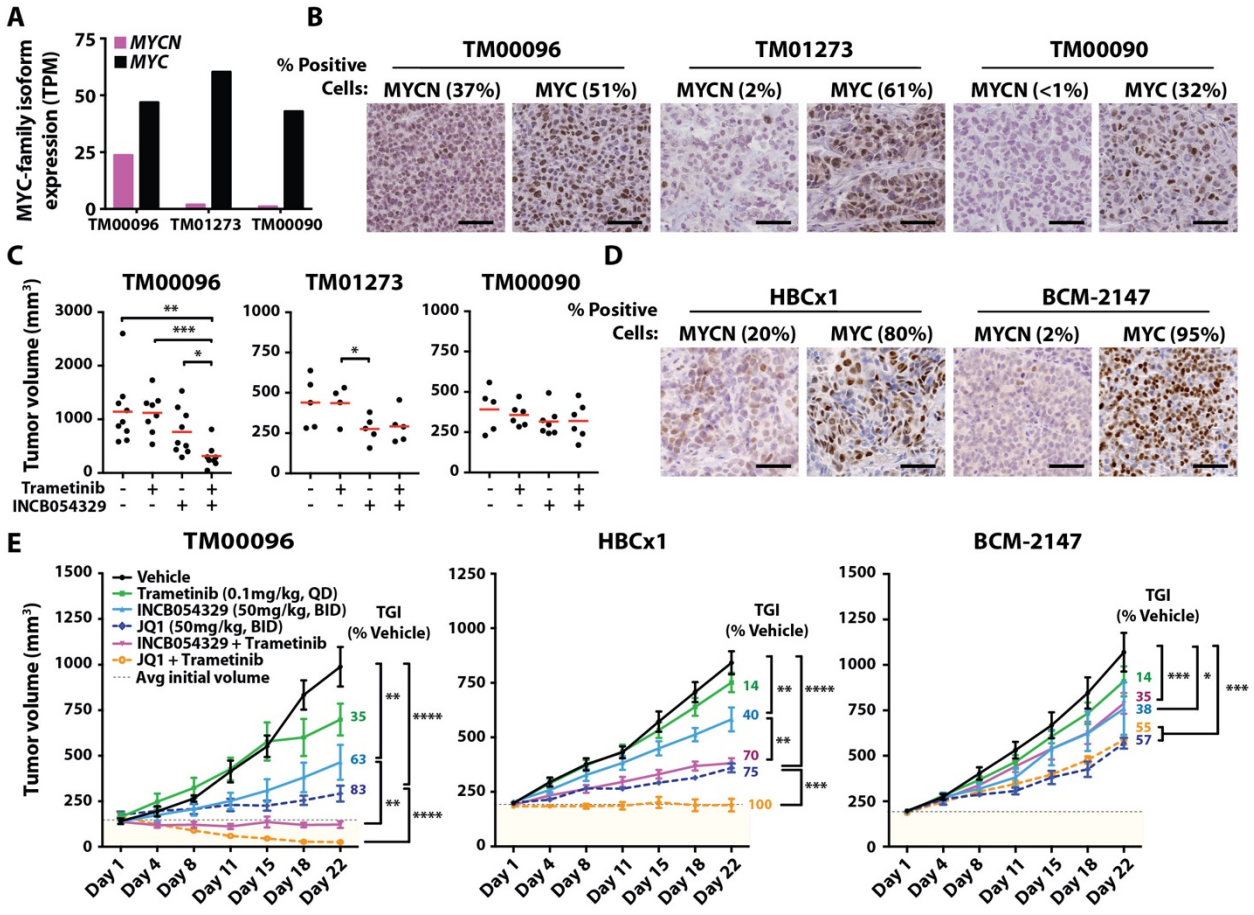

Figure 22. Evaluation of TNBC tumor growth after BETi and MEKi combination treatment *in vivo*. (**A**) *MYCN* and *MYC* expression (TPM) in three TNBC PDX models (TM00096, TM01273, and TM00090). (**B**) Representative IHC and quantification of percent positive cells for MYCN and MYC in TM00096, TM01273, and TM00090 sections. (**C**) Tumor volume (mm^3) of TM00096, TM01273, and TM00090 treated with trametinib (0.1mg/kg, QD) or INCB054329 (50mg/kg, BID) alone, or in combination for 14 days. Red bar represents mean. (**D**) Representative IHC and quantification of percent positive cells for MYCN and MYC in HBCx1 and BCM-2147 sections. (**E**) Tumor volume (mm^3) of TM00096, HBCx1, and BCM-2147 treated with trametinib, INCB054329, or JQ1 (50mg/kg, BID) alone, or either BETi in combination with trametinib for 22 days. TGI, tumor growth inhibition. QD, once daily. BID, twice daily. Data shown represent the means ± SEM. Unpaired t-test between vehicle, BETi, and corresponding combination treated tissue, *p<0.05, **p<0.01, ***p<0.001, ****p<0.0001.

with trametinib, INCB054329, or JQ1 (50 mg/kg, BID) as single-agents, or with the indicated BETi combined with trametinib. All compounds administered were well tolerated as all animals completed the study without excess weight loss (Figure 23) or limiting morbidities. We observed the greatest statistical difference from vehicle in response to either BETi treatment in the $MYCN^{High}$ model (TM00096) with a 63% TGI in response to INCB054329 treatment (compared to 40% and 38% in the $MYCN^{Intermediate}$ and $MYCN^{low}$ models, respectively) and an 83% TGI in response to JQ1 (compared to 75% and 57% in the $MYCN^{Intermediate}$ and $MYCN^{low}$ models, respectively) (Figure 22E). Combined MEKi and BETi resulted in a synergistic TGI in mice harboring either $MYCN^{High}$ and $MYCN^{Intermediate}$ tumors (Figure 22E) and an 11% and 85% reduction in tumor volume, compared to the starting treatment-naïve tumor volume, in the $MYCN^{High}$ PDX model when trametinib was combined with either INCB054329 or JQ1, respectively (left panel, yellow section; Figure 22E).

To determine the effects of the agents on pharmacodynamic markers *in vivo*, tumors were resected and protein extracted after the initial (two days) and final (22 days) treatments during the PDX study. Through immunoblot analyses, we observed that trametinib decreased pERK1/2 and both BETis decreased MYC and MYCN in all three PDX models, consistent with the agent's predicted biochemical activities (Figure 24A). To determine if decreased cell proliferation or increased apoptosis contributed to the observed decrease in tumor growth in the $MYCN^{High}$ and $MYCN^{Intermediate}$ models treated with the combination, we evaluated markers of proliferation (Ki67) and apoptosis (cleaved PARP and cleaved caspase-3) by IHC and immunoblot, respectively. Unlike the $MYCN^{Low}$ PDX model, Ki67 decreased in tissue from the $MYCN^{High}$ and $MYCN^{Intermediate}$ models

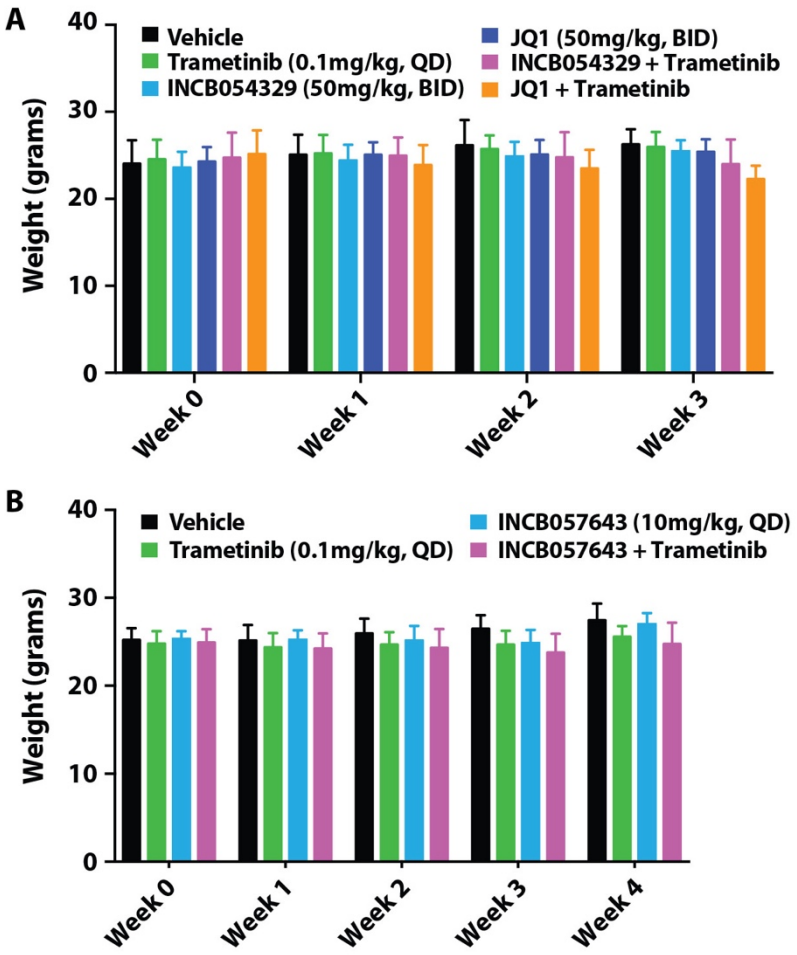

Figure 23. Effect of BETi and MEKi combination treatments on weight of treated mice. Averaged weight (grams) of mice measured weekly while treated with vehicle control (n=25), trametinib (0.1mg/kg, QD, n=25), INCB054329 (50mg/kg, BID, n=26), JQ1 (50mg/kg, BID, n=19), or the combination of trametinib with INCB054329 (n=25) or JQ1 (n=21) by orogastric gavage for 21 days (**A**) or with vehicle control (n=12), trametinib (0.1mg/kg, QD, n=12), or INCB057643 (10mg/kg, BID, n=11), or the combination of trametinib with INCB057643 (n=12) by orogastric gavage for 30 days (**B**). Data shown represent the means ± SD. QD, daily. BID, twice a day.

treated with either single-agent BETi or in combination with MEKi, after two days of treatment and to a greater extent at the end of treatment (Figure 24B). Only the $MYCN^{High}$ model displayed markers of apoptosis after two days of treatment with each single-agent alone or in combination (Figure 24A). These data suggest that BETis decreased both MYCN and MYC levels in tumor cells grown *in vivo*, and combination treatment resulted in a synergistic decrease in tumor volume in the MYCN-expressing TNBC models due to both anti-proliferative and pro-apoptotic mechanisms.

Changes in MYC-family isoform expression in vivo after BETi and MEKi combination treatment

To evaluate changes in cellular expression of MYCN and MYC during treatment, we performed IHC and dual MYC-family isoform TSA-IF on PDX tissue collected after initial and final doses. Similar to immunoblot results at the early treatment timepoint (Figure 24A), single-agent BETis decreased MYC levels in the $MYCN^{Low}$ PDX model and both MYC and MYCN levels in the $MYCN^{High}$ and $MYCN^{Intermediate}$ models (Figure 25A and Figure 26, A-C). Trametinib treatment alone transiently decreased both MYC-family isoforms in the $MYCN^{High}$ PDX model as protein expression returned to near basal, vehicle-treated levels by day 22 (Figure 25, A-C, and Figure 26, B and C). In contrast, trametinib combined with either BETi decreased MYCN and MYC levels to a greater extent than with either BETi alone throughout the time course of treatment in both $MYCN^{High}$ and $MYCN^{Intermediate}$ models (Figure 25, B and C). Taken together, treatment with either structurally distinct BETi, INCB054329 or JQ1, when combined with MEKi, continuously inhibited MYC-family isoform expression in PDX models with elevated

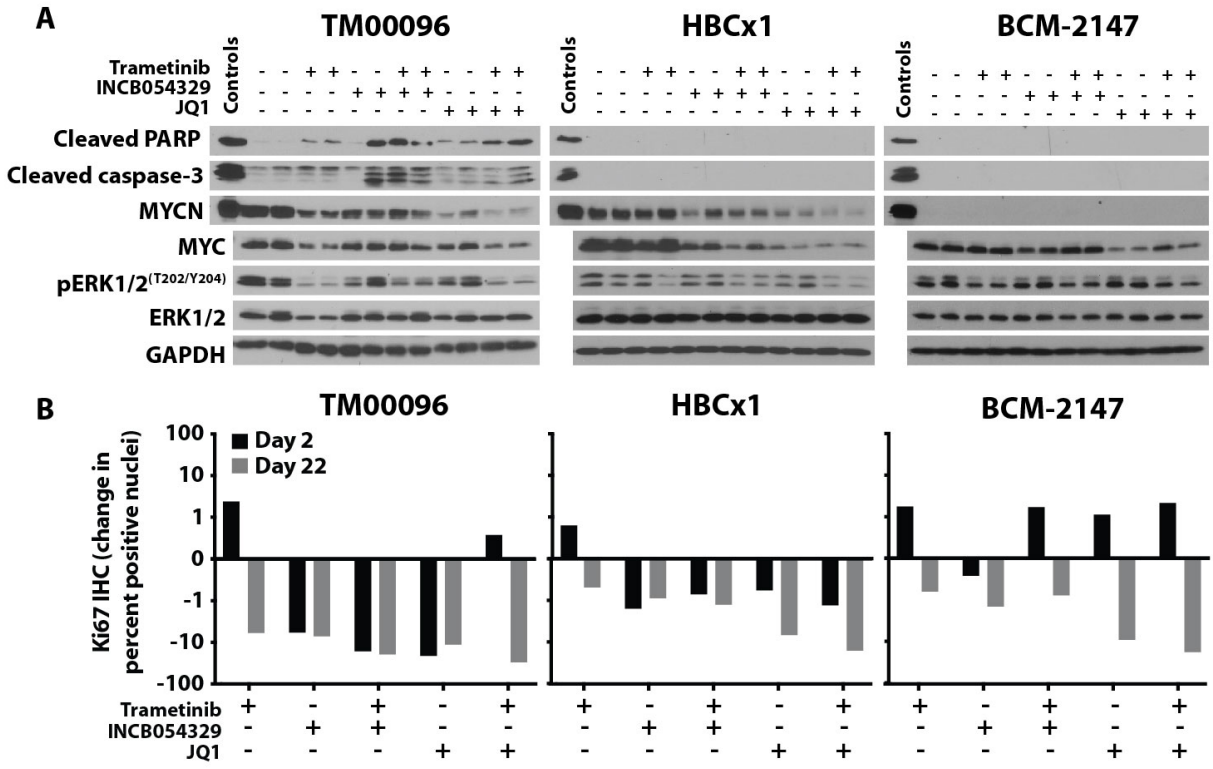

Figure 24. Evaluation of apoptosis and proliferation after BETi and MEKi treatment in TNBC PDX models. (**A**) Immunoblot analysis for pERK1/2, total ERK1/2, MYCN, MYC, cleaved PARP, cleaved caspase-3 and β-Actin, in TM00096, HBCx1, and BCM-2147 treated for two days with vehicle control, trametinib (0.1mg/kg, QD), INCB054329 (50mg/kg, BID), JQ1 (50mg/kg, BID), or the combination of trametinib with INCB054329 or JQ1. Two tumors per treatment condition. Controls represent SK-N-BE(2)C cell lysates for MYCN, and cell lysates prepared from irradiated CAL-51 Cln8 (50 J/m^2) for cleaved PARP and cleaved caspase-3. (**B**) Change in percent Ki67 positive nuclei in TM00096, HBCx1, and BCM-2147 tumor cells after treatment with compounds described in Part A.

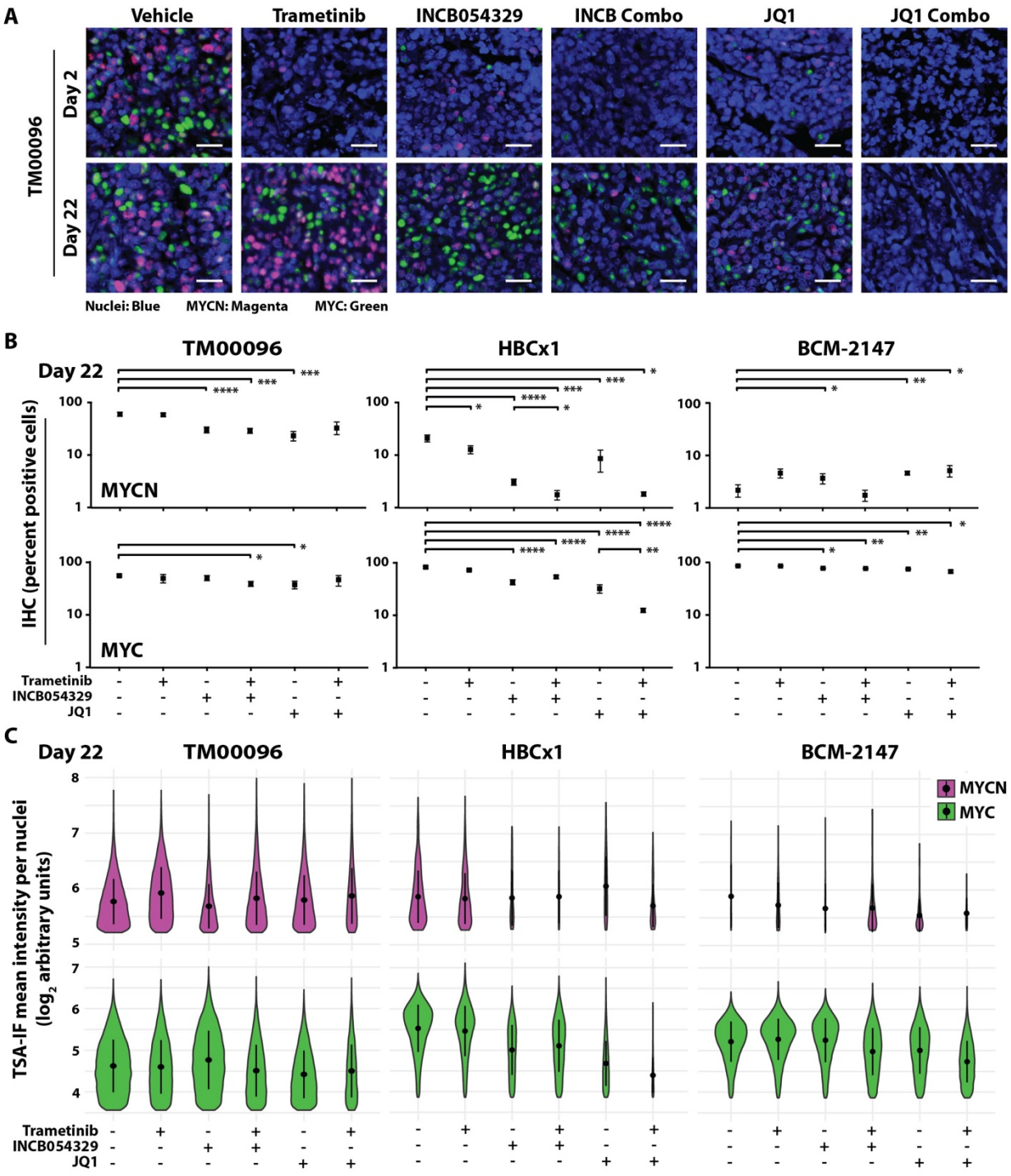

Figure 25. Evaluation of MYC-family isoform expression after BETi and MEKi combination treatment *in vivo*. (**A**) Representative TSA-IF of MYCN and MYC in TM00096 after two or 22 days of treatment with trametinib (0.1mg/kg, QD), INCB054329 (50mg/kg, BID), or JQ1 (50mg/kg, BID) alone, or either BETi in combination with trametinib. Colors represent cell nuclei (blue), MYCN (magenta), and MYC (green). Scale bar, 20 μM. (**B**) Quantification of IHC (percent positive cells) and (**C**) violin plots showing the distribution of TSA-IF intensity per

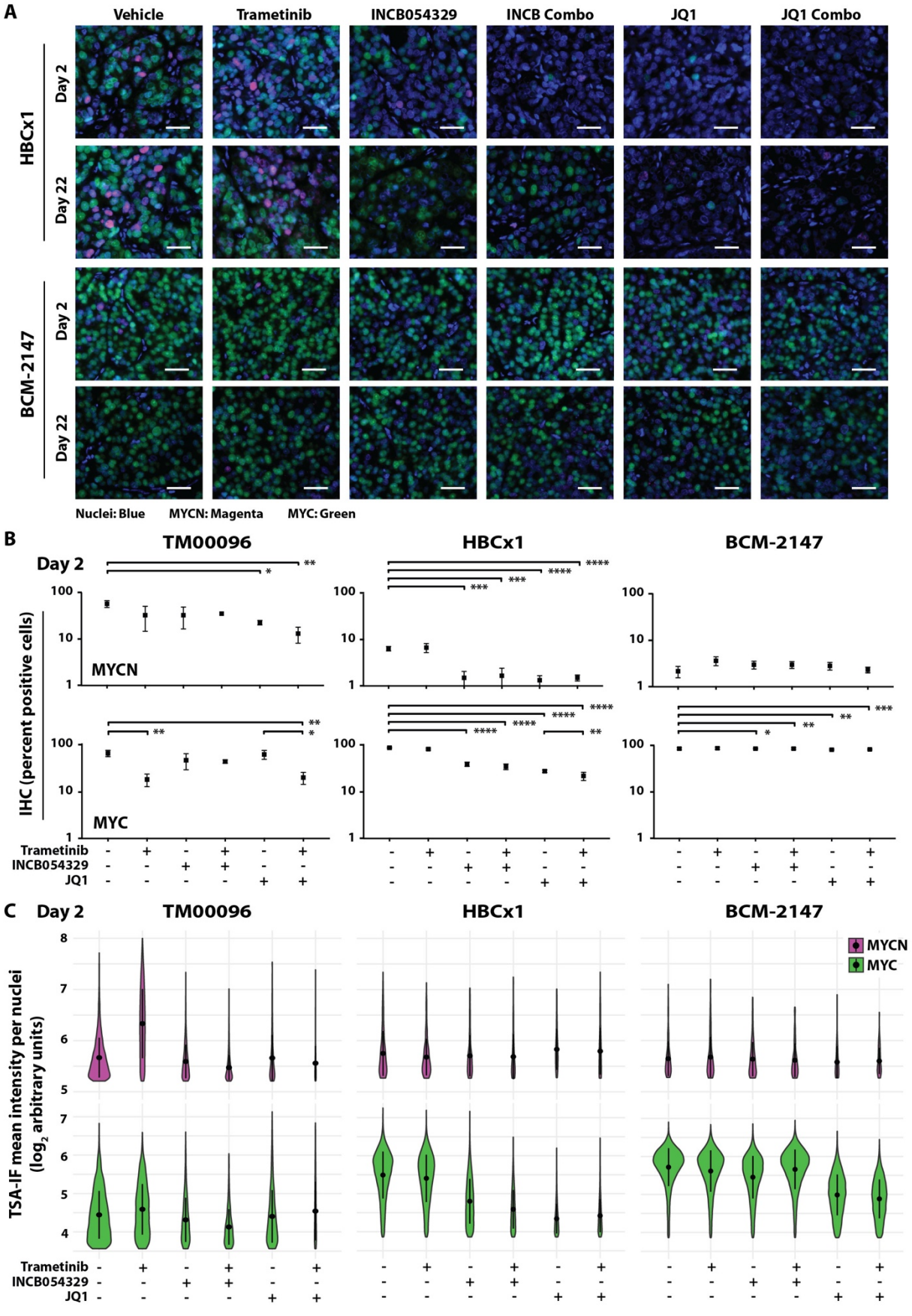
A
Vehicle
Trametinib
INCB054329
INCB Combo
JQ1
JQ1 Combo
HBCx1
Day 2
Day 22
BCM-2147
Day 2
Day 22
Nuclei: Blue
MYCN: Magenta
MYC: Green
B
TM00096
HBCx1
BCM-2147
Day 2
IHC (percent positive cells)
MYCN
MYC
Trametinib
INCB054329
JQ1
C
Day 2
TM00096
HBCx1
BCM-2147
MYCN
MYC
TSA-IF mean intensity per nuclei (log2 arbitrary units)
Trametinib
INCB054329
JQ1

Figure 26. Evaluation of MYC-family isoform expression after BETi and MEKi combination treatment *in vivo*. (**A**) Representative TSA-IF of MYCN and MYC in HBCx1 and BCM-2147 after two or 22 days of treatment with trametinib (0.1mg/kg, QD), INCB054329 (50mg/kg, BID), or JQ1 (50mg/kg, BID) alone, or with INCB054329 or JQ1 in combination with trametinib. Scale bar, 20 μM. (**B-C**) IHC (percent positive cells) (**B**) and TSA-IF intensity per nuclei (**C**) quantification of MYCN and MYC in TM00096, HBCx1, and BCM-2147 sections after treatments described in Part A for two days. Unpaired t-test between vehicle and treatment arms and between single-agent BETi and associated combination treated tissue, *p<0.05, **p<0.01, ***p<0.001, ****p<0.0001.

MYCN levels and resulted in synergistic tumor growth inhibition for both PDX models and tumor regression in the highest MYCN-expressing PDX model.

MYCN expression in primary and recurrent ER+ and HER2+ breast cancer

Despite there being effective first-line therapies for patients with HER2+ disease, patients with locally recurrent and/or metastatic HER2+ breast cancer have an unfavorable five-year survival and need additional therapeutic options *(25)*. To determine if we could extend our findings beyond TNBC, we analyzed *MYCN* expression across all primary, treatment-naïve breast cancer subtypes including estrogen receptor (ER)-expressing (ER+), HER2-amplified (HER2+), ER-expressing and HER2-amplified (ER+/HER2+), and TNBC within TCGA and METABRIC datasets. *MYCN* expression was highest in TNBC (p=<0.0001), as well as HER2+ (p=<0.0001) breast cancer, compared to ER+ tumors in both datasets (Figure 27, A and B). *MYCN* expression was also elevated in metastatic TNBC and HER2+ tumors compared to ER+ breast cancer in the MET500 dataset (Figure 27C) *(379)*.

Previously, we analyzed *MYCN* expression in TNBC cases from a recent study (37) evaluating transcriptional changes between primary and metastatic breast cancer. Similar to *MYCN* expression between primary TNBC and patient-matched metastases (Figure 10), *MYCN* levels in primary ER+ and HER2+ breast cancer were also elevated

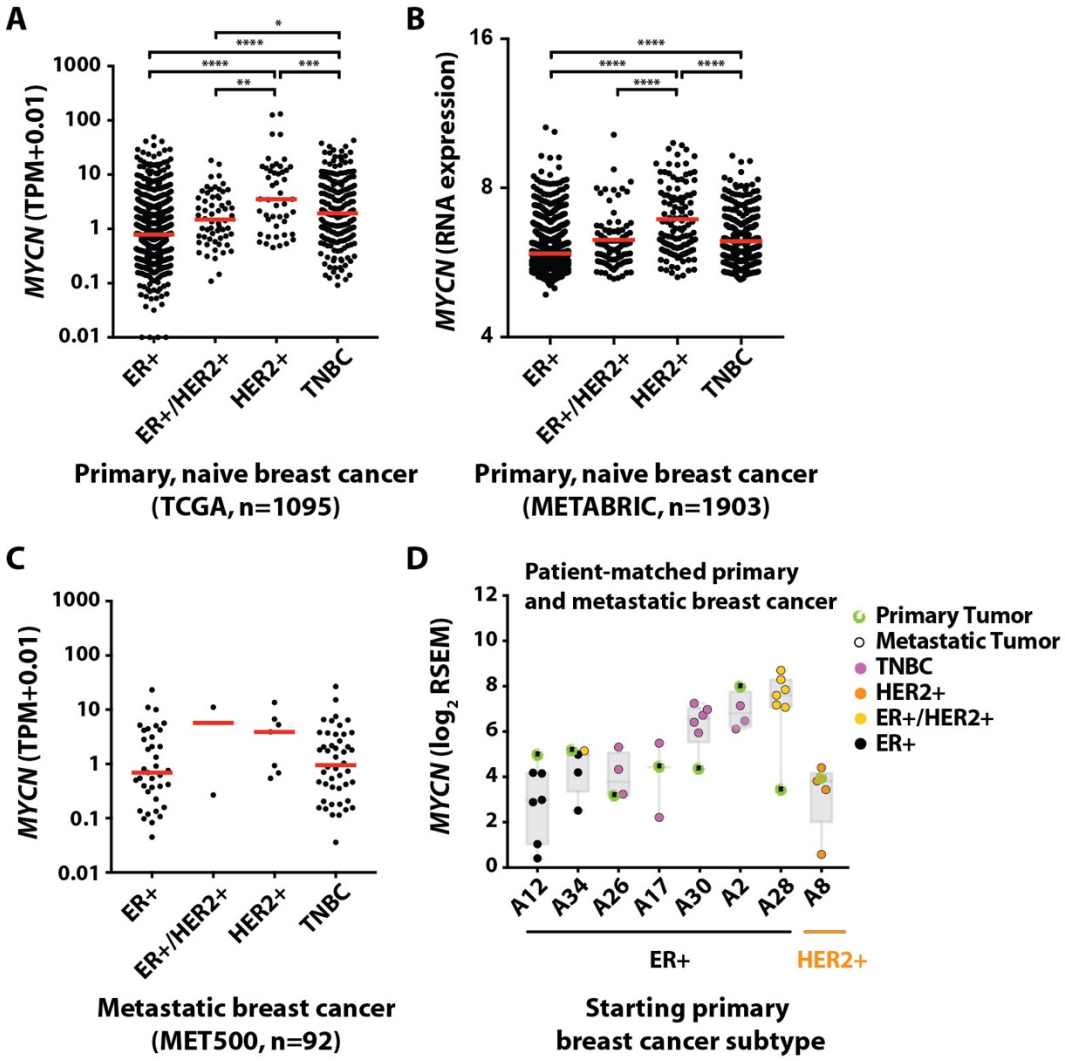

Figure 27. *MYCN* expression in primary and metastatic TNBC and ER+/HER2+ breast cancer. *MYCN* expression grouped according to breast cancer subtype (ER+ only, ER+/HER+, HER2+ only, TNBC) for primary, treatment-naïve cases from TCGA (BRCA) (**A**) and METABRIC (**B**) datasets. Unpaired t-test, *p<0.05, **p<0.01, ***p<0.001, ****p<0.0001. Red line represents mean. (**C**) *MYCN* expression (TPM) grouped according to breast cancer subtype for metastatic cases in the MET500 dataset. (**D**) *MYCN* expression in ER+ and HER2+ primary breast cancer and associated patient-matched metastatic lesions from Siegel *et al*. Primary and metastatic samples are circled in green and black, respectively. Colors represent TNBC (magenta), HER2+ only (orange), ER+/HER2+ (yellow), ER+ only (black) breast cancer samples.

or similarly expressed in nearly all associated metastatic specimens, except for one case with *ER* expression in both the primary tumor and associated metastases (Figure 27D). Of note, four of the seven patients with ER+ primary breast cancer lost *ER* expression in the metastatic setting and were redefined as TNBC; the majority of these metastatic lesions contained elevated MYCN expression compared to the primary tumor (Figure 27D). Similarly, the case that exhibited the greatest increase in *MYCN* expression in the metastatic setting was a primary ER+ tumor that had gained the expression of *HER2* during progression of the disease (Figure 27D). Although further analyses need to be conducted across larger datasets to determine the prevalence of MYCN expression in advanced HER2+ disease, the data presented in the previous chapter for TNBC may have implications for patients with HER2+ breast cancer.

Effect of BETi and MEKi treatment on in vivo growth of MYCN-expressing HER2+ breast xenograft tumors

To determine if the preclinical efficacy of BET and MEK inhibition observed for MYCN-expressing TNBC would be similar for MYCN-expressing HER2+ breast cancer, we first evaluated *MYCN* and *MYC* expression across a panel of HER2+ and TNBC PDX samples from Champions Oncology (CO) (Figure 28A). The only model with elevated *MYCN* expression was CTG-1475, a primary stage IV HER2+ invasive ductal breast carcinoma with little to no *MYC* expression (Figure 28A). To evaluated if RNA levels correlated with protein expression, we performed an immunoblot analysis for MYCN and MYC in CTG-1475 alongside the two other HER2+ breast cancer models and 16 TNBC PDX models (Figure 28B), including TM00096, the high MYCN-expressing TNBC PDX

model that demonstrated a synergistic response to combined BET and MEK inhibition (Figure 22A). Although MYCN levels in CTG-1475 were not as high as TM00096, they were elevated compared to the other breast cancer PDX models, and similar to *MYC* RNA expression, CTG-1475 had little to no MYC protein expression (Figure 28B). The inverse relationship between MYCN and MYC expression in this model was further validated through IHC and TSA-IF staining on tissue sections of CTG-1475 (Figure 28C). Based on these data, the CTG-1475 HER2+ PDX model was selected for *in vivo* tumor growth studies and evaluation of response to single-agent and combination BET and MEK inhibitors at CO.

For this study, CTG-1475 tumor fragments were subcutaneously implanted into the flank of female immunocompromised mice and when xenograft tumor volumes reached 150-300 mm^3, mice were treated with vehicle control, trametinib (0.1 mg/kg, QD), INCB057643 (10 mg/kg, BID), or the combination of the two agents at the indicated doses for 30 days. INCB057643 is a next-generation BETi and has a more favorable pharmacokinetic (PK) profile than INCB054329 *(380)*. Again, all compounds administered were well tolerated as all animals completed the study without excess weight loss (Figure 23B) or limiting morbidities. While both trametinib and INCB057643 had marked anti-tumor effects as single-agents, the combination resulted in a greater TGI than either agent alone and had a statistically significant reduction in tumor volume compared to vehicle control ($p=0.0201$, Figure 28D). Collectively, these data suggest that in addition to patients with advanced MYCN-expressing TNBC, those with advanced HER2+ MYCN-expressing breast cancer could also benefit from combined treatment with BET and MEK inhibitors.

A

Model	Doubling Time	Metadata: Subtype	Tumor Status	Histology	Harvest Site	Disease Stage	Tumor Grade	Treatment History	RNA log(RPKM+1): *MYCN*	*MYC*
CTG-1475	19 days	HER2+	Primary	Invasive ductal carcinoma	Breast	IV	Poorly differentiated	Pretreated	5.347	0.863
CTG-0018	20 days	TNBC	Metastatic	Colloid carcinoma	Lymph node	IV	Well differentiated	NA	3.319	2.695
CTG-1325	10 days	HER2+	Primary	Intraductal carcinoma	Breast	NA	Poorly differentiated	NA	2.887	6.482
CTG-1684	NA	HER2+	Metastatic	Adenocarcinoma	Liver	NA	Poorly differentiated	Pretreated	2.848	4.377
CTG-1408	38 days	TNBC	Metastatic	Invasive ductal carcinoma	Lymph node	IV	Poorly differentiated	Pretreated	2.827	6.626
CTG-1019	18 days	TNBC	Metastatic	Invasive ductal carcinoma	Liver	IV	Poorly differentiated	Pretreated	2.817	6.517
CTG-1340	9 days	TNBC	Metastatic	Invasive ductal carcinoma	Lymph node	III	Poorly differentiated	Pretreated	2.527	6.478
CTG-0869	9 days	TNBC	Metastatic	Invasive ductal carcinoma	Chest	IV	Poorly differentiated	Pretreated	2.522	7.545
CTG-1151	52 days	TNBC	Metastatic	Invasive ductal carcinoma	Lymph node	IV	Poorly differentiated	Pretreated	2.094	4.988
CTG-0017	20 days	TNBC	Metastatic	Carcinoma	Lymph node	IV	Poorly differentiated	Pretreated	1.850	6.166

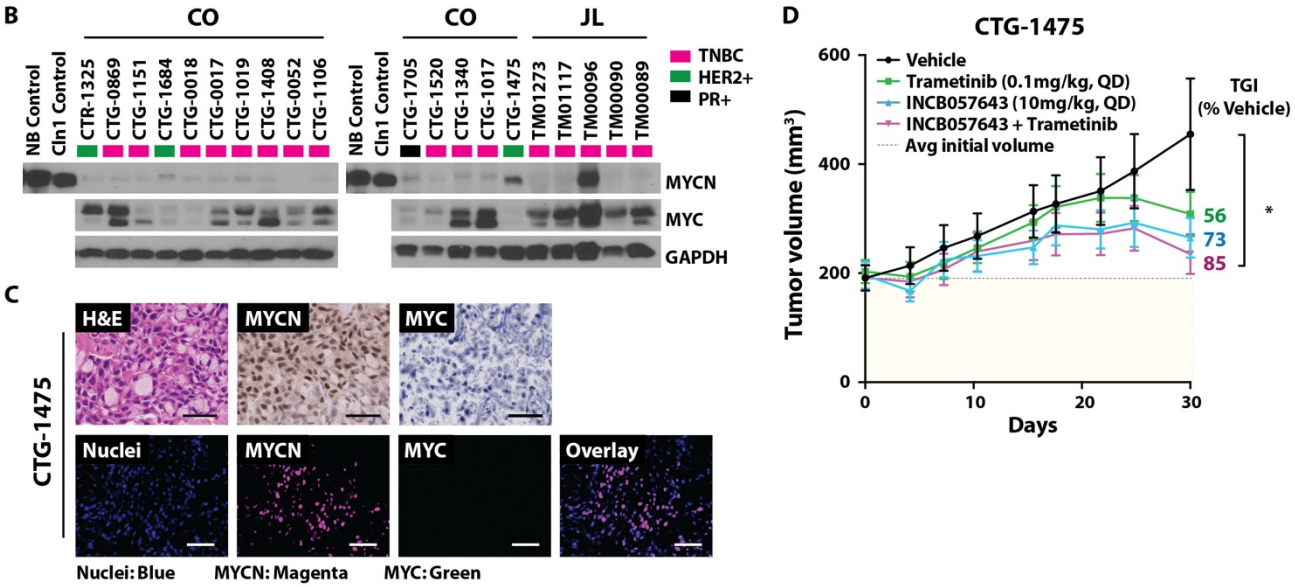

Figure 28. Evaluation HER2+ breast cancer tumor growth after BETi and MEKi combination treatment *in vivo.* (**A**) Metadata and MYC-family isoform (*MYCN* and *MYC*) expression for TNBC and HER2+ breast cancer PDX samples from Champions Oncology (CO). The PDX highlighted in red was the model selected for IHC/TSA-IF analyses and drug sensitivity studies as described in Fig. 28. (**B**) Immunoblot analysis for MYCN, MYC, and GAPDH in TNBC (magenta), HER2+ (green), and PR+ (black) breast cancer cases from CO and Jackson Laboratories (JL). (**C**) Representative hematoxylin and eosin (H&E), IHC, and TSA-IF stains of MYCN and MYC in the CTG-1475 HER2+ breast cancer PDX model. Colors represent cell nuclei (blue), MYCN (magenta), and MYC (green). Scale bars, 20 μM (IHC) and 50 μM (TSA-IF). (**D**) Tumor volume (mm^3) of CTG-1475 treated with vehicle control (n=12), trametinib (0.1mg/kg, QD, n=12), or INCB057643 (10mg/kg, BID, n=11), or the combination of trametinib with INCB057643 (n=12) by orogastric gavage for 30 days. TGI, tumor growth inhibition. Data shown represent the means ± SEM. Unpaired t-tests between treatment arms, *p<0.05.

Discussion

Previous studies have demonstrated MYCN and MYC preferentially regulate the same set of core genes involved in metabolism and cell growth, and while the MYCN allele can functionally replace MYC in murine development *(180)*, MYCN and MYC have separate temporal regulation over organogenesis in early vertebrate development *(358)*. *MYCN* expression is essential for the initial establishment of stem and progenitor populations; over the course of organ system development, *MYCN* expression switches to low *MYC* expression to support stem and progenitor cell maintenance, and during cell lineage commitment and expansion, elevated *MYC* levels drive highly proliferative cells until they reach terminal differentiation *(358)*. MYC-isoform expression within vertebrate development and in normal breast tissue will be discussed further in the Future Directions section. Of relevance to this discussion, developmental studies demonstrate the ability of cells to switch between MYCN and MYC expression over time while serving differing roles in progenitor cells, tissue homeostasis, and organogenesis. Similarly, an elegant study using endogenous fluorescent labels for MYCN and MYC demonstrate both isoforms are necessary for the survival of hematopoietic stem cells. They show that MYCN is involved in the self-renewal of quiescent stem cells and that MYCN expression switches to MYC expression upon differentiation to transit-amplifying progenitors *(349, 381)*. MYC-family isoform switching in our clonally-derived TNBC cell line models indicates tumor cells have retained the epigenetic ability to transition between MYCN and MYC, which may account for the large range (2-100%) of MYCN expression within heterogenous TNBC cell populations. Although a MYCN-to-MYC transition is typically observed, MYC-expressing

cells may revert to a MYCN-expressing state to provide a survival advantage in the presence of therapeutic perturbations.

By isolating and expanding single cells from heterogeneous TNBC tumor-derived cell line populations, we were able to generate novel MYCN- and MYC-expressing cell cultures with a similar genetic background, thus allowing us to assign the biological relevance of MYCN versus MYC expression to the sensitivity of compounds under preclinical investigation. We conducted a high-throughput 158-drug screen that included compounds from the NCI FDA-AOD library and identified inhibitors of the BRD-family of transcriptional regulators (e.g. BETi) that were preferentially effective in inhibiting MYCN-expressing tumor cell growth. BETis are a class of compounds currently under early stage clinical development that broadly targets the BRD family (predominantly BRD2, BRD3, and BRD4) of transcriptional regulators *(373)*. These compounds were of particular interest given a previous report of preferential sensitivity of BETis in TNBC compared to other breast cancer subtypes *(374)*. Further, the activity of BETis has been predominantly attributed to the selective disruption of super-enhancer-associated genes that deregulates transcription factor activity *(374, 382, 383)*. BRD4 regulates transcription of *MYCN* as well as occupies MYCN target-gene enhancers and super-enhancer genomic sites, and preclinical studies have suggested BETis as a promising strategy to target MYCN-driven neuronal [neuroblastoma *(271, 273)*, medulloblastoma *(384)*, embryonal tumors with multilayered rosettes *(385)*] and non-neuronal [ovarian cancer *(343)*, alveolar rhadomyosarcoma *(386)*] tumor cell growth.

While prior studies have focused on BRD-mediated targeting of MYC, we show that TNBC tumors are heterogeneously composed of MYC and MYCN-expressing cells

and MYCN-expressing cells have differential sensitivity to BETis in select tumor cells and model systems. Currently, BETis are in the initial stages of clinical assessment and have had their greatest single-agent clinical efficacy in hematopoietic and NUT midline malignancies *(373)*; however, favorable preclinical investigation with BETi combination treatments have catalyzed interventional trials to improve hematopoietic malignancy and solid tumor patient responses *(373, 387)*. The synergy between BETi and MEKi has been attributed to an upregulation of MAPK pathway signaling in response to BETi treatment *(388)* and the ability of BETis to disrupt adaptive bypass mechanisms induced by MEKi treatment *(389)*. While we did not observe an upregulation of MAPK pathway signaling after BETi treatment in either our TNBC cell lines or PDX tissue, we cannot rule out chromatin modulation or enhancer remodeling in response to treatment with either single-agent given the rebound/upregulation of MYC expression in response to BETi treatment in the CAL-51 clonal cell lines.

Conclusions

We discovered that single-agent BETi and MEKi treatments decreased both MYCN and MYC expression and had a greater effect when used in combination. Importantly, combined low-dose BETi and MEKi displayed a synergistic decrease in tumor cell viability in cell line cultures and in mice harboring TNBC PDXs with the heterogeneous expression of both MYCN and MYC. Based on our preclinical results using adherent and non-adherent *in vitro* TNBC cell lines models and *in vivo* TNBC and HER2+ breast cancer PDX models, we posit that BETi and MEKi combination treatment will induce regression of MYCN-expressing breast tumors and/or reduce the advent of

MYCN-mediated metastases. Given that patients with TNBC primarily receive systemic cytotoxic chemotherapies that frequently result in unfavorable outcomes, we initially propose the clinical development of combination BET and MEK inhibitors for patients with advanced or recurrent TNBC with the evaluation of MYCN as a relevant biomarker for patient selection. Any benefits observed clinically for TNBC will inform future studies for TNBC as well as non-TNBC MYCN-expressing tumors.

CHAPTER V

SYNOPSIS AND FUTURE DIRECTIONS

The poor prognosis associated with TNBC is primarily due to the lack of biomarkers used to direct effective therapeutic options for this very heterogeneous subtype. While patients with TNBC achieved a greater pathological complete response to neoadjuvant chemotherapy compared to the other breast cancer subtypes, the majority of patients with TNBC experience recurrence and succumb to their disease. To evaluate if MYCN, a proto-oncogene shown to be aberrantly expressed in a variety of neuronal and non-neuronal tissues, was also deregulated in TNBC, we performed a series of immunohistochemistry-based analyses on >300 TNBC specimens representing the main stages of disease progression, including: at diagnosis (primary, treatment-naïve tissue), after standard-of-care NAC treatment (NAC-treated residual disease), and after the onset of disease recurrence (locally-recurrently/metastatic lesions).

In conjunction with *MYCN* expression analyses from TNBC tumor cells, pre- and post-NAC treatment, and between primary and metastatic patient-matched tumors, we determined that: (i) MYCN-expressing tumor cells were present within a significant fraction (55%) of TNBC tumors; (ii) MYCN-expressing cells increased in expression level (mean H-score, 25 to 29) and frequency (45% to 64%) after NAC treatment primarily consisting of anthracyclines and taxols; (iii) both MYCN RNA and protein were detected in metastatic TNBC; and (iv) patients with TNBC tumors with elevated MYCN expression had decreased rates of overall survival by approximately 30%.

This dissertation research also led to the discovery that nearly half of all TNBC tumors heterogeneously co-express MYCN and MYC within intratumoral cell populations, and the majority of cell nuclei robustly expressed only one MYC family member. Through isolation and analysis of individual cells from a TNBC cell line that was derived from a metastatic lung lesion, we were able to confirm the heterogeneous nature of MYC and MYCN protein expression observed in clinical specimens and create unique TNBC clonal cell line models to evaluate differing growth properties and drug sensitives between MYCN- and MYC-expressing TNBC cells. By conducting high-throughput drug screens using 158 compounds, currently or previously under clinical development, we observed increased sensitivity of MYCN-expressing tumor cells to several drug classes including BET, Aurora-A, and MAPK pathway inhibitors. Drug combination studies, using BETi and MEKi on TNBC cell line and PDX models with heterogeneous expression of MYCN and MYC, resulted in a synergistic decrease in tumor cell growth and/or viability that mirrored cumulative MYC-family isoform expression levels after treatment. Many questions remain as to the biological relevance of MYCN-expressing cells in breast cancer, if MYCN- and MYC-expressing tumor cells have unique differentiation states, and if expression of one family member versus the other contributes to or is just a biomarker of disease progression.

MYCN- and MYC-expressing TNBC drug sensitivity and resistance

Standard-of-care chemotherapy for patients with primary, localized TNBC generally consists of the DNA damaging agents called anthracyclines (e.g. doxorubicin) and microtubule stabilizers known as taxanes (e.g. paclitaxel). The vast majority of the primary, NAC-treated tissue used to determine levels of MYCN-expressing cells after chemotherapy were surgical resections after treatment with either an anthracycline (85%) and/or a taxane (58%), collectively representing 96% of all samples. To identify oncogenic signaling pathways in residual disease after NAC that may be candidates for drug development, Balko and colleagues performed a comprehensive molecular analysis on 74 TNBC tumors after NAC using targeted next-generation sequencing and digital RNA expression analyses. After *TP53* alterations (89%), *MCL1* and *MYC* were amplified in 54% and 35% of NAC-treated TNBC, respectively *(321)*. While the frequency of amplified *MYC* was similar to that of primary, treatment-naïve TNBC, a greater number of *MCL1*-amplified TNBC was observed post-NAC compared to basal-like primary, treatment-naïve tumors in TCGA (54% post-NAC versus 19% treatment-naïve) *(321)*. These data demonstrate retention and/or acquisition of high-frequency *MYC* amplifications post-NAC. These tissue, as well as patient-matched primary and NAC-treated TNBC samples, were generously provided by Dr. Balko for our investigation of MYCN and MYC expression pre- and post-NAC described in Chapter III. While MYC levels and frequencies were similar between the independent cohorts of primary, treatment-naïve and NAC-treated TNBC cases, a significant fraction of specimens also expressed MYCN. The frequency of MYC-Only-expressing cases transitioned from 46% to 21% to 45% between the primary, treatment-naïve; primary, NAC-treated; and recurrent TNBC cohorts, respectively. Of

importance, the percentage of MYCN-Only- and dual MYCN/MYC-expressing cases increased post-NAC (MYCN-Only: 9% to 16%, both MYCN and MYC: 34% to 49%). Further, the majority (91%) of recurrent MYCN-expressing TNBC cases also express MYC. The IHC evaluations of MYC protein were similar to results from the Balko lab and suggest a cooperation between MYC and MYCN during tumor progression.

Through the use of single-cell sequencing, elevated *MYCN*-expression has been shown to associate with TNBC tumor cells that have a basal/stem-like differentiation state and seed metastatic lesions; *MYCN*-expressing low-burden tumors then expanded and differentiated into high *MYC*-expressing proliferative tumors with luminal gene expression *(261)*. Consistent with this report, MYC levels were higher in recurrent tumors compared to primary tumors [mean H-score: recurrent TNBC (86) versus primary, treatment-naïve (33) and NAC-treated TNBC (32)]. Whether the actual *MYCN*-expressing basal/stem-like cells that seeded metastatic lesions in the Lawson *et al.* study were just present at lower percentages within high-burden *MYC*-expressing tumors or they differentiated into *MYC*-expressing cells is unknown and should be investigated further.

In Chapter III, we generated MYC- and MYCN-expressing clonal cell lines through isolation of individual cells from the CAL-51 TNBC cell line cultured with and without in the presence of PI3Ki. The percentage of MYCN-expressing clonal cells increased from 6% to 86% after exposure to continuous PI3Ki exposure, implicating an association between MYCN expression and PI3Ki resistance. Along these same lines, Muellner and colleagues created isogenic cell lines from the human breast epithelial cell line MCF10A and performed a synthetic lethal screen *(390)*. Barcoded cells were transfected with cDNA for overexpression, or siRNAs for knockdown, of 70 cancer-related genes and then

evaluated for resistance to the dual PI3K/mTOR inhibitor, BEZ235 *(390)*. By validating "hits" from this screen, the authors reported *MYC* was one of the primary genes responsible for PI3Ki resistance *(390)*. Similar results have been described in several other studies evaluating mechanisms of resistance to PI3Kis *(391)*. Of note, two of the fourteen clonal cell lines generated from our PI3Ki-resistant TNBC cell population expressed MYC, indicating MYC-expressing cells were resistant to PI3Ki-induced senescence or cell death. However, unlike MYCN-expressing cells isolated from the same cell population, the MYC-expressing cells reverted back to a PI3Ki-sensitive state.

To evaluate mechanisms of PI3Ki-resistance and differential drug sensitivities between MYCN- and MYC-expressing TNBC cells, we performed a high-throughput drug screen described in Chapter IV using the NCI FDA-Approved AOD library and 44 additional compounds of interest. The additional compounds included the previously-mentioned inhibitors that target MYC-family isoform expression (i.e. BRD family, Aurora-A, and MAPK pathway inhibitors) as well as several inhibitors against proteins known to prevent apoptosis, including the anti-apoptotic proteins BCL2 (ABT737) and MCL1 (VU661013). The latter compound, along with two other MCL1 inhibitors, were generously provided by Dr. Stephen W. Fesik at VUMC. Mentioned in Chapter I, *MYCN*-amplified neuroblastoma cell lines have demonstrated sensitivity to BCL2 inhibitors *(316)*. In contrast to this study, we found the MYCN-expressing TNBC cell lines were resistant to the BCL1 inhibitor but hypersensitive to all three MCL1 inhibitors. To further explore MCL1-sensitivity in the context of PI3Ki-resistance, we treated two *PIK3CA*-mutant, PI3Ki-resistant TNBC cell lines, MDA-MB-453 and CAL-148 (previously generated alongside CAL-51 PI3Ki-resistant line), and corresponding parental cell line controls with

the MCL1 inhibitors. Given that there was no difference in MCL1-sensitivity between the MDA-MB-453 and CAL-148 PI3KiR and parental lines (data not shown, d.n.s), the MCL1-sensitivity observed in the CAL-51 MYCN-expressing PI3Ki-resistant clonal cell lines was either cell line-specific or related to the MYCN-expressing cell state.

As previously mentioned, EZH2 is an enzymatic component of the polycomb repressive complex that facilitates the NEPC cell state that is associated with expression of MYCN. Inhibitors targeting EZH2 have been shown to inhibit growth of MYCN-expressing NEPC cells *(256)*. Therefore, we included an inhibitor of EZH2 in our initial primary screen. We observed no difference in sensitivity between $MYCN^{High}$ and $MYCN^{Low}$ (MYC-expressing) cell lines. The CAL-51 $MYCN^{High}$ lines either have no expression or similar expression of CHGA, SYP, ENO2, and NCAM1, canonical neuroendocrine markers *(256)*, compared to the $MYCN^{Low}$ lines, indicating the MYCN-expressing TNBC cell line models do not associate with a neuroendocrine cell state and therefore, would not have increased drug sensitivity to EZH2 inhibitors. Previous studies have shown binding of Aurora-A stabilized MYCN protein and that inhibition of Aurora-A resulted in uncoupling of the Aurora-A complex from the degron of MYCN, leading to polyubiquitination and subsequent proteasomal degradation *(295)*. However, decreased tumor cell growth after Aurora-A inhibitor treatment has been observed for both MYC- and MYCN-expressing tumors *(316, 392)*. Allosteric Aurora-A inhibitors have also shown activity in the treatment of MYCN-amplified neuroblastoma *(298)*; therefore, we included the allosteric Aurora-A kinase, CD532, along with ATP-site competitive small molecule inhibitors, MLN8237 and MK-457, in our drugs screen. Compared to the TNBC $MYCN^{Low}$ (MYC-expressing) lines, the $MYCN^{High}$ cells in both the primary and validation screens

had increased sensitivity to MLN8237 and MK-457 but demonstrated no differential sensitivity to CD532, with all lines exhibiting similar relative sensitivity to CD532. These data suggest that allosteric Aurora-A inhibitors would not be selective for MYCN-expressing TNBC tumors.

The canonical MAPK pathway is activated by RAS-mediated mechanisms and signals through MEK1/2 and ERK1/2 to drive the transcription of genes involved in pathways that include proliferation, differentiation, and migration *(393)*. High-risk neuroblastoma is a subset of neuroblastic tumors characterized by pathological advanced disease and/or the presence of MYCN gene-amplifications *(394)*. In an analysis of chemotherapy-resistant relapsed disease, the vast majority of tumors demonstrated active RAS-MAPK pathway signaling predictive of MEK inhibition *in vitro* and *in vivo (376)*. Given that previous studies have also demonstrated the MAPK pathway contributes to MYC phosphorylation and stability *(287)*, we included several MAPK pathway inhibitors in our primary and validation drug screens, including the FDA-approved MEK inhibitor, trametinib. MAPK pathway inhibitors were the top “hits” in both screens. We show in Chapter IV that MAPK pathway inhibitors downstream of MEK resulted in decreased MYCN and MYC protein in all MYCN- and MYC-expressing CAL-51 cell line models, with trametinib resulting in the greatest decrease in protein levels. Whether changes in MYCN protein expression by trametinib treatment were due to altered transcriptional, translational, or protein stability is currently unknown and could be the basis of future studies.

MYCN- versus MYC-associated gene expression in TNBC

The discovery of both intertumoral and intratumoral heterogeneity of MYCN and MYC expression in TNBC led us to wonder if the associated gene expression differed between cells that express a given MYC-family isoform. We performed differential gene expression analyses using the TNBC587 dataset and compared TNBC tumors based on *MYCN* and *MYC* expression levels and the ratio of expression relative to each other. *MYCN*^{HighRatio} tumors have the highest *MYCN* expression and the lowest *MYC* expression. Conversely, *MYC*^{HighRatio} tumors have the highest *MYC* expression and the lowest *MYCN* expression. Selecting tumors based on expression levels as well as respective expression ratios allowed us to minimize the inclusion of heterogeneous tumors co-expressing both isoforms and therefore reduce confounding results. To ensure the optimal number of *MYCN*^{HighRatio} and *MYC*^{HighRatio} tumors were selected for differential gene expression analyses and that genes identified were not by chance, we performed a simulation between a percentage (1-10%) of tumors from the TNBC587 cohort selected at random compared to the same percentage of the top *MYCN*^{HighRatio} and *MYC*^{HighRatio} tumors. The top 7% of *MYCN*^{HighRatio} and *MYC*^{HighRatio} tumors demonstrated the greatest number of statistically significant differentially expressed genes compared to 7% of tumors selected at random (Figure 32, panel A). The tumors selected and the statistically significant differentially expressed genes compared between the two groups are presented in Figure 32, panel B and C.

To determine the degree of variance between all *MYCN*^{HighRatio} and *MYC*^{HighRatio} tumors selected for analysis, we performed a principal component analysis (PCA). Although the variation between subgroups was relatively small (PC1, 11%), *MYCN*^{HighRatio}

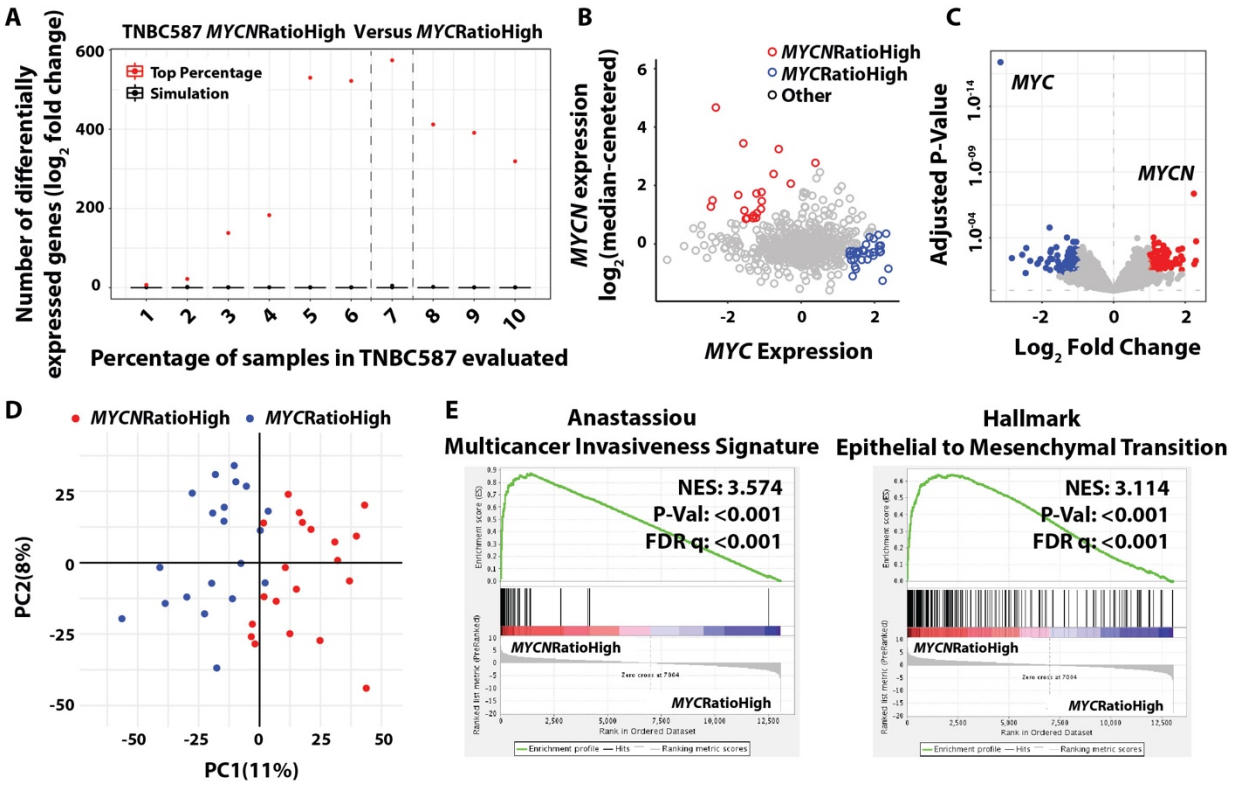

Figure 29. Differential gene expression analyses between *MYCN*$^{\text{RatioHigh}}$ and *MYC*$^{\text{RatioHigh}}$ TNBC. (**A**) Number of differentially expressed genes between a percentage (1-10) of TNBC samples in the TNBC587 dataset selected at random (simulation, black) versus samples selected for high expression of either MYC-family isoform (*MYCN* or *MYC*) relative to each other (top percentage, red). The dotted vertical lines represent the percent of samples from TNBC587 with the highest number of differentially expressed genes between samples with high *MYCN* expression relative to *MYC* expression (*MYCN*RatioHigh) versus high *MYC* expression relative to *MYCN* expression (*MYC*RatioHigh). These samples are highlighted in Panel B. (**B**) The top seven percent of *MYCN*RatioHigh (red) and *MYC*RatioHigh (blue) samples in the TNBC587 dataset and (**C**) corresponding differentially expressed genes. (**D**) Principal component analysis and (**E**) geneset enrichment analyses (GSEA) from statistically significant differentially expressed genes from samples described in Part A and B.

and *MYC*^{HighRatio} tumors clustered apart from each other, indicating tumors within each respective group have a greater similarity to each other than they do to tumors of the opposing group (Figure 32D). We show in Chapter III that MYCN is elevated in M-subtype TNBC, a subtype that associates with higher expression of genes involved in cell motility and EMT *(97)*. Consistent with this result, GSEA between *MYCN*^{HighRatio} and *MYC*^{HighRatio} tumors demonstrated an association between *MYCN* expression and pathways involved in EMT (Hallmark Epithelial to Mesenchymal Transition, p<0.001, false discovery rate [FDR] q=0.009) and invasion (Anastassiou Multicancer Invasiveness Signature p<0.0001, FDR q<0.001) (Figure 32E). Similarly, *MYCN* expression has also been associated with EMT in neuroendocrine prostate cancer *(256)*. Of note, MEK signaling is up in *MYCN*^{HighRatio} tumors compared to *MYC*^{HighRatio} tumors (El-Ashry MEK Up V1 Up p<0.001, FDR q=<0.001), providing more rationale to select a MEKi in combination with BETi to target MYCN-expressing TNBC (d.n.s.).

In Chapter III, we demonstrated that the majority of individual MYCN-expressing cells have little, if any, detectable expression of MYC. When analyzing *MYCN* expression across patient-matched primary and metastatic TNBC tumor samples, we found *MYCN* was elevated or similarly expressed between the primary tumor and sites of metastasis, indicating individual *MYCN*-expressing tumor cells may be able to migrate to distal sites. By evaluating gene expression in a publicly available RNA-seq dataset generated from circulating tumor cell (CTC) clusters *(347)*, we found one of ten breast cancer patients harbored *MYCN*-expressing CTC clusters. In a second RNA-seq dataset generated from CTC cluster cell cultures (from several of the same patients) *(395)*, we detected *MYCN*-expression in three of the six CTC cultures sequenced. Importantly, only the CTC cultures

that contained *MYCN* expression were able to generate CTC-derived xenografts in mice. In Chapter III, we stained 39 locally-advanced/metastatic TNBC and found over half contained MYCN expression. Collectively, these data reveal (i) similar or elevated *MYCN* expression between patient-matched primary TNBC and associated metastatic lesions, (ii) MYCN protein in tumor cell nuclei within recurrent TNBC, (iii) a positive correlation between MYCN and EMT/invasion through differential gene expression analyses, and (iv) *MYCN* expression within tumor-forming CTC clusters, implicating a role for MYCN in the metastatic progression of breast cancer.

While we demonstrate significance between *MYCN* expression and EMT/invasion through the GSEA, we did not determine a core set of genes responsible for this association. Functional evaluation of candidate genes could help elucidate how and why a small percentage of MYCN-expressing cells are retained within a large fraction of primary and metastatic tumors. Additional studies are needed to confirm the correlation we observed between cultured *MYCN*-expressing CTCs and CDX-forming ability and whether MYCN confers specific tumor cell biology that allows CTCs to exit the bloodstream and proliferate in distal sites in the human body. While we demonstrated the inhibitory effects of combination BETi and MEKi treatment on MYCN-expressing TNBC cell viability, understanding the biology of MYCN-expressing tumor cells and how it contributes to the progression of the disease could open up therapeutic avenues focused on preventing the metastatic spread of tumor cells.

Insights into the differentiation state of MYCN-expressing TNBC

The functional replacement of MYC alleles with the MYCN gene in murine development indicates the MYC-boxes and bHLHZip motif sequence homology between MYC and MYCN is sufficient to enable near-identical cell functions necessary for proper cell growth, survival, signaling, and differentiation of a developing mammal *(180)*. Therefore, differences observed between MYC- and MYCN-expressing cells likely reflect the differentiation state in which each isoform is expressed rather than the differences in MYC/MYCN amino acid sequence-specific structure-functions themselves. The various cell types in which each isoform is expressed have unique chromosomal architectures and sites of euchromatin, and therefore, each MYC-family isoform would be regulated differently based on variations in co-expressed proteins and would have differing target genes based on open chromatin and gene accessibility. MYC- and MYCN-associated drug sensitivities may actually relate to the cell state in which a given isoform regulates genes involved in cell growth and survival.

In Chapter IV, we demonstrated treatment with inhibitors that target the BRD family of transcriptional regulators (i.e. BETis) resulted in increased MYCN-expressing tumor cell growth inhibition compared to MYC-expressing models, both *in vitro* and in mice harboring TNBC PDX models. Previous studies on BRD inhibition have contributed increased effects of BETis to key tissue- or transcription factor-specific associations with enhancers and super-enhancers that mediate a cell state *(373)*. Therefore, the increased effects of BETis on MYCN-expressing cells may have more to do with the chromosomal architecture dictating the differentiation state of MYCN-expressing cells than an actual MYCN-specific protein function itself. MYCN has been shown to regulate the transcription

of thousands of genes at both gene promoters, enhancers, and super-enhancers *(167, 385, 396)*. BETi treatments result in displacement of BRD proteins from chromatin, thereby disrupting the transcription of *MYCN* as well as MYCN-mediated transcriptional regulation of its gene targets *(397)*. Cells that exhibit stemness are characterized by increased hypomethylation and a greater percentage of euchromatin *(398)*. Given the association of MYCN with stemness in vertebrate development and in the finding of a MYCN-containing basal/stem cell-like signature discussed above *(122, 261)*, we hypothesize the increase in MYCN-associated BETi-sensitivity is due to the cell state in which MYCN is expressed. Through fingerprinting analyses, we confirmed that our MYCN- and MYC-expressing cell line models originate from the same genetic background. A focus on enhancer RNAs and global transcription from the PRO-seq experiments, coupled with ATAC-seq (assay for transposase-accessible chromatin using sequencing) to assess genome-wide chromatin accessibility, and ChIP-seq (chromatin immunoprecipitation) to determine MYCN binding sites, could aid in the understanding of differing cell states between cells that express either MYCN or MYC.

A recently published pan-cancer study evaluated *MYC* and *MYCN*-associated genetic and epigenetic alterations across numerous cancer types from TCGA, including breast cancer (BRCA dataset) *(399)*, provides a resource for comparative analyses. In the pan-cancer study, pathways enriched in DNA replication and repair, chromatin, cell signaling, and extracellular matrix components were common between *MYC*- and *MYCN*-expressing cancers. *MYC*-expressing cancers were uniquely enriched in transcription, RNA processing, ribosomes, and rRNA pathways, while *MYCN*-expressing tumors were enriched in neuronal gene sets (glutamate receptor function, ligand-gated ion channels,

calcium ion transport, and acetylcholine binding) and developmental pathways. Of importance, several cancer types with the highest *MYCN* expression [LGG (low grade glioma), GBM (glioblastoma multiforme), TGCT (testicular germ cell tumors), and OV (ovarian)] displayed pathway enrichments that were consistent with canonical *MYC* signatures, suggesting tumors with *MYCN* expression above a certain threshold are more similar to *MYC*-driven cancers than to lower *MYCN*-expressing tumors.

Given the pan-cancer association between *MYCN* expression and neuronal gene sets, we analyzed our GSEA results from the previously described *MYCN*^{HighRatio} and *MYC*^{HighRatio} tumors in the context of the neuronal expression. Unlike *MYC*^{HighRatio} tumors, *MYCN*^{HighRatio} tumors exhibited neuro-associated gene expression, with the greatest correlation to gene sets describing axon extensions and ion transport (Table 7A). These results were particularly interesting given that none of the *MYCN*^{HighRatio} tumors were of neuroendocrine histology yet still associated with neuronal gene sets. To determine if the correlation between *MYCN*^{HighRatio} tumors and the neuronal gene sets should be attributed to *MYCN*-expressing tumor cells or tumor-infiltrating stromal/immune cells, we performed GSEA on gene expression from our CAL-51 MYCN^{High} and MYCN^{Low} clonal cell lines described and analyzed in the last two Chapters. Again, only the MYCN^{High} TNBC lines highly correlated with neuronal gene sets that relate to synaptic plasticity and ion channel activity (Table 7B).

While several of the gene sets related to neuronal synaptic transmission, these results may not actually relate to neurons but instead, provides a descriptor of a cell type with elevated cation channel activity. The combined activities of ion channels and transporters create an ionic gradient across cell membranes. All cells present a negative

A TNBC587 dataset

GO geneset name	Size	*MYCN*RatioHigh NES	P-value	FDR Q-value	*MYC*RatioHigh NES	P-value	FDR Q-value
MOTOR NEURON AXON GUIDANCE	22	2.13	0.0018	0.0013	NA	1.0000	1.0000
NEURON PROJECTION EXTENSION	48	2.09	<0.0001	0.0020	NA	1.0000	1.0000
NEURON FATE SPECIFICATION	22	2.08	<0.0001	0.0021	NA	1.0000	1.0000
AXON EXTENSION	34	2.08	<0.0001	0.0033	NA	1.0000	1.0000
POSITIVE REGULATION OF CALCIUM ION IMPORT	49	2.04	<0.0001	0.0031	NA	1.0000	1.0000
NEURON PROJECTION GUIDANCE	173	2.05	<0.0001	0.0043	NA	1.0000	1.0000
CALCIUM ION TRANSMEMBRANE TRANSPORTER ACTIVITY	99	2.01	<0.0001	0.0044	NA	1.0000	1.0000
VOLTAGE GATED CALCIUM CHANNEL COMPLEX	30	2.01	0.0020	0.0058	NA	1.0000	1.0000
NEURON RECOGNITION	29	1.99	<0.0001	0.0179	NA	1.0000	1.0000
VOLTAGE GATED CATION CHANNEL ACTIVITY	99	1.83	<0.0001	0.0058	NA	1.0000	1.0000
VOLTAGE GATED CALCIUM CHANNEL ACTIVITY	30	1.98	<0.0001	0.0059	NA	1.0000	1.0000
SPINAL CORD DEVELOPMENT	82	1.99	<0.0001	0.0059	NA	1.0000	1.0000
CALCIUM CHANNEL COMPLEX	46	1.95	<0.0001	0.0075	NA	1.0000	1.0000
NEURON FATE COMMITMENT	49	1.92	<0.0001	0.0100	NA	1.0000	1.0000
SODIUM ION TRANSMEMBRANE TRANSPORT	71	1.87	<0.0001	0.0133	NA	1.0000	1.0000

B CAL-51 clonally-derived cell lines

GO geneset name	Size	*MYCN*RatioHigh NES	P-value	FDR Q-value	*MYC*RatioHigh NES	P-value	FDR Q-value
REGULAITON OF NEURONAL SYNAPTIC PLASTICITY	29	1.96	<0.0001	0.2133	NA	1.0000	1.0000
EXTRACELLULAR LIGAND GATED ION CHANNEL ACTIVITY	26	1.93	<0.0001	0.1099	NA	1.0000	1.0000
PRESYNAPTIC ACTIVE ZONE	22	1.92	0.0021	0.0838	NA	1.0000	1.0000
SYNAPTIC TRANSMISSION GLUTAMATERGIC	17	1.92	0.0021	0.0760	NA	1.0000	1.0000
VOLTAGE GATED CATION CHANNEL ACTIVITY	59	1.91	<0.0001	0.0730	NA	1.0000	1.0000
EXCITATORY EXTRACELLULAR LIGAND GATED ION CHANNEL ACTIVITY	24	1.91	<0.0001	0.0652	NA	1.0000	1.0000
AMPA GLUTAMATE RECEPTOR COMPLEX	15	1.84	0.0045	0.1217	NA	1.0000	1.0000
VOLTAGE GATED CALCIUM CHANNEL ACTIVITY	20	1.80	<0.0001	0.1655	NA	1.0000	1.0000
CATION CHANNEL ACTIVITY	148	1.80	<0.0001	0.1499	NA	1.0000	1.0000
PRESYNAPTIC PROCESS INVOLVED IN SYNAPTIC TRANSMISSION	71	1.78	<0.0001	0.1543	NA	1.0000	1.0000
REGULATION OF NEUROTRANSMITTER RECEPTOR ACTIVITY	18	1.75	0.0043	0.2134	NA	1.0000	1.0000
MODULATION OF EXCITATORY POSTSYNAPTION PROTENTIAL	19	1.74	0.0045	0.2082	NA	1.0000	1.0000
REGULATION OF SYNAPTIC VESICLE TRANSPORT	28	1.74	0.0044	0.2028	NA	1.0000	1.0000
NEUROTRANSMITTER RECEPTOR ACTIVITY	25	1.71	0.0071	0.2400	NA	1.0000	1.0000
NEURON SYNAPTIC TRANSMISSION	29	1.71	0.0048	0.2271	NA	1.0000	1.0000

Table 7. Neuronal gene set pathway enrichments in *MYCN*$^{\text{RatioHigh}}$ TNBC tumor specimens and CAL-51 clonal cell lines. (**A-B**) GSEA between *MYCN*$^{\text{RatioHigh}}$ and *MYC*$^{\text{RatioHigh}}$ TNBC samples in the TNBC587 dataset (**A**) and CAL-51 clonally-derived cell lines (**B**). GO, gene ontology. NES, normalized enrichment score. NA, not applicable.

intracellular electric charge called transmembrane potential (Vm) *(400)*. Depolarization, the transient decrease of Vm, and repolarization, the transient increase of Vm, corresponds to cell cycle checkpoints and is critical for cell cycle progression in different cell types *(400)*. Several breast cancer studies have demonstrated transient depolarization initiates key signaling pathways that result in re-entry into the cell cycle, which enables malignant proliferation *(401)*.

The ion channel that predominates our GSEA results from both the TNBC587 dataset and our CAL-51 clonal cell line models involves the cation, calcium (Table 7, A and B). Calcium is a well-established signaling molecule prevalent in both normal physiology and pathological conditions. Finely controlled calcium gradients across the cell surface as well as the endoplasmic reticulum contribute to a diverse range of cellular processes, such as gene expression, proliferation, cell growth, apoptosis, and migration *(402, 403)* and have been linked to metastasis and invasion for many cancer cell types, including breast cancer *(404–406)*. Metabolomic studies evaluating the tumor cell media and plasma from patients with high MYCN-expressing disease could aid in the understanding of how these transport ions contribute to tumor cell function. With growing interest in the cancer research field on ion channel activity, pharmacological agents are being repurposed to investigate new therapeutic strategies. Studies have demonstrated that calcium channel blockers decreased proliferative tumor cell growth and voltage-gated Na+ channel inhibitors decreased migration and invasion *(407)*. Analyzing the presence, activity, and biological relevance of ion channels in MYCN-expressing tumors could enable additional avenues for therapeutic intervention.

MYCN expression in the normal mammary gland

To better understand the pathology of breast cancer progression and how deregulated HR signaling results in tumorigenesis, significant effort has been given towards determining the physiological roles of proto-oncoproteins, ER and PR, in normal mammary gland function. Likewise, understanding the role of MYCN in normal breast tissue could aid in an understanding to how cells that express this protein contribute to the onset or progression of breast cancer. In adult female humans and mice, the mammary gland contains continuous bilayers of epithelial cells structured as a network of ducts that branch out from a central duct and terminate at clustered alveolae or 'terminal ductal lobular units' (TDLU) *(408)*. Nearly 95% of human breast malignancies are adenocarcinomas that stem from the inner (luminal) layer of epithelial cells within ducts (ductal carcinomas) or at TDLUs (lobular carcinomas) *(409)*. The outer layer of cells are considered basal myoepithelial cells and express contractile proteins such as myosin and smooth muscle actin that enable vessel constriction and movement of secretions (i.e. milk) along the duct *(408)*.

The only evidence to date that indicates a presence of *MYCN* expression in normal breast tissue is from the previously-described study that characterized normal and tumor cell differentiation states over the course of TNBC disease progression *(261)*. Multiplex gene expression analyses were conducted on individual cells from normal breast epithelium using a 116 gene panel that associated with EMT, stemness, pluripotency, dormancy, mammary lineage specification, cell cycle, and proliferation *(261)*. *MYCN* expression associated with basal cell gene expression and stemness *(261)*, suggesting *MYCN* is expressed in the myoepithelium. While myoepithelial cells were once neglected

as being an essential part of breast cancer biology, we now know that myoepithelial cells, in general, have extensive stem cell-like properties, with ~65% of single-cell derived basal colonies capable of repopulating a mammary gland *(410)*. They also act as “natural tumor suppressors” by establishing epithelial cell polarity and in turn, inhibiting tumor formation and cell migration *(411)*.

Through the use of fluorescence lineage tracing, a seminal paper by Rios and colleagues elegantly revealed the existence of clonal epithelial patches of mammary stem cells (MaSC) that have both luminal and myoepithelial cell characteristics and stem from a primitive basal-cell precursor *(412)*. MaSCs were capable of long-lived self-renewal and through asymmetric division, contributed to the stem-cell population that maintains ducts *(412)*. ER and PR are generally co-expressed in 10-15% of human luminal breast epithelial cells and are evenly distributed across the mammary gland *(413)*. While ER is required for elongation of the mammary duct during puberty, PR is essential for epithelial cell proliferation of ductal side branches and alveologenesis during pregnancy *(21, 414)*. If MYCN expression contributes to mammary gland development, as it does with the hematopoietic system, skeletal tissue, and intestinal tract in murine development, we would hypothesize MYCN to have a higher expression at the onset of mammary gland organogenesis and possibly during puberty and pregnancy when the mammary duct and ductal side branches are extending. A better understanding of MYCN expression in normal breast tissue could aid in our understanding of its aberrant expression in TNBC and the identification of pathways or chromatin states that may be “targets” for drug development strategies.

Concluding Remarks

TNBC is a heterogeneous collection of tumors that lack the expression of therapeutic targets that direct treatment options for the other breast cancer subtypes; therefore, cytotoxic chemotherapy remains the primary means in which to treat patients with primary TNBC. With >70% of patients progressing or recurring upon treatment, patients with TNBC experience a shorter time to relapse and worse survival outcome compared to the other breast cancer subtypes. While PARP inhibitors and monoclonal antibodies are used to target *BRCA*-mutant and unresectable PD-L1-expressing disease, respectively, new therapeutic targets are needed to improve outcomes for patients with TNBC. Given that MYCN is an unfavorable prognostic feature detected in a wide variety of neuronal and non-neuronally-derived tumors, we sought to determine the prevalence of MYCN expression in TNBC and whether MYCN-expressing tumors represented a tumor population to direct clinical efforts. The work presented herein begins to characterize the phenotypic properties and drug sensitivities of this unique tumor type within TNBC and will hopefully lead to additional therapeutic options for patients with TNBC.

REFERENCES

1. F. Bray, Jacques Ferlay, Isabelle Soerjomataram, R. L. Siegel;, L. A. Torre;, A. Jemal, Global Cancer Statistics 2018: GLOBOCAN Estimates of Incidence and Mortality Worldwide for 36 Cancers in 185 Countries*CA. Cancer J. Clin.* **68**, 394–424 (2018).

2. K. A. Cronin, A. J. Lake, S. Scott, R. L. Sherman, A. M. Noone, N. Howlader, S. J. Henley, R. N. Anderson, A. U. Firth, J. Ma, B. A. Kohler, A. Jemal, Annual Report to the Nation on the Status of Cancer, part I: National cancer statistics, *Cancer* **124**, 2785–2800 (2018).

3. P. Y. Maximov, T. M. Lee, V. Craig, The discovery and development of selective estrogen receptor modulators (SERMs) for clinical practice, *Curr. Clin. Pharmacol.* **8**, 135–155 (2013).

4. D. J. Slamon, G. M. Clark, S. G. Wong, W. J. Levin, A. Ullrich, W. L. McGuire, Human breast cancer: correlation of relapse and survival with amplification of the HER-2/neu oncogene, *Science (80-.).* **235**, 177–182 (1987).

5. C. Shih, L. C. Padhy, M. Murray, R. A. Weinberg, Transforming genes of carcinomas and neuroblastomas introuced into mouse fibroblasts, *Nature* **290**, 261–264 (1981).

6. A. L. Schechter, D. F. Stern, L. Vaidyanathan, S. J. Decker, J. A. Drebin, M. I. Greene, R. A. Weinberg, The neu oncogene: an erb-B-related gene encoding a 185,000-Mr tumor antigen, *Nature* **312**, 513–516 (1984).

7. R. Nahta, F. J. Esteva, HER-2-Targeted Therapy: Lessons Learned and Future Directions, *Clin. Cancer Res.* **9**, 5078–5084 (2003).

8. J. M. Renoir, V. Marsaud, G. Lazennec, Estrogen receptor signaling as a target for novel breast cancer therapeutics, *Biochem. Pharmacol.* **85**, 449–465 (2013).

9. V. C. Jordan, Tamoxifen: A most unlikely pioneering medicine, *Nat. Rev. Drug Discov.* **2**, 205–213 (2003).

10. A. E. C. Lathrop, L. Loeb, Further investigations on the origin of tumors in mice, *J Exp Med* **28**, 1–19 (1918).

11. L. Björnström, M. Sjöberg, Mechanisms of Estrogen Receptor Signaling: Convergence of Genomic and Nongenomic Actions on Target Genes, *Mol. Endocrinol.* **19**, 833–842 (2005).

12. J. R. Skidmore, A. L. Walpole, J. Woodburn, Effect of some triphenylethylenes on oestradiol binding in vitro to macromolecules from uterus and anterior pituitary, *J. Endocrinol.* **52**, 289–298 (1972).

13. A. C. Lai, C. M. Crews, N. Haven, Induced protein degradation, *Nat. Rev. Drug Discov.* **16**, 101–114 (2017).

14. R. J. Santen, H. Brodie, E. R. Simpson, P. K. Siiteri, A. Brodie, History of aromatase: Saga of an important biological mediator and therapeutic target, *Endocr. Rev.* **30**, 343–375 (2009).

15. X. Dai, L. Xiang, T. Li, Z. Bai, Cancer hallmarks, biomarkers and breast cancer molecular subtypes, *J. Cancer* **7**, 1281–1294 (2016).

16. O. Abe, R. Abe, K. Enomoto, K. Kikuchi, H. Koyama, H. Masuda, Y. Nomura, Y. Ohashi, K. Sakai, K. Sugimachi, M. Toi, T. Tominaga, J. Uchino, M. Yoshida, J. L. Haybittle, C. F. Leonard, G. Calais, P. Geraud, V. Collett, C. Davies, A. Delmestri, J. Sayer, V. J. Harvey, I. M. Holdaway, R. G. Kay, B. H. Mason, J. F. Forbes, N. Wilcken, R. Bartsch, P. Dubsky, C. Fesl, H. Fohler, M. Gnant, R. Greil, R. Jakesz, A. Lang, G. Luschin-Ebengreuth, C. Marth, B. Mlineritsch, H. Samonigg, C. F. Singer, G. G. Steger, H. Stöger, P. Canney, H. M. A. Yosef, C. Focan, U. Peek, G. D. Oates, J. Powell, M. Durand, L. Mauriac, A. Di Leo, S. Dolci, D. Larsimont, J. M. Nogaret, C. Philippson, M. J. Piccart, M. B. Masood, D. Parker, J. J. Price, M. A. Lindsay, J. Mackey, M. Martin, P. S. G. J. Hupperets, T. Bates, R. W. Blamey, U. Chetty, I. O. Ellis, E. Mallon, D. A. L. Morgan, J. Patnick, S. Pinder, I. Olivotto, J. Ragaz, D. Berry, G. Broadwater, C. Cirrincione, H. Muss, L. Norton, R. B. Weiss, H. T. Abu-Zahra, S. M. Portnoj, S. Bowden, C. Brookes, J. Dunn, I. Fernando, M. Lee, C. Poole, D. Rea, D. Spooner, P. J. Barrett-Lee, R. E. Mansel, I. J. Monypenny, N. H. Gordon, H. L. Davis, J. Cuzick, Y. Lehingue, P. Romestaing, J. B. Dubois, T. Delozier, B. Griffon, J. Mace Lesec'h, P. Rambert, G. Mustacchi, L. Petruzelka, O. Pribylova, J. R. Owen, N. Harbeck, F. Jänicke, C. Meisner, M. Schmitt, C. Thomssen, P. Meier, Y. Shan, Y. F. Shao, X. Wang, D. B. Zhao, Z. M. Chen, H. C. Pan, A. Howell, R. Swindell, J. A. Burrett, M. Clarke, R. Collins, C. Correa, D. Cutter, S. Darby, C. Davies, K. Davies, A. Delmestri, P. Elphinstone, V. Evans, L. Gettins, J. Godwin, R. Gray, C. Gregory, D. Hermans, C. Hicks, S. James, A. Kerr, E. MacKinnon, M. Lay, P. McGale, T. McHugh, R. Peto, J. Sayer, C. Taylor, Y. Wang, J. Albano, C. F. De Oliveira, H. Gervásio, J. Gordilho, H. Johansen, H. T. Mouridsen, R. S. Gelman, J. R. Harris, D. Hayes, C. Henderson, C. L. Shapiro, E. Winer, P. Christiansen, B. Ejlertsen, M. Ewertz, M. B. Jensen, S. Møller, H. T. Mouridsen, B. Carstensen, T. Palshof, H. J. Trampisch, O. Dalesio, E. G. E. De Vries, S. Rodenhuis, H. Van Tinteren, R. L. Comis, N. E. Davidson, R. Gray, N. Robert, G. Sledge, L. J. Solin, J. A. Sparano, D. C. Tormey, W. Wood, D. Cameron, U. Chetty, J. M. Dixon, P. Forrest, W. Jack, I. Kunkler, J. Rossbach, J. G. M. Klijn, A. D. Treurniet-Donker, W. L. J. Van Putten, N. Rotmensz, U. Veronesi, G. Viale, H. Bartelink, N. Bijker, J. Bogaerts, F. Cardoso, T. Cufer, J. P. Julien, E. Rutgers, C. J. H. Van De Velde, M. P. Cunningham, R. Huovinen, H. Joensuu, A. Costa, C. Tinterri, G. Bonadonna, L. Gianni, P. Valagussa, L. J. Goldstein, J. Bonneterre, P. Fargeot, P. Fumoleau, P. Kerbrat, E. Luporsi, M. Namer, W. Eiermann, J. Hilfrich, W. Jonat, M. Kaufmann, R. Kreienberg, M. Schumacher, G. Bastert, H. Rauschecker, R. Sauer, W. Sauerbrei, A. Schauer, M. Schumacher, J. U. Blohmer, S. D. Costa, H. Eidtmann, B. Gerber, C. Jackisch, S. Loibl, G. Von Minckwitz, A. De Schryver, L. Vakaet, M. Belfiglio, A. Nicolucci, F. Pellegrini, M. C. Pirozzoli, M. Sacco, M. Valentini, C. S. McArdle, D. C. Smith, S. Stallard, D. M. Dent, C. A. Gudgeon, A. Hacking, E. Murray, E. Panieri, I. D.

Werner, E. Carrasco, M. Martin, M. A. Segui, E. Galligioni, M. Lopez, A. Erazo, J. Y. Medina, J. Horiguchi, H. Takei, I. S. Fentiman, J. L. Hayward, R. D. Rubens, D. Skilton, H. Scheurlen, M. Kaufmann, H. C. Sohn, M. Untch, U. Dafni, C. Markopoulos, U. Dafni, G. Fountzilas, D. Mavroudis, P. Klefstrom, C. Blomqvist, T. Saarto, M. Gallen, R. Margreiter, B. De Lafontan, J. Mihura, H. Roché, B. Asselain, R. J. Salmon, J. R. Vilcoq, R. Arriagada, C. Bourgier, C. Hill, S. Koscielny, A. Laplanche, M. G. Lê, M. Spielmann, R. A'Hern, J. Bliss, P. Ellis, L. Kilburn, J. R. Yarnold, J. Benraadt, M. Kooi, A. O. Van De Velde, J. A. Van Dongen, J. B. Vermorken, M. Castiglione, A. Coates, M. Colleoni, J. Collins, J. Forbes, R. D. Gelber, A. Goldhirsch, J. Lindtner, K. N. Price, M. M. Regan, C. M. Rudenstam, H. J. Senn, B. Thuerlimann, J. M. Bliss, C. E. D. Chilvers, R. C. Coombes, E. Hall, M. Marty, M. Buyse, K. Possinger, P. Schmid, M. Untch, D. Wallwiener, L. Foster, W. D. George, H. J. Stewart, P. Stroner, R. Borovik, H. Hayat, M. J. Inbar, E. Robinson, P. Bruzzi, L. Del Mastro, P. Pronzato, M. R. Sertoli, M. Venturini, T. Camerini, G. De Palo, M. G. Di Mauro, F. Formelli, P. Valagussa, D. Amadori, A. Martoni, F. Pannuti, R. Camisa, G. Cocconi, A. Colozza, R. Passalacqua, K. Aogi, S. Takashima, O. Abe, T. Ikeda, K. Inokuchi, K. Kikuchi, K. Sawa, H. Sonoo, S. Korzeniowski, J. Skolyszewski, M. Ogawa, J. Yamashita, E. Bastiaannet, C. J. H. Van De Velde, W. Van De Water, J. G. H. Van Nes, R. Christiaens, P. Neven, R. Paridaens, W. Van Den Bogaert, S. Braun, W. Janni, P. Martin, S. Romain, M. Janauer, M. Seifert, P. Sevelda, C. C. Zielinski, T. Hakes, C. A. Hudis, L. Norton, R. Wittes, G. Giokas, D. Kondylis, B. Lissaios, R. De La Huerta, M. G. Sainz, R. Altemus, K. Camphausen, K. Cowan, D. Danforth, A. Lichter, M. Lippman, J. O'Shaughnessy, L. J. Pierce, S. Steinberg, D. Venzon, J. A. Zujewski, C. D'Amico, M. Lioce, A. Paradiso, J. A. W. Chapman, K. Gelmon, P. E. Goss, M. N. Levine, R. Meyer, W. Parulekar, J. L. Pater, K. I. Pritchard, L. E. Shepherd, D. Tu, T. Whelan, Y. Nomura, S. Ohno, S. Anderson, G. Bass, A. Brown, J. Bryant, J. Costantino, J. Dignam, B. Fisher, C. Geyer, E. P. Mamounas, S. Paik, C. Redmond, S. Swain, L. Wickerham, N. Wolmark, M. Baum, I. M. Jackson, M. K. Palmer, E. Perez, J. N. Ingle, V. J. Suman, N. O. Bengtsson, S. Emdin, H. Jonsson, L. Del Mastro, M. Venturini, J. P. Lythgoe, R. Swindell, M. Kissin, B. Erikstein, E. Hannisdal, A. B. Jacobsen, J. E. Varhaug, B. Erikstein, S. Gundersen, M. Hauer-Jensen, H. Høst, A. B. Jacobsen, R. Nissen-Meyer, R. W. Blamey, A. K. Mitchell, D. A. L. Morgan, J. F. R. Robertson, H. Ueo, M. Di Palma, G. Mathé, J. L. Misset, M. Levine, K. I. Pritchard, T. Whelan, K. Morimoto, K. Sawa, Y. Takatsuka, E. Crossley, A. Harris, D. Talbot, M. Taylor, A. L. Martin, H. Roché, G. Cocconi, B. Di Blasio, V. Ivanov, R. Paltuev, V. Semiglazov, J. Brockschmidt, M. R. Cooper, C. I. Falkson, R. A'Hern, S. Ashley, M. Dowsett, A. Makris, T. J. Powles, I. E. Smith, J. R. Yarnold, J. C. Gazet, L. Browne, P. Graham, N. Corcoran, N. Deshpande, L. Di Martino, P. Douglas, A. Hacking, H. Høst, A. Lindtner, G. Notter, A. J. S. Bryant, G. H. Ewing, L. A. Firth, J. L. Krushen-Kosloski, R. Nissen-Meyer, H. Anderson, F. Killander, P. Malmström, L. Rydén, L. G. Arnesson, J. Carstensen, M. Dufmats, H. Fohlin, B. Nordenskjöld, M. Söderberg, T. J. Carpenter, N. Murray, G. T. Royle, P. D. Simmonds, K. Albain, W. Barlow, J. Crowley, D. Hayes, J. Gralow, S. Green, G. Hortobagyi, R. Livingston, S. Martino, C. K. Osborne, P. M. Ravdin, J. Adolfsson, J. Bergh, T. Bondesson, F. Celebioglu, K. Dahlberg, T. Fornander, I. Fredriksson, J. Frisell, E. Göransson, M. Iiristo, U. Johansson, E. Lenner, L. Löfgren, P. Nikolaidis, L. Perbeck, S. Rotstein, K. Sandelin, L. Skoog, G. Svane, E. Af Trampe, C. Wadström, M. Castiglione, A. Goldhirsch, R. Maibach, H. J. Senn, B. Thürlimann, M. Hakama, K. Holli, J. Isola, K. Rouhento, R. Saaristo, H. Brenner, A.

Hercbergs, A. L. Martin, H. Roché, M. Yoshimoto, A. H. G. Paterson, K. I. Pritchard, A. Fyles, J. W. Meakin, T. Panzarella, K. I. Pritchard, J. Bahi, M. Reid, M. Spittle, H. Bishop, N. J. Bundred, J. Cuzick, I. O. Ellis, I. S. Fentiman, J. F. Forbes, S. Forsyth, W. D. George, S. E. Pinder, I. Sestak, G. P. Deutsch, R. Gray, D. L. W. Kwong, V. R. Pai, R. Peto, F. Senanayake, F. Boccardo, A. Rubagotti, M. Baum, S. Forsyth, A. Hackshaw, J. Houghton, J. Ledermann, K. Monson, J. S. Tobias, C. Carlomagno, M. De Laurentiis, S. De Placido, L. Williams, D. Hayes, L. J. Pierce, K. Broglio, A. U. Buzdar, R. R. Love, J. Ahlgren, H. Garmo, L. Holmberg, G. Liljegren, H. Lindman, F. Wärnberg, L. Asmar, S. E. Jones, O. Gluz, N. Harbeck, C. Liedtke, U. Nitz, A. Litton, A. Wallgren, P. Karlsson, B. K. Linderholm, R. T. Chlebowski, H. Caffier, Relevance of breast cancer hormone receptors and other factors to the efficacy of adjuvant tamoxifen: Patient-level meta-analysis of randomised trials, *Lancet* **378**, 771–784 (2011).

17. E. A. Rakha, M. E. El-Sayed, A. R. Green, E. C. Paish, D. G. Powe, J. Gee, R. I. Nicholson, A. H. S. Lee, J. F. R. Robertson, I. O. Ellis, Biologic and clinical characteristics of breast cancer with single hormone receptor-positive phenotype, *J. Clin. Oncol.* **25**, 4772–4778 (2007).

18. T. A. Hopp, H. L. Weiss, S. G. Hilsenbeck, Y. Cui, D. C. Allred, K. B. Horwitz, S. A. W. Fuqua, Breast cancer patients with progesterone receptor PR-A-rich tumors have poorer disease-free survival rates., *Clin. Cancer Res.* **10**, 2751–60 (2004).

19. C. Brisken, Progesterone signalling in breast cancer: A neglected hormone coming into the limelight, *Nat. Rev. Cancer* **13**, 385–396 (2013).

20. S. L. Grimm, S. M. Hartig, D. P. Edwards, Progesterone Receptor Signaling Mechanisms, *J. Mol. Biol.* **428**, 3831–3849 (2016).

21. A. R. Daniel, C. R. Hagan, C. A. Lange, Progesterone receptor action: Defining a role in breast cancer, *Expert Rev. Endocrinol. Metab.* **6**, 359–369 (2011).

22. N. Iqbal, N. Iqbal, Human Epidermal Growth Factor Receptor 2 (HER2) in Cancers: Overexpression and Therapeutic Implications, *Mol. Biol. Int.* **2014**, 1–9 (2014).

23. I. Gingras, G. Gebhart, E. De Azambuja, M. Piccart-Gebhart, HER2-positive breast cancer is lost in translation: Time for patient-centered research, *Nat. Rev. Clin. Oncol.* **14**, 669–681 (2017).

24. S. Escrivá-de-Romaní, M. Arumí, M. Bellet, C. Saura, HER2-positive breast cancer: Current and new therapeutic strategies, *Breast* **39**, 80–88 (2018).

25. D. Mendes, C. Alves, N. Afonso, F. Cardoso, J. L. Passos-Coelho, L. Costa, S. Andrade, F. Batel-Marques, The benefit of HER2-targeted therapies on overall survival of patients with metastatic HER2-positive breast cancer - a systematic review, *Breast Cancer Res.* **17**, 1–14 (2015).

26. M. Scaltriti, P. Nuciforo, I. Bradbury, J. Sperinde, D. Agbor-Tarh, C. Campbell, A. Chenna, J. Winslow, V. Serra, J. L. Parra, L. Prudkin, J. Jimenez, C. Aura, N. Harbeck,

L. Pusztai, C. Ellis, H. Eidtmann, J. Arribas, J. Cortes, E. De Azambuja, M. Piccart, J. Baselga, High HER2 expression correlates with response to the combination of lapatinib and trastuzumab, *Clin. Cancer Res.* **21**, 569–576 (2015).

27. A. Schneeweiss, S. Chia, R. Hegg, C. Tausch, R. Deb, J. Ratnayake, V. McNally, G. Ross, A. Kiermaier, J. Corte´s, Evaluating the predictive value of biomarkers for efficacy outcomes in response to pertuzumab- and trastuzumab-based therapy: An exploratory analysis of the TRYPHAENA study, *Breast Cancer Res.* **16**, 1–12 (2014).

28. L. Zabaglo, O. Stoss, J. Rüschoff, D. Zielinski, J. Salter, M. Arfi, I. Bradbury, U. Dafni, M. Piccart-Gebhart, M. Procter, M. Dowsett, HER2 staining intensity in HER2-positive disease: Relationship with FISH amplification and clinical outcome in the HERA trial of adjuvant trastuzumab, *Ann. Oncol.* **24**, 2761–2766 (2013).

29. J. Baselga, J. Cortés, S. A. Im, E. Clark, G. Ross, A. Kiermaier, S. M. Swain, Biomarker Analyses in CLEOPATRA: A phase III, placebo-controlled study of pertuzumab in human epidermal growth factor receptor 2-positive, first-line metastatic breast cancer, *J. Clin. Oncol.* **32**, 3753–3761 (2014).

30. D. Theile, G. Lenz, J. A. Momand, S. E. Kane, in J. R. Prosperi, Ed. (Springer International Publishing, Cham, 2017), pp. 35–88.

31. B. E. Dogan, L. W. Turnbull, Imaging of triple-negative breast cancer, *Ann. Oncol.* **23**, vi23–vi29 (2012).

32. R. Dent, M. Trudeau, K. I. Pritchard, W. M. Hanna, H. K. Kahn, C. A. Sawka, L. A. Lickley, E. Rawlinson, P. Sun, S. A. Narod, Triple-Negative Breast Cancer: Clinical Features and Patterns of Recurrence, *Clin. Cancer Res.* **13**, 4429–4434 (2007).

33. J. M. Dolle, J. R. Daling, E. White, L. A. Brinton, D. R. Doody, P. L. Porter, K. E. Malone, Risk factors for triple-negative breast cancer in women under the age of 45 years, *Cancer Epidemiol. Biomarkers Prev.* **18**, 1157–1166 (2009).

34. M. E. H. Hammond, D. F. Hayes, M. Dowsett, D. C. Allred, K. L. Hagerty, S. Badve, P. L. Fitzgibbons, G. Francis, N. S. Goldstein, M. Hayes, D. G. Hicks, S. Lester, R. Love, P. B. Mangu, L. McShane, K. Miller, C. K. Osborne, S. Paik, J. Perlmutter, A. Rhodes, H. Sasano, J. N. Schwartz, F. C. G. Sweep, S. Taube, E. E. Torlakovic, P. Valenstein, G. Viale, D. Visscher, T. Wheeler, R. B. Williams, J. L. Wittliff, A. C. Wolff, American Society of Clinical Oncology/College of American Pathologists Guideline Recommendations for Immunohistochemical Testing of Estrogen and Progesterone Receptors in Breast Cancer, *J. Clin. Oncol.* **28**, 2784–2795 (2010).

35. A. C. Wolff, M. E. H. Hammond, D. G. Hicks, M. Dowsett, L. M. McShane, K. H. Allison, D. C. Allred, J. M. S. Bartlett, M. Bilous, P. Fitzgibbons, W. Hanna, R. B. Jenkins, P. B. Mangu, S. Paik, E. A. Perez, M. F. Press, P. A. Spears, G. H. Vance, G. Viale, D. F. Hayes, American Society of Clinical Oncology, College of American Pathologists, Recommendations for Human Epidermal Growth Factor Receptor 2 Testing in Breast Cancer: American Society of Clinical Oncology/College of American Pathologists Clinical

Practice Guideline Update, *J. Clin. Oncol.* **31**, 3997–4013 (2013).

36. C. Criscitiello, H. A. Azim, P. C. Schouten, S. C. Linn, C. Sotiriou, Understanding the biology of triple-negative breast cancer, *Ann. Oncol.* **23** (2012), doi:10.1093/annonc/mds188.

37. B. Weigelt, C. Eberle, C. F. Cowell, C. K. Y. Ng, J. S. Reis-Filho, Metaplastic breast carcinoma: more than a special type, *Nat. Rev. Cancer* **14**, 147–148 (2014).

38. B. T. Hennessy, S. Giordano, K. Broglio, Z. Duan, J. Trent, T. A. Buchholz, G. Babiera, G. N. Hortobagyi, V. Valero, Biphasic metaplastic sarcomatoid carcinoma of the breast., *Ann. Oncol. Off. J. Eur. Soc. Med. Oncol.* **17**, 605–13 (2006).

39. G. von Minckwitz, M. Untch, J.-U. Blohmer, S. D. Costa, H. Eidtmann, P. A. Fasching, B. Gerber, W. Eiermann, J. Hilfrich, J. Huober, C. Jackisch, M. Kaufmann, G. E. Konecny, C. Denkert, V. Nekljudova, K. Mehta, S. Loibl, Definition and Impact of Pathologic Complete Response on Prognosis After Neoadjuvant Chemotherapy in Various Intrinsic Breast Cancer Subtypes, *J. Clin. Oncol.* **30**, 1796–1804 (2012).

40. P. Cortazar, L. Zhang, M. Untch, K. Mehta, J. P. Costantino, N. Wolmark, H. Bonnefoi, D. Cameron, L. Gianni, P. Valagussa, S. M. Swain, T. Prowell, S. Loibl, D. L. Wickerham, J. Bogaerts, J. Baselga, C. Perou, G. Blumenthal, J. Blohmer, E. P. Mamounas, J. Bergh, V. Semiglazov, R. Justice, H. Eidtmann, S. Paik, M. Piccart, R. Sridhara, P. A. Fasching, L. Slaets, S. Tang, B. Gerber, C. E. Geyer, R. Pazdur, N. Ditsch, P. Rastogi, W. Eiermann, G. von Minckwitz, Pathological complete response and long-term clinical benefit in breast cancer: the CTNeoBC pooled analysis, *Lancet* **384**, 164–172 (2014).

41. C. A. Sawka, K. I. Pritchard, H. L. Lickley, G. A. Oldfield, J. A. Chapman, G. G. Allen, B. G. Mobbs, W. M. Hanna, H. Kahn, M. E. Trudeau, The Henrietta Banting Breast Centre database: a model for clinical research utilizing a hospital-based inception cohort., *J. Clin. Epidemiol.* **48**, 779–86 (1995).

42. M. Smid, Y. Wang, Y. Zhang, A. M. Sieuwerts, J. Yu, J. G. M. Klijn, J. A. Foekens, J. W. M. Martens, Subtypes of breast cancer show preferential site of relapse., *Cancer Res.* **68**, 3108–14 (2008).

43. J. C. Harrell, A. Prat, J. S. Parker, C. Fan, X. He, L. Carey, C. Anders, M. Ewend, C. M. Perou, Genomic analysis identifies unique signatures predictive of brain, lung, and liver relapse., *Breast Cancer Res. Treat.* **132**, 523–35 (2012).

44. N. U. Lin, E. Claus, J. Sohl, A. R. Razzak, A. Arnaout, E. P. Winer, Sites of distant recurrence and clinical outcomes in patients with metastatic triple-negative breast cancer, *Cancer* **113**, 2638–2645 (2008).

45. K. H. Vousden, X. Lu, Live or let die: the cell's response to p53., *Nat. Rev. Cancer* **2**, 594–604 (2002).

46. S. Nik-Zainal, H. Davies, J. Staaf, M. Ramakrishna, D. Glodzik, X. Zou, I. Martincorena,

L. B. Alexandrov, S. Martin, D. C. Wedge, P. Van Loo, Y. S. Ju, M. Smid, A. B. Brinkman, S. Morganella, M. R. Aure, O. C. Lingjærde, A. Langerød, M. Ringnér, S.-M. Ahn, S. Boyault, J. E. Brock, A. Broeks, A. Butler, C. Desmedt, L. Dirix, S. Dronov, A. Fatima, J. A. Foekens, M. Gerstung, G. K. J. Hooijer, S. J. Jang, D. R. Jones, H.-Y. Kim, T. A. King, S. Krishnamurthy, H. J. Lee, J.-Y. Lee, Y. Li, S. McLaren, A. Menzies, V. Mustonen, S. O'Meara, I. Pauporté, X. Pivot, C. A. Purdie, K. Raine, K. Ramakrishnan, F. G. Rodríguez-González, G. Romieu, A. M. Sieuwerts, P. T. Simpson, R. Shepherd, L. Stebbings, O. A. Stefansson, J. Teague, S. Tommasi, I. Treilleux, G. G. Van den Eynden, P. Vermeulen, A. Vincent-Salomon, L. Yates, C. Caldas, L. van't Veer, A. Tutt, S. Knappskog, B. K. T. Tan, J. Jonkers, Å. Borg, N. T. Ueno, C. Sotiriou, A. Viari, P. A. Futreal, P. J. Campbell, P. N. Span, S. Van Laere, S. R. Lakhani, J. E. Eyfjord, A. M. Thompson, E. Birney, H. G. Stunnenberg, M. J. van de Vijver, J. W. M. Martens, A.-L. Børresen-Dale, A. L. Richardson, G. Kong, G. Thomas, M. R. Stratton, Landscape of somatic mutations in 560 breast cancer whole-genome sequences, *Nature* **534**, 47–54 (2016).

47. J. M. R. Lambert, P. Gorzov, D. B. Veprintsev, M. Söderqvist, D. Segerbäck, J. Bergman, A. R. Fersht, P. Hainaut, K. G. Wiman, V. J. N. Bykov, PRIMA-1 Reactivates Mutant p53 by Covalent Binding to the Core Domain, *Cancer Cell* **15**, 376–388 (2009).

48. D. Malkin, F. P. Li, L. C. Strong, J. F. Fraumeni, C. E. Nelson, D. H. Kim, J. Kassel, M. A. Gryka, F. Z. Bischoff, M. A. Tainsky, Germ line p53 mutations in a familial syndrome of breast cancer, sarcomas, and other neoplasms., *Science (80-.).* **250**, 1233–1238 (1990).

49. C. C. Wu, S. Shete, C. I. Amos, L. C. Strong, Joint effects of germ-line p53 mutation and sex on cancer risk in Li-Fraumeni syndrome, *Cancer Res.* **66**, 8287–8292 (2006).

50. R. Roy, J. Chun, S. N. Powell, BRCA1 and BRCA2: different roles in a common pathway of genome protection., *Nat. Rev. Cancer* **12**, 68–78 (2011).

51. R. Wooster, B. L. Weber, Breast and Ovarian Cancer, *N. Engl. J. Med.* **348**, 2339–2347 (2003).

52. K. N. Stevens, C. M. Vachon, F. J. Couch, Genetic susceptibility to triple-negative breast cancer., *Cancer Res.* **73**, 2025–30 (2013).

53. A. Bhattacharyya, U. S. Ear, B. H. Koller, R. R. Weichselbaum, D. K. Bishop, The Breast Cancer Susceptibility Gene *BRCA1* Is Required for Subnuclear Assembly of Rad51 and Survival following Treatment with the DNA Cross-linking Agent Cisplatin, *J. Biol. Chem.* **275**, 23899–23903 (2000).

54. M. E. Moynahan, T. Y. Cui, M. Jasin, Homology-directed dna repair, mitomycin-c resistance, and chromosome stability is restored with correction of a Brca1 mutation., *Cancer Res.* **61**, 4842–50 (2001).

55. N. Turner, A. Tutt, A. Ashworth, Hallmarks of "BRCAness" in sporadic cancers., *Nat. Rev. Cancer* **4**, 814–9 (2004).

56. T. Byrski, T. Huzarski, R. Dent, J. Gronwald, D. Zuziak, C. Cybulski, J. Kladny, B. Gorski, J. Lubinski, S. A. Narod, Response to neoadjuvant therapy with cisplatin in BRCA1-positive breast cancer patients, *Breast Cancer Res. Treat.* **115**, 359–363 (2009).

57. E. Alba, J. I. Chacon, A. Lluch, A. Anton, L. Estevez, B. Cirauqui, E. Carrasco, L. Calvo, M. A. Segui, N. Ribelles, R. Alvarez, A. Sanchez-Muñoz, R. Sanchez, J. A. L. Garcia-Asenjo, C. Rodriguez-Martin, M. J. Escudero, J. Albanell, A randomized phase II trial of platinum salts in basal-like breast cancer patients in the neoadjuvant setting. Results from the GEICAM/2006-03, multicenter study, *Breast Cancer Res. Treat.* **136**, 487–493 (2012).

58. G. von Minckwitz, A. Schneeweiss, S. Loibl, C. Salat, C. Denkert, M. Rezai, J. U. Blohmer, C. Jackisch, S. Paepke, B. Gerber, D. M. Zahm, S. Kümmel, H. Eidtmann, P. Klare, J. Huober, S. Costa, H. Tesch, C. Hanusch, J. Hilfrich, F. Khandan, P. A. Fasching, B. V Sinn, K. Engels, K. Mehta, V. Nekljudova, M. Untch, Neoadjuvant carboplatin in patients with triple-negative and HER2-positive early breast cancer (GeparSixto; GBG 66): a randomised phase 2 trial., *Lancet. Oncol.* **15**, 747–56 (2014).

59. W. M. Sikov, D. A. Berry, C. M. Perou, B. Singh, C. T. Cirrincione, S. M. Tolaney, C. S. Kuzma, T. J. Pluard, G. Somlo, E. R. Port, M. Golshan, J. R. Bellon, D. Collyar, O. M. Hahn, L. A. Carey, C. A. Hudis, E. P. Winer, Impact of the Addition of Carboplatin and/or Bevacizumab to Neoadjuvant Once-per-Week Paclitaxel Followed by Dose-Dense Doxorubicin and Cyclophosphamide on Pathologic Complete Response Rates in Stage II to III Triple-Negative Breast Cancer: CALGB 40603 (Alliance), *J. Clin. Oncol.* **33**, 13–21 (2015).

60. Y. Fan, B. H. Xu, P. Yuan, F. Ma, J. Y. Wang, X. Y. Ding, P. Zhang, Q. Li, R. G. Cai, Docetaxel-cisplatin might be superior to docetaxel-capecitabine in the first-line treatment of metastatic triple-negative breast cancer., *Ann. Oncol. Off. J. Eur. Soc. Med. Oncol.* **24**, 1219–25 (2013).

61. X.-C. Hu, J. Zhang, B.-H. Xu, L. Cai, J. Ragaz, Z.-H. Wang, B.-Y. Wang, Y.-E. Teng, Z.-S. Tong, Y.-Y. Pan, Y.-M. Yin, C.-P. Wu, Z.-F. Jiang, X.-J. Wang, G.-Y. Lou, D.-G. Liu, J.-F. Feng, J.-F. Luo, K. Sun, Y.-J. Gu, J. Wu, Z.-M. Shao, Cisplatin plus gemcitabine versus paclitaxel plus gemcitabine as first-line therapy for metastatic triple-negative breast cancer (CBCSG006): a randomised, open-label, multicentre, phase 3 trial., *Lancet. Oncol.* **16**, 436–46 (2015).

62. A. Tutt, H. Tovey, M. C. U. Cheang, S. Kernaghan, L. Kilburn, P. Gazinska, J. Owen, J. Abraham, S. Barrett, P. Barrett-Lee, R. Brown, S. Chan, M. Dowsett, J. M. Flanagan, L. Fox, A. Grigoriadis, A. Gutin, C. Harper-Wynne, M. Q. Hatton, K. A. Hoadley, J. Parikh, P. Parker, C. M. Perou, R. Roylance, V. Shah, A. Shaw, I. E. Smith, K. M. Timms, A. M. Wardley, G. Wilson, C. Gillett, J. S. Lanchbury, A. Ashworth, N. Rahman, M. Harries, P. Ellis, S. E. Pinder, J. M. Bliss, Carboplatin in BRCA1/2-mutated and triple-negative breast cancer BRCAness subgroups: The TNT Trial, *Nat. Med.* **24**, 628–637 (2018).

63. H. E. Bryant, N. Schultz, H. D. Thomas, K. M. Parker, D. Flower, E. Lopez, S. Kyle,

M. Meuth, N. J. Curtin, T. Helleday, Specific killing of BRCA2-deficient tumours with inhibitors of poly(ADP-ribose) polymerase, *Nature* **434**, 913–917 (2005).

64. H. Farmer, N. McCabe, C. J. Lord, A. N. J. Tutt, D. A. Johnson, T. B. Richardson, M. Santarosa, K. J. Dillon, I. Hickson, C. Knights, N. M. B. Martin, S. P. Jackson, G. C. M. Smith, A. Ashworth, Targeting the DNA repair defect in BRCA mutant cells as a therapeutic strategy., *Nature* **434**, 917–21 (2005).

65. N. J. O'Neil, M. L. Bailey, P. Hieter, Synthetic lethality and cancer, *Nat. Rev. Genet.* **18**, 613–623 (2017).

66. P. C. Fong, D. S. Boss, T. A. Yap, A. Tutt, P. Wu, M. Mergui-Roelvink, P. Mortimer, H. Swaisland, A. Lau, M. J. O'Connor, A. Ashworth, J. Carmichael, S. B. Kaye, J. H. M. Schellens, J. S. de Bono, Inhibition of poly(ADP-ribose) polymerase in tumors from BRCA mutation carriers., *N. Engl. J. Med.* **361**, 123–34 (2009).

67. A. Tutt, M. Robson, J. E. Garber, S. M. Domchek, M. W. Audeh, J. N. Weitzel, M. Friedlander, B. Arun, N. Loman, R. K. Schmutzler, A. Wardley, G. Mitchell, H. Earl, M. Wickens, J. Carmichael, Oral poly(ADP-ribose) polymerase inhibitor olaparib in patients with BRCA1 or BRCA2 mutations and advanced breast cancer: a proof-of-concept trial., *Lancet (London, England)* **376**, 235–44 (2010).

68. M. Robson, S.-A. Im, E. Senkus, B. Xu, S. M. Domchek, N. Masuda, S. Delaloge, W. Li, N. Tung, A. Armstrong, W. Wu, C. Goessl, S. Runswick, P. Conte, Olaparib for Metastatic Breast Cancer in Patients with a Germline *BRCA* Mutation, *N. Engl. J. Med.* **377**, 523–533 (2017).

69. M. Papadimitriou, G. Mountzios, C. A. Papadimitriou, The role of PARP inhibition in triple-negative breast cancer: Unraveling the wide spectrum of synthetic lethality, *Cancer Treat. Rev.* **67**, 34–44 (2018).

70. H. S. Rugo, O. I. Olopade, A. DeMichele, C. Yau, L. J. van 't Veer, M. B. Buxton, M. Hogarth, N. M. Hylton, M. Paoloni, J. Perlmutter, W. F. Symmans, D. Yee, A. J. Chien, A. M. Wallace, H. G. Kaplan, J. C. Boughey, T. C. Haddad, K. S. Albain, M. C. Liu, C. Isaacs, Q. J. Khan, J. E. Lang, R. K. Viscusi, L. Pusztai, S. L. Moulder, S. Y. Chui, K. A. Kemmer, A. D. Elias, K. K. Edmiston, D. M. Euhus, B. B. Haley, R. Nanda, D. W. Northfelt, D. Tripathy, W. C. Wood, C. Ewing, R. Schwab, J. Lyandres, S. E. Davis, G. L. Hirst, A. Sanil, D. A. Berry, L. J. Esserman, I-SPY 2 Investigators, Adaptive Randomization of Veliparib-Carboplatin Treatment in Breast Cancer., *N. Engl. J. Med.* **375**, 23–34 (2016).

71. S. Loibl, J. O'Shaughnessy, M. Untch, W. M. Sikov, H. S. Rugo, M. D. McKee, J. Huober, M. Golshan, G. von Minckwitz, D. Maag, D. Sullivan, N. Wolmark, K. McIntyre, J. J. Ponce Lorenzo, O. Metzger Filho, P. Rastogi, W. F. Symmans, X. Liu, C. E. Geyer, Addition of the PARP inhibitor veliparib plus carboplatin or carboplatin alone to standard neoadjuvant chemotherapy in triple-negative breast cancer (BrighTNess): a randomised, phase 3 trial., *Lancet. Oncol.* **19**, 497–509 (2018).

72. C. K. Anders, V. Abramson, T. Tan, R. Dent, The Evolution of Triple-Negative Breast

Cancer: From Biology to Novel Therapeutics, *Am. Soc. Clin. Oncol. Educ. B.* **35**, 34–42 (2016).

73. C. Blank, T. F. Gajewski, A. Mackensen, Interaction of PD-L1 on tumor cells with PD-1 on tumor-specific T cells as a mechanism of immune evasion: implications for tumor immunotherapy., *Cancer Immunol. Immunother.* **54**, 307–14 (2005).

74. M. E. Keir, M. J. Butte, G. J. Freeman, A. H. Sharpe, PD-1 and Its Ligands in Tolerance and Immunity, *Annu. Rev. Immunol.* **26**, 677–704 (2008).

75. M. J. Butte, M. E. Keir, T. B. Phamduy, A. H. Sharpe, G. J. Freeman, Programmed death-1 ligand 1 interacts specifically with the B7-1 costimulatory molecule to inhibit T cell responses., *Immunity* **27**, 111–22 (2007).

76. T. Yamazaki, H. Akiba, H. Iwai, H. Matsuda, M. Aoki, Y. Tanno, T. Shin, H. Tsuchiya, D. M. Pardoll, K. Okumura, M. Azuma, H. Yagita, Expression of Programmed Death 1 Ligands by Murine T Cells and APC, *J. Immunol.* **169**, 5538–5545 (2002).

77. E. I. Buchbinder, A. Desai, CTLA-4 and PD-1 Pathways: Similarities, Differences, and Implications of Their Inhibition., *Am. J. Clin. Oncol.* **39**, 98–106 (2016).

78. S. Loi, N. Sirtaine, F. Piette, R. Salgado, G. Viale, F. Van Eenoo, G. Rouas, P. Francis, J. P. A. Crown, E. Hitre, E. de Azambuja, E. Quinaux, A. Di Leo, S. Michiels, M. J. Piccart, C. Sotiriou, Prognostic and predictive value of tumor-infiltrating lymphocytes in a phase III randomized adjuvant breast cancer trial in node-positive breast cancer comparing the addition of docetaxel to doxorubicin with doxorubicin-based chemotherapy: BIG 02-98., *J. Clin. Oncol.* **31**, 860–7 (2013).

79. Y. Issa-Nummer, S. Darb-Esfahani, S. Loibl, G. Kunz, V. Nekljudova, I. Schrader, B. V. Sinn, H.-U. Ulmer, R. Kronenwett, M. Just, T. Kühn, K. Diebold, M. Untch, F. Holms, J.-U. Blohmer, J.-O. Habeck, M. Dietel, F. Overkamp, P. Krabisch, G. von Minckwitz, C. Denkert, S. A. Glynn, Ed. Prospective validation of immunological infiltrate for prediction of response to neoadjuvant chemotherapy in HER2-negative breast cancer--a substudy of the neoadjuvant GeparQuinto trial., *PLoS One* **8**, e79775 (2013).

80. S. Ladoire, L. Arnould, L. Apetoh, B. Coudert, F. Martin, B. Chauffert, P. Fumoleau, F. Ghiringhelli, Pathologic Complete Response to Neoadjuvant Chemotherapy of Breast Carcinoma Is Associated with the Disappearance of Tumor-Infiltrating Foxp3+ Regulatory T Cells, *Clin. Cancer Res.* **14**, 2413–2420 (2008).

81. S. Loi, S. Michiels, R. Salgado, N. Sirtaine, V. Jose, D. Fumagalli, P.-L. Kellokumpu-Lehtinen, P. Bono, V. Kataja, C. Desmedt, M. J. Piccart, S. Loibl, C. Denkert, M. J. Smyth, H. Joensuu, C. Sotiriou, Tumor infiltrating lymphocytes are prognostic in triple negative breast cancer and predictive for trastuzumab benefit in early breast cancer: results from the FinHER trial., *Ann. Oncol.* **25**, 1544–50 (2014).

82. S. A. M. Urru, S. Gallus, C. Bosetti, T. Moi, R. Medda, E. Sollai, A. Murgia, F. Sanges, G. Pira, A. Manca, D. Palmas, M. Floris, A. M. Asunis, F. Atzori, C. Carru, M. D'Incalci,

M. Ghiani, V. Marras, D. Onnis, M. C. Santona, G. Sarobba, E. Valle, L. Canu, S. Cossu, A. Bulfone, P. C. Rocca, M. R. De Miglio, S. Orrù, Clinical and pathological factors influencing survival in a large cohort of triple-negative breast cancer patients., *BMC Cancer* **18**, 56 (2018).

83. M. Ono, H. Tsuda, C. Shimizu, S. Yamamoto, T. Shibata, H. Yamamoto, T. Hirata, K. Yonemori, M. Ando, K. Tamura, N. Katsumata, T. Kinoshita, Y. Takiguchi, H. Tanzawa, Y. Fujiwara, Tumor-infiltrating lymphocytes are correlated with response to neoadjuvant chemotherapy in triple-negative breast cancer, *Breast Cancer Res. Treat.* **132**, 793–805 (2012).

84. S. M. A. Mahmoud, E. C. Paish, D. G. Powe, R. D. Macmillan, M. J. Grainge, A. H. S. Lee, I. O. Ellis, A. R. Green, Tumor-Infiltrating CD8 $^{+}$ Lymphocytes Predict Clinical Outcome in Breast Cancer, *J. Clin. Oncol.* **29**, 1949–1955 (2011).

85. C. Denkert, S. Loibl, A. Noske, M. Roller, B. M. Müller, M. Komor, J. Budczies, S. Darb-Esfahani, R. Kronenwett, C. Hanusch, C. von Törne, W. Weichert, K. Engels, C. Solbach, I. Schrader, M. Dietel, G. von Minckwitz, Tumor-associated lymphocytes as an independent predictor of response to neoadjuvant chemotherapy in breast cancer., *J. Clin. Oncol.* **28**, 105–13 (2010).

86. V. A. Trinh, Current management of metastatic melanoma., *Am. J. Health. Syst. Pharm.* **65**, S3-8 (2008).

87. F. S. Hodi, S. J. O'Day, D. F. McDermott, R. W. Weber, J. A. Sosman, J. B. Haanen, R. Gonzalez, C. Robert, D. Schadendorf, J. C. Hassel, W. Akerley, A. J. M. van den Eertwegh, J. Lutzky, P. Lorigan, J. M. Vaubel, G. P. Linette, D. Hogg, C. H. Ottensmeier, C. Lebbé, C. Peschel, I. Quirt, J. I. Clark, J. D. Wolchok, J. S. Weber, J. Tian, M. J. Yellin, G. M. Nichol, A. Hoos, W. J. Urba, Improved Survival with Ipilimumab in Patients with Metastatic Melanoma, *N. Engl. J. Med.* **363**, 711–723 (2010).

88. C. Robert, J. Schachter, G. V. Long, A. Arance, J. J. Grob, L. Mortier, A. Daud, M. S. Carlino, C. McNeil, M. Lotem, J. Larkin, P. Lorigan, B. Neyns, C. U. Blank, O. Hamid, C. Mateus, R. Shapira-Frommer, M. Kosh, H. Zhou, N. Ibrahim, S. Ebbinghaus, A. Ribas, KEYNOTE-006 investigators, Pembrolizumab versus Ipilimumab in Advanced Melanoma, *N. Engl. J. Med.* **372**, 2521–2532 (2015).

89. P. Schmid, S. Adams, H. S. Rugo, A. Schneeweiss, C. H. Barrios, H. Iwata, V. Diéras, R. Hegg, S.-A. Im, G. Shaw Wright, V. Henschel, L. Molinero, S. Y. Chui, R. Funke, A. Husain, E. P. Winer, S. Loi, L. A. Emens, IMpassion130 Trial Investigators, Atezolizumab and Nab-Paclitaxel in Advanced Triple-Negative Breast Cancer, *N. Engl. J. Med.* **379**, 2108–2121 (2018).

90. C. M. Perou, T. Sørlie, M. B. Eisen, M. van de Rijn, S. S. Jeffrey, C. A. Rees, J. R. Pollack, D. T. Ross, H. Johnsen, L. A. Akslen, Ø. Fluge, A. Pergamenschikov, C. Williams, S. X. Zhu, P. E. Lønning, A.-L. Børresen-Dale, P. O. Brown, D. Botstein, Molecular portraits of human breast tumours, *Nature* **406**, 747–752 (2000).

91. L. A. Carey, C. M. Perou, C. A. Livasy, L. G. Dressler, D. Cowan, K. Conway, G. Karaca, M. A. Troester, C. K. Tse, S. Edmiston, S. L. Deming, J. Geradts, M. C. U. Cheang, T. O. Nielsen, P. G. Moorman, H. S. Earp, R. C. Millikan, Race, Breast Cancer Subtypes, and Survival in the Carolina Breast Cancer Study, *JAMA* **295**, 2492 (2006).

92. J. I. Herschkowitz, K. Simin, V. J. Weigman, I. Mikaelian, J. Usary, Z. Hu, K. E. Rasmussen, L. P. Jones, S. Assefnia, S. Chandrasekharan, M. G. Backlund, Y. Yin, A. I. Khramtsov, R. Bastein, J. Quackenbush, R. I. Glazer, P. H. Brown, J. E. Green, L. Kopelovich, P. A. Furth, J. P. Palazzo, O. I. Olopade, P. S. Bernard, G. A. Churchill, T. Van Dyke, C. M. Perou, Identification of conserved gene expression features between murine mammary carcinoma models and human breast tumors, *Genome Biol.* **8**, 1–17 (2007).

93. A. Prat, J. S. Parker, O. Karginova, C. Fan, C. Livasy, J. I. Herschkowitz, X. He, C. M. Perou, Phenotypic and molecular characterization of the claudin-low intrinsic subtype of breast cancer, *Breast Cancer Res.* **12** (2010), doi:10.1186/bcr2635.

94. F. Bertucci, P. Finetti, N. Cervera, B. Esterni, F. Hermitte, P. Viens, D. Birnbaum, How basal are triple-negative breast cancers?, *Int. J. Cancer* **123**, 236–240 (2008).

95. E. A. Rakha, M. E. El-Sayed, A. R. Green, A. H. S. Lee, J. F. Robertson, I. O. Ellis, Prognostic markers in triple-negative breast cancer, *Cancer* **109**, 25–32 (2007).

96. E. A. Rakha, S. E. Elsheikh, M. A. Aleskandarany, H. O. Habashi, A. R. Green, D. G. Powe, M. E. El-Sayed, A. Benhasouna, J. S. Brunet, L. A. Akslen, A. J. Evans, R. Blamey, J. S. Reis-Filho, W. D. Foulkes, I. O. Ellis, Triple-negative breast cancer: Distinguishing between basal and nonbasal subtypes, *Clin. Cancer Res.* **15**, 2302–2310 (2009).

97. B. D. Lehmann, J. A. Bauer, X. Chen, M. E. Sanders, A. B. Chakravarthy, Y. Shyr, J. A. Pietenpol, Identification of human triple-negative breast cancer subtypes and preclinical models for selection of targeted therapies., *J. Clin. Invest.* **121**, 2750–2767 (2011).

98. B. D. Lehmann, B. Jovanović, X. Chen, M. V. Estrada, K. N. Johnson, Y. Shyr, H. L. Moses, M. E. Sanders, J. A. Pietenpol, A. Sapino, Ed. Refinement of Triple-Negative Breast Cancer Molecular Subtypes: Implications for Neoadjuvant Chemotherapy Selection, *PLoS One* **11**, e0157368 (2016).

99. H. Masuda, K. A. Baggerly, Y. Wang, Y. Zhang, A. M. Gonzalez-Angulo, F. Meric-Bernstam, V. Valero, B. D. Lehmann, J. A. Pietenpol, G. N. Hortobagyi, W. F. Symmans, N. T. Ueno, Differential response to neoadjuvant chemotherapy among 7 triple-negative breast cancer molecular subtypes, *Clin. Cancer Res.* **19**, 5533–5540 (2013).

100. L. Gerratana, D. Basile, G. Buono, S. De Placido, M. Giuliano, S. Minichillo, A. Coinu, F. Martorana, I. De Santo, L. Del Mastro, M. De Laurentiis, F. Puglisi, G. Arpino, Androgen receptor in triple negative breast cancer: A potential target for the targetless subtype, *Cancer Treat. Rev.* **68**, 102–110 (2018).

101. B. Rahim, R. O'Regan, AR signaling in breast cancer, *Cancers (Basel).* **9** (2017), doi:10.3390/cancers9030021.

102. A. Gucalp, S. Tolaney, S. J. Isakoff, J. N. Ingle, M. C. Liu, L. A. Carey, K. Blackwell, H. Rugo, L. Nabell, A. Forero, V. Stearns, A. S. Doane, M. Danso, M. E. Moynahan, L. F. Momen, J. M. Gonzalez, A. Akhtar, D. D. Giri, S. Patil, K. N. Feigin, C. A. Hudis, T. A. Traina, Phase II trial of bicalutamide in patients with androgen receptor-positive, estrogen receptor-negative metastatic breast cancer, *Clin. Cancer Res.* **19**, 5505–5512 (2013).

103. D. F. Penson, A. J. Armstrong, R. Concepcion, N. Agarwal, C. Olsson, L. Karsh, C. Dunshee, F. Wang, K. Wu, A. Krivoshik, D. Phung, C. S. Higano, Enzalutamide versus bicalutamide in castration-resistant prostate cancer: The STRIVE trial, *J. Clin. Oncol.* **34**, 2098–2106 (2016).

104. N. D. Shore, S. Chowdhury, A. Villers, L. Klotz, D. Robert Siemens, D. Phung, S. van Os, N. Hasabou, F. Wang, S. Bhattacharya, A. Heidenreich, Efficacy and safety of enzalutamide versus bicalutamide for patients with metastatic prostate cancer (TERRAIN): A randomised, double-blind, phase 2 study, *Lancet Oncol.* **17**, 153–163 (2016).

105. B. D. Lehmann, J. A. Bauer, J. M. Schafer, C. S. Pendleton, L. Tang, K. C. Johnson, X. Chen, J. M. Balko, H. Gómez, C. L. Arteaga, G. B. Mills, M. E. Sanders, J. A. Pietenpol, PIK3CA mutations in androgen receptor-positive triple negative breast cancer confer sensitivity to the combination of PI3K and androgen receptor inhibitors., *Breast Cancer Res.* **16**, 406 (2014).

106. S. P. Shah, A. Roth, R. Goya, A. Oloumi, G. Ha, Y. Zhao, G. Turashvili, J. Ding, K. Tse, G. Haffari, A. Bashashati, L. M. Prentice, J. Khattra, A. Burleigh, D. Yap, V. Bernard, A. McPherson, K. Shumansky, A. Crisan, R. Giuliany, A. Heravi-Moussavi, J. Rosner, D. Lai, I. Birol, R. Varhol, A. Tam, N. Dhalla, T. Zeng, K. Ma, S. K. Chan, M. Griffith, A. Moradian, S. W. G. Cheng, G. B. Morin, P. Watson, K. Gelmon, S. Chia, S.-F. Chin, C. Curtis, O. M. Rueda, P. D. Pharoah, S. Damaraju, J. Mackey, K. Hoon, T. Harkins, V. Tadigotla, M. Sigaroudinia, P. Gascard, T. Tlsty, J. F. Costello, I. M. Meyer, C. J. Eaves, W. W. Wasserman, S. Jones, D. Huntsman, M. Hirst, C. Caldas, M. A. Marra, S. Aparicio, The clonal and mutational evolution spectrum of primary triple-negative breast cancers, *Nature* **486**, 1–5 (2012).

107. F. Janku, T. A. Yap, F. Meric-Bernstam, Targeting the PI3K pathway in cancer: are we making headway?, *Nat. Rev. Clin. Oncol.* **15**, 273–291 (2018).

108. B. S. Carver, C. Chapinski, J. Wongvipat, H. Hieronymus, Y. Chen, S. Chandarlapaty, V. K. Arora, C. Le, J. Koutcher, H. Scher, P. T. Scardino, N. Rosen, C. L. Sawyers, Reciprocal feedback regulation of PI3K and androgen receptor signaling in PTEN-deficient prostate cancer., *Cancer Cell* **19**, 575–86 (2011).

109. S. Bhatti, J. Heldstab, C. Lehn, O. Tawfik, R. M. Ash, D. R. Hout, R. S. Seitz, D. B. Bailey, A. P. O'Dea, R. A. Jensen, F. Fan, Q. J. Khan, A. K. Godwin, P. Sharma, Clinical Activity of Pembrolizumab in a Patient With Metastatic Triple-Negative Breast Cancer

Without Tumor Programmed Death-Ligand 1 Expression: A Case Report and Correlative Biomarker Analysis, *JCO Precis. Oncol.* , 1–6 (2017).

110. B. Z. Ring, D. R. Hout, S. W. Morris, K. Lawrence, B. L. Schweitzer, D. B. Bailey, B. D. Lehmann, J. A. Pietenpol, R. S. Seitz, Generation of an algorithm based on minimal gene sets to clinically subtype triple negative breast cancer patients, *BMC Cancer* **16**, 143 (2016).

111. C. Kandoth, M. D. McLellan, F. Vandin, K. Ye, B. Niu, C. Lu, M. Xie, Q. Zhang, J. F. McMichael, M. A. Wyczalkowski, M. D. M. Leiserson, C. A. Miller, J. S. Welch, M. J. Walter, M. C. Wendl, T. J. Ley, R. K. Wilson, B. J. Raphael, L. Ding, Mutational landscape and significance across 12 major cancer types., *Nature* **502**, 333–339 (2013).

112. V. G. Abramson, B. D. Lehmann, T. J. Ballinger, J. A. Pietenpol, Subtyping of triple-negative breast cancer: Implications for therapy*Cancer* (2015), doi:10.1002/cncr.28914.

113. Comprehensive molecular portraits of human breast tumours., *Nature* **490**, 61–70 (2012).

114. D. Horiuchi, L. Kusdra, N. E. Huskey, S. Chandriani, M. E. Lenburg, A. M. Gonzalez-Angulo, K. J. Creasman, A. V Bazarov, J. W. Smyth, S. E. Davis, P. Yaswen, G. B. Mills, L. J. Esserman, A. Goga, MYC pathway activation in triple-negative breast cancer is synthetic lethal with CDK inhibition., *J. Exp. Med.* **209**, 679–96 (2012).

115. Z. E. Stine, Z. E. Walton, B. J. Altman, A. L. Hsieh, C. V Dang, MYC, Metabolism, and Cancer., *Cancer Discov.* **5**, 1024–39 (2015).

116. C. V Dang, K. A. O'Donnell, K. I. Zeller, T. Nguyen, R. C. Osthus, F. Li, The c-Myc target gene network., *Semin. Cancer Biol.* **16**, 253–64 (2006).

117. N. Meyer, L. Z. Penn, Reflecting on 25 years with MYC, *Nat. Rev. Cancer* **8**, 976–990 (2008).

118. M. Vita, M. Henriksson, The Myc oncoprotein as a therapeutic target for human cancer*Semin. Cancer Biol.* **16**, 318–330 (2006).

119. V. Strieder, W. Lutz, Regulation of N-myc expression in development and disease., *Cancer Lett.* **180**, 107–19 (2002).

120. E. Legouy, R. DePinho, K. Zimmerman, R. Collum, G. Yancopoulos, L. Mitsock, R. Kriz, F. W. Alt, Structure and expression of the murine L-myc gene., *EMBO J.* **6**, 3359–66 (1987).

121. K. Zimmerman, E. Legouy, V. Stewart, R. Depinho, F. W. Alt, Differential regulation of the N-myc gene in transfected cells and transgenic mice., *Mol. Cell. Biol.* **10**, 2096–2103 (1990).

122. P. J. Hurlin, Control of vertebrate development by MYC, *Cold Spring Harb. Perspect.*

Med. **3** (2013), doi:10.1101/cshperspect.a014332.

123. K. A. Zimmerman, G. D. Yancopoulos, R. G. Collum, R. K. Smith, N. E. Kohl, K. A. Denis, M. M. Nau, O. N. Witte, D. Toran-Allerand, C. E. Gee, J. D. Minna, F. W. Alt, Differential expression of myc family genes during murine development, *Nature* **319**, 780–783 (1986).

124. C. Grandori, S. M. Cowley, L. P. James, R. N. Eisenman, The Myc/Max/Mad network and the transcriptional control of cell behavior., *Annu. Rev. Cell Dev. Biol.* **16**, 653–99 (2000).

125. C. E. Nesbit, J. M. Tersak, E. V Prochownik, MYC oncogenes and human neoplastic disease, *Oncogene* **18**, 3004–3016 (1999).

126. M. Schwab, MYCN in neuronal tumours., *Cancer Lett.* **204**, 179–87 (2004).

127. Z. Mladenov, U. Heine, D. Beard, J. W. Beard, Strain MC29 avian leukosis virus. Myelocytoma, endothelioma, and renal growths: pathomorphological and ultrastructural aspects., *J. Natl. Cancer Inst.* **38**, 251–85 (1967).

128. D. P. Bolognesi, A. J. Langlois, L. Sverak, R. A. Bonar, J. W. Beard, In vitro chick embryo cell response to strain MC29 avian leukosis virus., *J. Virol.* **2**, 576–86 (1968).

129. A. J. Langlois, S. Sankaran, P. H. Hsiung, J. W. Beard, Massive direct conversion of chick embryo cells by strain MC29 avian leukosis virus., *J. Virol.* **1**, 1082–4 (1967).

130. T. Graf, Two types of target cells for transformation with avian myelocytomatosis virus, *Virology* **54**, 398–413 (1973).

131. B. Royer-Pokora, H. Beug, M. Claviez, H.-J. Winkhardt, R. R. Friis, T. Graf, Transformation parameters in chicken fibroblasts transformed by AEV and MC29 avian leukemia viruses, *Cell* **13**, 751–760 (1978).

132. P. H. Duesberg, K. Bister, P. K. Vogt, The RNA of avian acute leukemia virus MC29., *Proc. Natl. Acad. Sci.* **74**, 4320–4324 (1977).

133. S. S. Hu, M. M. Lai, P. K. Vogt, Genome of avian myelocytomatosis virus MC29: analysis by heteroduplex mapping., *Proc. Natl. Acad. Sci.* **76**, 1265–1268 (1979).

134. D. Sheiness, L. Fanshier, J. M. Bishop, Identification of nucleotide sequences which may encode the oncogenic capacity of avian retrovirus MC29., *J. Virol.* **28**, 600–10 (1978).

135. D. Sheiness, J. M. Bishop, DNA and RNA from uninfected vertebrate cells contain nucleotide sequences related to the putative transforming gene of avian myelocytomatosis virus., *J. Virol.* **31**, 514–21 (1979).

136. M. Roussel, S. Saule, C. Lagrou, C. Rommens, H. Beug, T. Graf, D. Stehelin, Three new types of viral oncogene of cellular origin specific for haematopoietic cell

transformation, *Nature* **281**, 452–455 (1979).

137. B. Vennstrom, D. Sheiness, J. Zabielski, J. M. Bishop, Isolation and characterization of c-myc, a cellular homolog of the oncogene (v-myc) of avian myelocytomatosis virus strain 29., *J. Virol.* **42**, 773–9 (1982).

138. B. G. Neel, W. S. Hayward, H. L. Robinson, J. Fang, S. M. Astrin, Avian leukosis virus-induced tumors have common proviral integration sites and synthesize discrete new RNAs: oncogenesis by promoter insertion, *Cell* **23**, 323–334 (1981).

139. W. S. Hayward, B. G. Neel, S. M. Astrin, Activation of a cellular onc gene by promoter insertion in ALV-induced lymphoid leukosis, *Nature* **290**, 475–480 (1981).

140. G. S. Payne, S. A. Courtneidge, L. B. Crittenden, A. M. Fadly, J. M. Bishop, H. E. Varmus, Analysis of avian leukosis virus DNA and RNA in bursal tumours: viral gene expression is not required for maintenance of the tumor state., *Cell* **23**, 311–22 (1981).

141. R. Taub, I. Kirsch, C. Morton, G. Lenoir, D. Swan, S. Tronick, S. Aaronson, P. Leder, Translocation of the c-myc gene into the immunoglobulin heavy chain locus in human Burkitt lymphoma and murine plasmacytoma cells., *Proc. Natl. Acad. Sci.* **79**, 7837–7841 (1982).

142. R. Dalla-Favera, M. Bregni, J. Erikson, D. Patterson, R. C. Gallo, C. M. Croce, Human c-myc onc gene is located on the region of chromosome 8 that is translocated in Burkitt lymphoma cells., *Proc. Natl. Acad. Sci. U. S. A.* **79**, 7824–7 (1982).

143. M. L. Cher, G. S. Bova, D. H. Moore, E. J. Small, P. R. Carroll, S. S. Pin, J. I. Epstein, W. B. Isaacs, R. H. Jensen, Genetic alterations in untreated metastases and androgen-independent prostate cancer detected by comparative genomic hybridization and allelotyping., *Cancer Res.* **56**, 3091–102 (1996).

144. L. Thomas, J. Stamberg, I. Gojo, Y. Ning, A. P. Rapoport, Double minute chromosomes in monoblastic (M5) and myeloblastic (M2) acute myeloid leukemia: two case reports and a review of literature., *Am. J. Hematol.* **77**, 55–61 (2004).

145. K. Bhatia, K. Huppi, G. Spangler, D. Siwarski, R. Iyer, I. Magrath, Point mutations in the c-Myc transactivation domain are common in Burkitt's lymphoma and mouse plasmacytomas., *Nat. Genet.* **5**, 56–61 (1993).

146. M. Henriksson, A. Bakardjiev, G. Klein, B. Lüscher, Phosphorylation sites mapping in the N-terminal domain of c-myc modulate its transforming potential., *Oncogene* **8**, 3199–209 (1993).

147. C. A. Haiman, L. Le Marchand, J. Yamamato, D. O. Stram, X. Sheng, L. N. Kolonel, A. H. Wu, D. Reich, B. E. Henderson, A common genetic risk factor for colorectal and prostate cancer, *Nat. Genet.* **39**, 954–956 (2007).

148. M. M. Pomerantz, N. Ahmadiyeh, L. Jia, P. Herman, M. P. Verzi, H. Doddapaneni,

C. A. Beckwith, J. A. Chan, A. Hills, M. Davis, K. Yao, S. M. Kehoe, H.-J. Lenz, C. A. Haiman, C. Yan, B. E. Henderson, B. Frenkel, J. Barretina, A. Bass, J. Tabernero, J. Baselga, M. M. Regan, J. R. Manak, R. Shivdasani, G. A. Coetzee, M. L. Freedman, The 8q24 cancer risk variant rs6983267 shows long-range interaction with MYC in colorectal cancer., *Nat. Genet.* **41**, 882–4 (2009).

149. J. B. Wright, S. J. Brown, M. D. Cole, Upregulation of c-MYC in cis through a large chromatin loop linked to a cancer risk-associated single-nucleotide polymorphism in colorectal cancer cells., *Mol. Cell. Biol.* **30**, 1411–20 (2010).

150. T. C. He, A. B. Sparks, C. Rago, H. Hermeking, L. Zawel, L. T. da Costa, P. J. Morin, B. Vogelstein, K. W. Kinzler, Identification of c-MYC as a target of the APC pathway., *Science* **281**, 1509–12 (1998).

151. T. G. Oliver, L. L. Grasfeder, A. L. Carroll, C. Kaiser, C. L. Gillingham, S. M. Lin, R. Wickramasinghe, M. P. Scott, R. J. Wechsler-Reya, Transcriptional profiling of the Sonic hedgehog response: A critical role for N-myc in proliferation of neuronal precursors, *Proc. Natl. Acad. Sci.* **100**, 7331–7336 (2003).

152. A. P. Weng, J. M. Millholland, Y. Yashiro-Ohtani, M. L. Arcangeli, A. Lau, C. Wai, C. Del Bianco, C. G. Rodriguez, H. Sai, J. Tobias, Y. Li, M. S. Wolfe, C. Shachaf, D. Felsher, S. C. Blacklow, W. S. Pear, J. C. Aster, c-Myc is an important direct target of Notch1 in T-cell acute lymphoblastic leukemia/lymphoma., *Genes Dev.* **20**, 2096–109 (2006).

153. C. Schild, M. Wirth, M. Reichert, R. M. Schmid, D. Saur, G. Schneider, PI3K signaling maintains c-myc expression to regulate transcription of E2F1 in pancreatic cancer cells, *Mol. Carcinog.* **48**, 1149–1158 (2009).

154. J. Zhu, J. Blenis, J. Yuan, Activation of PI3K/Akt and MAPK pathways regulates Myc-mediated transcription by phosphorylating and promoting the degradation of Mad1., *Proc. Natl. Acad. Sci. U. S. A.* **105**, 6584–9 (2008).

155. M. Carroll, K. L. B. Borden, The Oncogene eIF4E: Using Biochemical Insights to Target Cancer, *J. Interf. Cytokine Res.* **33**, 227–238 (2013).

156. S. C. Schiavi, J. G. Belasco, M. E. Greenberg, Regulation of proto-oncogene mRNA stability., *Biochim. Biophys. Acta* **1114**, 95–106 (1992).

157. S. Akhoondi, D. Sun, N. von der Lehr, S. Apostolidou, K. Klotz, A. Maljukova, D. Cepeda, H. Fiegl, D. Dafou, D. Dofou, C. Marth, E. Mueller-Holzner, M. Corcoran, M. Dagnell, S. Z. Nejad, B. N. Nayer, M. R. Zali, J. Hansson, S. Egyhazi, F. Petersson, P. Sangfelt, H. Nordgren, D. Grander, S. I. Reed, M. Widschwendter, O. Sangfelt, C. Spruck, FBXW7/hCDC4 is a general tumor suppressor in human cancer., *Cancer Res.* **67**, 9006–12 (2007).

158. N. E. Kohl, N. Kanda, R. R. Schreck, G. Bruns, S. A. Latt, F. Gilbert, F. W. Alt, Transposition and amplification of oncogene-related sequences in human neuroblastomas, *Cell* **35**, 359–367 (1983).

159. M. M. Nau, B. J. Brooks, J. Battey, E. Sausville, A. F. Gazdar, I. R. Kirsch, O. W. McBride, V. Bertness, G. F. Hollis, J. D. Minna, L-myc, a new myc-related gene amplified and expressed in human small cell lung cancer, *Nature* **318**, 69–73 (1985).

160. M. Hartl, A.-M. Mitterstiller, T. Valovka, K. Breuker, B. Hobmayer, K. Bister, Stem cell-specific activation of an ancestral myc protooncogene with conserved basic functions in the early metazoan Hydra, *Proc. Natl. Acad. Sci.* **107**, 4051–4056 (2010).

161. W. P. Tansey, Mammalian MYC Proteins and Cancer, *New J. Sci.* **2014**, 1–27 (2014).

162. T. Blackwell, L. Kretzner, E. Blackwood, R. Eisenman, H. Weintraub, Sequence-specific DNA binding by the c-Myc protein, *Science (80-.).* **250**, 1149–1151 (1990).

163. G. Prendergast, E. Ziff, Methylation-sensitive sequence-specific DNA binding by the c-Myc basic region, *Science (80-.).* **251**, 186–189 (1991).

164. Z. Nie, G. Hu, G. Wei, K. Cui, A. Yamane, W. Resch, R. Wang, D. R. Green, L. Tessarollo, R. Casellas, K. Zhao, D. Levens, c-Myc is a universal amplifier of expressed genes in lymphocytes and embryonic stem cells., *Cell* **151**, 68–79 (2012).

165. C. Y. Lin, J. Lovén, P. B. Rahl, R. M. Paranal, C. B. Burge, J. E. Bradner, T. I. Lee, R. A. Young, Transcriptional amplification in tumor cells with elevated c-Myc, *Cell* **151**, 56–67 (2012).

166. B. T. Vo, E. Wolf, D. Kawauchi, A. Gebhardt, J. E. Rehg, D. Finkelstein, S. Walz, B. L. Murphy, Y. H. Youn, Y.-G. Han, M. Eilers, M. F. Roussel, The Interaction of Myc with Miz1 Defines Medulloblastoma Subgroup Identity., *Cancer Cell* **29**, 5–16 (2016).

167. B. King, F. Boccalatte, K. Moran-Crusio, E. Wolf, J. Wang, C. Kayembe, C. Lazaris, X. Yu, B. Aranda-Orgilles, A. Lasorella, I. Aifantis, The ubiquitin ligase Huwe1 regulates the maintenance and lymphoid commitment of hematopoietic stem cells, *Nat. Immunol.* (2016), doi:10.1038/ni.3559.

168. F. Lorenzin, U. Benary, A. Baluapuri, S. Walz, L. A. Jung, B. von Eyss, C. Kisker, J. Wolf, M. Eilers, E. Wolf, Different promoter affinities account for specificity in MYC-dependent gene regulation., *Elife* **5** (2016), doi:10.7554/eLife.15161.

169. A. Sabò, T. R. Kress, M. Pelizzola, S. de Pretis, M. M. Gorski, A. Tesi, M. J. Morelli, P. Bora, M. Doni, A. Verrecchia, C. Tonelli, G. Fagà, V. Bianchi, A. Ronchi, D. Low, H. Müller, E. Guccione, S. Campaner, B. Amati, Selective transcriptional regulation by Myc in cellular growth control and lymphomagenesis, *Nature* **511**, 488–492 (2014).

170. D. J. Murphy, M. R. Junttila, L. Pouyet, A. Karnezis, K. Shchors, D. A. Bui, L. Brown-Swigart, L. Johnson, G. I. Evan, Distinct thresholds govern Myc's biological output in vivo., *Cancer Cell* **14**, 447–57 (2008).

171. M. Eilers, R. N. Eisenman, Myc's broad reach, *Genes Dev.* **22**, 2755–2766 (2008).

172. C. V. Dang, MYC on the Path to Cancer, *Cell* **149**, 22–35 (2012).

173. H. Ji, G. Wu, X. Zhan, A. Nolan, C. Koh, A. De Marzo, H. M. Doan, J. Fan, C. Cheadle, M. Fallahi, J. L. Cleveland, C. V Dang, K. I. Zeller, M. V. Blagosklonny, Ed. Cell-type independent MYC target genes reveal a primordial signature involved in biomass accumulation., *PLoS One* **6**, e26057 (2011).

174. E. Guccione, F. Martinato, G. Finocchiaro, L. Luzi, L. Tizzoni, V. Dall' Olio, G. Zardo, C. Nervi, L. Bernard, B. Amati, Myc-binding-site recognition in the human genome is determined by chromatin context., *Nat. Cell Biol.* **8**, 764–70 (2006).

175. B.-K. Lee, A. A. Bhinge, A. Battenhouse, R. M. McDaniell, Z. Liu, L. Song, Y. Ni, E. Birney, J. D. Lieb, T. S. Furey, G. E. Crawford, V. R. Iyer, Cell-type specific and combinatorial usage of diverse transcription factors revealed by genome-wide binding studies in multiple human cells, *Genome Res.* **22**, 9–24 (2012).

176. F. Martinato, M. Cesaroni, B. Amati, E. Guccione, E. Abraham, Ed. Analysis of Myc-Induced Histone Modifications on Target Chromatin, *PLoS One* **3**, e3650 (2008).

177. T. K. Kundu, M. R. S. Rao, CpG Islands in Chromatin Organization and Gene Expression, *J. Biochem.* **125**, 217–222 (1999).

178. P. C. Fernandez, S. R. Frank, L. Wang, M. Schroeder, S. Liu, J. Greene, A. Cocito, B. Amati, Genomic targets of the human c-Myc protein., *Genes Dev.* **17**, 1115–29 (2003).

179. K. I. Zeller, X. Zhao, C. W. H. Lee, K. P. Chiu, F. Yao, J. T. Yustein, H. S. Ooi, Y. L. Orlov, A. Shahab, H. C. Yong, Y. Fu, Z. Weng, V. A. Kuznetsov, W.-K. Sung, Y. Ruan, C. V Dang, C.-L. Wei, Global mapping of c-Myc binding sites and target gene networks in human B cells., *Proc. Natl. Acad. Sci. U. S. A.* **103**, 17834–9 (2006).

180. B. A. Malynn, I. M. De Alboran, R. C. O'Hagan, R. Bronson, L. Davidson, R. A. DePinho, F. W. Alt, N-myc can functionally replace c-myc in murine development, cellular growth, and differentiation, *Genes Dev.* (2000).

181. E. Dmitrovsky, W. M. Kuehl, G. F. Hollis, I. R. Kirsch, T. P. Bender, S. Segal, Expression of a transfected human c-myc oncogene inhibits differentiation of a mouse erythroleukaemia cell line., *Nature* **322**, 748–50 (1986).

182. A. Nepveu, K. B. Marcu, A. I. Skoultchi, H. M. Lachman, Contributions of transcriptional and post-transcriptional mechanisms to the regulation of c-myc expression in mouse erythroleukemia cells., *Genes Dev.* **1**, 938–45 (1987).

183. G. P. Tonini, D. Radzioch, A. Gronberg, M. Clayton, E. Blasi, G. Benetton, L. Varesio, Erythroid differentiation and modulation of c-myc expression induced by antineoplastic drugs in the human leukemic cell line K562., *Cancer Res.* **47**, 4544–7 (1987).

184. A. Wilson, M. J. Murphy, T. Oskarsson, K. Kaloulis, M. D. Bettess, G. M. Oser, A.-C. Pasche, C. Knabenhans, H. R. Macdonald, A. Trumpp, c-Myc controls the balance

between hematopoietic stem cell self-renewal and differentiation., *Genes Dev.* **18**, 2747–63 (2004).

185. E. Laurenti, B. Varnum-Finney, A. Wilson, I. Ferrero, W. E. Blanco-Bose, A. Ehninger, P. S. Knoepfler, P.-F. Cheng, H. R. MacDonald, R. N. Eisenman, I. D. Bernstein, A. Trumpp, Hematopoietic stem cell function and survival depend on c-Myc and N-Myc activity., *Cell Stem Cell* **3**, 611–24 (2008).

186. S. Sawai, A. Shimono, Y. Wakamatsu, C. Palmes, K. Hanaoka, H. Kondoh, Defects of embryonic organogenesis resulting from targeted disruption of the N-myc gene in the mouse., *Development* **117**, 1445–55 (1993).

187. S. Ota, Z.-Q. Zhou, D. R. Keene, P. Knoepfler, P. J. Hurlin, Activities of N-Myc in the developing limb link control of skeletal size with digit separation., *Development* **134**, 1583–92 (2007).

188. D. ten Berge, S. A. Brugmann, J. A. Helms, R. Nusse, Wnt and FGF signals interact to coordinate growth with cell fate specification during limb development, *Development* **135**, 3247–3257 (2008).

189. Z.-Q. Zhou, C.-Y. Shung, S. Ota, H. Akiyama, D. R. Keene, P. J. Hurlin, F. Beier, Ed. Sequential and Coordinated Actions of c-Myc and N-Myc Control Appendicular Skeletal Development, *PLoS One* **6**, e18795 (2011).

190. B. R. Stanton, A. S. Perkins, L. Tessarollo, D. A. Sassoon, L. F. Parada, Loss of N-myc function results in embryonic lethality and failure of the epithelial component of the embryo to develop., *Genes Dev.* **6**, 2235–47 (1992).

191. J. Charron, B. A. Malynn, P. Fisher, V. Stewart, L. Jeannotte, S. P. Goff, E. J. Robertson, F. W. Alt, Embryonic lethality in mice homozygous for a targeted disruption of the N-myc gene., *Genes Dev.* **6**, 2248–57 (1992).

192. A. Trumpp, Y. Refaeli, T. Oskarsson, S. Gasser, M. Murphy, G. R. Martin, J. M. Bishop, c-Myc regulates mammalian body size by controlling cell number but not cell size, *Nature* **414**, 768–773 (2001).

193. A. C. Davis, M. Wims, G. D. Spotts, S. R. Hann, A. Bradley, A null c-myc mutation causes lethality before 10.5 days of gestation in homozygotes and reduced fertility in heterozygous female mice., *Genes Dev.* **7**, 671–82 (1993).

194. M. D. Delgado, J. Leon, Myc Roles in Hematopoiesis and Leukemia, *Genes Cancer* **1**, 605–616 (2010).

195. C. He, H. Hu, R. Braren, S.-Y. Fong, A. Trumpp, T. R. Carlson, R. A. Wang, c-myc in the hematopoietic lineage is crucial for its angiogenic function in the mouse embryo., *Development* **135**, 2467–77 (2008).

196. N. C. Dubois, C. Adolphe, A. Ehninger, R. A. Wang, E. J. Robertson, A. Trumpp,

Placental rescue reveals a sole requirement for c-Myc in embryonic erythroblast survival and hematopoietic stem cell function., *Development* **135**, 2455–65 (2008).

197. C. B. Moens, A. B. Auerbach, R. A. Conlon, A. L. Joyner, J. Rossant, A targeted mutation reveals a role for N-myc in branching morphogenesis in the embryonic mouse lung., *Genes Dev.* **6**, 691–704 (1992).

198. A. Nagy, C. Moens, E. Ivanyi, J. Pawling, M. Gertsenstein, A. K. Hadjantonakis, M. Pirity, J. Rossant, Dissecting the role of N-myc in development using a single targeting vector to generate a series of alleles., *Curr. Biol.* **8**, 661–4 (1998).

199. C. B. Moens, B. R. Stanton, L. F. Parada, J. Rossant, Defects in heart and lung development in compound heterozygotes for two different targeted mutations at the N-myc locus., *Development* **119**, 485–99 (1993).

200. T. Okubo, P. S. Knoepfler, R. N. Eisenman, B. L. M. Hogan, Nmyc plays an essential role during lung development as a dosage-sensitive regulator of progenitor cell proliferation and differentiation., *Development* **132**, 1363–74 (2005).

201. C. Harmelink, Y. Peng, P. DeBenedittis, H. Chen, W. Shou, K. Jiao, Myocardial Mycn is essential for mouse ventricular wall morphogenesis, *Dev. Biol.* **373**, 53–63 (2013).

202. H. Nakhai, J. T. Siveke, L. Mendoza-Torres, R. M. Schmid, Conditional inactivation of Myc impairs development of the exocrine pancreas, *Development* **135**, 3191–3196 (2008).

203. E. Domínguez-Frutos, I. López-Hernández, V. Vendrell, J. Neves, M. Gallozzi, K. Gutsche, L. Quintana, J. Sharpe, P. S. Knoepfler, R. N. Eisenman, A. Trumpp, F. Giráldez, T. Schimmang, N-myc controls proliferation, morphogenesis, and patterning of the inner ear., *J. Neurosci.* **31**, 7178–89 (2011).

204. P. S. Knoepfler, P. F. Cheng, R. N. Eisenman, N-myc is essential during neurogenesis for the rapid expansion of progenitor cell populations and the inhibition of neuronal differentiation., *Genes Dev.* **16**, 2699–712 (2002).

205. F. Mirzamohammadi, A. Kozlova, G. Papaioannou, E. Paltrinieri, U. M. Ayturk, T. Kobayashi, Distinct molecular pathways mediate Mycn and Myc-regulated miR-17-92 microRNA action in Feingold syndrome mouse models., *Nat. Commun.* **9**, 1352 (2018).

206. J. Celli, H. van Bokhoven, H. G. Brunner, Feingold syndrome: clinical review and genetic mapping., *Am. J. Med. Genet. A* **122A**, 294–300 (2003).

207. R. L. Waikel, Y. Kawachi, P. A. Waikel, X. J. Wang, D. R. Roop, Deregulated expression of c-Myc depletes epidermal stem cells., *Nat. Genet.* **28**, 165–8 (2001).

208. W. Shu, S. Guttentag, Z. Wang, T. Andl, P. Ballard, M. M. Lu, S. Piccolo, W. Birchmeier, J. A. Whitsett, S. E. Millar, E. E. Morrisey, Wnt/beta-catenin signaling acts upstream of N-myc, BMP4, and FGF signaling to regulate proximal-distal patterning in

the lung., *Dev. Biol.* **283**, 226–39 (2005).

209. M. C. Hu, N. D. Rosenblum, Smad1, -catenin and Tcf4 associate in a molecular complex with the Myc promoter in dysplastic renal tissue and cooperate to control Myc transcription, *Development* **132**, 215–225 (2004).

210. A. Gandarillas, F. M. Watt, c-Myc promotes differentiation of human epidermal stem cells, *Genes Dev.* **11**, 2869–2882 (1997).

211. A. Gandarillas, D. Davies, J. M. Blanchard, Normal and c-Myc-promoted human keratinocyte differentiation both occur via a novel cell cycle involving cellular growth and endoreplication., *Oncogene* **19**, 3278–89 (2000).

212. J. Zanet, S. Pibre, C. Jacquet, A. Ramirez, I. M. de Alboran, A. Gandarillas, Endogenous Myc controls mammalian epidermal cell size, hyperproliferation, endoreplication and stem cell amplification, *J. Cell Sci.* **118**, 1693–1704 (2005).

213. R. A. DePinho, N. Schreiber-Agus, F. W. Alt, in (1991), pp. 1–46.

214. M. Henriksson, B. Lüscher, in (1996), pp. 109–182.

215. K. I. Lin, Y. Lin, K. Calame, Repression of c-myc is necessary but not sufficient for terminal differentiation of B lymphocytes in vitro., *Mol. Cell. Biol.* **20**, 8684–95 (2000).

216. M. Couillard, M. Trudel, C-myc as a modulator of renal stem/progenitor cell population., *Dev. Dyn.* **238**, 405–14 (2009).

217. C. Bonal, F. Thorel, A. Ait-Lounis, W. Reith, A. Trumpp, P. L. Herrera, Pancreatic Inactivation of c-Myc Decreases Acinar Mass and Transdifferentiates Acinar Cells Into Adipocytes in Mice, *Gastroenterology* **136**, 309-319.e9 (2009).

218. J. Dong, S. Sutor, G. Jiang, Y. Cao, Y. W. Asmann, D. A. Wigle, S. Aerts, Ed. c-Myc Regulates Self-Renewal in Bronchoalveolar Stem Cells, *PLoS One* **6**, e23707 (2011).

219. T. Stoelzle, P. Schwarb, A. Trumpp, N. E. Hynes, c-Myc affects mRNA translation, cell proliferation and progenitor cell function in the mammary gland., *BMC Biol.* **7**, 63 (2009).

220. M. Moumen, A. Chiche, M.-A. Deugnier, V. Petit, A. Gandarillas, M. A. Glukhova, M. M. Faraldo, The Proto-Oncogene Myc Is Essential for Mammary Stem Cell Function, *Stem Cells* **30**, 1246–1254 (2012).

221. V. Muncan, O. J. Sansom, L. Tertoolen, T. J. Phesse, H. Begthel, E. Sancho, A. M. Cole, A. Gregorieff, I. M. de Alboran, H. Clevers, A. R. Clarke, Rapid Loss of Intestinal Crypts upon Conditional Deletion of the Wnt/Tcf-4 Target Gene c-Myc, *Mol. Cell. Biol.* **26**, 8418–8426 (2006).

222. M. D. Bettess, N. Dubois, M. J. Murphy, C. Dubey, C. Roger, S. Robine, A. Trumpp,

c-Myc is required for the formation of intestinal crypts but dispensable for homeostasis of the adult intestinal epithelium., *Mol. Cell. Biol.* **25**, 7868–78 (2005).

223. G. Bretones, M. D. Delgado, J. León, Myc and cell cycle control, *Biochim. Biophys. Acta - Gene Regul. Mech.* **1849**, 506–516 (2015).

224. S. K. Sjostrom, G. Finn, W. C. Hahn, D. H. Rowitch, A. M. Kenney, The Cdk1 complex plays a prime role in regulating N-myc phosphorylation and turnover in neural precursors., *Dev. Cell* **9**, 327–38 (2005).

225. C. Grandori, N. Gomez-Roman, Z. A. Felton-Edkins, C. Ngouenet, D. A. Galloway, R. N. Eisenman, R. J. White, c-Myc binds to human ribosomal DNA and stimulates transcription of rRNA genes by RNA polymerase I, *Nat. Cell Biol.* **7**, 311–318 (2005).

226. G. Xiao, S. Mao, G. Baumgarten, J. Serrano, M. C. Jordan, K. P. Roos, M. C. Fishbein, W. R. MacLellan, Inducible activation of c-Myc in adult myocardium in vivo provokes cardiac myocyte hypertrophy and reactivation of DNA synthesis., *Circ. Res.* **89**, 1122–9 (2001).

227. S. Pelengaris, T. Littlewood, M. Khan, G. Elia, G. Evan, Reversible activation of c-Myc in skin: induction of a complex neoplastic phenotype by a single oncogenic lesion., *Mol. Cell* **3**, 565–77 (1999).

228. H. Lee, G. Casadesus, A. Nunomura, X. Zhu, R. J. Castellani, S. L. Richardson, G. Perry, D. W. Felsher, R. B. Petersen, M. A. Smith, The Neuronal Expression of MYC Causes a Neurodegenerative Phenotype in a Novel Transgenic Mouse, *Am. J. Pathol.* **174**, 891–897 (2009).

229. K. Wartiovaara, F. Barnabe-Heider, F. D. Miller, D. R. Kaplan, N-myc promotes survival and induces S-phase entry of postmitotic sympathetic neurons., *J. Neurosci.* **22**, 815–24 (2002).

230. J. I. Partanen, A. I. Nieminen, T. P. Mäkelä, J. Klefstrom, Suppression of oncogenic properties of c-Myc by LKB1-controlled epithelial organization., *Proc. Natl. Acad. Sci. U. S. A.* **104**, 14694–9 (2007).

231. D. S. Rickman, J. H. Schulte, M. Eilers, The Expanding World of N-MYC–Driven Tumors, *Cancer Discov.* **8**, 150–163 (2018).

232. R. C. Seeger, G. M. Brodeur, H. Sather, A. Dalton, S. E. Siegel, K. Y. Wong, D. Hammond, Association of Multiple Copies of the N- *myc* Oncogene with Rapid Progression of Neuroblastomas, *N. Engl. J. Med.* **313**, 1111–1116 (1985).

233. G. Brodeur, R. Seeger, M. Schwab, H. Varmus, J. Bishop, Amplification of N-myc in untreated human neuroblastomas correlates with advanced disease stage, *Science (80-.).* **224**, 1121–1124 (1984).

234. F. J. Swartling, M. R. Grimmer, C. S. Hackett, P. A. Northcott, Q. W. Fan, D. D.

Goldenberg, J. Lau, S. Masic, K. Nguyen, S. Yakovenko, X. N. Zhe, H. C. Flynn Gilmer, R. Collins, M. Nagaoka, J. J. Phillips, R. B. Jenkins, T. Tihan, S. R. Vandenberg, C. D. James, K. Tanaka, M. D. Taylor, W. A. Weiss, L. Chesler, Pleiotropic role for MYCN in medulloblastoma, *Genes Dev.* **24**, 1059–1072 (2010).

235. S. Pfister, M. Remke, A. Benner, F. Mendrzyk, G. Toedt, J. Felsberg, A. Wittmann, F. Devens, N. U. Gerber, S. Joos, A. Kulozik, G. Reifenberger, S. Rutkowski, O. D. Wiestler, B. Radlwimmer, W. Scheurlen, P. Lichter, A. Korshunov, Outcome Prediction in Pediatric Medulloblastoma Based on DNA Copy-Number Aberrations of Chromosomes 6q and 17q and the *MYC* and *MYCN* Loci, *J. Clin. Oncol.* **27**, 1627–1636 (2009).

236. A. B. Hui, K. W. Lo, X. L. Yin, W. S. Poon, H. K. Ng, Detection of multiple gene amplifications in glioblastoma multiforme using array-based comparative genomic hybridization., *Lab. Invest.* **81**, 717–23 (2001).

237. P. W. Lewis, M. M. Müller, M. S. Koletsky, F. Cordero, S. Lin, L. A. Banaszynski, B. A. Garcia, T. W. Muir, O. J. Becher, C. D. Allis, Inhibition of PRC2 activity by a gain-of-function H3 mutation found in pediatric glioblastoma., *Science* **340**, 857–61 (2013).

238. L. Bjerke, A. Mackay, M. Nandhabalan, A. Burford, A. Jury, S. Popov, D. A. Bax, D. Carvalho, K. R. Taylor, M. Vinci, I. Bajrami, I. M. McGonnell, C. J. Lord, R. M. Reis, D. Hargrave, A. Ashworth, P. Workman, C. Jones, Histone H3.3 Mutations Drive Pediatric Glioblastoma through Upregulation of MYCN, *Cancer Discov.* **3**, 512–519 (2013).

239. W.-H. Lee, A. L. Murphree, W. F. Benedict, Expression and amplification of the N-myc gene in primary retinoblastoma, *Nature* **309**, 458–460 (1984).

240. D. MacPherson, K. Conkrite, M. Tam, S. Mukai, D. Mu, T. Jacks, Murine bilateral retinoblastoma exhibiting rapid-onset, metastatic progression and N-myc gene amplification., *EMBO J.* **26**, 784–94 (2007).

241. J. Squire, A. D. Goddard, M. Canton, A. Becker, R. A. Phillips, B. L. Gallie, Tumour induction by the retinoblastoma mutation is independent of N-myc expression, *Nature* **322**, 555–557 (1986).

242. D. E. Rushlow, B. M. Mol, J. Y. Kennett, S. Yee, S. Pajovic, B. L. Thériault, N. L. Prigoda-Lee, C. Spencer, H. Dimaras, T. W. Corson, R. Pang, C. Massey, R. Godbout, Z. Jiang, E. Zacksenhaus, K. Paton, A. C. Moll, C. Houdayer, A. Raizis, W. Halliday, W. L. Lam, P. C. Boutros, D. Lohmann, J. C. Dorsman, B. L. Gallie, Characterisation of retinoblastomas without RB1 mutations: genomic, gene expression, and clinical studies., *Lancet. Oncol.* **14**, 327–34 (2013).

243. H. Hirvonen, V. Hukkanen, T. T. Salmi, T.-T. Pelliniemi, R. Alitalo, L- *myc* and N-*myc* in Hematopoietic Malignancies, *Leuk. Lymphoma* **11**, 197–205 (1993).

244. M. van Lohuizen, M. Breuer, A. Berns, N-myc is frequently activated by proviral insertion in MuLV-induced T cell lymphomas., *EMBO J.* **8**, 133–6 (1989).

245. R. D. Williams, R. Al-Saadi, R. Natrajan, A. Mackay, T. Chagtai, S. Little, S. N. Hing, K. Fenwick, A. Ashworth, P. Grundy, J. R. Anderson, J. S. Dome, E. J. Perlman, C. Jones, K. Pritchard-Jones, Molecular profiling reveals frequent gain of MYCN and anaplasia-specific loss of 4q and 14q in wilms tumor, *Genes, Chromosom. Cancer* **50**, 982–995 (2011).

246. D. Driman, P. S. Thorner, M. L. Greenberg, S. Chilton-MacNeill, J. Squire, MYCN gene amplification in rhabdomyosarcoma, *Cancer* **73**, 2231–2237 (1994).

247. M. M. Nau, B. J. Brooks, D. N. Carney, A. F. Gazdar, J. F. Battey, E. A. Sausville, J. D. Minna, Human small-cell lung cancers show amplification and expression of the N-myc gene., *Proc. Natl. Acad. Sci. U. S. A.* **83**, 1092–6 (1986).

248. K. Fielitz, K. Althoff, K. De Preter, J. Nonnekens, J. Ohli, S. Elges, W. Hartmann, G. Klöppel, T. Knösel, M. Schulte, L. Klein-Hitpass, D. Beisser, H. Reis, A. Eyking, E. Cario, J. H. Schulte, A. Schramm, U. Schüller, Characterization of pancreatic glucagon-producing tumors and pituitary gland tumors in transgenic mice overexpressing MYCN in hGFAP-positive cells., *Oncotarget* **7**, 74415–74426 (2016).

249. H. Beltran, D. S. Rickman, K. Park, S. S. Chae, A. Sboner, T. Y. MacDonald, Y. Wang, K. L. Sheikh, S. Terry, S. T. Tagawa, R. Dhir, J. B. Nelson, A. de la Taille, Y. Allory, M. B. Gerstein, S. Perner, K. J. Pienta, A. M. Chinnaiyan, Y. Wang, C. C. Collins, M. E. Gleave, F. Demichelis, D. M. Nanus, M. A. Rubin, Molecular Characterization of Neuroendocrine Prostate Cancer and Identification of New Drug Targets, *Cancer Discov.* **1**, 487–495 (2011).

250. D. A. Morgenstern, J. Anderson, *MYCN* deregulation as a potential target for novel therapies in rhabdomyosarcoma, *Expert Rev. Anticancer Ther.* **6**, 217–224 (2006).

251. H. Kawagoe, A. Kandilci, T. A. Kranenburg, G. C. Grosveld, Overexpression of N-Myc rapidly causes acute myeloid leukemia in mice., *Cancer Res.* **67**, 10677–85 (2007).

252. Y. Fukuda, Y. Wang, S. Lian, J. Lynch, S. Nagai, B. Fanshawe, A. Kandilci, L. J. Janke, G. Neale, Y. Fan, B. P. Sorrentino, M. F. Roussel, G. Grosveld, J. D. Schuetz, Upregulated heme biosynthesis, an exploitable vulnerability in MYCN-driven leukemogenesis, *JCI Insight* **2** (2017), doi:10.1172/jci.insight.92409.

253. A. J. Wong, J. M. Ruppert, J. Eggleston, S. R. Hamilton, S. B. Baylin, B. Vogelstein, Gene amplification of c-myc and N-myc in small cell carcinoma of the lung., *Science* **233**, 461–4 (1986).

254. K. Funa, L. Steinholtz, E. Nou, J. Bergh, Increased expression of N-myc in human small cell lung cancer biopsies predicts lack of response to chemotherapy and poor prognosis., *Am. J. Clin. Pathol.* **88**, 216–20 (1987).

255. N. Clegg, C. Ferguson, L. D. True, H. Arnold, A. Moorman, J. E. Quinn, R. L. Vessella, P. S. Nelson, Molecular characterization of prostatic small-cell neuroendocrine carcinoma., *Prostate* **55**, 55–64 (2003).

256. E. Dardenne, H. Beltran, M. Benelli, K. Gayvert, A. Berger, L. Puca, J. Cyrta, A. Sboner, Z. Noorzad, T. MacDonald, C. Cheung, K. S. Yuen, D. Gao, Y. Chen, M. Eilers, J.-M. Mosquera, B. D. Robinson, O. Elemento, M. A. Rubin, F. Demichelis, D. S. Rickman, N-Myc Induces an EZH2-Mediated Transcriptional Program Driving Neuroendocrine Prostate Cancer., *Cancer Cell* **30**, 563–577 (2016).

257. K. Ellwood-Yen, T. G. Graeber, J. Wongvipat, M. L. Iruela-Arispe, J. Zhang, R. Matusik, G. V. Thomas, C. L. Sawyers, Myc-driven murine prostate cancer shares molecular features with human prostate tumors, *Cancer Cell* **4**, 223–238 (2003).

258. B. Gurel, T. Iwata, C. M. Koh, R. B. Jenkins, F. Lan, C. Van Dang, J. L. Hicks, J. Morgan, T. C. Cornish, S. Sutcliffe, W. B. Isaacs, J. Luo, A. M. De Marzo, Nuclear MYC protein overexpression is an early alteration in human prostate carcinogenesis., *Mod. Pathol.* **21**, 1156–67 (2008).

259. H. Beltran, D. Prandi, J. M. Mosquera, M. Benelli, L. Puca, J. Cyrta, C. Marotz, E. Giannopoulou, B. V. S. K. Chakravarthi, S. Varambally, S. A. Tomlins, D. M. Nanus, S. T. Tagawa, E. M. Van Allen, O. Elemento, A. Sboner, L. A. Garraway, M. A. Rubin, F. Demichelis, Divergent clonal evolution of castration-resistant neuroendocrine prostate cancer, *Nat. Med.* **22**, 298–305 (2016).

260. Y. Mizukami, A. Nonomura, T. Takizawa, M. Noguchi, T. Michigishi, S. Nakamura, T. Ishizaki, N-myc protein expression in human breast carcinoma: prognostic implications., *Anticancer Res.* **15**, 2899–905.

261. D. A. Lawson, N. R. Bhakta, K. Kessenbrock, K. D. Prummel, Y. Yu, K. Takai, A. Zhou, H. Eyob, S. Balakrishnan, C.-Y. Wang, P. Yaswen, A. Goga, Z. Werb, Single-cell analysis reveals a stem-cell program in human metastatic breast cancer cells., *Nature* **526**, 131–5 (2015).

262. E. R. Andrechek, R. D. Cardiff, J. T. Chang, M. L. Gatza, C. R. Acharya, A. Potti, J. R. Nevins, Genetic heterogeneity of Myc-induced mammary tumors reflecting diverse phenotypes including metastatic potential, *Proc. Natl. Acad. Sci.* **106**, 16387–16392 (2009).

263. M. Lefebure, R. W. Tothill, E. Kruse, E. D. Hawkins, J. Shortt, G. M. Matthews, G. P. Gregory, B. P. Martin, M. J. Kelly, I. Todorovski, M. A. Doyle, R. Lupat, J. Li, J. Schroeder, M. Wall, S. Craig, G. Poortinga, D. Cameron, M. Bywater, L. Kats, M. D. Gearhart, V. J. Bardwell, R. A. Dickins, R. D. Hannan, A. T. Papenfuss, R. W. Johnstone, Genomic characterisation of Eμ-Myc mouse lymphomas identifies Bcor as a Myc co-operative tumour-suppressor gene., *Nat. Commun.* **8**, 14581 (2017).

264. K. Althoff, A. Beckers, E. Bell, M. Nortmeyer, T. Thor, A. Sprüssel, S. Lindner, K. De Preter, A. Florin, L. C. Heukamp, L. Klein-Hitpass, K. Astrahantseff, C. Kumps, F. Speleman, A. Eggert, F. Westermann, A. Schramm, J. H. Schulte, A Cre-conditional MYCN-driven neuroblastoma mouse model as an improved tool for preclinical studies., *Oncogene* **34**, 3357–68 (2015).

265. C. Arvanitis, D. W. Felsher, Conditional transgenic models define how MYC initiates and maintains tumorigenesis, *Semin. Cancer Biol.* **16**, 313–317 (2006).

266. H. Chen, H. Liu, G. Qing, Targeting oncogenic Myc as a strategy for cancer treatment., *Signal Transduct. Target. Ther.* **3**, 5 (2018).

267. Z. Yang, J. H. N. Yik, R. Chen, N. He, M. K. Jang, K. Ozato, Q. Zhou, Recruitment of P-TEFb for Stimulation of Transcriptional Elongation by the Bromodomain Protein Brd4, *Mol. Cell* **19**, 535–545 (2005).

268. B. M. Peterlin, D. H. Price, Controlling the Elongation Phase of Transcription with P-TEFb, *Mol. Cell* **23**, 297–305 (2006).

269. J. E. Delmore, G. C. Issa, M. E. Lemieux, P. B. Rahl, J. Shi, H. M. Jacobs, E. Kastritis, T. Gilpatrick, R. M. Paranal, J. Qi, M. Chesi, A. C. Schinzel, M. R. McKeown, T. P. Heffernan, C. R. Vakoc, P. L. Bergsagel, I. M. Ghobrial, P. G. Richardson, R. A. Young, W. C. Hahn, K. C. Anderson, A. L. Kung, J. E. Bradner, C. S. Mitsiades, BET bromodomain inhibition as a therapeutic strategy to target c-Myc., *Cell* **146**, 904–17 (2011).

270. P. Filippakopoulos, J. Qi, S. Picaud, Y. Shen, W. B. Smith, O. Fedorov, E. M. Morse, T. Keates, T. T. Hickman, I. Felletar, M. Philpott, S. Munro, M. R. McKeown, Y. Wang, A. L. Christie, N. West, M. J. Cameron, B. Schwartz, T. D. Heightman, N. La Thangue, C. A. French, O. Wiest, A. L. Kung, S. Knapp, J. E. Bradner, Selective inhibition of BET bromodomains, *Nature* **468**, 1067–1073 (2010).

271. A. Puissant, S. M. Frumm, G. Alexe, C. F. Bassil, J. Qi, Y. H. Chanthery, E. A. Nekritz, R. Zeid, W. C. Gustafson, P. Greninger, M. J. Garnett, U. McDermott, C. H. Benes, A. L. Kung, W. A. Weiss, J. E. Bradner, K. Stegmaier, Targeting MYCN in neuroblastoma by BET bromodomain inhibition., *Cancer Discov.* **3**, 308–23 (2013).

272. J. E. Delmore, G. C. Issa, M. E. Lemieux, P. B. Rahl, J. Shi, H. M. Jacobs, E. Kastritis, T. Gilpatrick, R. M. Paranal, J. Qi, M. Chesi, A. C. Schinzel, M. R. McKeown, T. P. Heffernan, C. R. Vakoc, P. L. Bergsagel, I. M. Ghobrial, P. G. Richardson, R. A. Young, W. C. Hahn, K. C. Anderson, A. L. Kung, J. E. Bradner, C. S. Mitsiades, BET Bromodomain Inhibition as a Therapeutic Strategy to Target c-Myc, *Cell* **146**, 904–917 (2011).

273. A. Henssen, K. Althoff, A. Odersky, A. Beckers, R. Koche, F. Speleman, S. Scha fers, E. Bell, M. Nortmeyer, F. Westermann, K. De Preter, A. Florin, L. Heukamp, A. Spruessel, K. Astrahanseff, S. Lindner, N. Sadowski, A. Schramm, L. Astorgues-Xerri, M. E. Riveiro, A. Eggert, E. Cvitkovic, J. H. Schulte, Targeting MYCN-Driven Transcription By BET-Bromodomain Inhibition, *Clin. Cancer Res.* **22**, 2470–2481 (2016).

274. R. P. Fisher, Secrets of a double agent: CDK7 in cell-cycle control and transcription., *J. Cell Sci.* **118**, 5171–80 (2005).

275. J. Peng, N. F. Marshall, D. H. Price, Identification of a Cyclin Subunit Required for

the Function of *Drosophila* P-TEFb, *J. Biol. Chem.* **273**, 13855–13860 (1998).

276. R. Shiekhattar, F. Mermelstein, R. P. Fisher, R. Drapkin, B. Dynlacht, H. C. Wessling, D. O. Morgan, D. Reinberg, Cdk-activating kinase complex is a component of human transcription factor TFIIH, *Nature* **374**, 283–287 (1995).

277. M. Heidemann, C. Hintermair, K. Voß, D. Eick, Dynamic phosphorylation patterns of RNA polymerase II CTD during transcription, *Biochim. Biophys. Acta - Gene Regul. Mech.* **1829**, 55–62 (2013).

278. E. Chipumuro, E. Marco, C. Christensen, N. Kwiatkowski, T. Zhang, C. Hatheway, B. Abraham, B. Sharma, C. Yeung, A. Altabef, A. Perez-Atayde, K.-K. Wong, G.-C. Yuan, N. Gray, R. Young, R. George, CDK7 Inhibition Suppresses Super-Enhancer-Linked Oncogenic Transcription in MYCN-Driven Cancer, *Cell* **159**, 1126–1139 (2014).

279. N. Kwiatkowski, T. Zhang, P. B. Rahl, B. J. Abraham, J. Reddy, S. B. Ficarro, A. Dastur, A. Amzallag, S. Ramaswamy, B. Tesar, C. E. Jenkins, N. M. Hannett, D. McMillin, T. Sanda, T. Sim, N. D. Kim, T. Look, C. S. Mitsiades, A. P. Weng, J. R. Brown, C. H. Benes, J. A. Marto, R. A. Young, N. S. Gray, Targeting transcription regulation in cancer with a covalent CDK7 inhibitor, *Nature* **511**, 616–620 (2014).

280. M.-P. Garcia-Cuellar, E. Füller, E. Mäthner, C. Breitinger, K. Hetzner, L. Zeitlmann, A. Borkhardt, R. K. Slany, Efficacy of cyclin-dependent-kinase 9 inhibitors in a murine model of mixed-lineage leukemia., *Leukemia* **28**, 1427–35 (2014).

281. M.-A. Bjornsti, P. J. Houghton, The tor pathway: a target for cancer therapy, *Nat. Rev. Cancer* **4**, 335–348 (2004).

282. S. Wullschleger, R. Loewith, M. N. Hall, TOR Signaling in Growth and Metabolism, *Cell* **124**, 471–484 (2006).

283. D.-H. Kim, D. D. Sarbassov, S. M. Ali, J. E. King, R. R. Latek, H. Erdjument-Bromage, P. Tempst, D. M. Sabatini, mTOR interacts with raptor to form a nutrient-sensitive complex that signals to the cell growth machinery., *Cell* **110**, 163–75 (2002).

284. P. Frost, F. Moatamed, B. Hoang, Y. Shi, J. Gera, H. Yan, P. Frost, J. Gibbons, A. Lichtenstein, In vivo antitumor effects of the mTOR inhibitor CCI-779 against human multiple myeloma cells in a xenograft model, *Blood* **104**, 4181–4187 (2004).

285. N. Chapuis, J. Tamburini, A. S. Green, C. Vignon, V. Bardet, A. Neyret, M. Pannetier, L. Willems, S. Park, A. Macone, S.-M. Maira, N. Ifrah, F. Dreyfus, O. Herault, C. Lacombe, P. Mayeux, D. Bouscary, Dual inhibition of PI3K and mTORC1/2 signaling by NVP-BEZ235 as a new therapeutic strategy for acute myeloid leukemia., *Clin. Cancer Res.* **16**, 5424–35 (2010).

286. K. Yu, L. Toral-Barza, C. Discafani, W. G. Zhang, J. Skotnicki, P. Frost, J. J. Gibbons, mTOR, a novel target in breast cancer: the effect of CCI-779, an mTOR inhibitor, in preclinical models of breast cancer., *Endocr. Relat. Cancer* **8**, 249–258 (2001).

287. R. Sears, F. Nuckolls, E. Haura, Y. Taya, K. Tamai, J. R. Nevins, Multiple Ras-dependent phosphorylation pathways regulate Myc protein stability., *Genes Dev.* **14**, 2501–14 (2000).

288. R. Sears, G. Leone, J. DeGregori, J. R. Nevins, Ras enhances Myc protein stability, *Mol. Cell* (1999), doi:10.1016/S1097-2765(00)80308-1.

289. M. Welcker, A. Orian, J. Jin, J. E. Grim, J. A. Grim, J. W. Harper, R. N. Eisenman, B. E. Clurman, The Fbw7 tumor suppressor regulates glycogen synthase kinase 3 phosphorylation-dependent c-Myc protein degradation., *Proc. Natl. Acad. Sci. U. S. A.* **101**, 9085–90 (2004).

290. M. A. Gregory, Y. Qi, S. R. Hann, Phosphorylation by glycogen synthase kinase-3 controls c-myc proteolysis and subnuclear localization., *J. Biol. Chem.* **278**, 51606–12 (2003).

291. D. Xiao, M. Yue, H. Su, P. Ren, J. Jiang, F. Li, Y. Hu, H. Du, H. Liu, G. Qing, Polo-like Kinase-1 Regulates Myc Stabilization and Activates a Feedforward Circuit Promoting Tumor Cell Survival, *Mol. Cell* **64**, 493–506 (2016).

292. J. R. Bischoff, G. D. Plowman, The Aurora/Ipl1p kinase family: regulators of chromosome segregation and cytokinesis., *Trends Cell Biol.* **9**, 454–9 (1999).

293. J. den Hollander, S. Rimpi, J. R. Doherty, M. Rudelius, A. Buck, A. Hoellein, M. Kremer, N. Graf, M. Scheerer, M. A. Hall, A. Goga, N. von Bubnoff, J. Duyster, C. Peschel, J. L. Cleveland, J. A. Nilsson, U. Keller, Aurora kinases A and B are up-regulated by Myc and are essential for maintenance of the malignant state, *Blood* **116**, 1498–1505 (2010).

294. H. Yang, C. C. Ou, R. I. Feldman, S. V Nicosia, P. A. Kruk, J. Q. Cheng, Aurora-A kinase regulates telomerase activity through c-Myc in human ovarian and breast epithelial cells., *Cancer Res.* **64**, 463–7 (2004).

295. T. Otto, S. Horn, M. Brockmann, U. Eilers, L. Schüttrumpf, N. Popov, A. M. Kenney, J. H. Schulte, R. Beijersbergen, H. Christiansen, B. Berwanger, M. Eilers, Stabilization of N-Myc Is a Critical Function of Aurora A in Human Neuroblastoma, *Cancer Cell* **15**, 67–78 (2009).

296. M. Brockmann, E. Poon, T. Berry, A. Carstensen, H. E. Deubzer, L. Rycak, Y. Jamin, K. Thway, S. P. Robinson, F. Roels, O. Witt, M. Fischer, L. Chesler, M. Eilers, Small Molecule Inhibitors of Aurora-A Induce Proteasomal Degradation of N-Myc in Childhood Neuroblastoma, *Cancer Cell* **24**, 75–89 (2013).

297. C. A. Dodson, M. Kosmopoulou, M. W. Richards, B. Atrash, V. Bavetsias, J. Blagg, R. Bayliss, Crystal structure of an Aurora-A mutant that mimics Aurora-B bound to MLN8054: insights into selectivity and drug design., *Biochem. J.* **427**, 19–28 (2010).

298. W. C. Gustafson, J. G. Meyerowitz, E. A. Nekritz, J. Chen, C. Benes, E. Charron, E. F. Simonds, R. Seeger, K. K. Matthay, N. T. Hertz, M. Eilers, K. M. Shokat, W. A. Weiss,

Drugging MYCN through an allosteric transition in Aurora kinase A., *Cancer Cell* **26**, 414–27 (2014).

299. M. W. Richards, S. G. Burgess, E. Poon, A. Carstensen, M. Eilers, L. Chesler, R. Bayliss, Structural basis of N-Myc binding by Aurora-A and its destabilization by kinase inhibitors, *Proc. Natl. Acad. Sci.* **113**, 13726–13731 (2016).

300. E. Blackwood, R. Eisenman, Max: a helix-loop-helix zipper protein that forms a sequence-specific DNA-binding complex with Myc, *Science (80-.).* **251**, 1211–1217 (1991).

301. I. Uribesalgo, M. Buschbeck, A. Gutiérrez, S. Teichmann, S. Demajo, B. Kuebler, J. F. Nomdedéu, J. Martín-Caballero, G. Roma, S. A. Benitah, L. Di Croce, E-box-independent regulation of transcription and differentiation by MYC, *Nat. Cell Biol.* **13**, 1443–1449 (2011).

302. L. Soucek, M. Helmer-Citterich, A. Sacco, R. Jucker, G. Cesareni, S. Nasi, Design and properties of a Myc derivative that efficiently homodimerizes., *Oncogene* **17**, 2463–72 (1998).

303. D. Annibali, J. R. Whitfield, E. Favuzzi, T. Jauset, E. Serrano, I. Cuartas, S. Redondo-Campos, G. Folch, A. Gonzàlez-Juncà, N. M. Sodir, D. Massó-Vallés, M.-E. Beaulieu, L. B. Swigart, M. M. Mc Gee, M. P. Somma, S. Nasi, J. Seoane, G. I. Evan, L. Soucek, Myc inhibition is effective against glioma and reveals a role for Myc in proficient mitosis., *Nat. Commun.* **5**, 4632 (2014).

304. L. Soucek, S. Nasi, G. I. Evan, Omomyc expression in skin prevents Myc-induced papillomatosis., *Cell Death Differ.* **11**, 1038–45 (2004).

305. L. R. Thomas, Q. Wang, B. C. Grieb, J. Phan, A. M. Foshage, Q. Sun, E. T. Olejniczak, T. Clark, S. Dey, S. Lorey, B. Alicie, G. C. Howard, B. Cawthon, K. C. Ess, C. M. Eischen, Z. Zhao, S. W. Fesik, W. P. Tansey, Interaction with WDR5 promotes target gene recognition and tumorigenesis by MYC., *Mol. Cell* **58**, 440–52 (2015).

306. A. Guarnaccia, W. Tansey, Moonlighting with WDR5: A Cellular Multitasker, *J. Clin. Med.* **7**, 21 (2018).

307. E. R. Aho, J. Wang, R. D. Gogliotti, G. C. Howard, J. Phan, P. Acharya, J. D. Macdonald, K. Cheng, S. L. Lorey, B. Lu, S. Wenzel, A. M. Foshage, J. Alvarado, F. Wang, J. G. Shaw, B. Zhao, A. M. Weissmiller, L. R. Thomas, C. R. Vakoc, M. D. Hall, S. W. Hiebert, Q. Liu, S. R. Stauffer, S. W. Fesik, W. P. Tansey, Displacement of WDR5 from Chromatin by a WIN Site Inhibitor with Picomolar Affinity, *Cell Rep.* **26**, 2916-2928.e13 (2019).

308. M.-Z. Wu, Y.-P. Tsai, M.-H. Yang, C.-H. Huang, S.-Y. Chang, C.-C. Chang, S.-C. Teng, K.-J. Wu, Interplay between HDAC3 and WDR5 is essential for hypoxia-induced epithelial-mesenchymal transition., *Mol. Cell* **43**, 811–22 (2011).

309. A. Carugo, G. Genovese, S. Seth, L. Nezi, J. L. Rose, D. Bossi, A. Cicalese, P. K. Shah, A. Viale, P. F. Pettazzoni, K. C. Akdemir, C. A. Bristow, F. S. Robinson, J. Tepper, N. Sanchez, S. Gupta, M. R. Estecio, V. Giuliani, G. I. Dellino, L. Riva, W. Yao, M. E. Di Francesco, T. Green, C. D'Alesio, D. Corti, Y. Kang, P. Jones, H. Wang, J. B. Fleming, A. Maitra, P. G. Pelicci, L. Chin, R. A. DePinho, L. Lanfrancone, T. P. Heffernan, G. F. Draetta, In Vivo Functional Platform Targeting Patient-Derived Xenografts Identifies WDR5-Myc Association as a Critical Determinant of Pancreatic Cancer., *Cell Rep.* **16**, 133–147 (2016).

310. F. Wang, K. O. Jeon, J. M. Salovich, J. D. Macdonald, J. Alvarado, R. D. Gogliotti, J. Phan, E. T. Olejniczak, Q. Sun, S. Wang, D. Camper, J. P. Yuh, J. G. Shaw, J. Sai, O. W. Rossanese, W. P. Tansey, S. R. Stauffer, S. W. Fesik, Discovery of Potent 2-Aryl-6,7-dihydro-5 *H* -pyrrolo[1,2- *a*]imidazoles as WDR5-WIN-Site Inhibitors Using Fragment-Based Methods and Structure-Based Design, *J. Med. Chem.* **61**, 5623–5642 (2018).

311. J. D. Macdonald, S. Chacon Simon, C. Han, F. Wang, J. G. Shaw, J. E. Howes, J. Sai, J. Yuh, D. V. Camper, B. M. Alicie, J. Alvarado, S. Nikhar, W. G. Payne, E. R. Aho, J. Bauer, B. Zhao, J. Phan, L. R. Thomas, O. W. Rossanese, W. P. Tansey, A. G. Waterson, S. R. Stauffer, S. W. Fesik, Discovery and Optimization of Salicylic Acid-Derived Sulfonamide Inhibitors of the WD Repeat-Containing Protein 5 (WDR5)–MYC Protein–Protein Interaction, *J. Med. Chem.* , acs.jmedchem.9b01411 (2019).

312. Y. Sun, J. L. Bell, D. Carter, S. Gherardi, R. C. Poulos, G. Milazzo, J. W. H. Wong, R. Al-Awar, A. E. Tee, P. Y. Liu, B. Liu, B. Atmadibrata, M. Wong, T. Trahair, Q. Zhao, J. M. Shohet, Y. Haupt, J. H. Schulte, P. J. Brown, C. H. Arrowsmith, M. Vedadi, K. L. MacKenzie, S. Hüttelmaier, G. Perini, G. M. Marshall, A. Braithwaite, T. Liu, WDR5 Supports an N-Myc Transcriptional Complex That Drives a Protumorigenic Gene Expression Signature in Neuroblastoma., *Cancer Res.* **75**, 5143–54 (2015).

313. R. J. DeBerardinis, J. J. Lum, G. Hatzivassiliou, C. B. Thompson, The Biology of Cancer: Metabolic Reprogramming Fuels Cell Growth and Proliferation, *Cell Metab.* **7**, 11–20 (2008).

314. M. Yuneva, N. Zamboni, P. Oefner, R. Sachidanandam, Y. Lazebnik, Deficiency in glutamine but not glucose induces MYC-dependent apoptosis in human cells., *J. Cell Biol.* **178**, 93–105 (2007).

315. G. Qing, B. Li, A. Vu, N. Skuli, Z. E. Walton, X. Liu, P. A. Mayes, D. R. Wise, C. B. Thompson, J. M. Maris, M. D. Hogarty, M. C. Simon, ATF4 regulates MYC-mediated neuroblastoma cell death upon glutamine deprivation., *Cancer Cell* **22**, 631–44 (2012).

316. J. Ham, C. Costa, R. Sano, T. L. Lochmann, E. M. Sennott, N. U. Patel, A. Dastur, M. Gomez-Caraballo, K. Krytska, A. N. Hata, K. V Floros, M. T. Hughes, C. T. Jakubik, D. A. R. Heisey, J. T. Ferrell, M. L. Bristol, R. J. March, C. Yates, M. A. Hicks, W. Nakajima, M. Gowda, B. E. Windle, M. G. Dozmorov, M. J. Garnett, U. McDermott, H. Harada, S. M. Taylor, I. M. Morgan, C. H. Benes, J. A. Engelman, Y. P. Mossé, A. C. Faber, Exploitation of the Apoptosis-Primed State of MYCN-Amplified Neuroblastoma to Develop a Potent

and Specific Targeted Therapy Combination., *Cancer Cell* **29**, 159–72 (2016).

317. X. Chen, J. Li, W. H. Gray, B. D. Lehmann, J. A. Bauer, Y. Shyr, J. A. Pietenpol, TNBCtype: A Subtyping Tool for Triple-Negative Breast Cancer., *Cancer Inform.* **11**, 147–56 (2012).

318. T. J. Pugh, O. Morozova, E. F. Attiyeh, S. Asgharzadeh, J. S. Wei, D. Auclair, S. L. Carter, K. Cibulskis, M. Hanna, A. Kiezun, J. Kim, M. S. Lawrence, L. Lichenstein, A. McKenna, C. S. Pedamallu, A. H. Ramos, E. Shefler, A. Sivachenko, C. Sougnez, C. Stewart, A. Ally, I. Birol, R. Chiu, R. D. Corbett, M. Hirst, S. D. Jackman, B. Kamoh, A. H. Khodabakshi, M. Krzywinski, A. Lo, R. A. Moore, K. L. Mungall, J. Qian, A. Tam, N. Thiessen, Y. Zhao, K. A. Cole, M. Diamond, S. J. Diskin, Y. P. Mosse, A. C. Wood, L. Ji, R. Sposto, T. Badgett, W. B. London, Y. Moyer, J. M. Gastier-Foster, M. A. Smith, J. M. G. Auvil, D. S. Gerhard, M. D. Hogarty, S. J. M. Jones, E. S. Lander, S. B. Gabriel, G. Getz, R. C. Seeger, J. Khan, M. A. Marra, M. Meyerson, J. M. Maris, The genetic landscape of high-risk neuroblastoma, *Nat. Genet.* **45**, 279–284 (2013).

319. W. Abida, J. Cyrta, G. Heller, D. Prandi, J. Armenia, I. Coleman, M. Cieslik, M. Benelli, D. Robinson, E. M. Van Allen, A. Sboner, T. Fedrizzi, J. M. Mosquera, B. D. Robinson, N. De Sarkar, L. P. Kunju, S. Tomlins, Y. M. Wu, D. Nava Rodrigues, M. Loda, A. Gopalan, V. E. Reuter, C. C. Pritchard, J. Mateo, D. Bianchini, S. Miranda, S. Carreira, P. Rescigno, J. Filipenko, J. Vinson, R. B. Montgomery, H. Beltran, E. I. Heath, H. I. Scher, P. W. Kantoff, M.-E. Taplin, N. Schultz, J. S. deBono, F. Demichelis, P. S. Nelson, M. A. Rubin, A. M. Chinnaiyan, C. L. Sawyers, Genomic correlates of clinical outcome in advanced prostate cancer, *Proc. Natl. Acad. Sci.* **116**, 11428–11436 (2019).

320. M. B. Siegel, X. He, K. A. Hoadley, A. Hoyle, J. B. Pearce, A. L. Garrett, S. Kumar, V. J. Moylan, C. M. Brady, A. E. D. Van Swearingen, D. Marron, G. P. Gupta, L. B. Thorne, N. Kieran, C. Livasy, E. R. Mardis, J. S. Parker, M. Chen, C. K. Anders, L. A. Carey, C. M. Perou, Integrated RNA and DNA sequencing reveals early drivers of metastatic breast cancer, *J. Clin. Invest.* **128**, 1371–1383 (2018).

321. J. M. Balko, J. M. Giltnane, K. Wang, L. J. Schwarz, C. D. Young, R. S. Cook, P. Owens, M. E. Sanders, M. G. Kuba, V. Sánchez, R. Kurupi, P. D. Moore, J. A. Pinto, F. D. Doimi, H. Gómez, D. Horiuchi, A. Goga, B. D. Lehmann, J. A. Bauer, J. A. Pietenpol, J. S. Ross, G. A. Palmer, R. Yelensky, M. Cronin, V. A. Miller, P. J. Stephens, C. L. Arteaga, Molecular profiling of the residual disease of triple-negative breast cancers after neoadjuvant chemotherapy identifies actionable therapeutic targets., *Cancer Discov.* **4**, 232–45 (2014).

322. C. Kim, R. Gao, E. Sei, R. Brandt, J. Hartman, T. Hatschek, N. Crosetto, T. Foukakis, N. E. Navin, Chemoresistance Evolution in Triple-Negative Breast Cancer Delineated by Single-Cell Sequencing., *Cell* **173**, 879-893.e13 (2018).

323. A. Butler, P. Hoffman, P. Smibert, E. Papalexi, R. Satija, Integrating single-cell transcriptomic data across different conditions, technologies, and species, *Nat. Biotechnol.* **36**, 411–420 (2018).

324. A. A. Borisy, P. J. Elliott, N. W. Hurst, M. S. Lee, J. Lehar, E. R. Price, G. Serbedzija, G. R. Zimmermann, M. A. Foley, B. R. Stockwell, C. T. Keith, Systematic discovery of multicomponent therapeutics., *Proc. Natl. Acad. Sci. U. S. A.* **100**, 7977–82 (2003).

325. J. J. Wallin, J. Guan, W. W. Prior, L. B. Lee, L. Berry, L. D. Belmont, H. Koeppen, M. Belvin, L. S. Friedman, D. Sampath, GDC-0941, a Novel Class I Selective PI3K Inhibitor, Enhances the Efficacy of Docetaxel in Human Breast Cancer Models by Increasing Cell Death In Vitro and In Vivo, *Clin. Cancer Res.* **18**, 3901–3911 (2012).

326. M. Dodt, J. Roehr, R. Ahmed, C. Dieterich, FLEXBAR—Flexible Barcode and Adapter Processing for Next-Generation Sequencing Platforms, *Biology (Basel).* **1**, 895–905 (2012).

327. A. Dobin, C. A. Davis, F. Schlesinger, J. Drenkow, C. Zaleski, S. Jha, P. Batut, M. Chaisson, T. R. Gingeras, STAR: ultrafast universal RNA-seq aligner., *Bioinformatics* **29**, 15–21 (2013).

328. J. Harrow, A. Frankish, J. M. Gonzalez, E. Tapanari, M. Diekhans, F. Kokocinski, B. L. Aken, D. Barrell, A. Zadissa, S. Searle, I. Barnes, A. Bignell, V. Boychenko, T. Hunt, M. Kay, G. Mukherjee, J. Rajan, G. Despacio-Reyes, G. Saunders, C. Steward, R. Harte, M. Lin, C. Howald, A. Tanzer, T. Derrien, J. Chrast, N. Walters, S. Balasubramanian, B. Pei, M. Tress, J. M. Rodriguez, I. Ezkurdia, J. van Baren, M. Brent, D. Haussler, M. Kellis, A. Valencia, A. Reymond, M. Gerstein, R. Guigo, T. J. Hubbard, GENCODE: The reference human genome annotation for The ENCODE Project, *Genome Res.* **22**, 1760–1774 (2012).

329. C. Trapnell, B. A. Williams, G. Pertea, A. Mortazavi, G. Kwan, M. J. van Baren, S. L. Salzberg, B. J. Wold, L. Pachter, Transcript assembly and quantification by RNA-Seq reveals unannotated transcripts and isoform switching during cell differentiation., *Nat. Biotechnol.* **28**, 511–5 (2010).

330. M. I. Love, W. Huber, S. Anders, Moderated estimation of fold change and dispersion for RNA-seq data with DESeq2., *Genome Biol.* **15**, 550 (2014).

331. R. Kolde, pheatmap: Pretty Heatmaps. R package version 1.0.1 (2019) (available at https://cran.r-project.org/package=pheatmap).

332. A. Subramanian, P. Tamayo, V. K. Mootha, S. Mukherjee, B. L. Ebert, M. A. Gillette, A. Paulovich, S. L. Pomeroy, T. R. Golub, E. S. Lander, J. P. Mesirov, Gene set enrichment analysis: a knowledge-based approach for interpreting genome-wide expression profiles., *Proc. Natl. Acad. Sci. U. S. A.* **102**, 15545–50 (2005).

333. A. Liberzon, A. Subramanian, R. Pinchback, H. Thorvaldsdóttir, P. Tamayo, J. P. Mesirov, Molecular signatures database (MSigDB) 3.0., *Bioinformatics* **27**, 1739–40 (2011).

334. D. B. Mahat, H. Kwak, G. T. Booth, I. H. Jonkers, C. G. Danko, R. K. Patel, C. T. Waters, K. Munson, L. J. Core, J. T. Lis, Base-pair-resolution genome-wide mapping of

active RNA polymerases using precision nuclear run-on (PRO-seq)., *Nat. Protoc.* **11**, 1455–76 (2016).

335. R. Schmieder, R. Edwards, Quality control and preprocessing of metagenomic datasets., *Bioinformatics* **27**, 863–4 (2011).

336. H. Li, Toward better understanding of artifacts in variant calling from high-coverage samples., *Bioinformatics* **30**, 2843–51 (2014).

337. H. Li, B. Handsaker, A. Wysoker, T. Fennell, J. Ruan, N. Homer, G. Marth, G. Abecasis, R. Durbin, 1000 Genome Project Data Processing Subgroup, The Sequence Alignment/Map format and SAMtools, *Bioinformatics* **25**, 2078–2079 (2009).

338. J. Wang, Y. Zhao, X. Zhou, S. W. Hiebert, Q. Liu, Y. Shyr, Nascent RNA sequencing analysis provides insights into enhancer-mediated gene regulation., *BMC Genomics* **19**, 633 (2018).

339. A. E. Carpenter, T. R. Jones, M. R. Lamprecht, C. Clarke, I. H. Kang, O. Friman, D. A. Guertin, J. H. Chang, R. A. Lindquist, J. Moffat, P. Golland, D. M. Sabatini, CellProfiler: image analysis software for identifying and quantifying cell phenotypes., *Genome Biol.* **7**, R100 (2006).

340. D. C. Koboldt, R. S. Fulton, M. D. McLellan, H. Schmidt, J. Kalicki-Veizer, J. F. McMichael, L. L. Fulton, D. J. Dooling, L. Ding, E. R. Mardis, R. K. Wilson, A. Ally, M. Balasundaram, Y. S. N. Butterfield, R. Carlsen, C. Carter, A. Chu, E. Chuah, H.-J. E. Chun, R. J. N. Coope, N. Dhalla, R. Guin, C. Hirst, M. Hirst, R. A. Holt, D. Lee, H. I. Li, M. Mayo, R. A. Moore, A. J. Mungall, E. Pleasance, A. Gordon Robertson, J. E. Schein, A. Shafiei, P. Sipahimalani, J. R. Slobodan, D. Stoll, A. Tam, N. Thiessen, R. J. Varhol, N. Wye, T. Zeng, Y. Zhao, I. Birol, S. J. M. Jones, M. A. Marra, A. D. Cherniack, G. Saksena, R. C. Onofrio, N. H. Pho, S. L. Carter, S. E. Schumacher, B. Tabak, B. Hernandez, J. Gentry, H. Nguyen, A. Crenshaw, K. Ardlie, R. Beroukhim, W. Winckler, G. Getz, S. B. Gabriel, M. Meyerson, L. Chin, P. J. Park, R. Kucherlapati, K. A. Hoadley, J. Todd Auman, C. Fan, Y. J. Turman, Y. Shi, L. Li, M. D. Topal, X. He, H.-H. Chao, A. Prat, G. O. Silva, M. D. Iglesia, W. Zhao, J. Usary, J. S. Berg, M. Adams, J. Booker, J. Wu, A. Gulabani, T. Bodenheimer, A. P. Hoyle, J. V. Simons, M. G. Soloway, L. E. Mose, S. R. Jefferys, S. Balu, J. S. Parker, D. Neil Hayes, C. M. Perou, S. Malik, S. Mahurkar, H. Shen, D. J. Weisenberger, T. Triche Jr, P. H. Lai, M. S. Bootwalla, D. T. Maglinte, B. P. Berman, D. J. Van Den Berg, S. B. Baylin, P. W. Laird, C. J. Creighton, L. A. Donehower, G. Getz, M. Noble, D. Voet, G. Saksena, N. Gehlenborg, D. DiCara, J. Zhang, H. Zhang, C.-J. Wu, S. Yingchun Liu, M. S. Lawrence, L. Zou, A. Sivachenko, P. Lin, P. Stojanov, R. Jing, J. Cho, R. Sinha, R. W. Park, M.-D. Nazaire, J. Robinson, H. Thorvaldsdottir, J. Mesirov, P. J. Park, L. Chin, S. Reynolds, R. B. Kreisberg, B. Bernard, R. Bressler, T. Erkkila, J. Lin, V. Thorsson, W. Zhang, I. Shmulevich, G. Ciriello, N. Weinhold, N. Schultz, J. Gao, E. Cerami, B. Gross, A. Jacobsen, R. Sinha, B. Arman Aksoy, Y. Antipin, B. Reva, R. Shen, B. S. Taylor, M. Ladanyi, C. Sander, P. Anur, P. T. Spellman, Y. Lu, W. Liu, R. R. G. Verhaak, G. B. Mills, R. Akbani, N. Zhang, B. M. Broom, T. D. Casasent, C. Wakefield, A. K. Unruh, K. Baggerly, K. Coombes, J. N. Weinstein, D. Haussler, C. C. Benz, J. M. Stuart,

S. C. Benz, J. Zhu, C. C. Szeto, G. K. Scott, C. Yau, E. O. Paull, D. Carlin, C. Wong, A. Sokolov, J. Thusberg, S. Mooney, S. Ng, T. C. Goldstein, K. Ellrott, M. Grifford, C. Wilks, S. Ma, B. Craft, C. Yan, Y. Hu, D. Meerzaman, J. M. Gastier-Foster, J. Bowen, N. C. Ramirez, A. D. Black, R. E. XPATH ERROR: unknown variable “tname”., P. White, E. J. Zmuda, J. Frick, T. M. Lichtenberg, R. Brookens, M. M. George, M. A. Gerken, H. A. Harper, K. M. Leraas, L. J. Wise, T. R. Tabler, C. McAllister, T. Barr, M. Hart-Kothari, K. Tarvin, C. Saller, G. Sandusky, C. Mitchell, M. V. Iacocca, J. Brown, B. Rabeno, C. Czerwinski, N. Petrelli, O. Dolzhansky, M. Abramov, O. Voronina, O. Potapova, J. R. Marks, W. M. Suchorska, D. Murawa, W. Kycler, M. Ibbs, K. Korski, A. Spychała, P. Murawa, J. J. Brzeziński, H. Perz, R. Łaźniak, M. Teresiak, H. Tatka, E. Leporowska, M. Bogusz-Czerniewicz, J. Malicki, A. Mackiewicz, M. Wiznerowicz, X. Van Le, B. Kohl, N. Viet Tien, R. Thorp, N. Van Bang, H. Sussman, B. Duc Phu, R. Hajek, N. Phi Hung, T. Viet The Phuong, H. Quyet Thang, K. Zaki Khan, R. Penny, D. Mallery, E. Curley, C. Shelton, P. Yena, J. N. Ingle, F. J. Couch, W. L. Lingle, T. A. King, A. Maria Gonzalez-Angulo, G. B. Mills, M. D. Dyer, S. Liu, X. Meng, M. Patangan, F. Waldman, H. Stöppler, W. Kimryn Rathmell, L. Thorne, M. Huang, L. Boice, A. Hill, C. Morrison, C. Gaudioso, W. Bshara, K. Daily, S. C. Egea, M. D. Pegram, C. Gomez-Fernandez, R. Dhir, R. Bhargava, A. Brufsky, C. D. Shriver, J. A. Hooke, J. Leigh Campbell, R. J. Mural, H. Hu, S. Somiari, C. Larson, B. Deyarmin, L. Kvecher, A. J. Kovatich, M. J. Ellis, T. A. King, H. Hu, F. J. Couch, R. J. Mural, T. Stricker, K. White, O. Olopade, J. N. Ingle, C. Luo, Y. Chen, J. R. Marks, F. Waldman, M. Wiznerowicz, R. Bose, L.-W. Chang, A. H. Beck, A. Maria Gonzalez-Angulo, T. Pihl, M. Jensen, R. Sfeir, A. Kahn, A. Chu, P. Kothiyal, Z. Wang, E. Snyder, J. Pontius, B. Ayala, M. Backus, J. Walton, J. Baboud, D. Berton, M. Nicholls, D. Srinivasan, R. Raman, S. Girshik, P. Kigonya, S. Alonso, R. Sanbhadti, S. Barletta, D. Pot, M. Sheth, J. A. Demchok, K. R. Mills Shaw, L. Yang, G. Eley, M. L. Ferguson, R. W. Tarnuzzer, J. Zhang, L. A. L. Dillon, K. Buetow, P. Fielding, B. A. Ozenberger, M. S. Guyer, H. J. Sofia, J. D. Palchik, Comprehensive molecular portraits of human breast tumours, *Nature* **490**, 61–70 (2012).

341. E. Cerami, J. Gao, U. Dogrusoz, B. E. Gross, S. O. Sumer, B. A. Aksoy, A. Jacobsen, C. J. Byrne, M. L. Heuer, E. Larsson, Y. Antipin, B. Reva, A. P. Goldberg, C. Sander, N. Schultz, The cBio Cancer Genomics Portal: An Open Platform for Exploring Multidimensional Cancer Genomics Data: Figure 1., *Cancer Discov.* **2**, 401–404 (2012).

342. J. K. Lee, J. W. Phillips, B. A. Smith, J. W. Park, T. Stoyanova, E. F. McCaffrey, R. Baertsch, A. Sokolov, J. G. Meyerowitz, C. Mathis, D. Cheng, J. M. Stuart, K. M. Shokat, W. C. Gustafson, J. Huang, O. N. Witte, N-Myc Drives Neuroendocrine Prostate Cancer Initiated from Human Prostate Epithelial Cells, *Cancer Cell* **29**, 536–547 (2016).

343. M. G. Baratta, A. C. Schinzel, Y. Zwang, P. Bandopadhayay, C. Bowman-Colin, J. Kutt, J. Curtis, H. Piao, L. C. Wong, A. L. Kung, R. Beroukhim, J. E. Bradner, R. Drapkin, W. C. Hahn, J. F. Liu, D. M. Livingston, An in-tumor genetic screen reveals that the BET bromodomain protein, BRD4, is a potential therapeutic target in ovarian carcinoma, *Proc. Natl. Acad. Sci.* **112**, 232–237 (2015).

344. A. Berger, N. J. Brady, R. Bareja, B. Robinson, V. Conteduca, M. A. Augello, L. Puca, A. Ahmed, E. Dardenne, X. Lu, I. Hwang, A. M. Bagadion, A. Sboner, O. Elemento, J.

Paik, J. Yu, C. E. Barbieri, N. Dephoure, H. Beltran, D. S. Rickman, N-Myc-mediated epigenetic reprogramming drives lineage plasticity in advanced prostate cancer., *J. Clin. Invest.* **130**, 3924–3940 (2019).

345. Y. Liu, J. Easton, Y. Shao, J. Maciaszek, Z. Wang, M. R. Wilkinson, K. McCastlain, M. Edmonson, S. B. Pounds, L. Shi, X. Zhou, X. Ma, E. Sioson, Y. Li, M. Rusch, P. Gupta, D. Pei, C. Cheng, M. A. Smith, J. G. Auvil, D. S. Gerhard, M. V Relling, N. J. Winick, A. J. Carroll, N. A. Heerema, E. Raetz, M. Devidas, C. L. Willman, R. C. Harvey, W. L. Carroll, K. P. Dunsmore, S. S. Winter, B. L. Wood, B. P. Sorrentino, J. R. Downing, M. L. Loh, S. P. Hunger, J. Zhang, C. G. Mullighan, The genomic landscape of pediatric and young adult T-lineage acute lymphoblastic leukemia, *Nat. Genet.* **49**, 1211–1218 (2017).

346. H. Beltran, The N-myc Oncogene: Maximizing its Targets, Regulation, and Therapeutic Potential, *Mol. Cancer Res.* **12**, 815–822 (2014).

347. N. Aceto, A. Bardia, D. T. Miyamoto, M. C. Donaldson, B. S. Wittner, J. A. Spencer, M. Yu, A. Pely, A. Engstrom, H. Zhu, B. W. Brannigan, R. Kapur, S. L. Stott, T. Shioda, S. Ramaswamy, D. T. Ting, C. P. Lin, M. Toner, D. A. Haber, S. Maheswaran, Circulating Tumor Cell Clusters Are Oligoclonal Precursors of Breast Cancer Metastasis, *Cell* **158**, 1110–1122 (2014).

348. C. Curtis, S. P. Shah, S. F. Chin, G. Turashvili, O. M. Rueda, M. J. Dunning, D. Speed, A. G. Lynch, S. Samarajiwa, Y. Yuan, S. Gräf, G. Ha, G. Haffari, A. Bashashati, R. Russell, S. McKinney, S. Aparicio, J. D. Brenton, I. Ellis, D. Huntsman, S. Pinder, L. Murphy, H. Bardwell, Z. Ding, L. Jones, B. Liu, I. Papatheodorou, S. J. Sammut, G. Wishart, S. Chia, K. Gelmon, C. Speers, P. Watson, R. Blamey, A. Green, D. MacMillan, E. Rakha, C. Gillett, A. Grigoriadis, E. De Rinaldis, A. Tutt, M. Parisien, S. Troup, D. Chan, C. Fielding, A. T. Maia, S. McGuire, M. Osborne, S. M. Sayalero, I. Spiteri, J. Hadfield, L. Bell, K. Chow, N. Gale, M. Kovalik, Y. Ng, L. Prentice, S. Tavaré, F. Markowetz, A. Langerød, E. Provenzano, A. Purushotham, A. L. Børresen-Dale, C. Caldas, The genomic and transcriptomic architecture of 2,000 breast tumours reveals novel subgroups, *Nature* **486**, 346–352 (2012).

349. D. S. Rickman, J. H. Schulte, M. Eilers, The Expanding World of N-MYC-Driven Tumors., *Cancer Discov.* **8**, 150–163 (2018).

350. W. Zhang, B. Liu, W. Wu, L. Li, B. M. Broom, S. P. Basourakos, D. Korentzelos, Y. Luan, J. Wang, G. Yang, S. Park, A. K. Azad, X. Cao, J. Kim, P. G. Corn, C. J. Logothetis, A. M. Aparicio, A. M. Chinnaiyan, N. Navone, P. Troncoso, T. C. Thompson, Targeting the MYCN–PARP–DNA Damage Response Pathway in Neuroendocrine Prostate Cancer, *Clin. Cancer Res.* **24**, 696–707 (2018).

351. S. Herold, J. Kalb, G. Büchel, C. P. Ade, A. Baluapuri, J. Xu, J. Koster, D. Solvie, A. Carstensen, C. Klotz, S. Rodewald, C. Schülein-Völk, M. Dobbelstein, E. Wolf, J. Molenaar, R. Versteeg, S. Walz, M. Eilers, Recruitment of BRCA1 limits MYCN-driven accumulation of stalled RNA polymerase., *Nature* **567**, 545–549 (2019).

352. J. L. Harenza, M. A. Diamond, R. N. Adams, M. M. Song, H. L. Davidson, L. S. Hart,

M. H. Dent, P. Fortina, C. P. Reynolds, J. M. Maris, Transcriptomic profiling of 39 commonly-used neuroblastoma cell lines, *Sci. Data* **4**, 170033 (2017).

353. S. Piscuoglio, C. K. Y. Ng, F. C. Geyer, K. A. Burke, C. F. Cowell, L. G. Martelotto, R. Natrajan, T. Popova, C. A. Maher, R. S. Lim, I. de Bruijn, O. Mariani, L. Norton, A. Vincent-Salomon, B. Weigelt, J. S. Reis-Filho, Genomic and transcriptomic heterogeneity in metaplastic carcinomas of the breast, *npj Breast Cancer* **3**, 48 (2017).

354. V. Guarneri, K. Broglio, S.-W. Kau, M. Cristofanilli, A. U. Buzdar, V. Valero, T. Buchholz, F. Meric, L. Middleton, G. N. Hortobagyi, A. M. Gonzalez-Angulo, Prognostic value of pathologic complete response after primary chemotherapy in relation to hormone receptor status and other factors., *J. Clin. Oncol.* **24**, 1037–44 (2006).

355. C. Liedtke, C. Mazouni, K. R. Hess, F. André, A. Tordai, J. A. Mejia, W. F. Symmans, A. M. Gonzalez-Angulo, B. Hennessy, M. Green, M. Cristofanilli, G. N. Hortobagyi, L. Pusztai, Response to neoadjuvant therapy and long-term survival in patients with triple-negative breast cancer., *J. Clin. Oncol.* **26**, 1275–81 (2008).

356. J. M. Balko, R. S. Cook, D. B. Vaught, M. G. Kuba, T. W. Miller, N. E. Bhola, M. E. Sanders, N. M. Granja-Ingram, J. J. Smith, I. M. Meszoely, J. Salter, M. Dowsett, K. Stemke-Hale, A. M. González-Angulo, G. B. Mills, J. A. Pinto, H. L. Gómez, C. L. Arteaga, Profiling of residual breast cancers after neoadjuvant chemotherapy identifies DUSP4 deficiency as a mechanism of drug resistance., *Nat. Med.* **18**, 1052–9 (2012).

357. R. Gao, C. Kim, E. Sei, T. Foukakis, N. Crosetto, L.-K. Chan, M. Srinivasan, H. Zhang, F. Meric-Bernstam, N. Navin, Nanogrid single-nucleus RNA sequencing reveals phenotypic diversity in breast cancer, *Nat. Commun.* **8**, 228 (2017).

358. P. J. Hurlin, Control of vertebrate development by MYC., *Cold Spring Harb. Perspect. Med.* **3**, a014332 (2013).

359. J. Barretina, G. Caponigro, N. Stransky, K. Venkatesan, A. A. Margolin, S. Kim, C. J. Wilson, J. Lehár, G. V. Kryukov, D. Sonkin, A. Reddy, M. Liu, L. Murray, M. F. Berger, J. E. Monahan, P. Morais, J. Meltzer, A. Korejwa, J. Jané-Valbuena, F. A. Mapa, J. Thibault, E. Bric-Furlong, P. Raman, A. Shipway, I. H. Engels, J. Cheng, G. K. Yu, J. Yu, P. Aspesi, M. de Silva, K. Jagtap, M. D. Jones, L. Wang, C. Hatton, E. Palescandolo, S. Gupta, S. Mahan, C. Sougnez, R. C. Onofrio, T. Liefeld, L. MacConaill, W. Winckler, M. Reich, N. Li, J. P. Mesirov, S. B. Gabriel, G. Getz, K. Ardlie, V. Chan, V. E. Myer, B. L. Weber, J. Porter, M. Warmuth, P. Finan, J. L. Harris, M. Meyerson, T. R. Golub, M. P. Morrissey, W. R. Sellers, R. Schlegel, L. A. Garraway, The Cancer Cell Line Encyclopedia enables predictive modelling of anticancer drug sensitivity, *Nature* **483**, 603–607 (2012).

360. J. Gioanni, D. Le François, C. Mazeau, F. Ettore, J. C. Lambert, B. Dutrillaux, Establishment and characterisation of a new tumorigenic cell line with a normal karyotype derived from a human breast adenocarcinoma, *Br. J. Cancer* **62**, 8–13 (1990).

361. K. J. Chavez, S. V Garimella, S. Lipkowitz, Triple negative breast cancer cell lines: one tool in the search for better treatment of triple negative breast cancer., *Breast Dis.*

32, 35–48 (2010).

362. B. D. Lehmann, J. A. Bauer, J. M. Schafer, C. S. Pendleton, L. Tang, K. C. Johnson, X. Chen, J. M. Balko, H. Gómez, C. L. Arteaga, G. B. Mills, M. E. Sanders, J. A. Pietenpol, PIK3CA mutations in androgen receptor-positive triple negative breast cancer confer sensitivity to the combination of PI3K and androgen receptor inhibitors., *Breast Cancer Res.* **16**, 406 (2014).

363. S. J. Klempner, A. P. Myers, L. C. Cantley, What a tangled web we weave: emerging resistance mechanisms to inhibition of the phosphoinositide 3-kinase pathway., *Cancer Discov.* **3**, 1345–54 (2013).

364. A. H. Davies, H. Beltran, A. Zoubeidi, Cellular plasticity and the neuroendocrine phenotype in prostate cancer, *Nat. Rev. Urol.* **15**, 271–286 (2018).

365. M. Kirby, C. Hirst, E. D. Crawford, Characterising the castration-resistant prostate cancer population: a systematic review, *Int. J. Clin. Pract.* **65**, 1180–1192 (2011).

366. A. H. Davies, H. Beltran, A. Zoubeidi, Cellular plasticity and the neuroendocrine phenotype in prostate cancer, *Nat. Rev. Urol.* **15**, 271–286 (2018).

367. J. E. Delmore, G. C. Issa, M. E. Lemieux, P. B. Rahl, J. Shi, H. M. Jacobs, E. Kastritis, T. Gilpatrick, R. M. Paranal, J. Qi, M. Chesi, A. C. Schinzel, M. R. McKeown, T. P. Heffernan, C. R. Vakoc, P. L. Bergsagel, I. M. Ghobrial, P. G. Richardson, R. A. Young, W. C. Hahn, K. C. Anderson, A. L. Kung, J. E. Bradner, C. S. Mitsiades, BET bromodomain inhibition as a therapeutic strategy to target c-Myc., *Cell* **146**, 904–17 (2011).

368. D. Horiuchi, R. Camarda, A. Y. Zhou, C. Yau, O. Momcilovic, S. Balakrishnan, A. N. Corella, H. Eyob, K. Kessenbrock, D. A. Lawson, L. A. Marsh, B. N. Anderton, J. Rohrberg, R. Kunder, A. V Bazarov, P. Yaswen, M. T. McManus, H. S. Rugo, Z. Werb, A. Goga, PIM1 kinase inhibition as a targeted therapy against triple-negative breast tumors with elevated MYC expression, *Nat. Med.* **22**, 1321–1329 (2016).

369. R. Sears, G. Leone, J. DeGregori, J. R. Nevins, Ras Enhances Myc Protein Stability, *Mol. Cell* **3**, 169–179 (1999).

370. D. Dauch, R. Rudalska, G. Cossa, J.-C. Nault, T.-W. Kang, T. Wuestefeld, A. Hohmeyer, S. Imbeaud, T. Yevsa, L. Hoenicke, T. Pantsar, P. Bozko, N. P. Malek, T. Longerich, S. Laufer, A. Poso, J. Zucman-Rossi, M. Eilers, L. Zender, A MYC–aurora kinase A protein complex represents an actionable drug target in p53-altered liver cancer, *Nat. Med.* **22**, 744–753 (2016).

371. M. C. Stubbs, T. C. Burn, R. Sparks, T. Maduskuie, S. Diamond, M. Rupar, X. Wen, A. Volgina, N. Zolotarjova, P. Waeltz, M. Favata, R. Jalluri, H. Liu, X. M. Liu, J. Li, R. Collins, N. Falahatpisheh, P. Polam, D. DiMatteo, P. Feldman, V. Dostalik, P. Thekkat, C. Gardiner, X. He, Y. Li, M. Covington, R. Wynn, B. Ruggeri, S. Yeleswaram, C.-B. Xue, W. Yao, A. P. Combs, R. Huber, G. Hollis, P. Scherle, P. C. C. Liu, The Novel Bromodomain

and Extraterminal Domain Inhibitor INCB054329 Induces Vulnerabilities in Myeloma Cells That Inform Rational Combination Strategies, *Clin. Cancer Res.* , 1–13 (2018).

372. M. Boi, E. Gaudio, P. Bonetti, I. Kwee, E. Bernasconi, C. Tarantelli, A. Rinaldi, M. Testoni, L. Cascione, M. Ponzoni, A. A. Mensah, A. Stathis, G. Stussi, M. E. Riveiro, P. Herait, G. Inghirami, E. Cvitkovic, E. Zucca, F. Bertoni, The BET bromodomain inhibitor OTX015 affects pathogenetic pathways in preclinical B-cell tumor models and synergizes with targeted drugs, *Clin. Cancer Res.* **21**, 1628–1638 (2015).

373. A. Stathis, F. Bertoni, BET Proteins as Targets for Anticancer Treatment., *Cancer Discov.* **8**, 24–36 (2018).

374. S. Shu, C. Y. Lin, H. H. He, R. M. Witwicki, D. P. Tabassum, J. M. Roberts, M. Janiszewska, S. J. Huh, Y. Liang, J. Ryan, E. Doherty, H. Mohammed, H. Guo, D. G. Stover, M. B. Ekram, J. Brown, C. D'Santos, I. E. Krop, D. Dillon, M. McKeown, C. Ott, J. Qi, M. Ni, P. K. Rao, M. Duarte, S.-Y. Wu, C.-M. Chiang, L. Anders, R. A. Young, E. Winer, A. Letai, W. T. Barry, J. S. Carroll, H. Long, M. Brown, X. S. Liu, C. A. Meyer, J. E. Bradner, K. Polyak, K. Polyak, Response and resistance to BET bromodomain inhibitors in triple-negative breast cancer., *Nature* **529**, 413–417 (2016).

375. R. C. Sears, The life cycle of C-myc: from synthesis to degradation., *Cell Cycle* **3**, 1133–7 (2004).

376. T. F. Eleveld, D. A. Oldridge, V. Bernard, J. Koster, L. C. Daage, S. J. Diskin, L. Schild, N. B. Bentahar, A. Bellini, M. Chicard, E. Lapouble, V. Combaret, P. Legoix-Né, J. Michon, T. J. Pugh, L. S. Hart, J. Rader, E. F. Attiyeh, J. S. Wei, S. Zhang, A. Naranjo, J. M. Gastier-Foster, M. D. Hogarty, S. Asgharzadeh, M. A. Smith, J. M. Guidry Auvil, T. B. K. Watkins, D. A. Zwijnenburg, M. E. Ebus, P. van Sluis, A. Hakkert, E. van Wezel, C. E. van der Schoot, E. M. Westerhout, J. H. Schulte, G. A. Tytgat, M. E. M. Dolman, I. Janoueix-Lerosey, D. S. Gerhard, H. N. Caron, O. Delattre, J. Khan, R. Versteeg, G. Schleiermacher, J. J. Molenaar, J. M. Maris, Relapsed neuroblastomas show frequent RAS-MAPK pathway mutations, *Nat. Genet.* **47**, 864–871 (2015).

377. L. S. Hart, J. Rader, P. Raman, V. Batra, M. R. Russell, M. Tsang, M. Gagliardi, L. Chen, D. Martinez, Y. Li, A. Wood, S. Kim, S. Parasuraman, S. Delach, K. A. Cole, S. Krupa, M. Boehm, M. Peters, G. Caponigro, J. M. Maris, Preclinical Therapeutic Synergy of MEK1/2 and CDK4/6 Inhibition in Neuroblastoma., *Clin. Cancer Res.* **23**, 1785–1796 (2017).

378. H. Kim, P. Kumar, F. Menghi, J. Noorbakhsh, E. Cerveira, M. Ryan, Q. Zhu, G. Ananda, J. George, H. C. Chen, S. Mockus, C. Zhang, Y. Yang, J. Keck, R. K. M. Karuturi, C. J. Bult, C. Lee, E. T. Liu, J. H. Chuang, High-resolution deconstruction of evolution induced by chemotherapy treatments in breast cancer xenografts., *Sci. Rep.* **8**, 17937 (2018).

379. D. R. Robinson, Y. M. Wu, R. J. Lonigro, P. Vats, E. Cobain, J. Everett, X. Cao, E. Rabban, C. Kumar-Sinha, V. Raymond, S. Schuetze, A. Alva, J. Siddiqui, R. Chugh, F. Worden, M. M. Zalupski, J. Innis, R. J. Mody, S. A. Tomlins, D. Lucas, L. H. Baker, N.

Ramnath, A. F. Schott, D. F. Hayes, J. Vijai, K. Offit, E. M. Stoffel, J. S. Roberts, D. C. Smith, L. P. Kunju, M. Talpaz, M. Cieślik, A. M. Chinnaiyan, Integrative clinical genomics of metastatic cancer, *Nature* **548**, 297–303 (2017).

380. G. S. Falchook, S. Rosen, P. M. LoRusso, J. M. Watts, S. Gupta, C. C. Coombs, M. Talpaz, R. Kurzrock, M. M. Mita, R. D. Cassaday, W. Harb, J. A. Peguero, D. C. Smith, S. A. Piha-Paul, R. Z. Szmulewitz, M. S. Noel, S. Yeleswaram, P. Liu, J. Switzky, G. Zhou, F. Zheng, A. N. Mehta, Development of 2 Bromodomain and Extraterminal Inhibitors With Distinct Pharmacokinetic and Pharmacodynamic Profiles for the Treatment of Advanced Malignancies, *Clin. Cancer Res.* , clincanres.4071.2018 (2019).

381. B. King, F. Boccalatte, K. Moran-Crusio, E. Wolf, J. Wang, C. Kayembe, C. Lazaris, X. Yu, B. Aranda-Orgilles, A. Lasorella, I. Aifantis, The ubiquitin ligase Huwe1 regulates the maintenance and lymphoid commitment of hematopoietic stem cells., *Nat. Immunol.* **17**, 1312–1321 (2016).

382. B. Chapuy, M. R. McKeown, C. Y. Lin, S. Monti, M. G. M. Roemer, J. Qi, P. B. Rahl, H. H. Sun, K. T. Yeda, J. G. Doench, E. Reichert, A. L. Kung, S. J. Rodig, R. A. Young, M. A. Shipp, J. E. Bradner, Discovery and characterization of super-enhancer-associated dependencies in diffuse large B cell lymphoma., *Cancer Cell* **24**, 777–90 (2013).

383. J. Lovén, H. A. Hoke, C. Y. Lin, A. Lau, D. A. Orlando, C. R. Vakoc, J. E. Bradner, T. I. Lee, R. A. Young, Selective Inhibition of Tumor Oncogenes by Disruption of Super-Enhancers, *Cell* **153**, 320–334 (2013).

384. P. Bandopadhayay, G. Bergthold, B. Nguyen, S. Schubert, S. Gholamin, Y. Tang, S. Bolin, S. E. Schumacher, R. Zeid, S. Masoud, F. Yu, N. Vue, W. J. Gibson, B. R. Paolella, S. S. Mitra, S. H. Cheshier, J. Qi, K.-W. Liu, R. Wechsler-Reya, W. A. Weiss, F. J. Swartling, M. W. Kieran, J. E. Bradner, R. Beroukhim, Y.-J. Cho, BET Bromodomain Inhibition of MYC-Amplified Medulloblastoma, *Clin. Cancer Res.* **20**, 912–925 (2014).

385. P. Sin-Chan, I. Mumal, T. Suwal, B. Ho, X. Fan, I. Singh, Y. Du, M. Lu, N. Patel, J. Torchia, D. Popovski, M. Fouladi, P. Guilhamon, J. R. Hansford, S. Leary, L. M. Hoffman, J. M. Mulcahy Levy, A. Lassaletta, P. Solano-Paez, E. Rivas, A. Reddy, G. Y. Gillespie, N. Gupta, T. E. Van Meter, H. Nakamura, T.-T. Wong, Y.-S. Ra, S.-K. Kim, L. Massimi, R. G. Grundy, J. Fangusaro, D. Johnston, J. Chan, L. Lafay-Cousin, E. I. Hwang, Y. Wang, D. Catchpoole, J. Michaud, B. Ellezam, R. Ramanujachar, H. Lindsay, M. D. Taylor, C. E. Hawkins, E. Bouffet, N. Jabado, S. K. Singh, C. L. Kleinman, D. Barsyte-Lovejoy, X.-N. Li, P. B. Dirks, C. Y. Lin, S. C. Mack, J. N. Rich, A. Huang, A C19MC-LIN28A-MYCN Oncogenic Circuit Driven by Hijacked Super-enhancers Is a Distinct Therapeutic Vulnerability in ETMRs: A Lethal Brain Tumor., *Cancer Cell* **36**, 51-67.e7 (2019).

386. B. E. Gryder, M. E. Yohe, H.-C. Chou, X. Zhang, J. Marques, M. Wachtel, B. Schaefer, N. Sen, Y. Song, A. Gualtieri, S. Pomella, R. Rota, A. Cleveland, X. Wen, S. Sindiri, J. S. Wei, F. G. Barr, S. Das, T. Andresson, R. Guha, M. Lal-Nag, M. Ferrer, J. F. Shern, K. Zhao, C. J. Thomas, J. Khan, PAX3-FOXO1 Establishes Myogenic Super Enhancers and Confers BET Bromodomain Vulnerability., *Cancer Discov.* **7**, 884–899

(2017).

387. A. G. Cochran, A. R. Conery, R. J. Sims, Bromodomains: a new target class for drug development, *Nat. Rev. Drug Discov.* **18**, 609–628 (2019).

388. A. Wyce, J. J. Matteo, S. W. Foley, D. J. Felitsky, S. R. Rajapurkar, X.-P. Zhang, M. C. Musso, S. Korenchuk, N. O. Karpinich, K. M. Keenan, M. Stern, L. K. Mathew, C. F. McHugh, M. T. McCabe, P. J. Tummino, R. G. Kruger, C. Carpenter, O. Barbash, MEK inhibitors overcome resistance to BET inhibition across a number of solid and hematologic cancers., *Oncogenesis* **7**, 35 (2018).

389. J. S. Zawistowski, S. M. Bevill, D. R. Goulet, T. J. Stuhlmiller, A. S. Beltran, J. F. Olivares-Quintero, D. Singh, N. Sciaky, J. S. Parker, N. U. Rashid, X. Chen, J. S. Duncan, M. C. Whittle, S. P. Angus, S. H. Velarde, B. T. Golitz, X. He, C. Santos, D. B. Darr, K. Gallagher, L. M. Graves, C. M. Perou, L. A. Carey, H. S. Earp, G. L. Johnson, Enhancer Remodeling during Adaptive Bypass to MEK Inhibition Is Attenuated by Pharmacologic Targeting of the P-TEFb Complex., *Cancer Discov.* **7**, 302–321 (2017).

390. M. K. Muellner, I. Z. Uras, B. V Gapp, C. Kerzendorfer, M. Smida, H. Lechtermann, N. Craig-Mueller, J. Colinge, G. Duernberger, S. M. B. Nijman, A chemical-genetic screen reveals a mechanism of resistance to PI3K inhibitors in cancer, *Nat. Chem. Biol.* **7**, 787–793 (2011).

391. N. Dey, B. Leyland-Jones, P. De, MYC-xing it up with PIK3CA mutation and resistance to PI3K inhibitors: summit of two giants in breast cancers., *Am. J. Cancer Res.* **5**, 1–19 (2015).

392. G. Mollaoglu, M. R. Guthrie, S. Böhm, J. Brägelmann, I. Can, P. M. Ballieu, A. Marx, J. George, C. Heinen, M. D. Chalishazar, H. Cheng, A. S. Ireland, K. E. Denning, A. Mukhopadhyay, J. M. Vahrenkamp, K. C. Berrett, T. L. Mosbruger, J. Wang, J. L. Kohan, M. E. Salama, B. L. Witt, M. Peifer, R. K. Thomas, J. Gertz, J. E. Johnson, A. F. Gazdar, R. J. Wechsler-Reya, M. L. Sos, T. G. Oliver, MYC Drives Progression of Small Cell Lung Cancer to a Variant Neuroendocrine Subtype with Vulnerability to Aurora Kinase Inhibition., *Cancer Cell* **31**, 270–285 (2017).

393. A. S. Dhillon, S. Hagan, O. Rath, W. Kolch, MAP kinase signalling pathways in cancer., *Oncogene* **26**, 3279–90 (2007).

394. T. J. Pugh, O. Morozova, E. F. Attiyeh, S. Asgharzadeh, J. S. Wei, D. Auclair, S. L. Carter, K. Cibulskis, M. Hanna, A. Kiezun, J. Kim, M. S. Lawrence, L. Lichenstein, A. Mckenna, C. S. Pedamallu, A. H. Ramos, E. Shefler, A. Sivachenko, C. Sougnez, C. Stewart, A. Ally, I. Birol, R. Chiu, R. D. Corbett, M. Hirst, S. D. Jackman, B. Kamoh, A. H. Khodabakshi, M. Krzywinski, A. Lo, R. A. Moore, K. L. Mungall, J. Qian, A. Tam, N. Thiessen, Y. Zhao, K. A. Cole, M. Diamond, S. J. Diskin, Y. P. Mosse, A. C. Wood, L. Ji, R. Sposto, T. Badgett, W. B. London, Y. Moyer, J. M. Gastier-Foster, M. A. Smith, J. M. G. Auvil, D. S. Gerhard, M. D. Hogarty, S. J. M. Jones, E. S. Lander, S. B. Gabriel, G. Getz, R. C. Seeger, J. Khan, M. A. Marra, M. Meyerson, J. M. Maris, The genetic landscape of high-risk neuroblastoma, *Nat. Genet.* (2013), doi:10.1038/ng.2529.

395. M. Yu, A. Bardia, N. Aceto, F. Bersani, M. W. Madden, M. C. Donaldson, R. Desai, H. Zhu, V. Comaills, Z. Zheng, B. S. Wittner, P. Stojanov, E. Brachtel, D. Sgroi, R. Kapur, T. Shioda, D. T. Ting, S. Ramaswamy, G. Getz, A. J. Iafrate, C. Benes, M. Toner, S. Maheswaran, D. A. Haber, Ex vivo culture of circulating breast tumor cells for individualized testing of drug susceptibility, *Science (80-.).* **345**, 216–220 (2014).

396. R. Zeid, M. A. Lawlor, E. Poon, J. M. Reyes, M. Fulciniti, M. A. Lopez, T. G. Scott, B. Nabet, M. A. Erb, G. E. Winter, Z. Jacobson, D. R. Polaski, K. L. Karlin, R. A. Hirsch, N. P. Munshi, T. F. Westbrook, L. Chesler, C. Y. Lin, J. E. Bradner, Enhancer invasion shapes MYCN-dependent transcriptional amplification in neuroblastoma., *Nat. Genet.* **50**, 515–523 (2018).

397. J. Shi, C. R. Vakoc, The mechanisms behind the therapeutic activity of BET bromodomain inhibition., *Mol. Cell* **54**, 728–36 (2014).

398. M. Berdasco, M. Esteller, DNA methylation in stem cell renewal and multipotency., *Stem Cell Res. Ther.* **2**, 42 (2011).

399. F. X. Schaub, V. Dhankani, A. C. Berger, M. Trivedi, A. B. Richardson, R. Shaw, W. Zhao, X. Zhang, A. Ventura, Y. Liu, D. E. Ayer, P. J. Hurlin, A. D. Cherniack, R. N. Eisenman, B. Bernard, C. Grandori, S. J. Caesar-Johnson, J. A. Demchok, I. Felau, M. Kasapi, M. L. Ferguson, C. M. Hutter, H. J. Sofia, R. Tarnuzzer, Z. Wang, L. Yang, J. C. Zenklusen, J. (Julia) Zhang, S. Chudamani, J. Liu, L. Lolla, R. Naresh, T. Pihl, Q. Sun, Y. Wan, Y. Wu, J. Cho, T. DeFreitas, S. Frazer, N. Gehlenborg, G. Getz, D. I. Heiman, J. Kim, M. S. Lawrence, P. Lin, S. Meier, M. S. Noble, G. Saksena, D. Voet, H. Zhang, B. Bernard, N. Chambwe, V. Dhankani, T. Knijnenburg, R. Kramer, K. Leinonen, Y. Liu, M. Miller, S. Reynolds, I. Shmulevich, V. Thorsson, W. Zhang, R. Akbani, B. M. Broom, A. M. Hegde, Z. Ju, R. S. Kanchi, A. Korkut, J. Li, H. Liang, S. Ling, W. Liu, Y. Lu, G. B. Mills, K.-S. Ng, A. Rao, M. Ryan, J. Wang, J. N. Weinstein, J. Zhang, A. Abeshouse, J. Armenia, D. Chakravarty, W. K. Chatila, I. de Bruijn, J. Gao, B. E. Gross, Z. J. Heins, R. Kundra, K. La, M. Ladanyi, A. Luna, M. G. Nissan, A. Ochoa, S. M. Phillips, E. Reznik, F. Sanchez-Vega, C. Sander, N. Schultz, R. Sheridan, S. O. Sumer, Y. Sun, B. S. Taylor, J. Wang, H. Zhang, P. Anur, M. Peto, P. Spellman, C. Benz, J. M. Stuart, C. K. Wong, C. Yau, D. N. Hayes, J. S. Parker, M. D. Wilkerson, A. Ally, M. Balasundaram, R. Bowlby, D. Brooks, R. Carlsen, E. Chuah, N. Dhalla, R. Holt, S. J. M. Jones, K. Kasaian, D. Lee, Y. Ma, M. A. Marra, M. Mayo, R. A. Moore, A. J. Mungall, K. Mungall, A. G. Robertson, S. Sadeghi, J. E. Schein, P. Sipahimalani, A. Tam, N. Thiessen, K. Tse, T. Wong, A. C. Berger, R. Beroukhim, A. D. Cherniack, C. Cibulskis, S. B. Gabriel, G. F. Gao, G. Ha, M. Meyerson, S. E. Schumacher, J. Shih, M. H. Kucherlapati, R. S. Kucherlapati, S. Baylin, L. Cope, L. Danilova, M. S. Bootwalla, P. H. Lai, D. T. Maglinte, D. J. Van Den Berg, D. J. Weisenberger, J. T. Auman, S. Balu, T. Bodenheimer, C. Fan, K. A. Hoadley, A. P. Hoyle, S. R. Jefferys, C. D. Jones, S. Meng, P. A. Mieczkowski, L. E. Mose, A. H. Perou, C. M. Perou, J. Roach, Y. Shi, J. V. Simons, T. Skelly, M. G. Soloway, D. Tan, U. Veluvolu, H. Fan, T. Hinoue, P. W. Laird, H. Shen, W. Zhou, M. Bellair, K. Chang, K. Covington, C. J. Creighton, H. Dinh, H. Doddapaneni, L. A. Donehower, J. Drummond, R. A. Gibbs, R. Glenn, W. Hale, Y. Han, J. Hu, V. Korchina, S. Lee, L. Lewis, W. Li, X. Liu, M. Morgan, D. Morton, D. Muzny, J. Santibanez, M. Sheth, E. Shinbrot, L. Wang, M. Wang, D. A.

Wheeler, L. Xi, F. Zhao, J. Hess, E. L. Appelbaum, M. Bailey, M. G. Cordes, L. Ding, C. C. Fronick, L. A. Fulton, R. S. Fulton, C. Kandoth, E. R. Mardis, M. D. McLellan, C. A. Miller, H. K. Schmidt, R. K. Wilson, D. Crain, E. Curley, J. Gardner, K. Lau, D. Mallery, S. Morris, J. Paulauskis, R. Penny, C. Shelton, T. Shelton, M. Sherman, E. Thompson, P. Yena, J. Bowen, J. M. Gastier-Foster, M. Gerken, K. M. Leraas, T. M. Lichtenberg, N. C. Ramirez, L. Wise, E. Zmuda, N. Corcoran, T. Costello, C. Hovens, A. L. Carvalho, A. C. de Carvalho, J. H. Fregnani, A. Longatto-Filho, R. M. Reis, C. Scapulatempo-Neto, H. C. S. Silveira, D. O. Vidal, A. Burnette, J. Eschbacher, B. Hermes, A. Noss, R. Singh, M. L. Anderson, P. D. Castro, M. Ittmann, D. Huntsman, B. Kohl, X. Le, R. Thorp, C. Andry, E. R. Duffy, V. Lyadov, O. Paklina, G. Setdikova, A. Shabunin, M. Tavobilov, C. McPherson, R. Warnick, R. Berkowitz, D. Cramer, C. Feltmate, N. Horowitz, A. Kibel, M. Muto, C. P. Raut, A. Malykh, J. S. Barnholtz-Sloan, W. Barrett, K. Devine, J. Fulop, Q. T. Ostrom, K. Shimmel, Y. Wolinsky, A. E. Sloan, A. De Rose, F. Giuliante, M. Goodman, B. Y. Karlan, C. H. Hagedorn, J. Eckman, J. Harr, J. Myers, K. Tucker, L. A. Zach, B. Deyarmin, H. Hu, L. Kvecher, C. Larson, R. J. Mural, S. Somiari, A. Vicha, T. Zelinka, J. Bennett, M. Iacocca, B. Rabeno, P. Swanson, M. Latour, L. Lacombe, B. Têtu, A. Bergeron, M. McGraw, S. M. Staugaitis, J. Chabot, H. Hibshoosh, A. Sepulveda, T. Su, T. Wang, O. Potapova, O. Voronina, L. Desjardins, O. Mariani, S. Roman-Roman, X. Sastre, M.-H. Stern, F. Cheng, S. Signoretti, A. Berchuck, D. Bigner, E. Lipp, J. Marks, S. McCall, R. McLendon, A. Secord, A. Sharp, M. Behera, D. J. Brat, A. Chen, K. Delman, S. Force, F. Khuri, K. Magliocca, S. Maithel, J. J. Olson, T. Owonikoko, A. Pickens, S. Ramalingam, D. M. Shin, G. Sica, E. G. Van Meir, H. Zhang, W. Eijckenboom, A. Gillis, E. Korpershoek, L. Looijenga, W. Oosterhuis, H. Stoop, K. E. van Kessel, E. C. Zwarthoff, C. Calatozzolo, L. Cuppini, S. Cuzzubbo, F. DiMeco, G. Finocchiaro, L. Mattei, A. Perin, B. Pollo, C. Chen, J. Houck, P. Lohavanichbutr, A. Hartmann, C. Stoehr, R. Stoehr, H. Taubert, S. Wach, B. Wullich, W. Kycler, D. Murawa, M. Wiznerowicz, K. Chung, W. J. Edenfield, J. Martin, E. Baudin, G. Bubley, R. Bueno, A. De Rienzo, W. G. Richards, S. Kalkanis, T. Mikkelsen, H. Noushmehr, L. Scarpace, N. Girard, M. Aymerich, E. Campo, E. Giné, A. L. Guillermo, N. Van Bang, P. T. Hanh, B. D. Phu, Y. Tang, H. Colman, K. Evason, P. R. Dottino, J. A. Martignetti, H. Gabra, H. Juhl, T. Akeredolu, S. Stepa, D. Hoon, K. Ahn, K. J. Kang, F. Beuschlein, A. Breggia, M. Birrer, D. Bell, M. Borad, A. H. Bryce, E. Castle, V. Chandan, J. Cheville, J. A. Copland, M. Farnell, T. Flotte, N. Giama, T. Ho, M. Kendrick, J.-P. Kocher, K. Kopp, C. Moser, D. Nagorney, D. O'Brien, B. P. O'Neill, T. Patel, G. Petersen, F. Que, M. Rivera, L. Roberts, R. Smallridge, T. Smyrk, M. Stanton, R. H. Thompson, M. Torbenson, J. D. Yang, L. Zhang, F. Brimo, J. A. Ajani, A. M. Angulo Gonzalez, C. Behrens, J. Bondaruk, R. Broaddus, B. Czerniak, B. Esmaeli, J. Fujimoto, J. Gershenwald, C. Guo, A. J. Lazar, C. Logothetis, F. Meric-Bernstam, C. Moran, L. Ramondetta, D. Rice, A. Sood, P. Tamboli, T. Thompson, P. Troncoso, A. Tsao, I. Wistuba, C. Carter, L. Haydu, P. Hersey, V. Jakrot, H. Kakavand, R. Kefford, K. Lee, G. Long, G. Mann, M. Quinn, R. Saw, R. Scolyer, K. Shannon, A. Spillane, J. Stretch, M. Synott, J. Thompson, J. Wilmott, H. Al-Ahmadie, T. A. Chan, R. Ghossein, A. Gopalan, D. A. Levine, V. Reuter, S. Singer, B. Singh, N. V. Tien, T. Broudy, C. Mirsaidi, P. Nair, P. Drwiega, J. Miller, J. Smith, H. Zaren, J.-W. Park, N. P. Hung, E. Kebebew, W. M. Linehan, A. R. Metwalli, K. Pacak, P. A. Pinto, M. Schiffman, L. S. Schmidt, C. D. Vocke, N. Wentzensen, R. Worrell, H. Yang, M. Moncrieff, C. Goparaju, J. Melamed, H. Pass, N. Botnariuc, I. Caraman, M. Cernat, I. Chemencedji, A. Clipca, S. Doruc, G. Gorincioi, S. Mura, M. Pirtac, I. Stancul, D. Tcaciuc,

M. Albert, I. Alexopoulou, A. Arnaout, J. Bartlett, J. Engel, S. Gilbert, J. Parfitt, H. Sekhon, G. Thomas, D. M. Rassl, R. C. Rintoul, C. Bifulco, R. Tamakawa, W. Urba, N. Hayward, H. Timmers, A. Antenucci, F. Facciolo, G. Grazi, M. Marino, R. Merola, R. de Krijger, A.-P. Gimenez-Roqueplo, A. Piché, S. Chevalier, G. McKercher, K. Birsoy, G. Barnett, C. Brewer, C. Farver, T. Naska, N. A. Pennell, D. Raymond, C. Schilero, K. Smolenski, F. Williams, C. Morrison, J. A. Borgia, M. J. Liptay, M. Pool, C. W. Seder, K. Junker, L. Omberg, M. Dinkin, G. Manikhas, D. Alvaro, M. C. Bragazzi, V. Cardinale, G. Carpino, E. Gaudio, D. Chesla, S. Cottingham, M. Dubina, F. Moiseenko, R. Dhanasekaran, K.-F. Becker, K.-P. Janssen, J. Slotta-Huspenina, M. H. Abdel-Rahman, D. Aziz, S. Bell, C. M. Cebulla, A. Davis, R. Duell, J. B. Elder, J. Hilty, B. Kumar, J. Lang, N. L. Lehman, R. Mandt, P. Nguyen, R. Pilarski, K. Rai, L. Schoenfield, K. Senecal, P. Wakely, P. Hansen, R. Lechan, J. Powers, A. Tischler, W. E. Grizzle, K. C. Sexton, A. Kastl, J. Henderson, S. Porten, J. Waldmann, M. Fassnacht, S. L. Asa, D. Schadendorf, M. Couce, M. Graefen, H. Huland, G. Sauter, T. Schlomm, R. Simon, P. Tennstedt, O. Olabode, M. Nelson, O. Bathe, P. R. Carroll, J. M. Chan, P. Disaia, P. Glenn, R. K. Kelley, C. N. Landen, J. Phillips, M. Prados, J. Simko, K. Smith-McCune, S. VandenBerg, K. Roggin, A. Fehrenbach, A. Kendler, S. Sifri, R. Steele, A. Jimeno, F. Carey, I. Forgie, M. Mannelli, M. Carney, B. Hernandez, B. Campos, C. Herold-Mende, C. Jungk, A. Unterberg, A. von Deimling, A. Bossler, J. Galbraith, L. Jacobus, M. Knudson, T. Knutson, D. Ma, M. Milhem, R. Sigmund, A. K. Godwin, R. Madan, H. G. Rosenthal, C. Adebamowo, S. N. Adebamowo, A. Boussioutas, D. Beer, T. Giordano, A.-M. Mes-Masson, F. Saad, T. Bocklage, L. Landrum, R. Mannel, K. Moore, K. Moxley, R. Postier, J. Walker, R. Zuna, M. Feldman, F. Valdivieso, R. Dhir, J. Luketich, E. M. Mora Pinero, M. Quintero-Aguilo, C. G. Carlotti, J. S. Dos Santos, R. Kemp, A. Sankarankuty, D. Tirapelli, J. Catto, K. Agnew, E. Swisher, J. Creaney, B. Robinson, C. S. Shelley, E. M. Godwin, S. Kendall, C. Shipman, C. Bradford, T. Carey, A. Haddad, J. Moyer, L. Peterson, M. Prince, L. Rozek, G. Wolf, R. Bowman, K. M. Fong, I. Yang, R. Korst, W. K. Rathmell, J. L. Fantacone-Campbell, J. A. Hooke, A. J. Kovatich, C. D. Shriver, J. DiPersio, B. Drake, R. Govindan, S. Heath, T. Ley, B. Van Tine, P. Westervelt, M. A. Rubin, J. Il Lee, N. D. Aredes, A. Mariamidze, Pan-cancer Alterations of the MYC Oncogene and Its Proximal Network across the Cancer Genome Atlas, *Cell Syst.* **6**, 282-300.e2 (2018).

400. S. H. Wright, Generation of resting membrane potential, *Adv. Physiol. Educ.* **28**, 139–142 (2004).

401. M. Lobikin, B. Chernet, D. Lobo, M. Levin, Resting potential, oncogene-induced tumorigenesis, and metastasis: the bioelectric basis of cancer in vivo., *Phys. Biol.* **9**, 065002 (2012).

402. C. Wei, X. Wang, M. Zheng, H. Cheng, Calcium gradients underlying cell migration., *Curr. Opin. Cell Biol.* **24**, 254–61 (2012).

403. D. E. Clapham, Calcium Signaling, *Cell* **131**, 1047–1058 (2007).

404. C. L. So, J. M. Saunus, S. J. Roberts-Thomson, G. R. Monteith, Calcium signalling and breast cancer, *Semin. Cell Dev. Biol.* **94**, 74–83 (2019).

405. G. R. Monteith, N. Prevarskaya, S. J. Roberts-Thomson, The calcium-cancer signalling nexus., *Nat. Rev. Cancer* **17**, 367–380 (2017).

406. G. R. Monteith, D. McAndrew, H. M. Faddy, S. J. Roberts-Thomson, Calcium and cancer: targeting Ca2+ transport, *Nat. Rev. Cancer* **7**, 519–530 (2007).

407. F. Martin, C. Ufodiama, I. Watt, M. Bland, W. J. Brackenbury, Therapeutic Value of Voltage-Gated Sodium Channel Inhibitors in Breast, Colorectal, and Prostate Cancer: A Systematic Review., *Front. Pharmacol.* **6**, 273 (2015).

408. B. Gusterson, C. J. Eaves, Basal-like breast cancers: from pathology to biology and back again, *Stem Cell Reports* **10**, 1676–1686 (2018).

409. J. Makki, Diversity of breast carcinoma: Histological subtypes and clinical relevance, *Clin. Med. Insights Pathol.* **8**, 23–31 (2015).

410. M. D. Prater, V. Petit, I. Alasdair Russell, R. R. Giraddi, M. Shehata, S. Menon, R. Schulte, I. Kalajzic, N. Rath, M. F. Olson, D. Metzger, M. M. Faraldo, M.-A. Deugnier, M. A. Glukhova, J. Stingl, Mammary stem cells have myoepithelial cell properties, *Nat. Cell Biol.* **16**, 942–950 (2014).

411. K. Polyak, M. Hu, Do Myoepithelial Cells Hold the Key for Breast Tumor Progression?, *J. Mammary Gland Biol. Neoplasia* **10**, 231–247 (2005).

412. A. C. Rios, N. Y. Fu, G. J. Lindeman, J. E. Visvader, In situ identification of bipotent stem cells in the mammary gland, *Nature* **506**, 322–327 (2014).

413. C. Brisken, B. O'Malley, Hormone Action in the Mammary Gland, *Cold Spring Harb. Perspect. Biol.* **2** (2010).

414. T. Tanos, L. J. Rojo, P. Echeverria, C. Brisken, ER and PR signaling nodes during mammary gland development, *Breast Cancer Res.* **14** (2012), doi:10.1186/bcr3166.